

The role of inhibitor of apoptosis proteins and XAF1 in the resistance to anti-cancer treatment in brain tumor cells and high-grade gliomas

DISSERTATION

zur Erlangung des Grades
“Doktor rerum naturalium”

am Fachbereich 10 - Biologie
der Johannes Gutenberg-Universität
in Mainz

Thomas R. Reich
geboren am 05.07.1987
in Ludwigshafen am Rhein

Mainz, Januar 2017

Dekan: [REDACTED]

1. Berichterstatter: PD Dr. [REDACTED]

2. Berichterstatter: Prof. Dr. [REDACTED]

Tag der mündlichen Prüfung: 12.05.2017

Das hier vorgestellte Thema wurde in der Zeit von Januar 2013 bis Dezember 2016 am Institut für Toxikologie der Universitätsmedizin Mainz bearbeitet und wird als Dissertation am Fachbereich Biologie der Johannes Gutenberg Universität Mainz (**D77**) eingereicht.

„Du kannst alles schaffen, wovon du träumst. Es sei denn, es ist zu schwierig.“

Quichotte (deutscher Dichter und Autor)

Abstract

Introduction: High grade gliomas (HGG) are the most frequent and most aggressive type of brain tumors with WHO grade III and IV. Especially gliomas of grade IV (glioblastomas) remain incurable and are associated with a short median survival. Therefore, there is an urgent need for improving the understanding of biological markers involved in pathogenesis and therapy response of gliomas. Inhibitor of apoptosis proteins (IAPs) are essential for regulation of apoptosis. Particularly Survivin and the X linked inhibitor of apoptosis protein (XIAP) are strongly expressed in many tumors, driving malignant transformation, tumor progression, and most importantly enabling tumor cells to resist therapy induced apoptosis. In turn, IAPs are regulated themselves by pro apoptotic factors, amongst which the XIAP associated factor 1 (XAF1) is an important tumor suppressor, frequently downregulated in different tumor entities.

Methods: Cellular survival was analyzed by colony formation assay and cell viability assays in the background of ectopic Survivin overexpression in glioma cells. In this here established cell model, induction of apoptosis, necrosis, senescence, DNA damage, and DNA repair capacity was investigated depending on the subcellular localization of Survivin. The epigenetic regulation of *survivin* and *XAF1* was analyzed in glioma cells and HGG patient samples by methylation specific PCR and methylation sensitive high resolution melt analysis. Kaplan Meier survival estimates were calculated to determine survival differences in dependency of the *XAF1* methylation status in HGG patients.

Results: Predominantly cytoplasmic Survivin was found to mediate cellular resistance to the alkylating anti cancer drug temozolomide (TMZ). Upon overexpression, Survivin led to an improved cellular survival and a reduced proportion of senescent cells. Both observations could be linked to a lower induction of DNA damage (double strand breaks) that was caused by an increased homologous recombination repair (HRR) capacity. In contrast, cells with overexpression of mutant Survivin, accumulating within the cell nucleus, sensitized the cells towards the applied treatment and were associated with increased DNA damage and an impaired HRR activity. In search for putative biomarkers, the methylation in the promoter regions of *survivin* and *XAF1* was analyzed. In glioma cells, no clear gene regulation of *survivin* by promoter methylation was observed. However, CpG methylation in the *XAF1* promoter was found to be inversely correlated with *XAF1* mRNA and protein expression and furthermore to a strongly improved survival of patients with grade III gliomas. In these tumors, the occurrence of *XAF1* methylation was strictly associated to a specific mutation in the *IDH1* gene, which is widely used as prognostic marker for HGG.

Discussion: Here, a yet unknown participation of Survivin in the HRR is described in the response to TMZ. It was shown that this protective effect relies on the intracellular localization of Survivin. Thus, the expression and localization of Survivin might provide valuable information about the prognosis and the response to chemotherapy in HGG. Furthermore, *XAF1* methylation was determined as a prognostic marker for grade III gliomas, being associated with an improved survival and *IDH1* mutations. Thus, analyzing this factor may improve the accuracy of the prognosis in HGG and eventually predict the response to TMZ based therapy.

Abstract (deutsch)

Einleitung: Hochgradige Gliome (WHO Grad III und IV) stellen die häufigste und aggressivste Tumorform unter den Hirntumoren dar. Besonders Glioblastome (Grad IV) sind mit einer äußerst schlechten Prognose assoziiert und sind kaum therapierbar. Daher ist die Erforschung von prognose- oder therapieassoziierten Marker unabdingbar. *Inhibitor of apoptosis proteins* (IAPs) sind in der Regulation der Apoptose beteiligt und in Tumoren häufig überexprimiert. Die wohl wichtigsten IAP Vertreter Survivin und *X linked inhibitor of apoptosis protein* (XIAP) sind mitverantwortlich für die maligne Transformation von Zellen, die Tumorprogression und die Resistenzbildung gegenüber zytostatikainduzierter Apoptose. Die Inhibierung dieser IAPs kann durch das pro apoptotische Tumorsuppressorprotein *XIAP associated factor 1* (XAF1) erfolgen, welches seinerseits häufig in verschiedenen Tumorentitäten herunterreguliert ist.

Methoden: Zur Analyse des zellulären Überlebens wurden Koloniebildungstests und Zellviabilitätstests in Abhängigkeit von ektopischer Survivin Expression durchgeführt. In diesem hier etablierten Zellmodell wurden außerdem die Induktion von Apoptose/ Nekrose, Seneszenz, DNA Schäden und der DNA Reparaturkapazität in Abhängigkeit von der subzellulären Survivin Lokalisation bestimmt. Die epigenetische Regulation von *survivin* und *XAF1* wurde mittels methylierungsspezifischer PCR und *high resolution melt* Analyse untersucht. Um den Einfluss bei der epigenetischen Faktoren auf das Überleben von Gliompatienten zu ermitteln, wurden Kaplan Meier Überlebenszeitanalysen durchgeführt.

Ergebnisse: Zytoplasmatisch lokalisiertes Survivin vermittelte in den hier durchgeführten Experimenten eine Resistenz gegenüber dem alkylierenden Zytostatikum Temozolomid (TMZ). Nach der Überexpression von Survivin konnte ein stark verbessertes Überleben und eine Reduktion des Anteils seneszenten Zellen beobachtet werden. Beides konnte auf eine signifikant reduzierte Zahl an DNA Doppelstrangbrüchen und eine erhöhte DNA Reparaturkapazität zurückgeführt werden. Dagegen blieb dieser protektive Effekt in Zellen, in denen Survivin im Kern lokalisiert war, aus. Zur Evaluation von *survivin* und *XAF1* als potentielle Biomarker in hochgradigen Gliomen wurde die epigenetische Stilllegung beider Promotorregionen untersucht. Während für *survivin* keine epigenetische Regulation beobachtet werden konnte, wurde für *XAF1* eine eindeutige, inverse Korrelation zwischen der Promotormethylierung und der *XAF1* mRNA und Protein Expression festgestellt. Ein methylierter *XAF1* Promotor war positiv mit dem Überleben von Gliompatienten (Grad III) assoziiert und trat in dieser Tumorentität strikt in Zusammenhang mit einer Mutation im *IDH1* Gen auf, welche ein gut etablierter Biomarker für hochgradige Glioma darstellt.

Diskussion: In der vorliegenden Arbeit konnte eine neuartige Rolle von Survivin bei der Reparatur von TMZ induzierten Doppelstrangbrüchen über die Homologen Rekombination beschrieben werden. Dies war stark abhängig von der Lokalisation des Proteins. Die Information über die Expression und Lokalisation von Survivin in Gliomen könnte daher einen vielversprechenden molekularen Marker darstellen. Die prognostische Bedeutung der Methylierung des *XAF1* Promotors wurde für Grad III Gliome nachgewiesen und könnte aufgrund seiner strikten Assoziierung mit Mutationen im *IDH1* Gen zur Unterstützung der Prognose und der Vorhersage des Therapieansprechens herangezogen werden.

Table of contents

List of abbreviations	V
1 Introduction	1
1.1 Molecular markers in cancer therapy.....	1
1.2 Gliomas represent the most common type of malignant brain tumors.....	2
1.3 Isocitrate dehydrogenase family and IDH mutations in gliomas.....	8
1.4 DNA repair pathways involved in glioma therapy	11
1.4.1 TMZ: Induction of DNA double-strand breaks.....	12
1.4.2 Repair of DNA damage induced by ionizing radiation	16
1.4.3 The repair of DNA double-strand breaks: HR vs. NHEJ.....	16
1.4.3.1 From sensing DNA double-strand breaks to pathway choice.....	17
1.4.3.2 The ATM-Chk2 pathway	18
1.4.3.3 Homologous recombination repair of DNA double-strand breaks.....	19
1.5 The anti-apoptotic protein Survivin is selectively expressed in tumor cells.....	22
1.5.1 Apoptosis: the programmed cell death	22
1.5.2 IAPs: Apoptosis and beyond	24
1.5.3 Survivin: a versatile protein with distinct functions and subcellular localization.....	25
1.5.4 Inhibiting IAPs Tumor suppressor XAF1 counteracts XIAP and Survivin	30
1.6 Aims.....	32
2 Material & Methods	33
2.1 Lists.....	33
2.2 Cell culture.....	35
2.2.1 Mycoplasma detection	36
2.2.2 Treatment of cells with cytostatic drugs	36
2.2.3 γ -Irradiation of cells.....	36
2.2.4 Generation of transgenic cell lines/ stable transfections	37
2.2.4.1 Plasmids.....	37
2.2.4.2 Stable/ transient transfection of GB cell lines	38
2.2.5 Transient siRNA-mediated gene knockdown	40
2.3 Protein extracts & Western blot.....	40
2.3.1 Cell lysates	40

2.3.2	SDS Polyacrylamid-Gel electrophoresis (SDS-PAGE) & Western blotting.....	41
2.4	Cytotoxicity assays.....	43
2.4.1	Cell viability assay (MTT)	43
2.4.2	Colony formation assay (CFA).....	44
2.4.3	Senescence	44
2.4.4	Caspase 3/ 7 activation.....	46
2.4.5	Cell Proliferation ELISA, BrdU-Incorporation assay	46
2.4.6	Flow cytometry.....	48
2.4.6.1	Analysis of the cell cycle distribution and apoptotic cell fraction by PI-staining.....	48
2.4.6.2	Analysis of apoptosis/ necrosis by AnnexinV-PI co-staining.....	49
2.4.6.3	Cell clone growth curve (CountBright Absolute Counting Beads)	50
2.5	Real-time RT-PCR.....	51
2.5.1	RNA isolation and cDNA synthesis.....	51
2.5.2	qPCR	51
2.6	Epigenetic Analyses	52
2.6.1	PCI DNA-Extraction	52
2.6.2	Bisulfite-induced modification of genomic DNA	53
2.6.3	Design of primers specific for bisulfite-converted DNA	53
2.6.4	Generation of DNA methylation standards by in vitro methylation.....	55
2.6.5	Analysis methods for detecting methylation in bisulfite-treated DNA	55
2.6.5.1	Methylation specific PCR (MSP)	56
2.6.5.2	Methylation-sensitive high resolution melt analysis (MS-HRM)	57
2.6.5.3	Bisulfite Pyrosequencing (PSQ)	59
2.7	Sequencing	61
2.7.1	Pyrosequencing	61
2.7.2	Sanger-Sequencing	61
2.8	Immunofluorescence.....	62
2.8.1	Immunofluorescence staining of fixed cells for foci detection.....	62
2.8.2	Immunofluorescence staining of fixed cells for detection of Survivin	63
2.8.3	Immunofluorescence staining of FFPE tumor sections (IHC).....	63
2.8.4	Live cell imaging	64
2.9	Survival analysis & statistics	64
2.9.1	HGG patient's cohort.....	64
2.9.2	Ethics statement.....	65

2.9.3	Kaplan-Meier Survival estimates & Correlations	65
2.9.4	Bivariate correlations	65
2.9.5	Statistical hypothesis testing	66
2.10	Assays for determining DNA repair	66
2.10.1	DNA-dependent protein kinase assay	66
2.10.2	Homologous Recombination assay	68
3	Results	70
3.1	Cell model.....	70
3.1.1	Stable expression of a Survivin-GFP fusion protein in glioblastoma cells	70
3.1.2	NES-inactivating mutation in SurvNESmut-GFP clones	73
3.1.3	Doubling time of Surv-GFP cell clones.....	73
3.2	Localization of Survivin in the response to anticancer drugs	74
3.2.1	Localization of Survivin-GFP upon CRM1-inhibition, TPT, and IR	75
3.2.2	Localization of endogenous Survivin in glioma cell lines.....	77
3.2.3	Localization of endogenous Survivin after IR	79
3.2.4	Localization of Survivin in high-grade glioma tumor sections	81
3.2.5	Screening for NES inactivating somatic mutations in HGG tumor samples.....	82
3.3	Impact of Survivin expression and localization on the response to TMZ	84
3.3.1	Survivin protects glioblastoma cells from TMZ-induced cell death.....	84
3.3.2	Induction of apoptosis and necrosis in LN229 cell clones	85
3.3.3	Activation of Caspase 3/ 7 in LN229 cell clones	86
3.3.4	Induction of senescence	87
3.3.5	Cellular response to TMZ-induced DNA damage.....	88
3.4	Induction of DNA double-strand breaks in Survivin cell clones.....	89
3.4.1	γ H2AX and co-localization with 53BP1	90
3.4.2	γ H2AX induction after TMZ treatment in Survivin clones	91
3.4.3	Influence of NHEJ on TMZ-induced DNA damage in Survivin clones.....	94
3.4.3.1	DNA-PK activity assay	94
3.4.3.2	Inhibition of NHEJ	95
3.4.4	Survivin in the homologous recombination repair of TMZ-induced DSB	97
3.4.4.1	Survivin expression rescues survival of Rad51-knockdown clones	97
3.4.4.2	Survivin expression reduces DNA DSB in RAD51-knockdown clones	98
3.4.5	Survivin increases capacity of HR DSB repair	99

3.5	Evaluation of Survivin as biomarker in high grade gliomas	100
3.6	IAP-antagonist XAF1 is epigenetically silenced in glioblastoma cell lines	103
3.6.1	Establishing MS-HRM promoter methylation analysis for XAF1 in GB cell lines	103
3.6.2	XAF1 methylation predicts XAF1 mRNA expression in glioma cells	106
3.6.3	Methylation of the XAF1 promoter in high-grade brain tumors	108
3.6.3.1	Patient characteristics	108
3.6.3.2	Receiver operating characteristics: Verification of the promoter methylation threshold in HGG patient samples	109
3.6.3.3	XAF1 methylation is associated with an improved survival in malignant gliomas ..	111
3.6.3.4	Identification of a false-negative IDH1-wt diagnosis using XAF1 methylation	117
3.6.4	A lack of XAF1 changes response of glioma cells to TMZ	118
3.6.4.1	XAF1 knockdown abrogates the TMZ-induced G2-arrest.....	118
3.6.4.2	XAF1 knockdown abrogates TMZ-induced cell cycle arrest in glioma cells.....	119
3.6.4.3	Implications of XAF1 knockdown for proliferation.....	121
3.6.5	Overexpression of XAF1 TMZ-treated glioma cells.....	122
4	Discussion	124
4.1	Survivin in the resistance of glioma cells to TMZ-induced cell death.....	125
4.1.1	Survivin reduces the number of TMZ-induced double-strand breaks	126
4.1.2	Survivin enhances double-strand break repair via HRR	129
4.1.3	The use of nuclear Survivin as predictive marker for TMZ-based chemotherapy.....	131
4.2	Evaluation of BIRC5 as epigenetic prognostic marker in gliomas.....	132
4.3	XAF1 promoter methylation is a promising biomarker in high-grade gliomas.....	134
4.3.1	XAF1 promoter methylation accounts for gene silencing in high-grade gliomas.....	134
4.3.2	XAF1 promoter methylation is strictly linked to 2-HG-producing IDH1 mutations and prolonged survival in grade III gliomas.....	135
4.3.3	XAF1 methylation as surrogate marker for IDH mutations	136
4.3.4	The contradictory role of XAF1 silencing in the response of glioma cells to TMZ.....	138
5	Literature	141
6	Appendix.....	156
6.1	Supplementary data	156
6.2	Acknowledgments	165
6.3	Curriculum Vitae.....	166

List of abbreviations

2-HG	2-hydroxyglutarate
3meA	N3-methyladenine
53BP1	p53-binding protein 1
5-mC	5 methylcytosine
7meG	N7-methylguanine
AA	anaplastic astrocytoma
Ab	antibody
ACTB	β -Actin
aKG	α -ketoglutarate
AML	acute myeloid leukemia
AO	anaplastic oligodendroglioma
AOA	anaplastic oligoastrocytoma
AP	apurnic site
APC	allophycocyanin
AT	Ataxia-telangiectasia
ATBA	American Brain Tumor Association
ATM	ataxia-telangiectasia-mutated
ATR	AT and Rad3-related protein
ATRX	alpha thalassemia/mental retardation syndrome X-linked (somatic mutations)
AUC	area under the curve
β -Gal	β -Galactosidase
BC	breast cancer
BH	BCL2 homology domain
BIR	baculovirus inhibitor of apoptosis protein repeat
BIRC5	Baculoviral IAP Repeat Containing 5
BRAD	BRCA1-associated RING domain 1
BRCA	BRCA1-associated
BrdU	Bromodeoxyuridine
CAD	caspase-activated Dnase
CARD	Caspase recruitment domain
CDE	cycle-dependent element
CDK	cyclin-dependent kinase
CDS	coding sequence
CFA	colony formation assay
CHR	cell cycle genes homology region
CNS	central nervous system
code1	codeletion
CPC	Chromosomal passenger complex
CpG	cytosine, guanine dinucleotide
CRC	colorectal cancer
CT	chemotherapy
CtIP	CtBP-interacting protein
Cyt c	cytochrome c
DDR	DNA damage response
DIC	differential interference contrast
DNA-PKcs	DNA-dependent protein kinase
DSB	DNA double-strand break
DSB	double-strand break
EFS	event-free survival
ER	estrogen receptor
ESCC	esophageal squamous-cell carcinoma
EtOH	ethanol
FACS	fluorescence-activated cell scanner/ sorter
FCS	fetal calf serum
FFPE	formalin-fixed and paraffin-embedded
GB	glioblastoma
G-CIMP	glioma CpG island methylator phenotype
gDNA	genomic DNA

GFP	green fluorescent protein
Gy	gray (absorbed dose)
HER2	human epidermal growth receptor 2
HGG	high-grade glioma
HJ	Holliday-junctions
HNSCC	head and neck squamous cell carcinoma
HR	homologous recombination
HRM	high resolution melt
IAP	inhibitor of apoptosis protein
IDH	isocitrate dehydrogenase
IR	ionizing radiation
LMB	leptomycin B
M	methylated
MDC1	mediator of DNA damage checkpoint protein 1
MGMT	O6-methylguanine-DNA methyltransferase
MHC	Major histocompatibility complex
MMR	mismatch repair
MRE11	meiotic recombination 11 homolog
MS-HRM	methylation sensitive high resolution melt (analysis)
MSP	methylation specific PCR
mut	mutated
NBS1	Nijmegen breakage syndrome protein 1
NES	nuclear export sequence
NHEJ	non-homologous end-joining
NLS	nuclear localization signal
NPC	nuclear pore complex
ns	not significant
NSCLC	Non-Small Cell Lung Cancer
O ⁶ meG	O6-methylguanine
OS	overall survival
PCI	phenol-chloroform-isoamyl alcohol
PCV	procarbazine, CCNU, vincristine
PDB	protein database
PI	propidium iodide
PIKK	phosphatidylinositol 3-kinase-like protein kinase
PR	progesterone receptor
PS	phosphatidylserine
PSQ	pyrosequencing
RAD50	radiation sensitive 50 homolog
RCC	renal cell carcinoma
RING	Really Interesting New Gene (protein domain)
RNF8	RING finger protein 8
ROS	reactive oxygen species
RT	radiotherapy/ room temperature
scr	scramble (siRNA)
SeqP	sequencing primer
SMAC	second mitochondria-derived activator of caspases
SN1	nucleophilic substitution (first order)
SSB	single-strand break
TET	ten-eleven translocation
TMZ	temozolomide (alkylating anti-cancer drug)
TPT	topotecan (TOP1 inhibitor used for glioma therapy)
TRAIL	TNF-related apoptosis-inducing ligand
Ub	ubiquitin
UM	unmethylated
WHO	World Health Organization
wt	wild-type
XAF1	XIAP-associated factor 1
XIAP	X-linked inhibitor of apoptosis protein (BIRC4)

1 Introduction

The constantly increasing knowledge of genes involved in tumorigenesis and the pathology of tumors is the basis of modern tumor biology. Identification of new biological tumor markers, either specific for certain tumor types, or ubiquitous among different tumor entities, allows a highly differential diagnosis and clears the way for a precise and personalized therapy approaches. Also, the identification of genetic markers that are associated with a predisposition to cancer help to improve treatment possibilities due to preventive medical checkups. At present, there are well established prognostic and therapy guiding markers for different cancer types. A well characterized example is breast cancer (BC). Two decades ago, certain heterozygous germline mutations in *BRCA1* and *BRCA2* were linked to a predisposition for developing breast and ovarian cancer [1,2]. Mechanistically, this susceptibility to cancer was explained when both gene products were identified to be involved in repair of DNA double strand breaks (DSB) via homologous recombination (HR) [3,4]. These markers became increasingly important not only for prognosis but also for the choice of therapy, indicating a treatment with platinum drugs and PARP inhibitors [5]. A “BRCAness” could also be observed in non hereditary/ sporadic breast cancer, ovarian cancer and other cancers which opened the possibility of a wider application of BC treatment regimens [6], emphasizing the huge importance of molecular markers.

1.1 Molecular markers in cancer therapy

In BC, combining molecular markers with other (classical) predictive markers like estrogen receptor (ER), progesterone receptor (PR), or human epidermal growth factor receptor 2 (HER2) positivity has provided a good basis for an individual therapy of BC. Hormone receptor positive tumors are responsive to an anti hormonal therapy with selective ER response modulators, ER downregulators, and others. HER2 positive BCs are sensitive to trastuzumab (inter alia), a humanized monoclonal antibody against HER2. Triple negative BCs on the other hand, not showing ER, PR, or HER2 positivity, require a different type of treatment. The importance of guiding an effective molecular therapy of these biologically different tumors by clinical testing has been emphasized by recent efforts for standardization of the diagnostic methods for detecting the hormone receptor status and HER2 status [7,8].

Introduction

In case of gliomas, the use of molecular markers in therapy is less advanced. Most of the time, a diagnosis of this disease is devastating for the patients, as therapy options are still missing. The current standard type of care usually involves a combination of surgery and radiation therapy (RT) and chemotherapy (CT). Indeed, there is a constant progress with regard to the discovery of new markers and the possibility of a precise molecular subgrouping of tumor entities, but these efforts are mostly of sheer prognostic implications.

1.2 Gliomas represent the most common type of malignant brain tumors

Gliomas belong to tumors of the central nervous system (CNS) which are mainly affecting the brain and brain stem (95 %) [9]. The remaining 5 % represent very rare tumors of the meninges, cerebral nerves, the spinal cord amongst others [*ibid.*]. Depending on the histopathology and more and more on the use of molecular markers, CNS tumors are subdivided into different tumor types with distinct pathological features. Since over 100 tumor entities are described, diagnosing a tumor correctly is a demanding task, as prognosis and further clinical treatment depend on this initial histopathological work. Clinicians and neuropathologists can find advice for their diagnosis in the “WHO Classification of Tumours of the Central Nervous System”, which is released by the World Health Organization (WHO) with regular updates. The WHO grading of tumors ranges from grade I – IV and is performed in parallel to the classification system, based on histological criteria. This grade provides an important tool for defining the malignancy and aggressiveness of the tumor to aid therapy decisions. The criteria for WHO grading of CNS tumors are summarized in **Table 1** according to Kleinhues *et al.* [10]. Besides the grading, the WHO guideline gives an overview of all tumor entities currently being implemented (**Table 2**) [11].

Table 1: WHO grading for tumors of the CNS. The different WHO tumor grades depend on distinct histopathological features. The occurrence of several features at once suggest the classification into a higher grade. Tumor grading was summarized according to Kleinhues et al. [10].

WHO grade	Tumor characteristics	histopathological features
I	lesions with low proliferative potential, frequently discrete nature, and the possibility of cure by surgical resection alone	
II	lesions are generally infiltrating and show low mitotic activity; tumors might also progress to lesions of higher grades	0 or 1 feature; usually nuclear atypia
III	clear histological signs of malignancy: increased mitotic activity, infiltrative growth, anaplasia	2 features; usually nuclear atypia and mitotic activity
IV	mitotically active neoplasms that are necrosis prone and associated with a rapid pre and postoperative disease progression; strong infiltration of neighboring tissue might add to the tumor properties	3 features; usually nuclear atypia, mitoses, endothelial proliferation, and/ or necrosis

Gliomas are tumors originating from probably different glial progenitor cells which make up the non neuronal supportive CNS tissue. This includes astrocytes, oligodendrocytes, ependymal cells, and microglia. Gliomas account for 30 – 40 % of all primary intracranial tumors [12] or 27 % according to the American Brain Tumor Association (ATBA) in 2016 [13]. With this high percentage, gliomas are also representing the majority (~80 %) of all primary malignant brain neoplasms [13], while 32.8 % of brain and CNS tumors are diagnosed as being malignant, and more than two thirds are of benign nature [14]. In the age group of adolescents and young adults (15 – 39 years), malignant brain and CNS tumors are the 3rd most common cause of cancer death [15], whereas in adults they rank on place 8., despite being a relatively rare cancer overall with about 3 % of the estimated new cases in the US in 2016 [16]. The 5 year survival rates of CNS tumors of about 22 % or even only 8 % for glioblastomas (GB) are miserable in comparison to other cancers (breast cancer: 80 %; colorectal cancer: 52 %; overall men: 52 %; overall women: 58 %) [9] and have not improved much in the last decade. These facts underline the importance of research aiming at the discovery of new glioma markers and thereby potential therapy targets especially for high grade gliomas (HGG).

Most cases of malignant gliomas (> 50 %) are astrocytomas of WHO grade IV, also referred to as GB, with the worst prognosis among the brain tumors [17,18]. Despite the advances in the treatment by a combination of surgery (maximum safe resection) with subsequent RT with concomitant plus adjuvant temozolomide(TMZ) based CT, median overall survival (OS) is

Introduction

14.6 months only [19]. This is a minor improvement in comparison to 12.1 months after surgery and RT alone [*ibid.*] and demonstrates the destructive nature of this disease. Beside GB, WHO II diffuse or WHO III anaplastic astrocytomas (AA) make up 15.9 % of the gliomas and WHO II oligodendrogliomas or WHO III anaplastic oligodendrogliomas (AO) are found in 13.6 % of the cases [17]. The residual percentages are allotted to ependymomas, pilocytic astrocytomas, and others. Together, AA (WHO III), AO (WHO III), and GB (WHO IV) represent the group of HGG which are highly invasive tumors that remain largely incurable. A small entity of WHO III tumors referred to as anaplastic oligoastrocytoma (AOA) also belongs to this group. These tumors show histological features of astrocytes and oligodendrocytes and thus cannot be classified as either tumor entity by classic histology. However, the diagnosis of AOA is strongly discouraged by the recent WHO guideline, as nearly all of these tumors can be classified as either astrocytoma or oligodendroglioma by genetic testing [20].

For now, steering glioma therapy on the basis of molecular markers is not performed generally. In some cases, molecular markers can help to indicate the choice of treatment combinations. In GB patients with 1p/ 19q codeletion (codeletion) for instance, a combination of RT and CT with procarbazine, CCNU, vincristine (PCV) can achieve a doubling of the survival time as compared to RT alone [21]. Though, a combined chemotherapy with PCV also clearly improves the prognosis of patients without 1p/ 19q codeletion, and therefore stratification upon this marker is not realized in all centers [21]. Furthermore, the methylation status of the O⁶ methylguanine DNA methyltransferase (*MGMT*) promoter is usually analyzed but not relevant for the choice of therapy, e.g. whether to use alkylating agents or not. First evidence indicating a predictive value of *MGMT* promoter methylation had already been published in 2005 by Stupp *et al.* and Hegi *et al.*, who demonstrated an improved OS for patients with methylated *MGMT* promoter upon concomitant TMZ treatment [19,22]. In subsequent phase 3 trials, a predictive value of the *MGMT* status for the treatment with TMZ was only found for elderly (> 65 years) patients (NOA 08 [23] and Nordic [24]). NOA 08 revealed that patients with anaplastic astrocytoma (AA) and GB older than 65 years, showing *MGMT* promoter methylation, benefit in terms of an improved event free survival (EFS) from TMZ based chemotherapy alone, when compared to the standard RT alone. An improved OS was not observed. The authors suggested to make use of the *MGMT* status as predictive biomarker for the treatment of this particular patient group.

Table 2: 2016 WHO Classification list of tumor entities of the central nervous system. The British English spelling was adopted from the original source. *Reproduced with permission from Louis, DN, Ohgaki, H, Wiestler, OD, Cavenee, WK, Ellison, DW, Figarella-Branger, D, Perry, A, Reifenberger, G, Von Deimling, A. World Health Organization Classification of Tumours of the Central Nervous System, Fourth Edition revised. IARC, Lyon, 2016 (see appendix (p. 164) for reprint permission).*

Diffuse astrocytic and oligodendroglial tumours		Neuronal and mixed neuronal-glia tumours	
Diffuse astrocytoma, IDH-mutant	9400/3	Dysembryoplastic neuroepithelial tumour	9413/0
Gemistocytic astrocytoma, IDH-mutant	9411/3	Gangliocytoma	9492/0
<i>Diffuse astrocytoma, IDH-wildtype</i>	9400/3	Ganglioglioma	9505/1
Diffuse astrocytoma, NOS	9400/3	Anaplastic ganglioglioma	9505/3
Anaplastic astrocytoma, IDH-mutant	9401/3	Dysplastic cerebellar gangliocytoma (Lhermitte–Duclos disease)	9493/0
<i>Anaplastic astrocytoma, IDH-wildtype</i>	9401/3	Desmoplastic infantile astrocytoma and ganglioglioma	9412/1
Anaplastic astrocytoma, NOS	9401/3	Papillary glioneuronal tumour	9509/1
Glioblastoma, IDH-wildtype	9440/3	Rosette-forming glioneuronal tumour	9509/1
Giant cell glioblastoma	9441/3	<i>Diffuse leptomeningeal glioneuronal tumour</i>	
Gliosarcoma	9442/3	Central neurocytoma	9506/1
<i>Epithelioid glioblastoma</i>	9440/3	Extraventricular neurocytoma	9506/1
Glioblastoma, IDH-mutant	9445/3*	Cerebellar liponeurocytoma	9506/1
Glioblastoma, NOS	9440/3	Paraganglioma	8693/1
Diffuse midline glioma, H3 K27M–mutant	9385/3*	Tumours of the pineal region	
Oligodendroglioma, IDH-mutant and 1p/19q-codeleted	9450/3	Pineocytoma	9361/1
Oligodendroglioma, NOS	9450/3	Pineal parenchymal tumour of intermediate differentiation	9362/3
Anaplastic oligodendroglioma, IDH-mutant and 1p/19q-codeleted	9451/3	Pineoblastoma	9362/3
<i>Anaplastic oligodendroglioma, NOS</i>	9451/3	Papillary tumour of the pineal region	9395/3
<i>Oligoastrocytoma, NOS</i>	9382/3	Embryonal tumours	
<i>Anaplastic oligoastrocytoma, NOS</i>	9382/3	Medulloblastomas, genetically defined	
Other astrocytic tumours		Medulloblastoma, WNT-activated	9475/3*
Pilocytic astrocytoma	9421/1	Medulloblastoma, SHH-activated and <i>TP53</i> -mutant	9476/3*
Pilomyxoid astrocytoma	9425/3	Medulloblastoma, SHH-activated and <i>TP53</i> -wildtype	9471/3
Subependymal giant cell astrocytoma	9384/1	Medulloblastoma, non-WNT/non-SHH <i>Medulloblastoma, group 3</i>	9477/3*
Pleomorphic xanthoastrocytoma	9424/3	<i>Medulloblastoma, group 4</i>	
Anaplastic pleomorphic xanthoastrocytoma	9424/3	Medulloblastomas, histologically defined	
Ependymal tumours		Medulloblastoma, classic	9470/3
Subependymoma	9383/1	Medulloblastoma, desmoplastic/nodular	9471/3
Myxopapillary ependymoma	9394/1	Medulloblastoma with extensive nodularity	9471/3
Ependymoma	9391/3	Medulloblastoma, large cell / anaplastic	9474/3
Papillary ependymoma	9393/3	Medulloblastoma, NOS	9470/3
Clear cell ependymoma	9391/3	Embryonal tumour with multilayered rosettes, C19MC-altered	9478/3*
Tanycytic ependymoma	9391/3	<i>Embryonal tumour with multilayered rosettes, NOS</i>	9478/3
Ependymoma, <i>RELA</i> fusion–positive	9396/3*	Medulloepithelioma	9501/3
Anaplastic ependymoma	9392/3	CNS neuroblastoma	9500/3
Other gliomas		CNS ganglioneuroblastoma	9490/3
Chordoid glioma of the third ventricle	9444/1	CNS embryonal tumour, NOS	9473/3
Angiocentric glioma	9431/1	Atypical teratoid/rhabdoid tumour	9508/3
Astroblastoma	9430/3	<i>CNS embryonal tumour with rhabdoid features</i>	9508/3
Choroid plexus tumours		Tumours of the cranial and paraspinal nerves	
Choroid plexus papilloma	9390/0	Schwannoma	9560/0
Atypical choroid plexus papilloma	9390/1	Cellular schwannoma	9560/0
Choroid plexus carcinoma	9390/3	Plexiform schwannoma	9560/0

Introduction

Melanotic schwannoma	9560/1	Osteochondroma	9210/0
Neurofibroma	9540/0	Osteosarcoma	9180/3
Atypical neurofibroma	9540/0		
Plexiform neurofibroma	9550/0	Melanocytic tumours	
Perineurioma	9571/0	Meningeal melanocytosis	8728/0
Hybrid nerve sheath tumours		Meningeal melanocytoma	8728/1
Malignant peripheral nerve sheath tumour	9540/3	Meningeal melanoma	8720/3
Epithelioid MPNST	9540/3	Meningeal melanomatosis	8728/3
MPNST with perineurial differentiation	9540/3		
Meningiomas		Lymphomas	
Meningioma	9530/0	Diffuse large B-cell lymphoma of the CNS	9680/3
Meningothelial meningioma	9531/0	Immunodeficiency-associated CNS lymphomas	
Fibrous meningioma	9532/0	AIDS-related diffuse large B-cell lymphoma	
Transitional meningioma	9537/0	EBV-positive diffuse large B-cell lymphoma, NOS	
Psammomatous meningioma	9533/0	Lymphomatoid granulomatosis	9766/1
Angiomatous meningioma	9534/0	Intravascular large B-cell lymphoma	9712/3
Microcystic meningioma	9530/0	Low-grade B-cell lymphomas of the CNS	
Secretory meningioma	9530/0	T-cell and NK/T-cell lymphomas of the CNS	
Lymphoplasmacyte-rich meningioma	9530/0	Anaplastic large cell lymphoma, ALK-positive	9714/3
Metaplastic meningioma	9530/0	Anaplastic large cell lymphoma, ALK-negative	9702/3
Chordoid meningioma	9538/1	MALT lymphoma of the dura	9699/3
Clear cell meningioma	9538/1		
Atypical meningioma	9539/1	Histiocytic tumours	
Papillary meningioma	9538/3	Langerhans cell histiocytosis	9751/3
Rhabdoid meningioma	9538/3	Erdheim–Chester disease	9750/1
Anaplastic (malignant) meningioma	9530/3	Rosai–Dorfman disease	
		Juvenile xanthogranuloma	
		Histiocytic sarcoma	9755/3
Mesenchymal, non-meningothelial tumours		Germ cell tumours	
Solitary fibrous tumour / haemangiopericytoma**		Germinoma	9064/3
Grade 1	8815/0	Embryonal carcinoma	9070/3
Grade 2	8815/1	Yolk sac tumour	9071/3
Grade 3	8815/3	Choriocarcinoma	9100/3
Haemangioblastoma	9161/1	Teratoma	9080/1
Haemangioma	9120/0	Mature teratoma	9080/0
Epithelioid haemangioendothelioma	9133/3	Immature teratoma	9080/3
Angiosarcoma	9120/3	Teratoma with malignant transformation	9084/3
Kaposi sarcoma	9140/3	Mixed germ cell tumour	9085/3
Ewing sarcoma / PNET	9364/3		
Lipoma	8850/0	Tumours of the sellar region	
Angiolipoma	8861/0	Craniopharyngioma	9350/1
Hibernoma	8880/0	Adamantinomatous craniopharyngioma	9351/1
Liposarcoma	8850/3	Papillary craniopharyngioma	9352/1
Desmoid-type fibromatosis	8821/1	Granular cell tumour of the sellar region	9582/0
Myofibroblastoma	8825/0	Pituicytoma	9432/1
Inflammatory myofibroblastic tumour	8825/1	Spindle cell oncocytoma	8290/0
Benign fibrous histiocytoma	8830/0		
Fibrosarcoma	8810/3	Metastatic tumours	
Undifferentiated pleomorphic sarcoma / malignant fibrous histiocytoma	8802/3		
Leiomyoma	8890/0		
Leiomyosarcoma	8890/3		
Rhabdomyoma	8900/0		
Rhabdomyosarcoma	8900/3		
Chondroma	9220/0		
Chondrosarcoma	9220/3		
Osteoma	9180/0		

The morphology codes are from the International Classification of Diseases for Oncology (ICD-O) [742A]. Behaviour is coded /0 for benign tumours; /1 for unspecified, borderline, or uncertain behaviour; /2 for carcinoma in situ and grade III intraepithelial neoplasia; and /3 for malignant tumours. The classification is modified from the previous WHO classification, taking into account changes in our understanding of these lesions. *These new codes were approved by the IARC/WHO Committee for ICD-O. *Italics*: Provisional tumour entities. **Grading according to the 2013 WHO Classification of Tumours of Soft Tissue and Bone.

In principle, these data are in line with the Nordic study by Malmström *et al* 2012 [24]. Here, a total of 342 patients with GB were randomized into three treatment groups, comparing TMZ treatment vs. hypofractionated RT vs. standard RT. Median OS was reported to be longer in TMZ treated group (8.3 months) than in the group that received standard RT (6.0 months) with a hazard ration of 0.70 (95 % CI 0.52 – 0.93; p = 0.01). In contrast, there was no significant

difference when compared to hypofractionated RT (7.5 months; hazard ratio: 0.85 (95 % CI 0.64 – 1.12; $p = 0.24$). A clear influence of the *MGMT* methylation status, however, could not be demonstrated, as survival differences were not statistically significant. Nevertheless, the authors concluded that for elderly patients (>70) the use of the *MGMT* promoter methylation status could indicate the option of a TMZ based therapy. Although these and other reports speak in favor of the use of *MGMT* methylation as therapy determining marker, “stratification of patients by the use of one biomarker (still) is not an established approach in neuro oncology [...]” [23].

As demonstrated above, the use of molecular markers for glioma therapy is heterogeneous and inconsequent. However, recent advances in tumor characterization by means of genetic and epigenetic analyses have led to a complete revision of the WHO classification system published in 2016 [20]. The so far valid classification system published 2007 mostly utilizes histopathological and immunohistochemical parameters for tumor classification [25]. Now, for the first time, molecular markers are utilized in addition to classic histological characteristics to define many tumor entities [11]. One groundbreaking discovery that might have paved the way into the molecular era of brain tumor classification was made in 2008. A mutation in the isocitrate dehydrogenase gene (*IDH1*) was identified by sequencing 20661 protein coding genes in GB, and it was found to have huge implications for the prognosis of GB patients [26]. The transition of guanine to adenine (G395A) causes a substitution of an arginine with a histidine in the active site of the protein (R132H) and was evident in 12 % of GB patients analyzed [*ibid.*]. It was noticeable that this *IDH1* mutation preferentially occurred in younger GB patients (mean age of 33 years in *IDH1* mut vs. 53 years in *IDH1* wt) and surprisingly in nearly all patients with secondary GB. Furthermore, the *IDH1* mut was associated with a significantly improved prognosis (median OS of 3.8 years as compared to 1.1 years). In the following, *IDH1* mutation status advanced to one of the most important and researched molecular markers for the diagnosis of gliomas and the definition of different glioma entities. This discovery did not only lead to the recent fundamental revision of tumor classification (**Figure 1**), but also generated a molecular understanding of distinct glioma subgroups with significantly different clinical pictures and cell physiology.

Classification of diffuse gliomas according to the 2016
„WHO Classification of Tumours of the Central Nervous System“

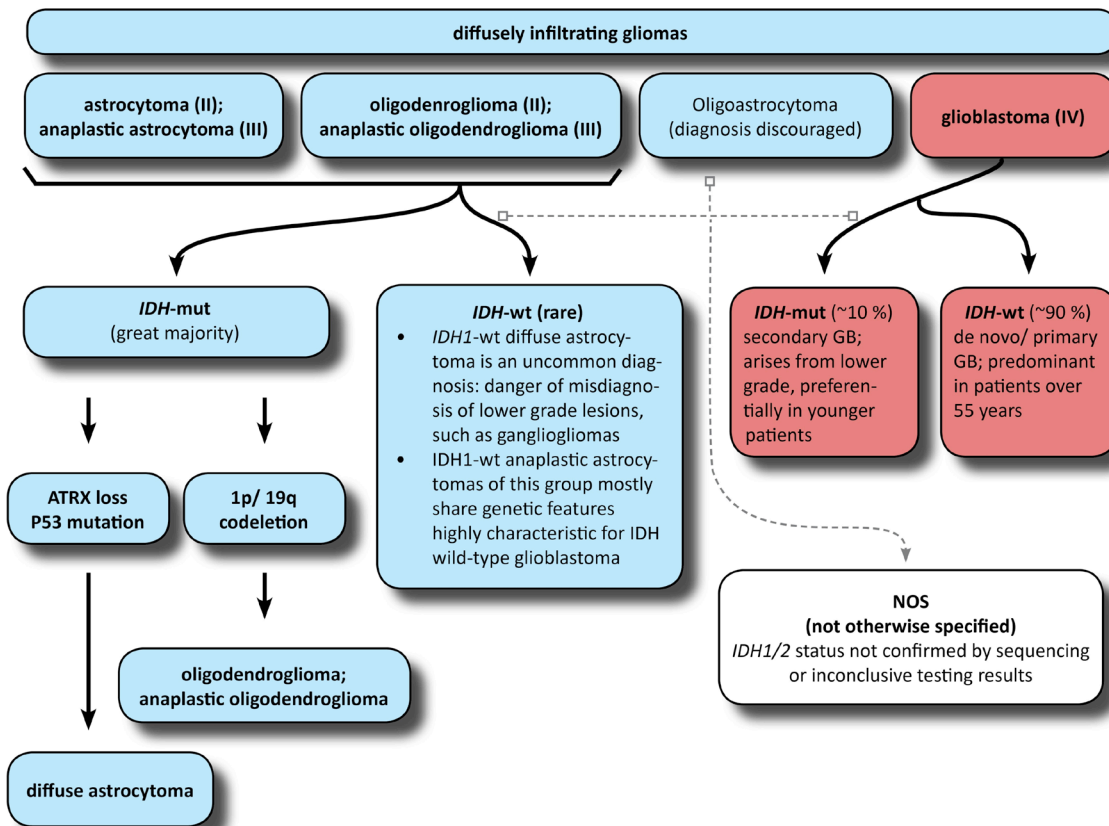


Figure 1: Classification procedure for diffuse gliomas involving histologic and genetic features according to the 2016 WHO guidelines. This new classification incorporates grade II and III astrocytic tumors, the grade II and grade III oligodendroglial tumors, and grade IV glioblastomas (GB) to the group of diffuse gliomas. The controversial group of oligoastrocytomas of grade II and III are suggested to be assigned to the NOS category (not otherwise specified) which is also used in the case of inconclusive IDH testing results. The diagnosis of oligodendroglioma or anaplastic oligodendroglioma requires the demonstration of an IDH mutation and a 1p/19q co-deletion. Asterisks indicate a characteristic but not required genetic testing result. Based on a review of the WHO guidelines by Louis et al. (2016) [11].

1.3 Isocitrate dehydrogenase family and IDH mutations in gliomas

The influence of *IDH1* mutations on the behavior of astrocytomas has yet not been fully understood. IDHs catalyze the reversible oxidative decarboxylation of isocitrate to α ketoglutarate (α KG), utilizing NAD^+ or NADP^+ as electron acceptor, depending on the IDH class [27]. IDH1 is one of three highly similar human isoforms, which uses NADP^+ as co factor. IDH1 is localized in the cytosol, the peroxisomes, and mitochondria [28]. The NAD^+ dependent enzymes (IDH3 isoforms) catalyze a key step in the citric acid cycle in the mitochondria and act as heterooctamer [29]. NADP^+ dependent cytosolic IDH1 and mitochondrial IDH2 act as homodimers and have also been shown to contribute to the cellular defense against oxidative

damage [30]. The heterozygous, cancer related mutations in conserved amino acid residues are found in the genes of *IDH1* and *IDH2* and are predominant for a subset of gliomas and also AML [31]. These mutations mainly affect the amino acid 132 or the corresponding R172 in *IDH2*. For *IDH1*, the substitution of Arg with His (R132H) occurs in more than 92 % of the mutations [32]. These changes are crucial for the enzyme's function as they affect the active site of the protein and thereby the binding of the ligands (**Figure 2**). Substitutions at the position R132 have been reported to reduce the protein's ability of converting isocitrate to α KG and have originally been interpreted to dominantly inhibit the wild type *IDH1* activity through heterodimer formation [33]. However, these mutations have been identified as gain of function mutations that allow the neomorphic conversion of α KG to 2 hydroxyglutarate (2 HG) [34,35]. Upon metabolite profiling, about 100 fold elevated levels of 2 HG were found in astrocytoma cells expressing mutated (mut) *IDH1* compared to *IDH1* wildtype (wt) expressing control cells. Noticeable amounts of 2 HG were also found in glioma samples, whereat no significant reduction in α KG levels was observed. Furthermore, there is strong evidence showing that the *IDH1* gain of function, to produce 2 HG, contributes to tumorigenesis by several molecular mechanisms. Biologically, the onco metabolite 2 HG functions as competitive inhibitor of non heme iron dioxygenases that utilize α KG as a redox co factor [36]. Important enzymes involved in processes of epigenetic regulation belong to this group, including JmjC domain containing histone demethylases [37] and the ten eleven translocation (TET) family enzymes that oxidize 5 methylcytosine (5 mC) to 5 hydroxymethylcytosine [38]. The inhibition of these enzymes by 2 HG causes enormous changes to the epigenome in terms of an extensive, coordinated hypermethylation at specific loci which accounts for the so called G CIMP (glioma CpG island methylator phenotype) [36,39]. This cancer related phenotype is associated with malignant transformation, increased proliferation, and an inhibition of differentiation and tightly linked to *IDH* mutations [40]. In gliomas, an *IDH1* mutation is sufficient to establish the G CIMP by mechanistically causing DNA hypermethylation of a large number of genes [41,42]. Alongside with this characteristic methylation pattern, interestingly, also a small number of hypomethylated genes was found [*ibid.*].

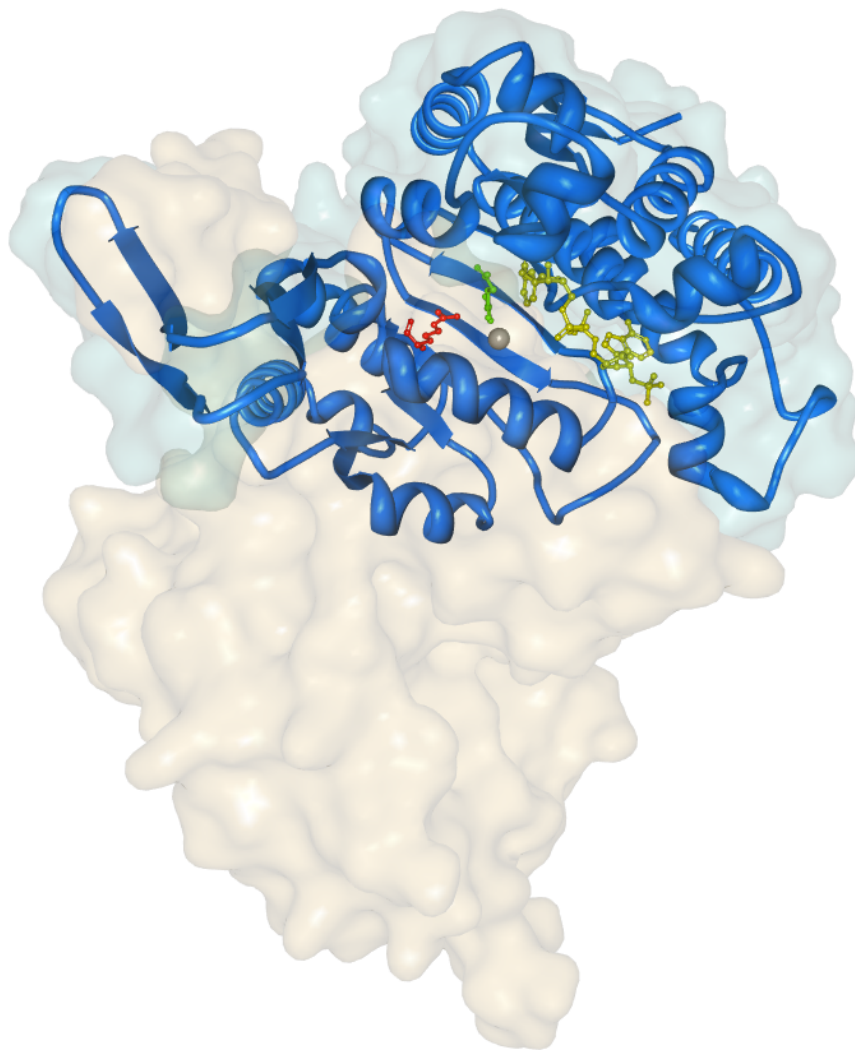


Figure 2: Crystal structure of human IDH1 homodimer in complex with NADP⁺ and Ca²⁺/αKG. Protein chain of the first monomer is shown in blue with α-KG (green), Ca²⁺ (grey), NADP⁺ (yellow). The arginine 132 in the active site is colored in red. Position 132 is frequently mutated in different glioma entities. For reasons of clarity, the second monomer is shown as surface model only (pale orange). This structural view was created using RCSB Protein Workshop [43,44] with structural data of PDB entry 4L04 [36].

The discovery of *IDH1* mutation in GB by Parsons *et al.* led to the awareness of this neomorphic metabolic enzyme and its broad clinical implications [26]. Further studies identified *IDH* mutations as being specific for WHO II and III oligodendrogliomas and astrocytomas and GB, having evolved from the aforementioned, since more than 70 % of these tumors show *IDH* mutations [45]. In contrast, *IDH1* mutations are very rare events in patients with primary GB (3 %), whereas they are found in about 50 – 82 % of secondary GB [46 48].

Because of the association with lower grade tumors, *IDH1* mutations are discussed to occur early during gliomagenesis and therefore might represent driver mutations that occur in stem/progenitor cells of the brain, causally linked to tumor development [32,49]. Despite a better genetic understanding of gliomas, IDH1 targeting therapies have not brought a breakthrough in glioma therapy, yet. Small molecule inhibitors targeting mutant IDH1 and vaccine immunotherapy with mutant IDH1 loaded onto MHC class II complexes are currently under investigation [50], but effectiveness in clinical trials has not been proven, yet. Hence, the demanding search for new markers and, even more important, of new therapeutic targets is of utmost importance. Of special interest in this context are proteins that exhibit a tumor specific expression, as they would be highly suitable for selective cancer targeting strategies. Such factors additionally involved in resistance mediating pathways like the inhibition of apoptosis or activation of DNA repair processes further provide a promising target for this approach.

1.4 DNA repair pathways involved in glioma therapy

Types of DNA damage are manifold and so are the mechanisms involved in the repair of the DNA and the maintenance of the genome. In normal cells, DNA repair pathways are essential to avoid mutations and maintain the genomic stability upon various exogenous DNA damaging influences like UV irradiation, food carcinogens, e.g. aflatoxins, N nitroso compounds, and others. Also, endogenous sources of DNA damage, like reactive oxygen species (ROS) or collapse of replication forks, lead to different DNA lesions. The instances of DNA repair protect cells from malignant transformation and thereby ultimately prevent cancer formation. Vice versa, defects in DNA repair pathways or upstream signaling pathways are associated with a predisposition for cancer. Interestingly, tumors with such defects provide the possibility to target the remaining “backup” pathways of DNA repair which creates a tumor specific “synthetic lethality”. On the other hand, DNA repair can also contribute to the cellular resistance to CT or RT.

In the therapy of gliomas, ionizing radiation (IR) and the alkylating anti cancer drug TMZ are used in the standard treatment regimen (see 1.2). These approaches aim at the induction of apoptosis in cancer cells via causing different types of DNA damage. However, the most lethal type of DNA damage in both cases are DSBs. DSBs are the source of chromosomal breaks and exchanges and may cause a fatal loss of genetic information by which these lesions unfold their enormous genotoxic potential.

1.4.1 TMZ: Induction of DNA double-strand breaks

Ironically, in case of the alkylating anti cancer drug TMZ, the generation of DSBs involves DNA repair mechanisms themselves. Alkylating agents or their intermediates are highly electrophilic reaction partners that are prone to a nucleophilic attack by ring nitrogen and extracyclic oxygen atoms of DNA bases. In aqueous solution, temozolomide is converted to its intermediates in a spontaneous and pH dependent reaction, ultimately releasing a highly electrophilic methyldiazonium cation (**Figure 3**) [51]. Depending on the starting substance, covalent base adducts are formed with methyl groups or larger alkyl moieties. Furthermore, the number of reactive sites within an alkylating compound, in particular if they are monofunctional or bifunctional, gives rise to different base alkylation patterns [52]. Also, the nucleophilic reactivity of the “target” atoms and the underlying mechanism of the nucleophilic substitution (one step S_N1 vs. two step/ S_N2) play a crucial role for the alkylation frequency of different base positions. The N7 position of guanine has a high nucleophilic reactivity and thus N7 methylguanine (7meG) is the major DNA lesion found in 60 – 80 % of all alkylations upon exposure to an S_N1 type alkylating drug like TMZ (**Figure 3**) [52]. Although 7meG has no mutagenic or cytotoxic effects on its own, it is susceptible to spontaneous depurination. The resulting apurinic site (AP) can inhibit DNA polymerases and is a source of mutations due to misincorporations during DNA replication [53,54]. The monofunctional S_N1 methylating chemotherapeutic drug TMZ, together with dacarbazine and procarbazine, belongs to the group of triazine compounds. Beside 7meG, these agents form N3 methyladenine (3meA) in about 10 – 20 % of the cases [55]. In contrast to 7meG, alkylations in N3 of adenine are highly cytotoxic, as most DNA polymerases cannot bypass this lesion which leads to sister chromatid exchanges, chromosome gaps/ breaks, and finally to S phase arrest [56]. The N1 position of adenine and the N3 position of guanine can also be alkylated by monofunctional agents, which leads to the formation of the mispairing and replication blocking lesions 1meA and 3meG, respectively [52,57]. However, in double stranded DNA, these positions are mainly protected from alkylation as consequence of the base pairing. These lesions are thus predominantly found in single stranded DNA [*ibid.*]. Despite being a rather rare product of S_N1 type alkylations (0.3 to 8 %), the methylation of the extracyclic oxygen of guanine (O^6 meG) accounts for the major mutagenic and cytotoxic effects of alkylating anti cancer drugs [58]. The mutagenic effect of O^6 meG is caused by its ability to mispair with thymine during DNA replication [59].

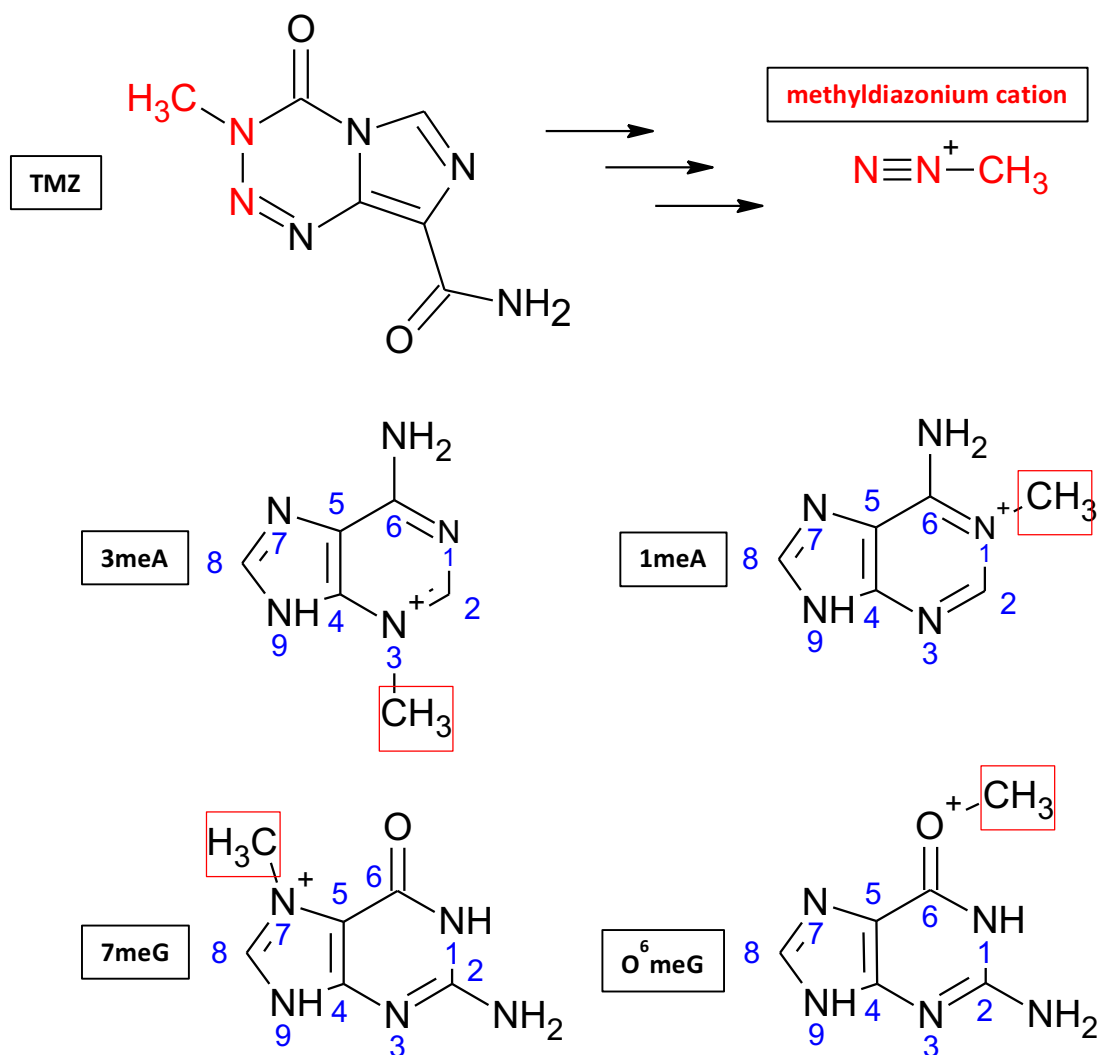


Figure 3: Formation of DNA base alkylations by TMZ. In aqueous solution, temozolomide is converted to its intermediates in a spontaneous and pH-dependent reaction, releasing a methyldiazonium cation. This cation can give rise to DNA base alkylations but also the methylation of RNA and protein. The most common DNA base methylation products are N7-methylguanine (7meG), N3-methyladenine (3meA), N1-methyladenine (1meA), and the most cytotoxic lesion caused by TMZ O⁶-methylguanine (O⁶meG).

Introduction

The resulting O⁶meG : T base pair gives rise to complicated subsequent repair processes (**Figure 4**). Once the mispairing lesion is recognized by the MUTS α heterodimer (MSH2 MSH6), MUTL α (PMS2 MSH1) is recruited and the mismatch repair (MMR) machinery causes a nick in the DNA, which serves as starting point for the resection of the strand opposing the O⁶meG by EXO1 [52]. As the problematic lesion (O⁶meG) persists in the DNA, a reinsertion of T is performed during the DNA synthesis step of the MMR. Thus, MMR is not able to correctly process the lesion, which culminates in several futile MMR cycles [60]. Gapped DNA is formed as a consequence of these futile cycles, which in turn give rise to DSBs during further replication. These DSB are the main cytotoxic event upon TMZ exposure, ultimately leading to apoptosis [58,61]. If not recognized by the repair machinery, O⁶meG : T would give rise to transition mutations after a second cycle of replication, which explains the tumor initiating properties of this base adduct and thereby the carcinogenicity of TMZ.

To circumvent the futile MMR cycles and to avoid mutations, the cellular defense against alkylation damage also provides a fast and direct damage reversal by alkyltransferases. In case of O⁶meG, the ubiquitously expressed protein MGMT transfers the methylgroup to a cysteine residue in its active site (Cys145) and thereby restores the damaged base [62]. The MGMT mediated repair is not limited to methyl groups alone but also can target O⁶ chloroethylguanine introduced by nitrosourea compounds like carmustine (BCNU) for example. The characteristic feature of this direct damage reversal is its stoichiometric nature. Upon accepting the alkyl group, MGMT is inactivated and is marked for proteasomal degradation by ubiquitination [63]. This mechanism implies that one MGMT protein can repair one damaged base only, and therefore MGMT often is referred to as “suicide enzyme”. N methylations of DNA bases are thought to be critical at higher doses and only if O⁶meG is repaired [64,65]. However, the repair of these lesions is not of minor importance. While the major methylation adduct 7meG is repaired via the multistep pathway of BER, 1meA, 3meC, 3meT, and 1meG are also repaired in a direct damage reversal by the α ketoglutarate dependent dioxygenases ALKBH2 and ALKBH3 in an oxidative dealkylation [52,66].

Beside the direct damage reversal and translesion synthesis [52], the DSB repair can additionally contribute to the tolerance of O⁶meG lesions. In contrast to the DNA damage induced by IR, there is strong evidence that DSBs originating from O⁶meG formation are mainly repaired

via HR [65,67]. HR thereby provides the ultimate survival mechanism in TMZ mediated genotoxicity. Thus, enhancement of DSB repair in cancer cells would provide an ideal mechanism to escape therapy induced apoptosis. As discussed later, Survivin has been reported to play a supportive role in the repair of IR induced DSBs via the non homologous end joining (NHEJ) (1.5.3). However, the exact nature of Survivin's participation is yet not well understood but is attributed to an interaction with different repair factors [68].

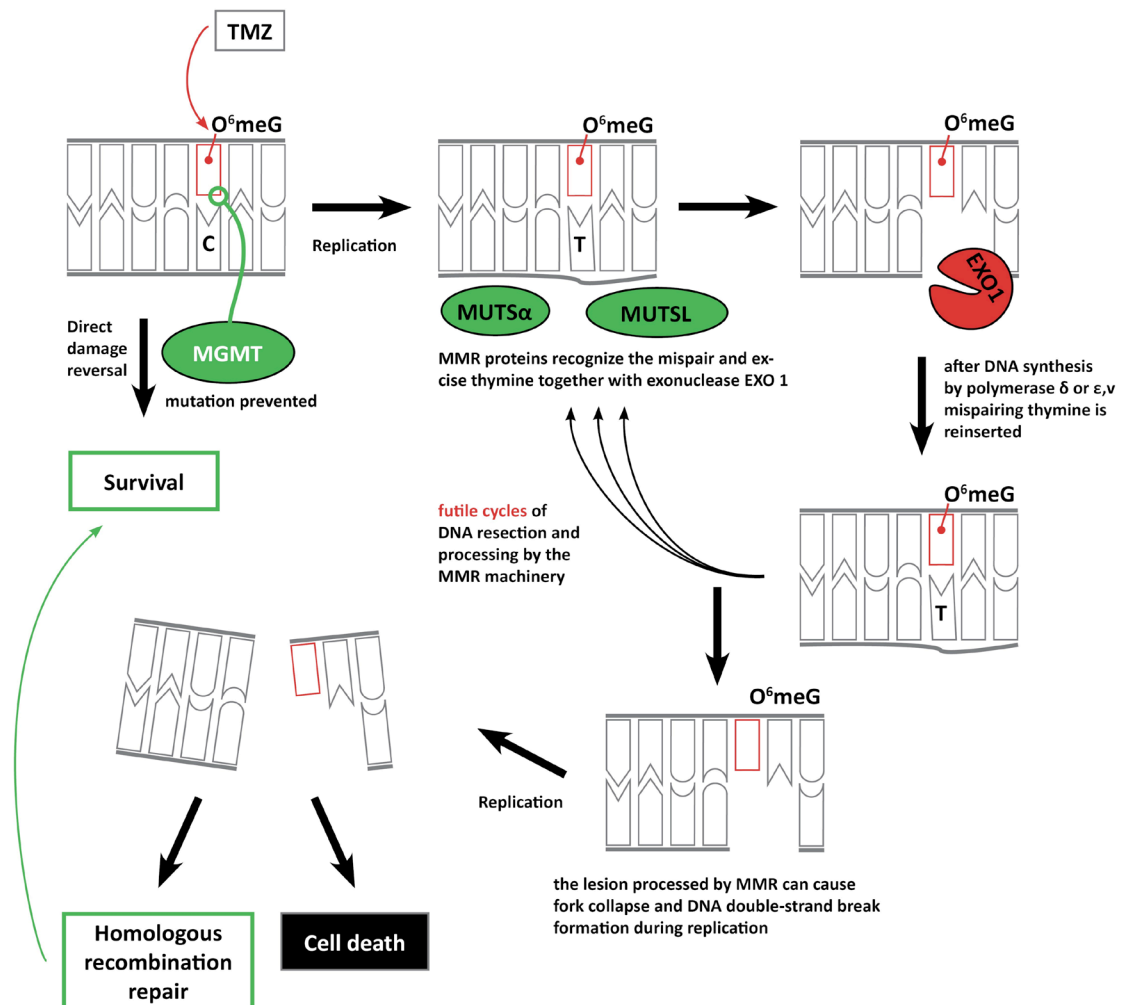


Figure 4: Mechanism of action of TMZ-induced cell death. Especially the base alkylations at the O^6 -position of guanine (O^6 meG) exhibit highly cytotoxic properties. If not repaired by MGMT, O^6 meG can mispair with thymine after one replication cycle. This mispair is recognized by the mismatch repair (MMR) complex MUTS α and MUTSL which introduce a nick in the strand bearing the mispairing lesion. After resection by the exonuclease EXO1, polymerase δ or ϵ can fill the gap. Since the O^6 meG lesion persists in the DNA, the polymerases reinsert thymine, which in turn is recognized by MMR. This leads to several futile MMR cycles, ultimately causing single-stranded DNA that can give rise to double-strand breaks (DSB) during replication. From here, either DNA repair by homologous recombination repair can help the cell to survive the DNA damage or unrepaired DSBs cause cell death.

Introduction

1.4.2 Repair of DNA damage induced by ionizing radiation

The cytotoxic effects of different types of radiation are utilized in the cancer treatment with IR. IR can hit and ionize the DNA directly and induce breaks in the sugar phosphate backbone or ionize water molecules in proximity to the DNA which then attack the DNA as highly nucleophilic hydroxyl radicals (OH•) [69]. Aqueous free radicals like ROS can be generated in the same manner but are of less importance for the induction of highly toxic DNA lesions [70,71]. Upon irradiation of 1 Gy (Gray; absorbed dose) approximately 3000 damaged bases, 1000 single strand breaks (SSBs) and 40 DSB can be found in one single cell [72]. This massive amount of DNA damage demands sophisticated repair techniques that ensure the genomic stability and thus survival. In the case of IR, these mechanisms involve pathways of the DNA DSB repair which are of utmost importance, as the processing of the highly toxic DSBs are of priority. In addition, base excision repair and SSB repair deal with less severe DNA lesions. The main repair pathway for dealing with IR induced DSB is the error prone NHEJ.

1.4.3 Repair of DNA double-strand breaks: HR vs. NHEJ

Depending on the nature of the arising DSB, different repair pathways become active due to a sophisticated DNA damage signaling. Beside NHEJ, a competing pathway for processing DSBs is provided by the HR. Similar to the process of genetic recombination during meiosis I, HR repair (HRR) can only be performed if (undamaged) sister chromatids are available. This limits the repair pathway to the S or G2 phase of the cell cycle, while NHEJ is active throughout the cell cycle but is favored during G1 or G0 [73]. The molecular decision making for the “selection” of either of these two major pathways is highly complex. In NHEJ, a heterodimer consisting of Ku70 and Ku80 binds to the free dsDNA end, thereby preventing 5' resection (the first step of HRR) and holding the DSB ends in proximity to each other (**Figure 5, B**) [74]. The NHEJ machinery ligates free double stranded DNA ends, irrespective of their initial origin. Thus, this repair process allows a very fast way to get rid of DSB and to ban the danger of a loss of genetic material. However, this goes at the cost of possible translocations and chromosomal rearrangements or di / acentric chromosomes [74]. In contrast, HR enzymes process DSB ends by generating 3' ssDNA overhangs, which are then immediately covered and thereby protected by replication protein A (RPA). The so processed DNA ends can then no longer be targeted by NHEJ.

1.4.3.1 From sensing DNA double strand breaks to pathway choice

Detection of DNA damage starts with the recognition of certain DNA lesions by damage sensors. These can trigger signal transduction processes which mediate the DNA damage checkpoint activation. The activated checkpoints prevent the progression through the cell cycle and allow the repair of DNA damage before it can become manifest in the genome. Thereby, checkpoints are the starting point of the complex signal transduction pathway of the DNA damage response (DDR). If the damage is not minimal, the checkpoint signaling is activated [75], initiating multi layered programs of decision making processes that determine whether a cell will survive (through DNA repair), initiate a program of permanent duplication arrest (senescence), or will undergo apoptosis [76]. The orchestration of the appropriate DNA repair pathway in the correct place and at the right time is also mediated by the checkpoint signaling. The DDR is initiated by the serine threonine protein kinases ATM, ATR, and DNA PK_{cs}, which belong to the phosphatidylinositol 3 kinase like protein kinase (PIKK) family. These proximal or initiating kinases associate with other factors and serve as damage sensors that recognize structural abnormalities of damaged DNA or chromatin and transduce the signal to distal transducer kinases like CHK1 and CHK2 [77]. These transducer kinases can block the transition from G1 to S phase (G1/ S checkpoint), slow down S phase (intra S checkpoint), or block entry into mitosis (G2/ M checkpoint) via inhibition of cyclin dependent kinases (CDKs) [78]. ATM (ataxia telangiectasia mutated) is a specific sensor of DSBs (occurring outside of the S phase) and phosphorylates hundreds of downstream substrates involved in the cell cycle checkpoint control, apoptosis induction, and DNA repair, including p53, H2AX, CHK2, and BRCA1 [77,79,80]. The identification of ATM as essential part of the DSB repair was possible by the analysis of a severe but rare genetic disorder affecting the *ATM* gene: Ataxia telangiectasia (AT). AT patients suffer from cerebellar degeneration, immunodeficiency, genome instability, clinical radiosensitivity, and most notably cancer predisposition [81]. These symptoms can be attributed to an impaired ability to cope with DNA DSBs due to a lack of functional ATM. Beside ATM, DSBs can also activate the DNA dependent protein kinase (DNA PK_{cs}) which in turn phosphorylates a own set of proteins involved in the NHEJ [80]. AT and Rad3 related protein (ATR) most commonly becomes activated by SSBs and thus responds to stalled replication or collapsed forks during the S phase [82]. However, also processed DNA lesions like resected DSB ends and ssDNA gaps can activate ATR. This leads to a complex but non redundant overlap between the ATM CHK2 and the ATR CHK1 pathway.

Introduction

1.4.3.2 The ATM CHK2 pathway

Initial sensing of free DSBs ends is not primarily performed by ATM itself. The proteins MRE11 (meiotic recombination 11 homolog), RAD50 (radiation sensitive 50 homolog), and NBS1 (Nijmegen breakage syndrome protein 1) form the MRN complex which quickly covers the free DNA ends of a DSB (**Figure 5, A1**). Then, ATM is recruited by Nbs1 [83] and phosphorylates Ser139 residues of the histone variant H2AX in proximity to the DNA break (**Figure 5, A2**). This posttranslational histone modification serves as recognition signal and leads to the recruitment of MDC1 (mediator of DNA damage checkpoint protein 1). The binding of MDC1 creates a positive feedback loop, as it recognizes autophosphorylated ATM and is recognized by the MRN complex itself. This enables the binding of further MRN complexes and ATM to the chromatin [84]. Providing the scaffold for this ATM/ MRN accumulation, MDC1 allows the amplification of the damage signaling in terms of a phosphorylation of H2AX along larger chromosomal regions flanking the DSB site (**Figure 5, A3**). Due to this accumulation of phospho H2AX, also called γ H2AX, DSBs can be visualized by immunofluorescent methods as distinct foci by γ H2AX staining. Upon phosphorylation by ATM, MDC1 can recruit the E3 ubiquitin (Ub) ligase RNF8 (RING finger protein 8) which then catalyzes the ubiquitination of histones near the break site (**Figure 5, A4**) [85]. This non proteolytic chromatin ubiquitination is thought to provide docking sites for the association of further signaling and repair factors [78]. After the recruitment of additional E3 ligases this process is even extended leading to the accumulation of repair factors like BRCA1 BARD1 (BRCA1 associated RING domain 1) and 53BP1 (p53 binding protein 1) [84,86]. In association with CtIP (CtBP interacting protein), BRCA1 BARD1 drives the end resection via the MRN complex [78] which paves the way for the start of the HRR. The decision between HRR and NHEJ can be re directed at several stages. The end resection is mainly impeded by the tight binding of the hetero dimer Ku70 Ku80 (**Figure 5, B**) under conditions when CDK activity is low, i.e. in G1 [87]. Furthermore, the ATM dependent phosphorylation of 53BP1 leads to its interaction with RIF1 (Rap1 interacting factor 1 homolog) (**Figure 5, A5b**). Especially in G1, both factors antagonize the initiation of the end resection by BRCA1 and CtIP, thereby favoring NHEJ [88]. Upon the entry into the S phase, CtIP gets phosphorylated by CDK2 which promotes its interaction with BRCA1 BARD1. The complex is then recruited to the Ub docking sites next to the DNA break, in turn antagonizing the attachment of 53BP1 RIF1 [89]. Importantly, this CDK dependent phosphorylation of CtIP in the S phase ensures the preference of HRR over the error prone NHEJ.

1.4.3.3 Homologous recombination repair of DNA double strand breaks

In the presence of phosphorylated CtIP, MRE11 introduces a nick into the 5' terminated DNA strand about 15 – 20 nucleotides away from the break (**Figure 5**, A6) [90]. Due to its 5' 3' exonuclease activity, the MRN complex can then degrade the nicked strand towards the DSB which generates a short overhang of the 3' terminated strand (7) [90,91]. Longer 5' to 3' resection is then taken over by EXO1 (8) [87]. The so generated 3' overhang is quickly covered by hetero trimeric RPA complexes which is subsequently displaced by the central recombinase RAD51 to form a nucleoprotein filament capable of strand invasion. To facilitate the homology search and the invasion into sister chromatid, additional factors localize to the nucleoprotein filament. Mediated by the interaction with BRCA1, PALB2 (partner and localizer of BRCA2) recruits BRCA2 to the damaged site [92]. Via its binding sites BRCA2 can deliver the recombinase RAD51, thereby assisting the filament formation, and stabilizing the repair structure [78]. This process is further stimulated by the remodeling of the RAD51 filaments by its paralogs RAD51B, RAD51C, RAD51D, XRCC2, and XRCC3 [93]. In its search for a homologous sequence, the filament invades the donor duplex for base pairing, forming the characteristic displacement loop (D loop). The synthesis of new DNA at the 3' end of the invading strand is initiated by the translesion DNA polymerase η and ν [94,95]. Depending on which free end of the damaged DNA duplex is primed for DNA synthesis, different possible outcomes can arise from this point (**Figure 5**, A11). First: after strand invasion, the newly synthesized strand is reannealed to the second end of the break, thereby leaving the donor DNA unaffected and generating non crossover products [96]. This outcome is referred to as synthesis dependent strand annealing (SDSA). Second: the alternative 3' priming of the second break end causes the formation of a more complex DNA structure with both duplexes being covalently linked and twisted with each other [*ibid.*]. These so called Holliday junctions (HJ) are then resolved by the endonucleases GEN1, MUS81/ EME1, or SLX1/ SLX4 to generate either crossover or non crossover DNA duplexes [97 100]. The enhancement of the cellular DNA repair capacity provides a survival advantage for cancer cells during anti cancer treatment. For TMZ based CT, the expression of MGMT provides such a mechanism [66]. Additionally, proteins facilitating HRR would also render the tumor cells less susceptible to TMZ induced apoptosis as illustrated in **Figure 4**. A protein that is being discussed to play an important role during DSB repair is Survivin. However, whether Survivin also participates in HRR is not known.

Introduction

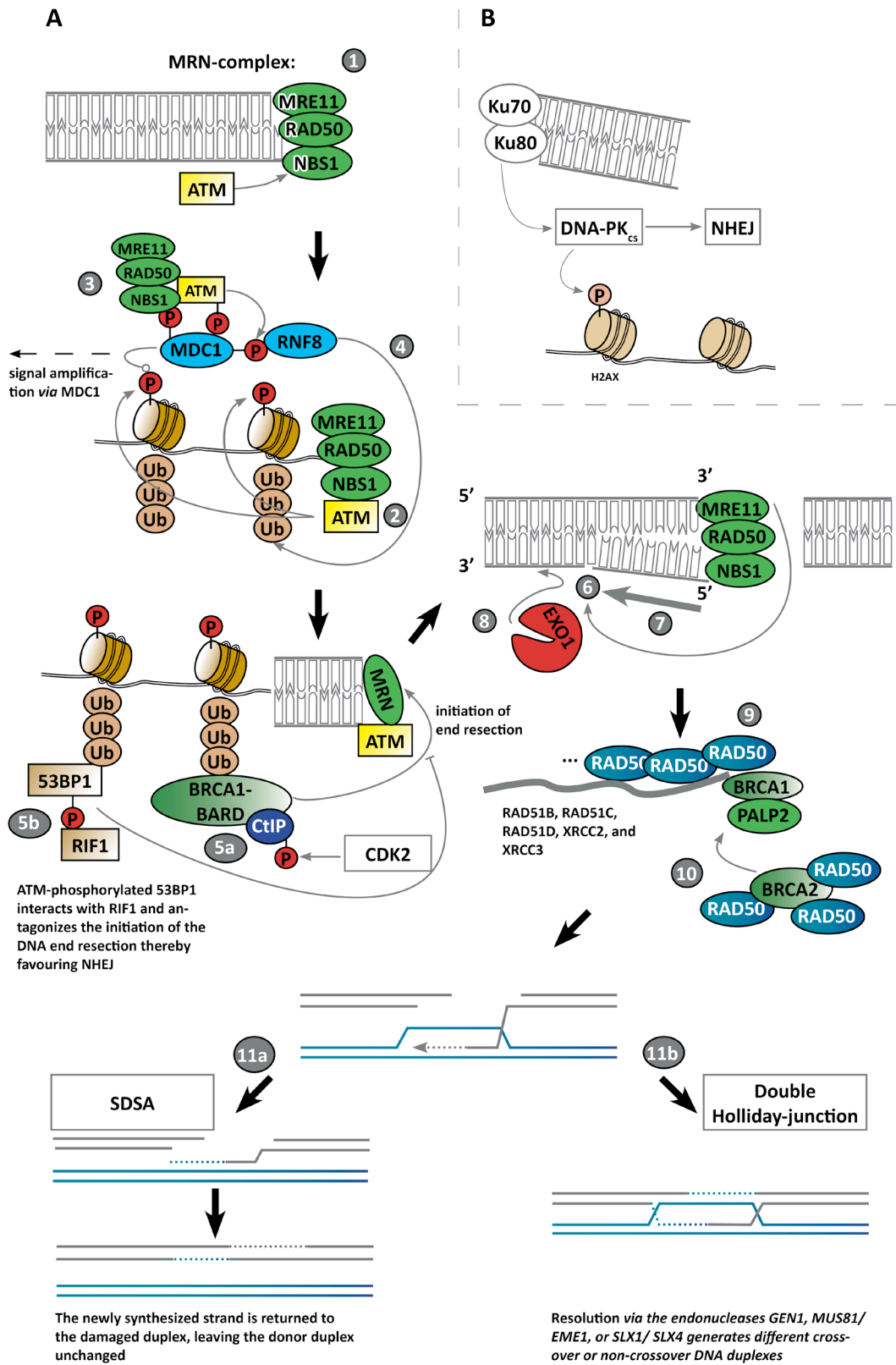


Figure 5: ATM-mediated DNA damage response and the homologous recombination repair of DNA double-strand breaks. 1) The proteins MRE11, RAD50, and NBS1 form the MRN-complex which quickly covers the free DNA ends of a DSB. 2) ATM is recruited by Nbs1 and phosphorylates Ser139 residues of the histone variant H2AX in proximity to the DNA break. 3) MDC1 is recruited and serves as binding site for additional MRN-complexes/ ATM, which creates a positive feedback loop by further phosphorylation of H2AX. 4) MDC1 recruits E3 Ub-ligase RNF8 which carries out a non-proteolytic chromatin ubiquitination on histones adjacent to the DSB site. The Ub-signal serves as docking site for the repair factors (5a) BRCA1-BARD1, and the (5b) end-protecting factor 53BP1. 6) In association with CtIP (CtBP-interacting protein) BRCA1-BARD1 drives the end-resection via the MRN-complex by introducing a nick in the 5'-terminated strand. 7) The nicked strand is degraded by the 5'-3'-exonuclease activity of the MRN-complex. 8) Further end-resection is accomplished by EXO1 which marks the beginning of the HRR. 9) The ssDNA is quickly covered by RPA (not shown) which is then subsequently displaced by the central recombinase RAD51 to form a nucleo-protein filament capable of strand invasion. Filament formation and stabilization is further aided by the association with BRCA2 the RAD51 paralogs RAD51B, RAD51C, RAD51D, XRCC2, and XRCC3. 10) In its search for a homologous sequence, the filament invades the donor duplex for base pairing, forming the characteristic displacement-loop (D-loop). The homologous strand is then used as template for DNA synthesis. 11a) The newly synthesized strand can be reannealed to the second end of the break, thereby leaving the donor DNA unaffected and generating non-crossover products (synthesis-dependent strand annealing (SDSA)). 11b) Alternatively, 3'-priming of the second break end causes the formation of Holliday-junctions (HJ) with both duplexes being covalently linked and twisted with each other. The resolution of these structures requires the activity of different endonucleases.

1.5 The anti-apoptotic protein Survivin is selectively expressed in tumor cells

One of the most tumor specifically expressed genes is *BIRC5* which encodes for the Survivin protein. The transcription of *BIRC5* gives rise to the expression of four alternative splice variants (Δ Ex3, 2B, 3B, and 2 α) all of which play different roles alongside Survivin and have a different subcellular localization [101,102]. While almost undetectable in normal differentiated adult tissues, Survivin is expressed in embryonic/ fetal tissues and is found in virtually every human tumor [103 105]. Because of this sharp differential expression in tumors and its involvement in multiple tumor pathways, the protein has been subject of intensive research, aiming for cancer specific targeting strategies [106 110].

1.5.1 Apoptosis: the programmed cell death

Conventional RT and CT aim at the induction of cell death to fight tumor growth or eliminate remaining tumor cells after surgery. Targeting the tumor tissue selectively is mostly an unrealistic notion. Since normal tissues are affected in almost all therapy approaches as well, unwanted side effects, e.g. apoptosis induction, often limit the treatment schemes. However, recent advances in high precision radiation therapy, for instance, have minimized the side effects on healthy tissues and thereby allowed to increase the dose that can be directed at the tumor cells. IR and chemotherapeutic drugs damage the DNA. If the damage cannot be repaired adequately, a coordinated cellular death protocol is induced. The main pathway of programmed cell death is apoptosis. The Greek term “apoptosis” (ἀπόπτωσης) was shaped by Kerr, Wyllie, and Currie in 1972 and illustrates “falling off” of petals from flowers or leaves from trees in autumn [111]. For multicellular organisms, apoptosis is a key mechanism in eliminating dangerous mutations and thus prevents malignant transformation of cells, which otherwise might ultimately lead to tumor formation. Apoptosis also contributes to tissue homeostasis and is important for developing organs and digits during ontogenesis [111]. Decades after its first detailed morphologic description, the process of apoptosis has turned out to comprise a plethora of different signaling cascades to perform a genetic program of cellular suicide.

Apoptosis is driven by a family of cysteine **aspartyl** specific proteases (caspases) that cleave peptide bonds C terminal to aspartic acid residues [112]. Caspases exist as inactive zymogens/ pro caspases within a cell and are activated by proteolytic cleavage themselves [113].

Two major pathways for initiating apoptosis can be distinguished: the extrinsic and the intrinsic one. Although the initiating caspases of both pathways are different, both ways converge at later stages and lead to the activation of the same effector caspases. Excessive DNA damage (and other stimuli) leads to changes in the mitochondrial transmembrane potential, which in turn alters the membrane permeability. Upon these changes, proteins, most notably cytochrome c (cyt c) and SMAC [106], are released from the mitochondrial intermembrane space into the cytoplasm. Cyt c then binds to the apoptotic protease activating factor 1 (APAF1) to form a multimeric complex, named apoptosome, which favors the recruitment and the proteolytic activation of pro caspase 9 [114,115]. The activation of caspase 9 leads to the subsequent activation of proteolytic cascades via the activation of the executioner/ effector caspases 3, 6, and 7 [116]. Intracellularly, these proteases cleave various substrates and activate other proteases that degrade nuclear or cytoskeletal proteins [*ibid.*]. Most importantly, caspase 3 promotes the degradation of chromosomal DNA by the activation of the endonuclease CAD (caspase activated DNase) [117]. This leads to a characteristic internucleosomal DNA fragmentation into ~180 bp fragments, thus putting the final nail into the cellular coffin.

Crucial for the cellular “decision” between life and death in this pathway is the influence of regulatory proteins. At the mitochondrial level, members of the BCL2 family tightly regulate the mitochondrial transmembrane potential. The 20 mammalian members of the BCL2 family exhibit at least one conserved BCL2 homology (BH) domain [118]. The complex balance between opposing pro and anti apoptotic factors determines the release of mitochondrial proteins into the cytoplasm and thus controls the cellular fate. These factors either increase (BAX, BAD, BAK, BIM, NOXA, PUMA ...) or decrease (BCL2, BCL X_L, BCL w ...) mitochondrial permeability [105,119]. While BCL2 mediated regulation of apoptosis induction resides rather upstream in the apoptotic cell death, the second group of regulatory proteins comes into play after caspase activation: the family of inhibitor of apoptosis proteins (IAPs). The ability to evade cellular suicide is a key step during tumorigenesis and is essential for malignant transformation, as the tumor cells usually have to overcome multiple stressors like hypoxia or nutrient deprivation [120,121]. Thus, the upregulation of IAP expression, in particular, Survivin and XIAP, provides a perfect survival strategy for tumor cells. Furthermore, the overexpression of IAPs is a major cause of therapy failure, as cancer therapies mainly aim at the induction of apoptosis in proliferative tumor cells. Ironically, these therapies can lead to the selection of cell clones with strong IAP expression which then causes the inexorable relapse of the tumor.

1.5.2 IAPs: Apoptosis and beyond

IAPs were first described in baculoviruses over two decades ago [122,123]. Here, the genes *cpIAP* and *OpIAP* encode for proteins that are able to interfere with apoptosis in insect host cells after viral infection. Preventing the host cell from undergoing apoptosis allows the virus to complete its replication cycle. A common characteristic feature of IAPs was identified: the occurrence of a zinc finger like protein domain called baculovirus IAP repeat (BIR) [124]. This domain promotes important protein protein interactions with different IAP targets. Following this discovery, IAP homologues were also identified in yeast, nematodes, flies, and higher vertebrates [125]. In mammals, the evolutionary conserved BIR domain consists of ~70 amino acids, coordinating a zinc atom via histidine and cysteine residues [*ibid.*]. Eight members of the IAP family are known in humans, containing one to three BIRs: NAIP, cIAP1, cIAP2, XIAP, Survivin, BRUCE/ Apollon, Livin, and Ts IAP (genes: *BIRC 1 – 8*) [126]. Survivin was discovered in 1997, containing only one BIR domain, while other IAP specific protein features are missing [103]. These can include a carboxyl terminal RING domain (Really Interesting New Gene) that functions as E3 ubiquitin ligase and CARDs (caspase recruitment domains) of less clear function [127]. The X linked inhibitor of apoptosis protein (XIAP) is encoded by the *BIRC4* gene and contains three BIR domains. In addition, XIAP contains the aforementioned carboxyl terminal RING domain, capable of self ubiquitination and ubiquitination of associated proteins [125]. The RING domain thereby controls the stability of XIAP itself and mediates the proteasomal degradation of bound proteins (e.g. caspase 3) [128]. Furthermore, a conserved ubiquitin associated (UBA) domain for recognizing highly polymerized ubiquitin chains is located between BIR 3 and the RING domain [129]. XIAP unfolds its anti apoptotic properties by binding directly to initiator caspase 9 and the effector caspases 3 and 7 and suppressing their enzymatic activity [130,131]. The binding of caspase 3 and 7 occurs at the linker region between BIR 1 and BIR 2 [132,133], while caspase 9 inhibition is achieved by a critical hydrophobic pocket in the BIR 3 surface [132]. Here, two important mitochondrial proteins (encoded in the nucleus) come into play as pro apoptotic factors: SMAC/ DIABLO (second mitochondria derived activator of caspases/ direct IAP binding protein with low pI) and Omi/ HtrA2. Due to sequence homologies with the N terminus of the active caspase 9 APAF1 holoenzyme, SMAC and Omi can bind to the BIR 3 of XIAP, thereby neutralizing the caspase's inhibition [134]. In the case of the protease Omi/ HtrA2, the proteolytic cleavage of XIAP is part of this negative regulation [135]. Beyond its anti apoptotic role, XIAP also participates in different signaling pathways reviewed

by Lewis *et al.* [136]. Most prominently, XIAP stimulates NF KB and MAP kinase activation by TAB1 (MAP3K7IP1) recruitment and TAK1 (MAP3K7) activation via the BIR 1 and thus is involved in developmental processes [137]. Due to its role in these pro survival pathways and its ability to prevent apoptosis, XIAP is tightly interlaced with the malignant progression, and thus is often found to be overexpressed in tumors. A study of a panel of 60 cancer cell lines by Tamm *et al.* revealed a variable but wide protein expression in different tumor entities [138]. Paradoxically, the overexpression of XIAP correlated with an increased sensitivity to cytarabine, cycloctidine, and other cytostatic drugs and could mechanistically not be explained by the authors [*ibid.*]. Furthermore, the impact of high vs. low expression levels of XIAP is controversially discussed in the literature. While no prognostic value of XIAP expression for prognosis and response to chemotherapy was found in patients with advanced stages of Non Small Cell Lung Cancer (NSCLC) [139], a high XIAP level was predictive for a lower risk of tumor recurrence in prostate cancer [140]. However, there is also evidence that higher levels of XIAP correlate with a shorter overall survival OS and metastasis in esophageal squamous cell carcinoma (ESCC) [141] and a poor differentiation (higher stage), shorter median survival [142], and shorter postoperative disease specific survival in renal cell carcinoma (RCC) [143]. In head and neck squamous cell carcinoma (HNSCC), high levels of XIAP are associated with cisplatin resistance and a poor clinical outcome [144]. Also, AML patients showing low XIAP levels benefited in terms of an improved OS [145]. Taken together, the discrepancies, regarding the prognostic impact of XIAP expression in different cancer entities illustrate that XIAP either plays pivotal roles in different tissues, or that methods for categorizing as “high” or “low” are not well standardized. In both cases, a therapeutic targeting of XIAP might be considered with caution.

1.5.3 Survivin: a versatile protein with distinct functions and subcellular localization

Among the IAPs, Survivin has an exceptional role as being the smallest member (16.5 kDa) of this family with one BIR domain only. The human *Survivin* gene (*BIRC5*) is located at the end of chromosome 17 (17q25) with a TATA less promoter, containing two critical SP1 sites, essential for basal transcription [146]. Canonical CDE/ CHR boxes guide the sharp cell cycle dependent expression, which peaks in the G2/ M phase [147]. Interestingly, this cell cycle dependent transcriptional control is largely lost in most cancer cells [148]. A canonical CpG island can be found in the promoter region of *BIRC5*. However, it was described to be unmethylated

Introduction

in both neoplastic and normal tissue [146]. Furthermore, the CpG methylation in the exon 1 was linked to a reduced expression of Survivin in ovarian cancer [149]. Strikingly, the CpGs analyzed were unmethylated in ovarian cancer but methylated in non cancerous ovarian tissues [*ibid.*]. Other reports show no association with survival/ carcinogenesis in AML, as the promoter region analyzed by MSP was unmethylated in all samples of AML patients and healthy peripheral blood mononuclear cells [150]. As convincing data speaking in favor of an epigenetic regulation of *BIRC5* in cancers are missing [151,152], the impact of Survivin promoter methylation remains controversial. In astrocytomas, *BIRC5* was among the genes showing a uniformly unmethylated pattern [153]. Interestingly, Nabils *et al.* were able to show an increased Survivin expression (instead of a gene silencing) in hypermethylated endometrial tumors [154]. Since p53 is a transcriptional suppressor of Survivin [155], an impaired binding upon methylation of the binding sites in the *BIRC5* promoter was found [154]. Thus, the opposed effects of *BIRC5* methylation strongly depend on the exact promoter region analyzed.

Survivin is a very versatile protein involved in diverse cellular networks. Its functions are reaching far beyond being a “simple” anti apoptotic protein. Nuclear Survivin **(1)** plays a role as essential member of the chromosomal passenger complex (CPC). Survivin associates with Aurora B, INCENP, Borealin and ensures the proper cell division (**Figure 6**). The hetero tetrameric CPC orchestrates the correct chromatid segregation and is thereby crucial for maintaining genomic stability [reviewed in 156]. **(2)** A newly described and not yet fully explored role of nuclear Survivin is its putative participation in DNA repair pathways. DNA repair is important for preventing cancer formation but also serves as resistance mechanism in tumors to evade radio and chemotherapy induced cell death. Upon IR, Survivin was shown to facilitate the repair of DSBs by stimulating DNA repair via the pathway of the NHEJ in brain tumor and CRC cells [68,157]. This repair enhancing effect was also shown to coincide with a nuclear accumulation of Survivin after IR and co localization with MDC1, γ H2AX, 53BP1, and DNA PK_{cs}. siRNA mediated downregulation of Survivin caused a reduced activity of the DNA PK_{cs}, leading to an increased amount of γ H2AX foci and apoptosis [*ibid.*]. Interestingly, the interaction with factors of the DSB repair machinery was also confirmed in colorectal cancer (CRC) cells after irradiation [157]. In line with the findings of Reichert *et al.*, a reduced DNA PK_{cs} activity was measured after Survivin knockdown [68]. **(3)** The view on Survivin as inhibitor of apoptosis has changed much since its discovery in 1997. First being described as inhibitor of caspases, Survivin was supposed to unfold its anti apoptotic properties by direct inhibition of caspase 3/7

in vitro [158]. However, further research demonstrated that a binding of Survivin to caspases does not occur under physiological conditions. Instead, it associates with XIAP and thereby increases its stability against polyubiquitination and proteasomal degradation [159]. This leads to a synergistic, indirect inhibition of the caspases 3, 7, and 9 by Survivin [159,160], as XIAP is the only mammalian IAP capable of binding and inhibiting caspases [108,125]. Adding another layer of complexity to this, a subcellular mitochondrial pool of Survivin was shown to be able to sequester the pro apoptotic XIAP antagonist SMAC away from XIAP [161] or to prevent SMAC release during the intrinsic pathway of apoptosis [162]. Besides, cytosolic Survivin also participates in the cellular stress response as interaction partner of different chaperones like HSP90 [163].

The diverse roles of Survivin strongly depend on its intracellular localization and therefore on a tightly regulated intracellular transport. Due to its small size (16.5 kDa), Survivin can enter different cellular compartments by diffusion [164], while a nuclear localization signal (NLS) for an active import is missing [165,166]. However, an active nuclear export was shown to be involved in the regulation of Survivin's subcellular localization [166]. The leucine rich nuclear export signal (NES) in the Survivin protein serves as recognition site for the export receptor CRM1 (chromosomal region maintenance 1), also known as Exportin 1 (XPO1) [167]. To allow proteins to pass the nuclear membrane, structures that facilitate this transport are embedded in the nuclear envelope. These nuclear pore complexes (NPCs) permit the diffusion of proteins of up to 40 – 65 kDa, while larger proteins are transported in association with specific transport receptors [168]. Transport receptors like CRM1 mainly belong to the karyopherin β family of proteins [169]. Not only the transport of large proteins involves these mechanisms, but also active transport processes require this export machinery. Including Survivin, CRM1 actively shuttles NES bearing proteins out of the nucleus in a RanGTP dependent manner [170]. RanGTP is a small GTPase molecule (25 kDa) present in high concentrations in the nucleus [168]. The RanGTP concentration gradient is thought to provide the energy for the active export process [171]. In complex with the transport receptor (CRM1) and the NES bearing cargo protein, RanGTP enhances the binding affinity of the interaction partners and promotes the export by facilitated diffusion [172]. After the transition to the cytoplasm, RanGTP is hydrolyzed by a RanGTPase, and the transport complex dissociates, releasing the cargo protein into the cytoplasm [168] (**Figure 6**).

Introduction

The NES of Survivin was found to be located between the amino acids 89 – 98, containing two leucine residues being essential for the recognition process [167]. This NES has been shown not only to be indispensable for the nucleo cytoplasmic shuttling of Survivin but also is essential for tethering the CPC to the centromere [166]. The authors could show that CRM1 inhibition by leptomycin B (LMB) or the loss of function mutations in the NES prevent the centromeric targeting of Survivin, leading to mitotic defects and multinucleate cells. This was caused by an impaired CRM1 Survivin interaction rather than blocking Survivin's ability to dimerize with CPC proteins. Furthermore, the predominant cytoplasmic localization of Survivin was changed upon LMB treatment or NES mutation, causing an equal distribution between both compartments. HeLa cells expressing a NES deficient (L98A) Survivin mutant were sensitized to IR and showed an increased activation of caspase 3 upon TRAIL treatment [173]. Thus, the mutation of the NES abrogates the cytoprotective effect of Survivin. Beside this important nucleo cytoplasmic shuttling, wt Survivin also translocates into mitochondria (see above). Upon apoptotic stimuli like DNA damage, this mitochondrial Survivin pool can rapidly be released into the cytosol to block apoptosis and was shown to be linked to tumorigenesis [174]. This means that Survivin is released from the mitochondrial intermembrane space alongside death amplifiers like cyt c, during intrinsic induction apoptosis (**Figure 6**, 3a). This release was shown to be dependent on the activation of CHK2, since CHK2 targeting caused an increased DNA damage induced apoptosis due to an impaired release of Survivin from the mitochondria [175]. However, the exact molecular mechanism underlying the anti apoptotic role of mitochondrial Survivin remains controversial. As mentioned above, some reports attribute the anti apoptotic properties of mitochondrial Survivin to its ability to bind to and prevent the release of SMAC [161,162], thus, causing an abrogation of the XIAP inhibition via SMAC and increasing caspase inhibition. Undoubtedly, mitochondrial Survivin contributes to the anti apoptotic survival signaling during DNA damage induced apoptosis.

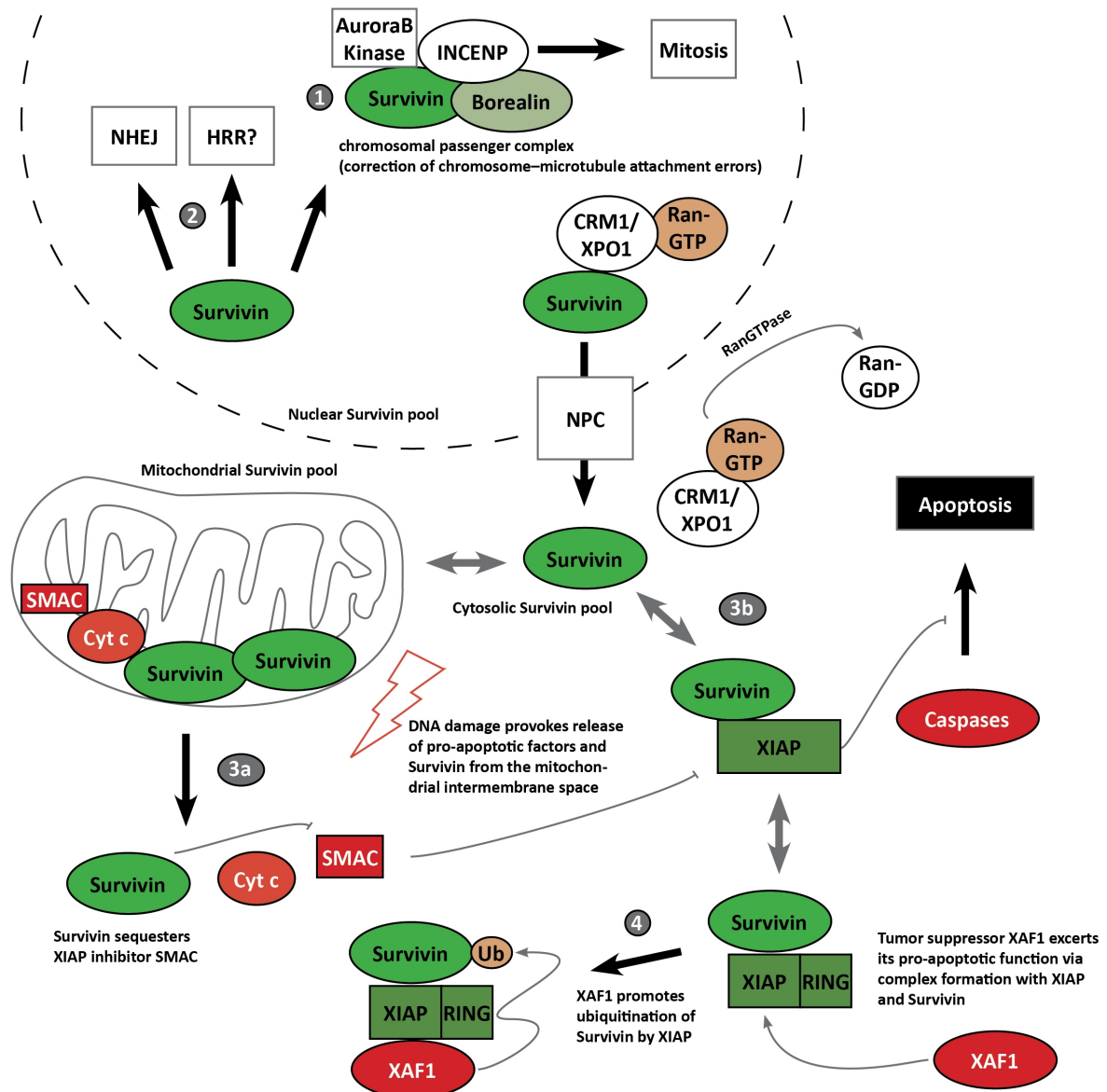


Figure 6: Different cellular localizations and functions of Survivin. The 16.5 kDa Survivin protein may enter different cellular compartments by passive diffusion, whereas no nuclear localization signal is contained within the protein's structure. Nuclear Survivin **1)** plays an essential role as member of the chromosomal passenger complex (CPC) in the chromatid segregation during mitosis. **2)** Furthermore, links to DNA repair processes have been described. After IR-induced DNA damage, Survivin was shown to facilitate DNA repair by NHEJ. A putative role of Survivin in the homologous recombination repair (HRR) is investigated in this work. Upon recognition of the leucine-rich nuclear export sequence (NES), the export receptor CRM1/XPO1 actively shuttles Survivin out of the nucleus via the nuclear pore complex (NPC). This active transport also involves a nuclear-cytosolic RanGTP gradient. Once in the cytoplasm, Survivin can also localize to mitochondria **3a)** where it is released upon DNA damage alongside pro-apoptotic factors like cyt c and SMAC. A sequestration of the XIAP-inhibitor SMAC might also contribute to Survivin's anti-apoptotic functions. **3b)** Cytosolic Survivin associates with XIAP, protecting it from polyubiquitination and proteasomal degradation, thereby facilitating caspase inhibition. **4)** Upon formation of a trimeric complex, the tumor-suppressor XAF1 counteracts this process by promoting Survivin's ubiquitination via the RING domain of XIAP (see 1.5.4).

1.5.4 Inhibiting IAPs – Tumor suppressor XAF1 counteracts XIAP and Survivin

Complex regulatory pathways like the interaction of BCL 2 proteins at the mitochondrial membrane balance the cellular decision between apoptosis and survival. IAPs tilt this balance towards survival by interfering with the executing proteins of apoptosis – the caspases. Targeting IAPs by intrinsic regulators in turn provides an ideal point of attack for pro apoptotic factors. The mitochondrial XIAP inhibitors SMAC and Omi are described for their pro apoptotic functions (see 1.5.2). With XIAP being a central protein in the inhibition of apoptosis, the regulation of this protein is crucial. XIAP associated factor 1 (XAF1) was shown to antagonize XIAP mediated caspase inhibition and interestingly to be expressed at low levels in cancer cell lines compared to normal human liver tissue [176]. XAF1 is a nuclear protein and was shown to cause the sequestration of XIAP to the nucleus and reversed its cyto protective effects [177]. On the contrary, adenoviral knockdown of XAF1 did enhance the resistance to apoptosis. Later studies revealed that the pro apoptotic role of XAF1 could not only be attributed to caspase dependent mechanisms. Interestingly, the overexpression of XAF1 leads to a down regulation of Survivin despite no direct interaction between these two proteins [178]. The Survivin expression was restored in the presence of a proteasome inhibitor (MG132) or an XIAP RING mutant (defective in its E3 ubiquitin ligase activity), pointing to an XAF1 induced proteasomal degradation of Survivin in the trimeric complex (**Figure 6**, 4). These findings support the importance of XAF1 as a tumor suppressor, since it simultaneously targets two important survival factors frequently overexpressed in cancer. Thus, a loss of XAF1 might be a common event during cancer development. Hereby, the epigenetic silencing via promoter methylation seems to play a crucial role in *XAF1* inactivation. In a large study on 123 gastric adenocarcinomas, normal gastric tissues, and 15 gastric cancer cell lines, a tumor specific downregulation of XAF1 was found to be strongly correlated to a higher tumor stage and grade [179]. Nearly all gastric tumors with abnormal *XAF1* expression (18 out of 20) showed an aberrant CpG methylation in *XAF1* promoter. In contrast, no methylation of these CpG sites was found in tumors with normal expression and normal tissues, respectively. To detect aberrant methylation patterns, two fragments of the *XAF1* promoter were analyzed by bisulfite DNA sequencing ranging from 1831 to 23 bp upstream of the transcription start site, covering 34 CpGs. Especially seven CpGs in the region proximal to the transcription start (23 to 234 bp) were found to be tightly linked to mRNA expression of *XAF1*. Additionally, *XAF1* expression

could be reactivated by treatment with 5-aza-2'-deoxycytidine (decitabine) in four non-expressing cell lines. The regulatory importance of this promoter region was also confirmed by Zou *et al.*, who link the major impact on transcriptional inactivation of the *XAF1* promoter to two CpG dinucleotides proximal (14 to 109 bp) to the transcription start [180]. In urogenital tumors and cancer cell lines, the methylation of the promoter region ranging from 23 to 692, containing 14 CpG sites, could also be linked to a reduced mRNA expression [181]. Recently, it was shown that methylation-associated silencing of the *XAF1* promoter is caused by the loss of the binding of the gene regulator CTCF which normally promotes the open chromatin configuration of the *XAF1* promoter [182].

Due to the pro-apoptotic mode of action of *XAF1*, the restoration of its expression in tumors might be an interesting therapy approach. Indeed, it was shown that tumor growth and angiogenesis is inhibited in HCC xenografts in mice upon expression of *XAF1* [183]. Furthermore, a high *XAF1* expression was shown to be prognostic for the OS of pancreatic cancer patients [184]. Here, an abnormal (low) *XAF1* level was also linked to advanced tumor stage and higher grade of bladder and kidney malignancies. However, convincing clinical studies clarifying the implications of *XAF1* expression are rare, and data elucidating the predictive or prognostic potential of *XAF1* methylation are still missing.

1.6 Aims

This work deals with the role of inhibitor of apoptosis proteins (IAPs) and IAP related proteins in the resistance of high grade glioma cells to anti cancer therapies. In the focus of this research is the role of the expression of the IAP Survivin (*BIRC5*) in the survival, the induction of apoptosis, and senescence upon DNA damage caused by the alkylating anti cancer drug temozolomide. **1)** To allow the molecular analysis of Survivin's expression and localization in these experimental approaches, a glioblastoma cell model should be established first. The aim was to generate a cell system with overexpression of a Survivin GFP fusion protein and a Survivin GFP variant with mutated nuclear export sequence. The GFP tag should serve for the analysis of changes of the intracellular localization of the protein upon DNA damage by live cell microscopy. **2)** Particularly, the influence of Survivin's subcellular localization on these endpoints should be addressed by colony formation assay, flow cytometric analysis of apoptosis/necrosis induction, and senescence associated β galactosidase staining. **3)** One main objective of this work is to elucidate the involvement of the IAP Survivin in non homologous end joining and homologous recombination repair of TMZ induced DNA double strand breaks by means of radioactive DNA PK activity assay and qPCR based HR activity assay, respectively. The amount of DNA damage should be quantified by immunofluorescence staining of γ H2AX and visualization by confocal laser scanning microscopy.

In search of better classification possibilities and molecular targets of anticancer therapy, the second part of this project aimed at the evaluation of Survivin and the IAP antagonist XAF1 as putative biomarkers in high grade gliomas. **4)** First, the epigenetic regulation of *BIRC5* and *XAF1* should be addressed by methylation specific PCR in glioma cell lines, and then a high throughput method for methylation analysis should be established, being suitable for analyzing DNA methylation in formalin fixed and paraffin embedded samples. **5)** The epigenetic regulation of both factors should then be analyzed in a cohort of 80 high grade glioma patients. The promoter silencing of either factor should be investigated for an association with clinical parameters including overall survival, progression free survival, age, and tumor grade.

2 Material & Methods

2.1 Lists

Consumable	Manufacturer
Amersham ECL Western Blotting Reagent (Detection Reagent 1 + 2)	GE Healthcare Europe GmbH, Freiburg, Germany
Amersham Hyperfilm ECL	GE Healthcare Europe GmbH, Freiburg, Germany
Aqua ad iniectionabilia (aliquoted for PCR and DNA storage)	B. Braun Melsungen AG, Melsungen
Cell culture flask 5 ml/ 10 ml	Nunc A/S Kamstrupvej, Denmark
Cell culture microscope: Zeiss Axiovert 40C	Carl Zeiss GmbH, Oberkochen, Germany
Cell culture work bench: HeraSafe	Heraeus GmbH, Hanau
Cellstar cell culture plates: 96-, 24-, 6-well; 35 mm, 60 mm, 100 mm	Greiner Bio-One GmbH, Frickenhausen
Cover slips H875 0.13 - 0.16 mm	Carl Roth GmbH + Co. KG, Karlsruhe
Cryo vials, Cryo.s	Greiner Bio-One GmbH, Frickenhausen
Film: Amersham Hyperfilm™ ECL	GE Healthcare Europe GmbH, Freiburg, Germany
FlowCytometry tubes	Sarstedt AG & CO., Nümbrecht, Germany
Hard-Shell PCR Plates 96-Well Clear well, white shell	Bio-Rad Laboratories GmbH, Hercules (CA), USA
Kodak GBX developer and replenisher	Sigma-Aldrich St. Louis (MO), USA
Kodak GBX fixer and replenisher	Sigma-Aldrich St. Louis (MO), USA
Microseal 'B' PCR Plate Sealing Film, adhesive	Bio-Rad Laboratories GmbH, Hercules (CA), USA
Mikrotiter plate (Bradford-Assay): Rotilabor F-Profile	Carl Roth GmbH + Co. KG, Karlsruhe
Nitrocellulose membrane 0.2 µm Amersham Protran	GE Healthcare Europe GmbH, Freiburg, Germany
Nunclon Delta Surface	Nunc A/S, Kamstrupvej, Denmark
Polypropylen Röhrchen, konischer Boden, 50 ml und 15 ml	Greiner Bio-One GmbH, Frickenhausen, Germany
Whatman-Filter	GE Healthcare Europe GmbH, Freiburg, Germany

Equipment	Manufacturer
Axiovert 35 microscope	Carl Zeiss GmbH, Oberkochen, Germany
Biofuge Pico	Heraeus GmbH, Hanau, Germany
Branson Sonifier 250	Branson Ultrasonics Corporation, Danbury (CT), USA
Centrifuge 5424R with rotor FA-45-24-11	Eppendorf AG, Hamburg, Germany
Centrifuge for cell culture: Megafuge 1.0 with rotor #2704	Heraeus GmbH, Hanau, Germany
CFX96 Real-Time PCR Detection System	Bio-Rad Laboratories GmbH, Hercules (CA), USA
ColorView SoftImagingSystem	Olympus Soft Imaging Solutions, Münster, Germany
Confocal microscope: LSM 710	Carl Zeiss GmbH, Oberkochen, Germany
Cryobox: Cryo 1 °C Freezing Container, "Mr. Frosty"	Nalgene (Thermo Scientific Inc.), Waltham (MA), USA
Eppendorf Safe-Lock tubes 1.5 ml/ 2.0 ml	Eppendorf AG, Hamburg, Germany
Flow cytometer FACS CANTO II	BD Biosciences, Heidelberg, Germany

Material & Methods

Gammacell Irradiator 2000 (Cs ³⁷)	Nuklear Data, Frankfurt, Germany
Incubator: Hera cell 150	Heraeus GmbH, Hanau, Germany
Liquid Scintillation Analyzer TRI-CARB 2100TR	Canberra Packard Central Europe GmbH, Schwadorf, Austria
Luminometer Tristar ² Multimode reader LB942	Berthold Technologies GmbH & Co. KG, Bad Wildbad, Germany
NanoDrop 2000 Spectrometer	Thermo Scientific Inc., Waltham (MA), USA
Odyssey infrared imaging 9120	LI-COR, Lincoln (NE), USA
PyroMark Q96 ID (Pyrosequencer)	Qiagen, Venlo, Netherlands
SDS-PAGE PowerPac Basic 75W	Bio-Rad Laboratories GmbH, Hercules (CA), USA
SDS-PAGE chamber Trans-Blot Cell	Bio-Rad Laboratories GmbH, Hercules (CA), USA
T100 Thermal Cycler	Bio-Rad Laboratories GmbH, Hercules (CA), USA
Thermomixer compact	Eppendorf AG, Hamburg, Germany
UV-Vis Spectrophotometer NanoDrop 2000	Thermo Scientific Inc., Waltham (MA), USA
Vortexer REAX 2000	Heidolph Instruments GmbH & Co. KG, Schwabach, Germany
VWR Rocking Platform	VWR International, LLC, Radnor (PA), USA

Software	Developer
BD FACSDiva Version 6	BD Biosciences, Heidelberg, Germany
Cell [^] A Imaging Software for Life Science Microscopy	Olympus Soft Imaging Solutions, Münster, Germany
CFX Manager 3.1	Bio-Rad Laboratories GmbH, Hercules (CA), USA
ChemSketch	ACD/Labs, Toronto, Canada
EndNote Version X6	Thomson Reuters, New York City (NY), USA
Geneious 6.0	Biomatters, Auckland, New Zealand
GraphPad Prism Version 6	GraphPad Software, La Jolla (CA), USA
ICE software	Berthold Technologies, Bad Wildbad, Germany
Image Studio Lite 5.2 (Western Blot Analysis Software)	LI-COR, Lincoln (NE), USA
ImageJ	U. S. National Institutes of Health, Bethesda (MD), USA
IMB SPSS Statistics version 23	IBM corp., Armonk, NY, USA
InDesign CS5.5	Adobe Systems Software Ireland Limited, Dublin, Ireland
MS Office Version 2016	Microsoft, Unterschleißheim, Germany
Odyssey Version 3.0	LI-COR, Lincoln (NE), USA
Precision Melt Analysis Software 1.2	Bio-Rad Laboratories GmbH, Hercules (CA), USA
Pyromark assay Designer 2.0	Qiagen, Venlo, Netherlands
Pyromark CpG Software	Qiagen, Venlo, Netherlands
SnapGene Viewer 2.8.2/ SnapGene Trial	GSL Biotech, Chicago (IL), USA
ZEISS ZEN Imaging Software 2.1	Carl Zeiss GmbH, Oberkochen, Germany

2.2 Cell culture

Human glioblastoma and astrocytoma cell lines, provided from the Institute's central cell stock, were used for in vitro analyses (**Table 3**). The cells were kept in appropriate cell culture medium (DMEM) at constant temperature (37 °C) and water vapor saturated atmosphere with 7 % CO₂. To provide complete growth medium, DMEM was supplemented with 10 % fetal calf serum (FCS). Cells were kept in culture for up to three months. For long term storage cell lines were frozen in DMEM + 10 % FCS and 10 % DMSO in a freezing container filled with 2 propanol at -80 °C and then stored in liquid nitrogen (gas phase). Normal passaging of cell lines was performed twice a week before reaching confluence. Culture medium was removed and residual medium was washed away with the same amount of PBS. Cells were then treated with trypsin EDTA (1/10 of the culture medium) for 2 – 5 min at 37 °C until they had detached from the culture vessel. An appropriate volume, usually one tenth of the cell suspension was kept for culturing and refilled to the initial volume with fresh culture medium. Left over cells were seeded for further experiments or rejected. For harvesting, the cells were treated in the same way. To seed a defined number of cells, the cell amount was determined using a "Neubauer improved" counting chamber, counting at least 100 cells. Cell densities, i.e. seeded cell numbers were adjusted for each experiment to avoid confluence of the monolayer at the day of the analysis. Specific cell numbers are indicated in the particular sections.

Table 3: List of glioma cell lines used with the corresponding medium used. Information obtained from ATCC and Cellosaurus knowledge resource on cell lines provided by the Swiss Institute of Bioinformatics (<http://web.expasy.org/cellosaurus/>)

Cell line	Origin*	Medium	Supplement
U118MG	GB	DMEM	10 % FCS
U343	AA	DMEM	10 % FCS
LN428	GB	DMEM	10 % FCS
GBP61	GB	DMEM	10 % FCS
A172	GB	DMEM	10 % FCS
LN308	GB	DMEM	10 % FCS
U87MG	GB	DMEM	10 % FCS
LN229	GB	DMEM	10 % FCS
LN319	AA	DMEM	10 % FCS
LN18	GB	DMEM	10 % FCS
U251	GB	DMEM	10 % FCS
U373MG	GB	DMEM	10 % FCS
D247	GB	DMEM	10 % FCS
U138MG	GB	DMEM	10 % FCS
M059K	GB	DMEM	10 % FCS
M059J	GB	DMEM	10 % FCS
GBP44	GB	DMEM	10 % FCS
T98G	GB	DMEM	10 % FCS

Material & Methods

2.2.1 Mycoplasma detection

In order to detect “Mycoplasma” contaminations, maintenance cell cultures were routinely controlled for the presence of different mollicutes, such as Mycoplasma, Acholeplasma, and Spiroplasma DNA. Cell culture supernatants were subjected to PCR (Venor GeM Classic, Minerva Biolabs), detecting common types of mollicutes. PCR products were run on a 1 % agarose gel and evaluated on the basis of positive and negative controls provided by the kit.

2.2.2 Treatment of cells with cytostatic drugs

To study the response of tumor cells to anti cancer drugs, relevant for the treatment of gliomas, cells were treated with adequate concentrations of TMZ or topotecan (TPT). The first line therapeutic drug TMZ was administered in a time frame of 24 – 144 h. A working solution of 35 mM was generated from 113.3 mM stock solved in DMSO by dilution with sterile water. Both solutions were stored at 80 °C. Treatment was performed by adding working stock directly to the culture medium to reach an end concentration of 50/ 100 µM or others. In case of low volumes to be pipetted (< 1 µl), a pre dilution step in cell culture medium was performed. The corresponding amount of DMSO in H₂O was added to the control cells in each experiment. TPT stock was provided as patient’s formulation by the pharmacy of the University Medical Center Mainz dissolved as 1 mg/ ml (2.18 mM) in H₂O and stored at 80 °C. Working solutions were freshly prepared for each experiment with fresh cell culture medium and then added to cell culture vessels directly. Control cells received treatment with the corresponding amount of fresh culture medium. TMZ/ TPT treated cells were incubated up to the desired end point under normal cell culture conditions.

2.2.3 γ -Irradiation of cells

For investigation of the cellular response to IR, cells were plated in 60 mm dishes and irradiated using a Cs¹³⁷ radiation source (Gammacell 2000). To reach a dose equivalent of 4 Gy, cells were irradiated for 80 sec. Control cells were kept under the same conditions during the whole procedure.

2.2.4 Generation of transgenic cell lines/ stable transfections

2.2.4.1 Plasmids

Plasmids for expression of the Survivin GFP (Surv GFP) fusion protein and the NES mutated Survivin variant were kindly provided by Prof. Dr. [REDACTED] (Fakultät für Biologie Universität Duisburg Essen). The 432 bp CDS of *BIRC5* (*survivin*) was cloned via BamHI and NheI in front of *EGFP* (711 bp) to generate Surv GFP plasmid (Figure 7). To verify the plasmid sequence identity, plasmids were sequenced with standard T7 and SP6 primers by Sanger sequencing by Starseq (Mainz). Both reads confirmed the error free sequence of the genes. For inactivation of the NES, a second plasmid was generated by cloning of a mutated SurvivinNESmut variant to pcDNA3.1 analogously (see 3.1.2). Neomycin resistance (aminoglycoside 3' phosphotransferase) was used as selection marker for positively transfected cells.

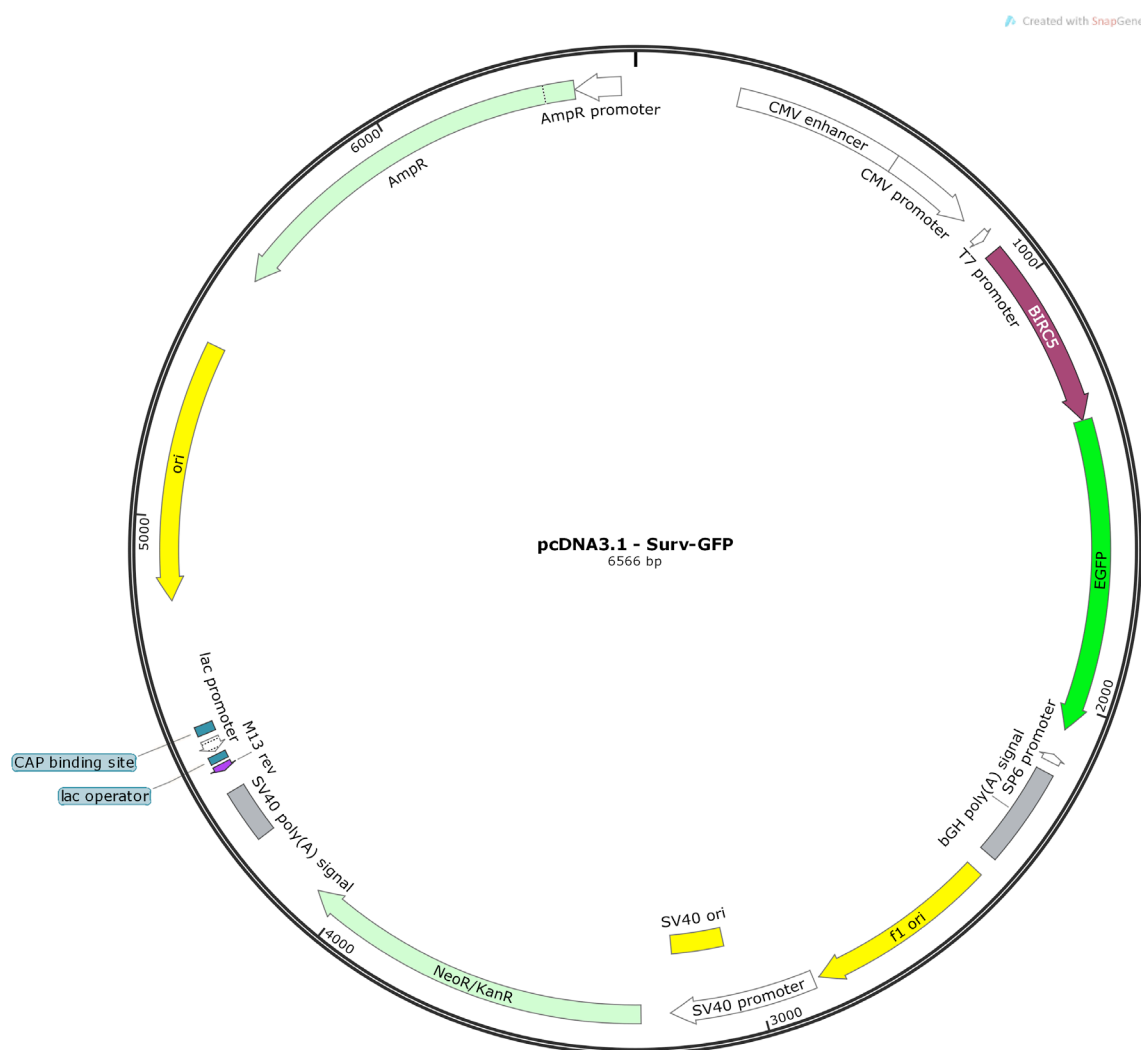


Figure 7: Map of pcDNA3.1 vector with fused CDS of BIRC5 and EGFP. One vector carried wt BIRC5 sequence whereas second vector carried NES mutated BIRC5 with mutations in codon 96 (TTA \Rightarrow GCA) and 98 (CTT \Rightarrow GCT). Vector map was generated using SnapGene Viewer 2.8.2.

Material & Methods

Plasmids were amplified and purified by plasmid midi preparation. Chemically competent *E. coli* (strain DH5 α) were generated by pretreatment with CaCl₂. In brief, over night culture was grown in 250 ml Luria broth (LB) medium to an OD₆₀₀ of 0.35 – 0.45. After centrifugation (2 min; 8000 g; 4 °C), bacteria were resuspended in 50 mM CaCl₂ and incubated for 20 min on ice. A second step of centrifugation was carried out and aliquots of the *E. coli* were prepared in 50 mM CaCl₂ + 10 % glycerol at 80 °C.

1 ng of plasmid DNA was used for transformation of 100 μ l competent bacteria suspension. Plasmids and bacteria were incubated for 30 min on ice followed by 90 s at 42 °C. 300 μ l LB medium w/o antibiotics was then added to the suspension for incubation period of 1 h at 37 °C. For plating on LB agar plates with 100 μ g/ml ampicillin, transformation mixture was spun down and bacteria were resuspended in 100 μ l of the supernatant. Plated bacteria were incubated over night at 37 °C. Positive colonies were then picked to inoculate ~300 ml LB medium in a 1000 ml Erlenmeyer flask. Bacteria were grown at 37 °C at constant shaking (240 rpm) for approximately 18 h (overnight). Bacteria were spun down (2 min; 8000 g; 4 °C) and plasmids were isolated from the pellet with NucleoBond Xtra Midiprep kit (Macherey & Nagel) according to the manufacturer's instructions. After isolation and purification, plasmids were reconstituted and stored in an appropriate volume of TE buffer, typically 600 – 800 μ l. Purity of plasmid DNA was verified by UV spectrophotometry (NanoDrop 2000, Thermo Scientific). Concentration, A_{260/280} and A_{260/230} ratios are provided in **Table 4**.

Table 4: DNA concentration following Midiprep plasmid isolation.

	ng/ μ l	A _{260/280}	A _{260/230}
pcDNA3.1 Surv GFP	4079.0	1.63	1.83
pcDNA3.1 SurvNESmut GFP	2080.1	1.79	2.04

2.2.4.2 Stable/ transient transfection of GB cell lines

The described plasmids were used for generation of stably transfected cell lines with the non liposomal lipid transfection reagent Effectene (Qiagen). In brief, cells were seeded on a 60 mm dish to reach 60 – 70 % confluency on the day of transfection. According to the manufacturer's conditions, 1 μ g plasmid DNA was diluted with DNA condensation buffer to a total volume of 150 μ l. 8 μ l enhancer were added and DNA was mixed by vortexing (1 s). After an incubation period of 2 – 5 min the mixture was spun down and 25 μ l Effectene reagent were added and mixed by vortexing (10 s). During formation of the transfection complexes (5 – 10 min),

growth medium on the cells was aspirated, the cells were washed with PBS and 4 ml fresh growth medium (with FCS) were added to the cells. 1 ml complete growth medium was added to the transfection complexes, suspension was mixed by pipetting up and down twice, and the complexes were added dropwise onto the cells immediately. Cells were then incubated under appropriate cell culture conditions. For transient transfection, cells were analyzed or treated at the desired time point after the transfection, usually 24 – 48 h. For stable transfection, cells were passaged 1:10 after 48 h into selective medium. Medium was replaced twice a week until colonies of resistant cell clones appeared. In case of Surv GFP and SurvNESmut GFP colonies, positive for GFP, were picked under a fluorescence microscope and transferred to a 24 well plate. Different Neo and GFP positive cell clones could be generated by this process. Clones were kept under constant selection pressure with 0.75 µg/ ml G418 and/ or 1 µg/ ml puromycin (different antibiotic combinations are provided in **Table 5**).

The GB cell line LN229 was used for generation of Surv GFP, SurvNESmut GFP, and Rad51_sh + Surv GFP clones. LN229 con and LN229 Rad51_sh were generated by Quiros *et al.* [185]. For comparability reasons with Rad51_sh cells, SurvivinGFP expressing cell clones were generated on basis of LN229 con cells. The LN229 con cell clone carries the empty pSuper and pSV2neo vector as described [185]. pcDNA3.1 Surv GFP was co transfected with a puromycin resistance plasmid for selection (**Table 5**) into LN229 con. pcDNA3.1 SurvNESmut GFP was transfected directly into parental LN229.

Table 5: Genetic background of the generated LN229 Surv-GFP and SurvNESmut-GFP clones. The transgenic cell lines used, were either generated on the basis of LN229 or LN229 con cells.

#	Clone	Plasmid	Parental cell line	Resistance/ selection marker
1	LN229 con	pSuper pSV2neo	LN229	G418
2	LN229 Surv GFP	pSuper pSV2neo pcDNA3.1 pSV2puro	LN229 con (#1)	G418 Puromycin
3	LN229 SurvNESmut GFP	pcDNA3.1 Surv GFP	LN229	G418
4	LN229 Rad51_sh	pSuper Rad51sh pSV2neo	LN229	
5	LN229 Rad51_sh + Surv GFP	pSuper Rad51sh pSV2neo pcDNA3.1 pSV2puro	LN229 Rad51_sh	G418

Material & Methods

This cell model was utilized to investigate the impact of Surv GFP expression and localization in LN229 cells and allowed the direct comparison with Surv GFP expression in a Rad51 knock down cells after genotoxic stimuli.

2.2.5 Transient siRNA-mediated gene knockdown

To achieve a temporary gene knockdown, cells were transfected with siRNA against targeted gene products (*BIRC5*, *XAF1*). Lipofectamine RNAiMAX Reagent (Invitrogen) was used for transfection. For knockdown of *XAF1*, LN229 cells were seeded in 6 well plates containing 26000/ well in 1.5 ml medium. After 24 h, 0.1 nmol siRNA were diluted in a total volume of 250 μ l with DMEM (w/o serum). 3 μ l transfection reagent were added to 247 μ l DMEM (w/o serum) and both preparations were combined and incubated for 5 min to allow complex formation. siRNA lipid complexes (500 μ l) were then added to the cells dropwise, yielding a final concentration of 50 nM siRNA. Cells were then incubated until analysis (24 – 96 h). Additional treatment with TMZ was carried out 24 h after the transfection.

For analysis of HR efficiency under knockdown of *BIRC5*, cells were grown in 24 well plates containing 10000/ well in 1 ml medium for treatment and 5000/ well in 1 ml for control cells, respectively. Transfection was performed with volumes adjusted for 24 well format using 3 μ l Lipofectamine RNAiMAX Reagent with 50 nM siRNA (final concentration) as described. Additional transfection with HR assay plasmids (see 2.10.2) were conducted after 24 h.

2.3 Protein extracts & Western blot

2.3.1 Cell lysates

To generate protein lysates different methods were used, depending on the subsequent analysis. For whole cell extracts and fractionated cell extracts, cells were harvested as described in 2.2. The cell pellet was then washed with PBS once.

Whole cell lysis was performed in NP 40 lysis buffer containing 25 mM Tris HCl (pH 8.0), 5 mM EDTA, 0.5 % NP 40 and 500 mM NaCl. Protease inhibitors were added freshly to the buffer as 2 mM DTT, 1 mM PMSF and 1x Complete inhibitor (Roche). Samples were kept on ice and lysis step was performed at 4 °C on a rotary shaker for 15 – 20 min, depending on the size of the pellet. After incubation, insoluble parts were removed by centrifugation (20 min, 18407 g, 40

4 °C) and supernatant could be used for western blot. Bradford protein quantification was used for determining protein concentration using a BSA standard curve [186]. Bradford reagent was prepared with 0.01 % Coomassie Brilliant Blue G 250, 25 ml EtOH and 50 ml phosphoric acid filled to 500 ml with dest. H₂O. After stirring and filtration, the solution was stored at 4 °C.

For fractionated cellular extracts two separate buffers for nuclear and cytoplasmic extracts were used. The cell pellet was resuspended in 500 µl PBS and split in half. To isolate cytoplasmic protein fraction only, the first pellet was lysed in 200 µl **lysis buffer 1** (10 mM NaCl, 3 mM MgCl₂, 10 mM Tris HCl (pH 7.4)) with freshly added 1 mM DTT and 1 mM PMSF on ice for 5 min. After adding 1 % NP 40, suspension was incubated for 3 min and the centrifuged (1 min, 18407 g, 4 °C). To extract the nuclear protein fraction of the cells, the second pellet was first lysed with lysis buffer 1 on ice for 5 min and then for additional 6 min with 1 % NP 40. Nuclei were centrifuged (5 min, 3550 g, 4 °C), then resuspended in 500 µl lysis buffer 1 and directly centrifuged. The so purified nuclei were then lysed in 100 µl **lysis buffer 2** (20 mM Tris HCl (pH 7.4), 40 mM Na₄P₂O₇, 5 mM MgCl₂, 10 mM EDTA, 1 % Triton X100, 1 % SDS) with freshly added 1 mM DTT and 1 mM PMSF. To ensure complete lysis of the nuclear membrane, samples were sonicated with 3 x 10 pulses at 40 % duty cycle. After centrifugation of the lysate (1 min, 18407 g, 4 °C), supernatant was frozen for further analysis. To avoid interference with buffer components, protein quantification was carried out according to Lowry *et al* [187] using a BSA standard curve.

“Blue” whole cell extracts were prepared for the analysis of protein phosphorylation. In brief, cell culture vessels with adherent cells were washed with PBS once. After complete removal of the washing medium, 100 – 200 µl preheated (96 °C) 1x RotiLoad (Carl Roth) was added directly onto the cells. Cell lysate was transferred to Eppendorf tubes and sonicated with 3 x 10 pulses at 40 % duty cycle.

2.3.2 SDS Polyacrylamid-Gel electrophoresis (SDS-PAGE) & Western blotting

The desired amount of total protein, usually 20 µg, was filled with H₂O to a total volume of 30 µl. 10 µl 4x loading buffer (RotiLoad) were added and the samples were boiled for 5 min at 95 °C before loading on a denaturing SDS polyacrylamid (PAA) gel. “Blue” whole cells extracts were loaded directly onto the gel. Gels with 12 % acrylamid (37.5 : 1 acrylamid – bisacrylamid)

Material & Methods

were used for protein separation. Spectra Multicolor Broad Range Protein Ladder (Thermo Scientific) was run on each gel for protein size verification. Stacking gel separation was performed at 60 V using 1x running buffer (50 mM Tris HCl, 384 mM glycine, 0.1 % SDS). As soon as the bromphenol blue front had entered the separation gel, voltage was increased to 120 V. Shortly before reaching the lower gel border electrophoresis was stopped. The gel was rinsed with blotting buffer once (25 mM Tris HCl, 192 mM glycine, 20 % MeOH). Proteins were then blotted onto a nitrocellulose membrane in a tank blot system at constant current of 300 mA for 2.5 h on ice. After the blotting procedure, protein transfer was confirmed by ponceau S staining which was washed away with Tris buffered saline and Tween20 (TBST) washing buffer (20 mM Tris, 137 mM NaCl, 0.2 % Tween®20, pH 7.6) for 3 times for 5 min.

Unsaturated membrane binding sites were then blocked with 5 % nonfat dried milk (NFDM) or BSA (w/v) in TBST for 1 h at constant shaking.

Incubation with primary antibody (Ab) followed for 2 h at RT or overnight at 4 °C, depending on the Ab specifications, at constant shaking (Table 6). Before incubating with appropriate secondary Ab, the membrane was washed with TBST 3 times for 5 min. After the incubation period of 1 h at RT, washing was repeated and Ab signal could be detected either by conventional ECL method or at the Odyssey infrared imaging system. For ECL detection the blot was incubated with a 1:1 mixture of ECL detection reagent 1 + 2 for 2 min at RT. A film was exposed, depending on the proteins expression, for 30 s – 5 min and then transferred to developer for 1 min. After being rinsed with water, the stop of the developing reaction was introduced by incubating the film for 1 min in fixer solution. Detection via Odyssey infrared imaging system required an incubation with an infra red fluorescent Ab. After incubation with secondary Ab, the blot was washed with TBST 3 times for 5 min and scan of the membrane was performed on an Odyssey 9120 either in channel 700 (excitation at 685 nm) or in channel 800 (excitation at 785 nm) depending on the secondary Ab. Oversaturation was avoided by adjusting excitation intensity.

Table 6: List of primary and secondary antibodies (Ab) used for Western blot detection. (abbr.: rb. rabbit; m. mouse; d. donkey; g. goat; mAb. monoclonal antibody; pAb. polyclonal antibody)

Antibody	Host/ re-activity	Provider (cat.-no.)	Incubation
primary antibodies			
Survivin	rb. pAb.	R&D Systems (#AF886)	1:1000 TBST + 5 % NFDm
XAF1	rb. pAb.	Pro-Sci (#3207)	1:1000 TBST + 5 % NFDm
HSP90	m. mAb.	Santa Cruz Biotechnology, Inc. (#13119)	1:1000 TBST
γH2AX (Ser139)	m. mAb.	Millipore (JBW301)	1:1000 TBST + 5 % BSA
pCHK1 (Ser345)	rb. pAb.	Cell Signaling Technology, Inc. (#2341)	1:1000 TBST + 5 % BSA
CHK1	m. mAb.	Cell Signaling Technology, Inc. (#2360)	
secondary antibodies			
Anti-m. peroxidase conjugated	g. pAb.	Rockland Immunochemicals Inc. (610-1302)	1:2000 TBST + 5 % NFDm
Anti-rb. peroxidase conjugated	g. pAb.	Rockland Immunochemicals Inc. (611-1302)	1:2000 TBST + 5 % NFDm
IRDye 680LT anti-mouse	d. pAb.	LI-COR	1:10000 TBST
IRDye 800CW anti-rabbit	d. pAb.	LI-COR	1:10000 TBST

2.4 Cytotoxicity assays

To measure different end points of DNA damaging/ cytotoxic treatment, cell lines were investigated by the analysis of metabolic activity (MTT), reproductive survival (colony formation assay), induction of senescence, activation of caspase 3/ 7 as well as induction of apoptosis and/ or necrosis. Furthermore, doubling time of different cell clones was determined as described in the flow cytometry section (see 2.4.6.3).

2.4.1 Cell viability assay (MTT)

The reduction of the water soluble 3 (4,5 dimethylthiazol 2 yl) 2,5 diphenyltetrazolium bromide (MTT) by metabolically active cells was determined in 96 plates [188]. Cells were seeded in 200 µl medium at densities of 1500 – 5000 cells/ well depending on the observation period. For measurement, cell culture medium was removed carefully and replaced with 100 µl DMEM w/o phenol red, containing 0.5 mg/ ml MTT. The stock solution was prepared by dissolving 5 mg/ ml MTT in PBS. After filtration, aliquots were stored at 20 °C for up to 3 months. To allow the reduction of MTT to a water insoluble, purple formazan product, plates were

Material & Methods

incubated under normal cell culture conditions for 3 h. To solubilize the formazan crystals, medium was removed carefully and 100 μ l acidified isopropanol (containing 0.04 N HCl) was added. After moderate shaking (550 rpm) absorbance at 570 nm was measured at TriStar² LB 942 multimode reader (Berthold, Bad Wildbad). Viability (%) was determined after normalization to control treated cells, using Prism 6 (GraphPad Software).

2.4.2 Colony formation assay (CFA)

Reproductive capability of glioma cells was determined by colony formation assay (CFA). Changes in clonogenic/ reproductive survival were monitored upon treatment with cytotoxic stimuli. 1000 cells were plated in 5 ml medium on 60 mm plates. After 24 h, particular treatment was applied. The plates were then incubated under cell culture conditions for 10 – 14 days depending on the size of the colonies. Cells were fixed on the plates with pure methanol (5 min, RT), after removing the culture medium and washing the cells once with PBS. Staining was performed for 30 min at RT by incubation with staining solution (1.25 % Giemsa solution, 0.125 % crystal violet (w/v)). After removing excess staining solution (water), and drying the plates, distinctly visible colonies of >50 cells were counted on each dish. Normalization to control and semi logarithmic graphing was performed, using Prism 6 (GraphPad Software).

2.4.3 Senescence

Induction of permanent cell cycle arrest as one possible result of exogenous DNA damage was determined via senescence associated (SA) β D galactosidase (β gal) activity. This stress induced senescence is a cellular protection mechanism to limit the replicative capacity of damaged cells with tumorigenic potential [189]. An increase of lysosomal β Gal activity is frequently used as cellular marker of senescence [190,191]. Other than in non senescent cells, where β Gal activity is detectable at the optimal pH of 4 only. The increased SA β Gal activity can also be measured at a suboptimal pH of 6 [192]. However, a direct involvement of the enzyme in the senescent phenotype has yet not been established [193]. LN229 cell clones were seeded on 35 mm dishes (3500/ control; 7000/ treatment) and cultured 24 h before treatment. After 120 h or 140 h cells were fixed on the plates by treatment with 1 ml fixative solution (2 % formaldehyde, 0.2 % glutaraldehyde in PBS) for 10 min at RT. After washing with

PBS, β Gal staining was performed by over night incubation at 37 °C (no CO₂) with 1 ml staining solution containing 5 mM K₃[Fe(CN)₆], 5 mM K₄[Fe(CN)₆], 2 mM MgCl₂, 150 mM NaCl, 1 mg/ml X Gal¹ dissolved in DMF. Staining solution was prepared in citric acid – Na₂HPO₄ – buffer (pH 6), generated by mixing 36.85 ml of 0.1 M citric acid with 63.15 ml of 0.2 Na₂HPO₄. pH was adjusted to 6.0, if necessary. During the staining, cell culture dishes were kept in a humidified chamber sealed with parafilm, to avoid drying of the samples. Characteristic blue coloring, was visible after ~18 h. Excess staining solution was then removed, plates were washed and cells were covered in 75 % glycerol for preservation. Phase contrast or bright field images, covering different spots of the growth area, were obtained on a Axiovert 35 microscope (Carl Zeiss GmbH) and digitalized with the Cell^A Software and a connected ColorView SoftImagingSystem camera (Olympus Soft Imaging Solutions) within a week upon fixation. Images were analyzed for total cell number and senescent cell number by manual counting using ImageJ (U. S. National Institutes of Health) Cells were considered as “senescence positive” if strong blue staining was visible in the cell body, as illustrated in **Figure 8**.

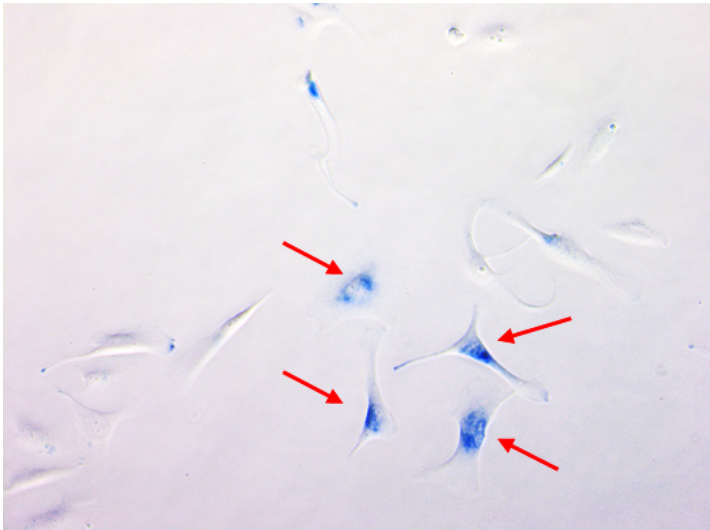


Figure 8. Example of senescent LN229 cells after the treatment with 100 μ M TMZ. Cells evaluated as senescence-positive are marked with red arrows (phase-contrast, 40x).

¹ X-Gal also 5-bromo-4-chloro-3-indoxyl- β -D-galactopyranoside is a chromogenic substrate for β -Gal. Upon hydrolysis into galactose and 5-Bromo-4-chloro-hydroxyindole the latter spontaneously dimerizes and is oxidized into a blue indigo compound (5,5'-dibromo-4,4'-dichloro-indigo).

Material & Methods

2.4.4 Caspase 3/ 7 activation

One central intersection of different cell death pathways is the activation of effector caspases. Among these, caspases 3 and 7 carry out crucial pro apoptotic functions. Therefore, the activation of these enzymes is a measure of the apoptotic signaling, induced by treatment with toxic agents. The activity of caspase 3 and 7 was determined in a luminescent multiwell plate assay (Caspase Glo 3/ 7 Assay, Promega). The assay relies on the cleavage of a luminogenic caspase substrate (Z DEVD), generating aminoluciferin + ATP + O₂. Luciferase, contained in Caspase Glo reagent, then generates a light signal depending on the available substrate. Thus, luminescence is proportional to the caspase activity. LN229 cell clones were seeded in 50 µl per well in a 96 well plate (half area, white walled) in appropriate densities (72 h: 2000/ 50 µl; 144 h: 1000/ 50 µl). Treatment occurred after 24 h, followed by an incubation of up to 144 h. After the indicated period, cells were lysed by adding 50 µl Caspase Glo reagent directly to the medium and mixing for 30 s at 500 rpm. Detection of luminescence was performed at a TriStar² LB 942 microplate reader (Berthold) after 1 h at RT. Values of a blank reaction, containing reagent and cell culture medium (w/o cells) was subtracted from the sample values.

2.4.5 Cell Proliferation ELISA, BrdU-Incorporation assay

Influence of XAF1 knockdown on cell proliferation was analyzed with Cell Proliferation ELISA, BrdU (colorimetric, Roche). Incorporation of the thymine analogue Bromodesoxyuridine (BrdU) into the DNA of replicating cells is measured to quantitate cell proliferation. A mouse anti BrdU mAb conjugated with HRP is used for detection. Oxidation of the peroxidase substrate 3,3',5,5' tetramethylbenzidine causes a color change to blue which can be quantified by absorbance measurement at 450 nm.

For analysis of TMZ induced effects on proliferation, cells were reseeded after XAF1/ con siRNA knockdown in 35 mm dishes. Knockdown was carried out with 50 nM final concentration of siRNA as described (see 2.2.5). 750 cells were reseeded in a 96 well plate in triplicates for each time point, ranging from 24 – 144 h. Inverse treatment with 100 µM TMZ was performed according to following time scheme (**Figure 9**).

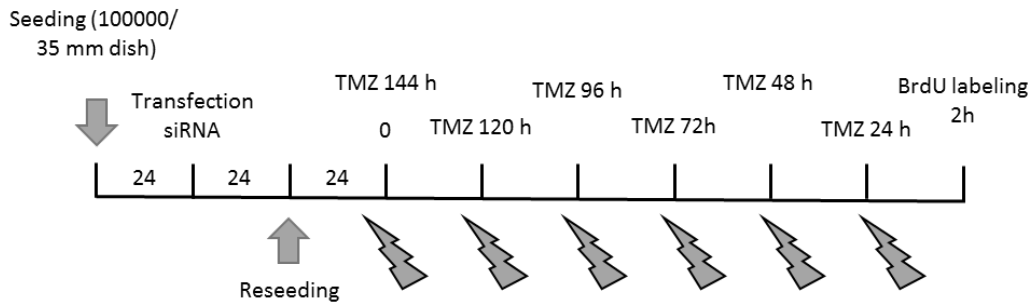


Figure 9: Seeding, transfection and treatment time scheme for the cell proliferation ELISA (BrdU incorporation assay).

At the end of the treatment period, BrdU labeling solution was added into the cell culture medium, yielding a final concentration of 10 μ M. Cells were incubated for DNA labelling for 2 h under normal conditions. Subsequent steps were performed as described in the manufacturer's protocol. In brief, cells were fixed on the MTP after BrdU labeling and then incubated with HRP labeled anti BrdU antibody for 90 min at RT. After several washing steps, 100 μ l substrate solution as added to each well and the reaction was stopped after 30 min by adding 25 μ l of 1 M H_2SO_4 . The absorbance was measured at 450 nm with a reference wavelength of 690 nm at the TriStar² LB 942 reader.

Material & Methods

2.4.6 Flow cytometry

Flow cytometric analyses were conducted on a FACSCanto II cell analyzer (BD).

2.4.6.1 Analysis of the cell cycle distribution and apoptotic cell fraction by PI staining

To determine the proportion of cells in G1, S and G2 phase and apoptotic (SubG1) cells, samples were subjected to propidium iodide (PI) staining. During apoptosis endonucleases (caspase activated DNases (CAD)) cleave the DNA inter nucleosomally in fragments of approx. 180 bp. Upon fixation with EtOH, the cell membrane gets permeable for this small oligonucleotides (and other substances) which can leak out of apoptotic cells. By DNA staining with PI, differences in the DNA content can thus be visualized [194,195]. PI intercalates into the DNA base stacks, allowing a quantification of the DNA content of a cell. G1 cells with diploid (unreplicated) genome (2n2c) give rise to a peak, since these cells are representing the majority in vital cell populations (**Figure 10, A**). Cells that have gone through replication are characterized by a doubled PI fluorescence, representing cells in G2 (2n4c). A DNA content between G1 and G2 is attributed to cells in the S phase. Furthermore, an amount of DNA below G1 can be found in apoptotic cells, that have lost parts of their genome (see above). Therefore, this method is suitable for the analysis of apoptosis induction and cell cycle distribution.

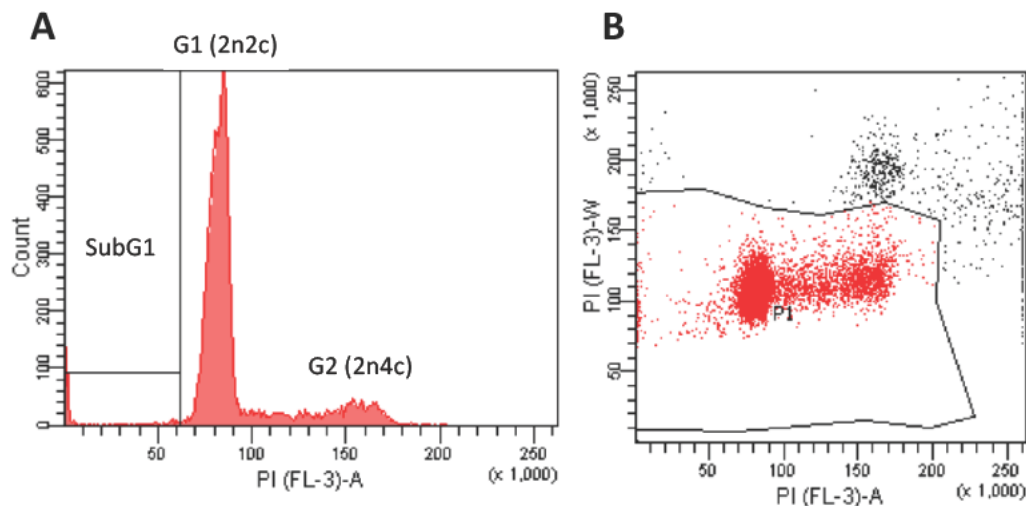


Figure 10: Example of the SubG1 analysis, showing a histogram and dot-plot for gating the SubG1 fractions. A) Histogram with SubG1 gate of the distribution of the PI fluorescence. Total counts of the PI-fluorescence measured as peak area (PI (FL-3)-A) are shown. Different cell cycle phases are indicated in the diagram. **B)** Gating for the exclusion of duplets was performed by blotting PI-fluorescence peak width (PI (FL-3)-W) vs. PI-fluorescence peak area (PI (FL-3)-A). Cells/ events inside gate P1 were considered for determination of the SubG1 fraction.

Figure 10 also shows exemplary “gating” of the SubG1 fraction. Gating defines a subpopulation of cells, e.g. cells in SubG1/ G1 or others. To ensure accurate analysis of single cells, duplet cells were excluded by a separate superordinate gate (**Figure 10, B**). Duplets were identified and excluded by blotting PI fluorescence (Width) vs. PI fluorescence (Area).

Cells were seeded in appropriate numbers in 60 mm dishes. After the indicated incubation period, cell culture medium was transferred to a centrifugation tube. The dishes were washed with PBS, which was also collected in the tubes. Remaining cells on the plate were detached by trypsinization and harvested with the cell culture medium and transferred to the corresponding tube. After centrifugation (4 min, 1500 rpm, RT), supernatant was removed and cell pellet was resuspended in 200 µl PBS. For fixation and membrane permeabilization, cells were fixed by dropwise addition of 2 ml ice cold 70 % EtOH under constant vortexing. Samples were kept for 1 up to 14 days at 20 °C. Before analysis of the cells, EtOH was removed by centrifugation (4 min, 1500 rpm, RT) and the pellets were allowed to dry. 330 µl PBS containing 0.1 mg/ml RNase H (Roche) were used to resuspend the pellet. To reduce background staining, RNase H digestion was performed for 30 min at RT and kept on ice until analysis. 170 µl PI solution (50 µg/ml in PBS) was added to the samples directly before the measurement. Data were analyzed using BD FACSDiva Software for quantification of the SubG1 fraction. Cell cycle distribution was analyzed with the DNA analysis software ModFit LT 3.3 (Verity Software House). Analysis was performed utilizing the diploid CC model 1nnOA_DSF.

2.4.6.2 Analysis of apoptosis/ necrosis by AnnexinV PI co staining

In contrast to SubG1 analysis, fixation was not performed for AnnexinV Pi staining. AnnexinV (A5) is a protein, capable of binding to phosphatidylserine (PS) residues which reside in the inner plasma membrane of cells. During apoptosis PS residues flip to the outside of the membrane and are accessible to A5. APC tagged A5 is thus used for detection of apoptotic cells. Necrosis is characterized by a rupture of the cellular membrane, allowing PI and A5 to enter the cell. Necrotic cells are therefore PI and A5 positive. However, also cells in late stages of apoptosis, show a disintegrated membrane and cannot not be distinguished from necrotic cells. Living cells appear unstained in this analysis. Determination of necrotic/ late apoptotic and apoptotic cells was achieved by dot blot analysis of PI fluorescence vs. APC fluorescence (**Figure 11**) using BD FACSDiva Software.

Material & Methods

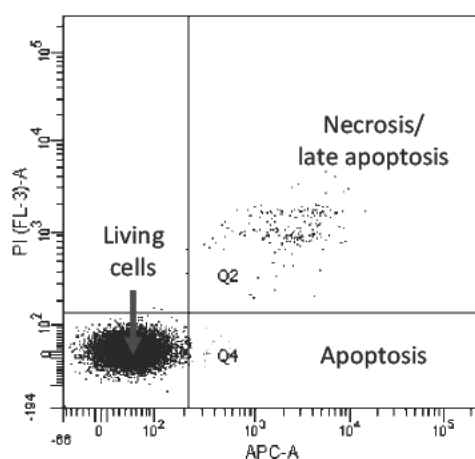


Figure 11: Example of a AnnexinV-PI co-staining dot-plot showing the PI-fluorescence peak area (PI (FL-3)-A) vs. APC-fluorescence peak area (APC-A). The apoptotic, necrotic/late apoptotic, and living cell fractions were gated in quadrants labeled in the diagram.

Cell pellets were obtained as described above (before EtOH fixation). Harvested cells were resuspended in 48.5 μ l AnnexinV binding buffer (BD Pharmingen). 1.5 μ l AnnexinV APC (Invitrogen) were added to the samples and incubation was carried out for 20 min on ice (in the dark). 440 μ l AnnexinV binding buffer, containing 10 μ l PI (50 μ g/ml) were added. After vortexing the samples were kept on ice until measurement.

2.4.6.3 Cell clone growth curve (CountBright Absolute Counting Beads)

To determine the growth rate of different cell clones and to compare these to the doubling time of the parental cell line, clones were seeded on 60 mm dishes in a starting density of 35000 cells. Every 24 h (24 – 96) cells were harvested (w/o supernatant) and fixed with EtOH, as described (see 2.4.6.1). Upon EtOH removal, the cell pellet was resuspended in 500 μ l PBS and 20 μ l CountBright Absolute Counting Beads (Molecular Probes) were added to each sample. Cell number was determined by flow cytometry. 2500 events of CountBright Absolute Counting Beads were counted, as gated in the FSC/SSC dot blot. Cell number was determined using the number of total events, the Lot specific beads concentration and the total volume:

$$n = \frac{events_{total} - events_{beads}}{events_{beads}} * \frac{beads (Lot)}{volume} * volume_{total}$$

Exponential growth curves were then plotted in Excel 2016 (Microsoft) and doubling times were calculated from the derived growth equations.

2.5 Real-time RT-PCR

Two step real time RT PCR was performed for quantification of *XAF1* gene expression. RNA was isolated from cell lines, reverse transcribed to cDNA and then amplified by real time PCR.

2.5.1 RNA isolation and cDNA synthesis

Cell pellets of 16 glioma cell lines were generated and RNA was isolated with the silica membrane based RNA extraction kit NucleoSpin RNA (Macherey Nagel). In brief, the cells were lysed, lysate was cleared by filtration and then, upon establishing appropriate high salt binding conditions, loaded onto silica membrane column. After DNase digestion and several washing steps, RNA was eluted in RNase free H₂O. RNA concentration and purity was determined by UV spectrophotometry (NanoDrop 2000, Thermo Scientific). Absorbance quotients $A_{260/280}$ of ~1.8 and $A_{260/230}$ ratios of 2.0 – 2.2 were generally accepted as pure. RNA was then reverse transcribed to generate the cDNA first strand with Verso cDNA kit (Thermo Scientific). 1 µg total RNA was used for the reverse transcription with random hexamer primers for 1 h at 42 °C. After inactivation of the added “RT Enhancer” 2 min at 95 °C, samples were diluted with DNase free H₂O to 50 µl and stored at 20 °C.

2.5.2 qPCR

Quantification of gene expression was performed in triplicates on a CFX96 Real Time PCR Detection System (Bio Rad) using 10 µl GoTaq qPCR Master Mix 2x (Promega), 300 nM primer and 4 ng cDNA filled with water to a total volume of 20 µl. After reference gene analysis (geNorm Kit, Primerdesign) and reference gene evaluation with the BestKeeper software [196], *ENOX2* and β *actin* (ACTB) were used as reference genes for normalization of *XAF1* mRNA expression. *ENOX2* and β *actin* primers were obtained from PrimerDesign (UK), and *XAF1* primers were self designed during this study and synthesized by Eurofins Genomics. PCR amplification was performed according to the indicated protocol (**Table 7**). Fluorescence of the intercalating DNA dye BRYT Green was detected after each run. The cycle of threshold is the amplification cycle, at which fluorescence exceeds the defined threshold (determined by the CFX manager software) and thereby the background fluorescence. Resulting C_T values were then used for calculation of the normalized fold (NFE) gene expression according to the $2^{-\Delta\Delta CT}$ method [197] with the Bio Rad CFX Manager 2.1 software. *XAF1* mRNA expression of

Material & Methods

cell line GBP61 was used as calibrator. Melting curves were assessed after each run and were checked for primer specificity (primer dimers, multiple amplification products). Samples with unspecific amplification products were excluded from the analysis.

Table 7: qPCR protocol for quantification of gene expression of XAF1, ENOX2, and ACTB.

Step	°C	min	cycle
1	50	2:00	-
2	95	10:00	-
3	95	0:10	45x
4	56	0:20	
5	72	0:20	
detection of fluorescence			
6	95	0:10	-
7	65 95 (0.5 increments)	0:05	-
detection of melting curves			

2.6 Epigenetic Analyses

Epigenetic regulation of *XAF1* and *BIRC5* via CpG methylation was analyzed in genomic DNA isolated from cell lines and formalin fixed and paraffin embedded (FFPE) tumor sections. Tumor cells in marked tumor areas on the slides were scraped off and transferred to a reaction tube.

2.6.1 PCI DNA-Extraction

Extraction of genomic DNA was performed by phenol chloroform isoamyl alcohol extraction with ethanol precipitation. Glioma cell pellets and scraped off FFPE tumor tissues were lysed in 300 µl TE9 buffer (50 mM TRIS, 20 mM EDTA, 10 mM NaCl, pH 9) containing SDS (1 %) and 182.5 µg proteinase K (Roche). To ensure complete lysis, samples were kept at 48 °C for 18 h under constant shaking (1100 rpm). An additional 125 µg proteinase K were added to the samples and incubation was prolonged for 2 h at RT. DNA extraction was started using 700 µl PCI (25:25:1; Carl Roth). After vortexing for 15 s, samples were centrifuged (5 min, 18407 g, RT) and upper aqueous layer was transferred to a new tube. This procedure was repeated once. Precipitation of the DNA was performed by adding 750 µl EtOH C₂H₃O₂NH₄ (8:1, 7.5 M C₂H₃O₂NH₄) with 2 µl glycogen (20 mg/ml; Roche). After 1 h at RT, samples were centrifuged (45 min, 18407 g, 4 °C). Supernatant was then discarded and the pellet retained was washed with 70 % EtOH. Remaining EtOH was removed by centrifugation (45 min, 18407 g, 4 °C) and the DNA was dissolved in 50 µl LoTE buffer (3 mM TRIS, 0.2 mM EDTA, pH 8) and evaluated by

UV spectrophotometry (NanoDrop 2000, Thermo Scientific). Absorbance quotients $A_{260/280}$ of ~ 2.0 and $A_{260/230}$ ratios of 2.0 – 2.2 were generally accepted as pure.

2.6.2 Bisulfite-induced modification of genomic DNA

To make a differential methylation at CpGs of interest accessible for analysis, DNA has been subjected to bisulfite induced modification (conversion). The bisulfite or hydrogen sulfite ion (HSO_3^-) is used for introducing sequence differences into DNA templates, depending on the methylation of the CpGs contained. While 5 methylcytosine is protected from this conversion, cytosine is converted during the reaction to uracil [198]. The resulting sequence alterations can be analyzed by different methods, as elucidated in chapter 2.6.5. Here, EZ DNA Methylation Kit (Zymo Research) was used for bisulfite conversion of 500 ng DNA according to the manufacturer's protocol. After conversion, DNA was eluted in 25 μl DNase free water.

2.6.3 Design of primers specific for bisulfite-converted DNA

The sequence of the *XAF1* gene was obtained from the NCBI database sequence of chromosome 17 NC_000017.11 (6755411..6775647) from reference assembly GRCh38.p7. The promoter region and the transcription start site of -5338 to +248 (**Figure 12**) was screened for CpGs putatively involved in gene regulation using the Geneious 6 software (Biomatters). Interesting areas were marked for further investigation. For primer design, the sequence was bisulfite converted *in silico*, whereat all Cs contained in a CpG dinucleotide were treated as methylated (5 mC). For these Cs no change was introduced into the DNA sequence. All Cs, not contained in CpG dinucleotides, were converted to T. Primers were designed with the help of Pyromark assay Designer software 2.0 (Bio Rad). Seven CpGs previously described by Byun *et al.* were included in this promoter region [179] (see also 3.6.1). Two regions were found to provide suitable primer binding sites for analysis of CpG methylation.

Material & Methods

For methylation analysis by methylation sensitive high resolution melt analysis (MS HRM), HRM region 1 (HRM1) and 2 (HRM2) were chosen as depicted in **Figure 12**. Both *XAF1* HRM primer pairs covered three CpG sites. Primers previously published by Chen *et al.* were used for methylation specific PCR (MSP) [199].

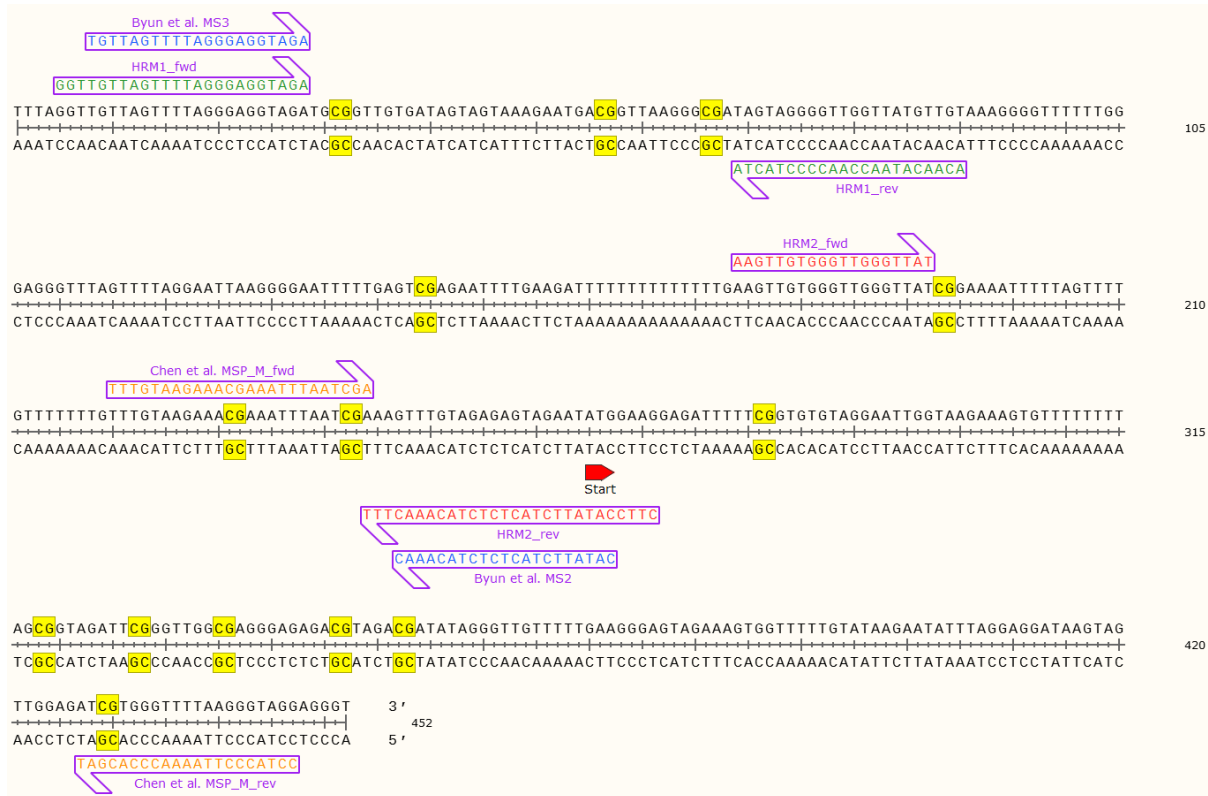


Figure 12: Bisulfite-converted DNA sequence of the *XAF1* promoter and transcription start site (red arrow) as excerpt from chromosome reference assembly GRCh38.p7. The *XAF1* gene is located at position 6755411..6775647 from where the sequence was retrieved. Primer binding sites for MSP primers (methylated template) and HRM primers are indicated. CpG dinucleotides are highlighted in yellow. The HRM1 primer pair upstream of the transcription start site was used for the analysis. In validation experiments HRM2 region was used to compare the methylation of both regions.

Analogously, HRM primers for *BIRC5* were designed on the basis of the same reference assembly (GRCh38.p7), extracting the region of 78214196..78225635 to analyze the promoter region reaching into the exon 1 of *BIRC5* commonly described as CpG island (**Figure 13**). For methylation analysis by MS HRM, HRM_fwd was used as forward primer in combination with HRM_rev2 as reverse primer containing 36 CpGs within the amplicon. The combination of HRM_fwd and HRM_rev1 was discarded due to low primer specificity.



Figure 13: Bisulfite-converted DNA sequence of the BIRC5 promoter and transcription site as excerpt from chromosome reference assembly GRCh38.p7. The BIRC5 gene is located at position 78214196..78225635 from where the sequence was retrieved. Primer binding sites for MSP primers (methylated template) and HRM primers are indicated. CpG dinucleotides are highlighted in yellow.

2.6.4 Generation of DNA methylation standards by in vitro methylation

Fully methylated DNA and unmethylated DNA was kindly provided by Olivier J. Switzeny. Genomic DNA was isolated from the buccal mucosa of a healthy donor and subjected to whole genome amplification (REPLI g Midi Kit, Qiagen) to generate the unmethylated standard DNA. CpG methylation of an aliquot of this DNA was performed with 400 U SssI methyltransferase and 640 μ M S adenosylmethionine according to the manufacturer's instructions (NEB) to generate the methylated standard. For a detailed description please refer to Switzeny *et al.* [200]. In vitro methylated and unmethylated DNA standards were then bisulfite converted, as described (see 2.6.2). To obtain 25 %, 50 % and 75 % methylation standards, bisulfite treated unmethylated DNA (0 %) and methylated DNA (100 %) were mixed in different proportions (3:1; 1:1 and 1:3).

2.6.5 Analysis methods for detecting methylation in bisulfite-treated DNA

Depending on the downstream method for analyzing bisulfite treated genomic DNA different approaches for primer design had to be followed. For MSP (see 2.6.5.1), primers covering CpG sites had to be used. Two primer pairs served for detection of either the methylated or unmethylated template. Primer sequences for MSP on *XAF1* and *BIRC5*, adopted from Chen *et al.* [199] and Wagner *et al.* [150], respectively. In contrast, only one primer pair was needed

Material & Methods

for each region of interest in MS HRM (see 2.6.5.2). Primers were designed to flank CpG sites, while not containing any within the actual binding site. Thereby, preferential binding to either the methylated or the unmethylated sequence was prevented, since C to T transitions resulting from bisulfite conversion did not affect primer DNA annealing. Optimal annealing temperatures were detected using a PCR gradient and are provided in the corresponding tables.

2.6.5.1 Methylation specific PCR (MSP)

MSP was carried out, using primer pairs (**Table 8**), detecting methylated or unmethylated template DNA. HotStarTaq Plus Master Mix Kit (Qiagen) was used for PCR, with 1 μ M forward and reverse primer and 40 ng of bisulfite converted genomic DNA. The initial denaturation step (5 min, 95 C) was followed by 35 cycles of denaturing (30 s, 94 °C), annealing (30 s, *BIRC5*: 61 °C/ *XAF1*: 57 °C) and elongation (15 s, 72 °C) with a final elongation step (10 min, 72 °C).

Table 8: Sequences of the methylation-specific primers used for MSP targeted at XAF1 and BIRC5. MSP primers specific for the unmethylated (UM) and methylated (M) template are provided.

Primer	Sequence (5'-3')	Length	T _m (°C)
<i>XAF1</i> MSP_M_fwd	TTTGTAAAGAAACGAAATTTAATCGA	25 mer	51
<i>XAF1</i> MSP_M_rev	CTCCATATTCTACTCTCTACAACTTT	28 mer	54
<i>XAF1</i> MSP_UM_fwd	TTTGTAAGAAATGAAATTTAATTGA	25 mer	48
<i>XAF1</i> MSP_UM_rev	CTCCTACCCTTAAAACCCACAAT	23 mer	55
<i>XAF1</i> Primers were previously described by Chen <i>et al.</i> [199].			
<i>BIRC5</i> MSP_M_fwd	TTCGGTATATTCGCGTCGT	20 mer	55
<i>BIRC5</i> MSP_M_rev	AACGTCGAAACACCCATACC	20 mer	56
<i>BIRC5</i> MSP_UM_fwd	GGTGTGGTGTGTGGGTGT	20 mer	59
<i>BIRC5</i> MSP_UM_rev	CCAACAAATCCCACAATTCA	20 mer	52

BIRC5 Primers were previously described by Wagner *et al.* [150].

Different annealing temperatures for MSP *BIRC5* and *XAF1* primers were tested in a temperature gradient using bisulfite treated gDNA of cell line LN308. **Figure 14** shows an exemplary agarose gel electrophoresis for *BIRC5* MSP. No band was observed for the M primer pair, whereas a specific band at ~200 bp (197 bp) was obtained for UM primers at all tested temperatures with no unspecific products. To increase primer binding specificity, for *BIRC5* M and UM a T_M of 61 °C was chosen and *XAF1* MSP was conducted at a T_M of 57 °C.

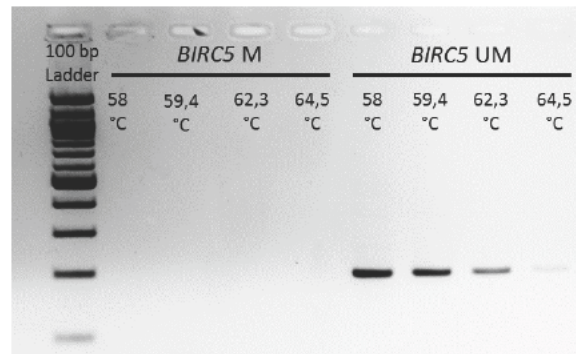


Figure 14: Amplification products of a gradient PCR with MSP BIRC5 primers using gDNA extracted from LN308 cells. Products were separated on a 1 % agarose gel.

2.6.5.2 Methylation sensitive high resolution melt analysis (MS HRM)

To allow a large, quantitative screening of patient samples and cell lines for methylation in the *XAF1* gene (and *BIRC5*), a high throughput method for methylation analysis was established. CpG flanking primers allowed the amplification of amplicons covering CpG putatively involved in gene regulation. Depending on the methylation status of these CpGs in the template gDNA, sequence differences were introduced by bisulfite conversion as described (see 2.6.2). Un methylated C are converted to T, causing weaker base base interactions in the corresponding A = T pairing, than in G ≡ C base pairs resulting from 5mC. These differences in the numbers of H bonds can be measured in high resolution melting analysis. Over a wide temperature range, the melting of the amplicons is monitored in high resolution (0.2 °C) which generates detailed melting curves for all samples, as show for *XAF1* HRM1 amplicon (**Figure 15**). Here, products for the amplification of *XAF1* using UM DNA (lower T_M) and M standard DNA (higher T_M) as template. Clear separation of both DNA templates was achieved during HRM.

Table 9: Different primer sequences used for MS-HRM targeted at *XAF1* and *BIRC5*.

Primer	Sequence (5'-3')	Length	T_m (°C)
<i>XAF1</i> HRM1_fwd	GGTTGTTAGTTTTAGGGAGGTAGA	24 mer	55
<i>XAF1</i> HRM1_rev	ACAACATAACCAACCCCTACTA	22 mer	54
<i>XAF1</i> HRM2_fwd	AAGTTGTGGGTTGGGTTAT	19 mer	51
<i>XAF1</i> HRM2_rev	CTCCATATTCTACTCTCTACAACTTT	28 mer	54
<i>BIRC5</i> HRM_fwd	GTTAGGTGTGGGTAGGGA	18 mer	53
<i>BIRC5</i> HRM_rev1	TAAAAAAAAAACTACCAAACAAAAA	25 mer	49
<i>BIRC5</i> HRM_rev2	ACCCTCCAAAAAAAACCAATTC	22 mer	53

Material & Methods

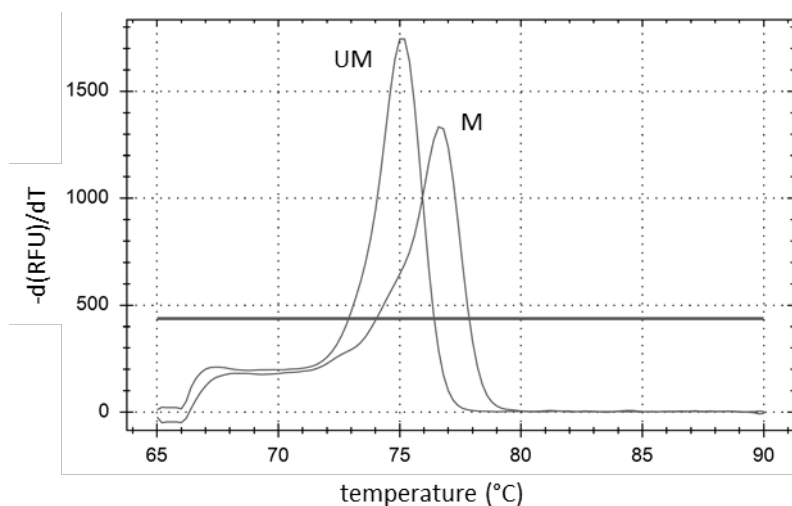


Figure 15: qPCR Melting curves for XAF1 MS-HRM1 amplicon for unmethylated (UM) and methylated (M) bisulfite-converted DNA standards as template.

qPCR was performed using a CFX96 Real Time PCR Detection System (Bio Rad) in 15 μ l preparations. 7.5 μ l 2x Precision Melt Supermix (Bio Rad) was used for amplification of 20 ng² bisulfite converted DNA with 400 nM fwd and rev HRM primer (**Table 9**). Amplification was started with an initial activation step at 95 °C, 2 min, followed by 45 cycles of denaturation (95 °C, 10 s), annealing (60.3 °C, 30 s), and at elongation (72 °C, 15 s) with a fluorescence read after every cycle. After the amplification cycles, the HRM step was performed as follows: 95 °C for 30 s, 60 °C for 60 s, heating up to 90 °C with detection of melt curves at a 0.2 °C increments. Appropriate annealing temperatures for specific primer binding were established in a temperature gradient. For cell lines and HGG tumor DNA analysis was performed in technical duplicates. Standards with a defined theoretical percentage of methylation (0 %, 25 %, 50 %, 75 %, 100 %) were amplified alongside the samples in every run for sample interpolation. These standards were generated by mixing methylated (M) and unmethylated (UM) DNA (see 2.6.4). For more accuracy of the HRM, the actual methylation of the standard DNA was determined for the XAF1 promoter by pyrosequencing. The methylation percentage of each of the three CpGs in the HRM1 region was determined (see 3.6.1). In brief, mean methylation for the XAF1 amplicon was 84.1 % for M DNA and 2.6 % for UM DNA. Correspondingly, the generated standards had methylation percentage of 23.0 % (3:4), 43.35 % (1:1) and 63.73 % (1:3). For sample interpolation, high resolution melting curves were then normalized to defined pre

² DNA amount of 20 ng represents theoretical amount assuming no loss of DNA during bisulfite conversion

melting and post melting areas, using the Precision Melt Analysis Software 1.2 (Bio Rad). These melting areas define the start of the melting process and are used for normalization. Normalized melt curves of XAF1 MS HRM1 amplification of standard DNA with theoretical methylation of 0 %, 25 %, 50 %, 75 % and 100 % are shown in **Figure 16** for technical duplicates each.

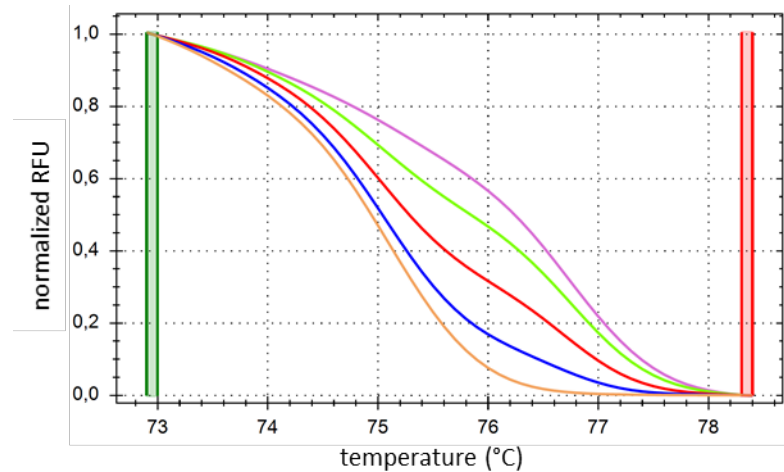


Figure 16: Normalized melt curves for XAF1 MS-HRM1 amplicon for methylation standards in technical duplicates for 0% (beige), 25% (blue), 50% (red), 75% (green) and 100% (violet) methylation level. The normalized relative fluorescence units (RFU) are plotted against the temperature.

Normalized relative fluorescence units (RFU) were then exported to Prism 6.0c for Mac (GraphPad Software) to calculate the area under the curve (AUC) of standard curves and samples. A linear regression analysis was performed ($R^2 \geq 0.98$) which allowed the interpolation of sample methylation values as percentage of methylation.

2.6.5.3 Bisulfite Pyrosequencing (PSQ)

Bisulfite converted gDNA was subjected to pyrosequencing for quantification of single CpG methylation values. Prior to sequencing, regions of interest were amplified by PCR optimized for pyrosequencing (PyroMark PCR, Qiagen). 12.5 μ l 2x PyroMark PCR Master Mix was used with 2.5 μ l CoralLoad Concentrate (10x), 280 nM fwd primer, 5' biotinylated rev primer for amplification of 20 ng DNA (**Table 10**). PCR mix was filled to 25 μ l with DNase free H₂O. After initial HotStarTaq activation (95 °C, 15 min), 45 cycles of denaturing (94 °C, 30 s), annealing (60 °C, 30 s) and elongation (72 °C, 30 s) was performed on a T100 Thermal Cycler (Bio Rad) with a final elongation step (10 °C, 72 min). PCR products were separated on an agarose gel for pre testing or analyzed by PSQ.

Material & Methods

20 µl of the PCR product were pipetted into a 96 well PCR plate and diluted with 20 µl DNase free water. 40 µl binding buffer (Qiagen) were added. To avoid sedimentation 3 µl Streptavidin Sepharose High Performance Beads (GE Healthcare) were added in the last step, before incubating under constant shaking for 5 min. Meanwhile, PSQ plate was prepared by dispensing 38.4 µl annealing buffer (Qiagen) and 1.6 µl sequencing primer (with 10 pmol/ µl) to each well. After the shaking, PCR products, bound to sepharose beads, were attached to a Vacuum Workstation (Qiagen). The system was kept under constant vacuum to avoid the loss of the sepharose beads. The beads on the preparation tool were washed by aspiration of 70 % EtOH for 5 s. To extract the anti sense strand with biotinylated 5' end only, sense strand was washed away by aspirating denaturation buffer (NaOH) for additional 5 s. A second washing step was performed and the prep. tool was carefully positioned over the PSQ plate. Pressure was released from the system slowly and each nozzle was dipped in the corresponding well of the PSQ plate, thereby releasing the biotinylated anti sense strands. Before sequencing, the sequencer cartridge was filled with all four ddNTPs (A, T, C, G), enzyme mix and substrate mix (PyroMark Gold Q96 Reagents, Qiagen) in appropriated amounts, as calculated by the PyroMark Assay Design Software 2.0 (Qiagen). Sequencing reaction was then performed on a PyroMark Q96 ID sequencer (Qiagen). Sequencing data was evaluated with Pyromark CpG Software (Qiagen).

Table 10: Primer sequences used for pyrosequencing.

Primer	Sequence (5'-3')	Length	T _m (°C)
IDH1_fwd	AAATATCCCCCGGCTTG	17 mer	52
IDH1_rev_biotin	TTGCCAACATGACTTACTTGATC	23 mer	59
IDH1_seqP	GGGTA AACCTATCATCATA	20 mer	52
IDH2_fwd	GTTCAAGCTGAAGAAGATGTGG	22 mer	55
IDH2_rev_biotin	TGTGGCCTTGTACTGCAGAG	20 mer	58
IDH2_seqP	AAGCCCATCACCATT	15 mer	47
XAF1 HRM1_fwd	GGTTGTTAGTTTTAGGGAGGTAGA	24 mer	55
XAF1 HRM1_rev_biotin	ACAACATAACCAACCCCTACTA	22 mer	54
NESmut_fwd	CGCTGTTGTTTTGATTTT	21 mer	47
NESmut_rev	CCAATACATACAATTTTGTT	21 mer	50
NESmut_SeqP	TTTCTGTCAAGAAGCAGT	18 mer	49

2.7 Sequencing

2.7.1 Pyrosequencing

PSQ of gDNA targeting *BIRC5* NES mutations was performed according to the bisulfite PSQ protocol (see 2.6.5.3), with up to 500 ng of non bisulfite converted DNA. Primer annealing in the PyroMark PCR was performed at 56 °C. Primer sequences are provided in **Table 10**.

2.7.2 Sanger-Sequencing

Purified plasmid DNA were sent to StarSEQ GmbH (Mainz) for sanger sequencing with and standard T7 and SP6 primers and designed primers for sequencing of the plasmid backbone in subsequent reads (primer walking) (**Table 11**). Chromatograms were retrieved as raw data, and base calling was performed using the SnapGene Software (trial version) 3.1.2 (GSL Bio tech, Chicago, IL). Overlapping T7 and SP6 reads were aligned using this software.

Table 11: Primer sequences used for Sanger sequencing.

Primer	Sequence (5'-3')	Length	Tm (°C)
T7	standard primer (StarSEQ GmbH)		
SP6	standard primer (StarSEQ GmbH)		
P1	GCATCACTCACGGCATGG	18 mer	58
P2	GCCGATTTCGGCCTATTGGT	20 mer	59

2.8 Immunofluorescence

Expression, localization and foci formation of different proteins of interest were analyzed by immunofluorescent staining with appropriate primary and fluorochrome conjugated secondary antibodies (**Table 12**). Techniques for imaging of stained fixed cells and FFPE tumor tissue sections, and living cells, respectively, are described subsequently.

Table 12: List of primary and secondary antibodies (Ab) used for immunofluorescence and immunohistochemistry. (abbr.: rb. rabbit; m. mouse; d. donkey; g. goat; mAb. monoclonal antibody; pAb. polyclonal antibody)

Antibody	Host/ re-activity	Provider (cat.-no.)	IF ¹ dilutions	IHC ² dilutions
primary antibodies				
Survivin	rb. pAb.	Cell Signaling Technology (#71G4)	1:1000	1:400
XIAP	m. mAb.	Becton Dickinson (#610716)	-	1:50
γH2AX (S139)	m. mAb.	Millipore (#JBW301)	1:1000	-
53BP1	m. mAb.		1:1000	-
Rad51	r. pAb.	Abcam (#638019)	1:1000	-
secondary antibodies				
anti-mouse-Cy3	g. pAb.	Dianova (#115165146)	1:1000	-
anti-rabbit-488	g. pAb.	Invitrogen (A-11008)	1:1000/2000	-
anti-mouse-488	g. pAb.	Invitrogen (A-11017)	1:1000	-
: diluted in 1:1000 in PBS + 0.25 % Triton X-100; ² : diluted in PBS + 2 % BSA + 0.1 % TritonX 100				

2.8.1 Immunofluorescence staining of fixed cells for foci detection

To study DNA damage associated formation of DNA repair foci of repair proteins, Ab against γH2AX, 53BP1, and Rad51 were used. The cells were seeded on sterilized cover slips in 35 mm cell culture dishes. Appropriate cell numbers were seeded, depending on different time points, and incubated for 48 h before treatment. Cells were fixed after the indicated treatment period. For fixation, medium was aspirated and the cell monolayer was washed with PBS once. 1 ml 4.5 % formaldehyde in PBS solution (Roti® Histofix 4,5 %, Carl Roth) was added under a fume hood and incubated for 15 min at RT. After washing (PBS), cells were covered in 1 – 2 ml ice cold MeOH and kept for 10 min at 20 °C. For rehydration samples were washed with PBS for 3 x 5 min. Blocking of unspecific intracellular antigens was performed with 40 μl PBS + 0.25 % Triton X 100 + 10 % normal goat serum (Thermo Scientific) that was dipped onto the cover slip and incubated for 1 h at RT. During this blocking step and all subsequent staining steps, the 35 mm were kept in a humidified incubation chamber to prevent drying. Blocking

solution was rinsed off with PBS and 40 µl primary Ab dilution in PBS + 0.25 % Triton X 100 was added onto the cover slip (γH2AX: 1:1000; 53BP1: 1:1000; RAD51: 1:5000). Staining was performed over night at 4 °C. Before secondary Ab was applied, cover slips were washed with PBS 2 x 5 min, rinsed with PBS_{high salt} (+ 0.4 M NaCl) and washed with PBS 1 x 5 min. After incubation of 40 µl of secondary Ab dilution (1:1000 in PBS + 0.25 % Triton X 100) for 1 h at RT in the dark, washing procedure was repeated. Nuclear DNA staining was achieved using 40 µl TO PRO 3 (10 µM in PBS, Thermo Scientific) for 15 min at RT. After washing with PBS, cover slips were mounted upside down on microscope slides using Vectashield Antifade Mounting Medium (Vector Laboratories Inc.) for preservation. Edges were sealed with nail polish (transparent) and foci and nuclear staining were visualized on a confocal laser scanning microscope: LSM 710 (Carl Zeiss GmbH) using a Plan Apochromat 63x/1.40 Oil DIC objective.

2.8.2 Immunofluorescence staining of fixed cells for detection of Survivin

A different fixation and staining method was applied for detecting Survivin's intracellular localization to avoid washing the protein out of the cytoplasm due to its small size. The cells were seeded and fixed with formaldehyde as described above. After fixation, the cover slips were washed with PBS for 3 x 5 min and blocking was performed (see 2.8.2). Incubation with Survivin rabbit mAb followed over night at 4 °C with 40 µl of a 1:1000 dilution. After the staining, washing was repeated (PBS for 3 x 5 min) and incubation with secondary Ab (1:2000; in PBS + 0.25 % Triton X 100) was carried out for 1 h at RT. Subsequent specimen preparation and visualization was performed as described above.

2.8.3 Immunofluorescence staining of FFPE tumor sections (IHC)

For immunohistochemistry (IHC) of FFPE tumor sections, specimens had to undergo deparaffinization and epitope retrieval. Sections, mounted on a microscopic slide, were pre heated at 60 °C for 30 min in an incubator. Afterwards, the tissue specimens were incubated in xylene 3 x 5 min, followed by an ethanol series (100/ 100/ 96/ 90/ 80/ 70 % EtOH) with an incubation time of 5 min each. Rehydration was carried out by rinsing the sections 2 x in H₂O_{dest} and 1 x in PBS. Specimen were incubated in pre heated citrate buffer (Target Retrieval Solution, Dako GmbH, Hamburg) in a steamer for 20 min. For additional 20 min, the samples were then allowed to cool down at RT. After rinsing 2 x in PBS, the sections were subjected to immunoflu

Material & Methods

orescent staining. To reduce the amount of Ab needed, tumor areas on the slide were encircled with a water repelling pen (Dako Pen, Dako GmbH) and blocked for 3 h with blocking solution (Dako GmbH) in a humidified chamber at RT. Antibodies used for detection are listed in **Table 12**. Incubation with anti Survivin mAb (1:400) or anti XIAP mAb. (1:50) diluted in PBS + 2 % BSA + 0.1 % TritonX 100 followed after one washing step of 5 min PBS over night at 4 °C. On the following day, Ab solution was washed off (3 x 10 min with PBS + 0.1 % Tween 20), before incubating with secondary goat anti rabbit 488 in PBS + 2 % BSA (1:500) for 2 h at RT (dark). Samples were washed again (3 x 10 min with PBS + 0.1 % Tween 20), rinsed 1 x in PBS, stained with TO PRO 3 (1:100) for 30 min and preserved with Vectashield Antifade Mounting Medium (Vector Laboratories Inc.) under a cover slip. Edges were sealed with nail polish (transparent). Tissues were visualized on an LSM 710 (Carl Zeiss GmbH) using an EC Plan Neofluar 10x/0.3, or C Apochromat 40x/1,2 W Korr M27 objective.

2.8.4 Live cell imaging

For live cell imaging cells were seeded in 4 well Tissue Culture Chambers (Sarstedt, Nümbrecht) with cover glass bottom for high resolution microscopy. For imaging, medium was replaced with appropriate supplemented medium without phenol red. At the time points indicated, images were acquired on an LSM 710 (Carl Zeiss GmbH) using a Plan Apochromat 63x/1.40 Oil DIC objective. LN229 Surv GFP and LN229 SurvNESmut GFP cell clones were analyzed for intracellular localization of the Surv GFP fusion protein.

2.9 Survival analysis & statistics

2.9.1 HGG patient's cohort

Tumor material was obtained from high grade glioma patients (first diagnosis) treated at the Department of Neurosurgery of the University Medical Center Mainz (Germany), between February 2011 and June 2013. Tumor specimens were obtained by resection, performed before the initiation of treatment and were FFPE immediately. Tumor FFPE sections were prepared at Institute of Neuropathology of the University Medical Center Mainz and were evaluated by a neuropathologist (Prof. Dr. C. Sommer) in hematoxylin and eosin (HE) stainings. Based on the tumor histology, the tumors were assigned to AA, OA, and AOA or GB of the

WHO grade III or IV, respectively. Furthermore, tumor areas haven been demarked from normal tissue. GB patients in appropriate postoperative clinical condition underwent combined radio and TMZ based chemotherapy according to Stupp *et al.* [19,201]. Patients with anaplastic gliomas received treatment according to the findings of the NOA 04 study [202,203].

2.9.2 Ethics statement

All patients provided a written informed consent prior to data assessment, and the study was approved by the institutional ethics committee of the University Medical Center Mainz.

2.9.3 Kaplan-Meier Survival estimates & Correlations

IBM SPSS Statistics version 23 was used for managing the patient's data and to calculate survival curves according to Kaplan Meier for the endpoints of experiencing a progress (PFS) or death (OS) with case censoring [204]. To compare different patient groups, survival curves were dichotomized for different parameters, e.g., *XAF1* status or *IDH1* mutation. Test for statistical significance of the group differences, was determined by Log rank test (Mantel Cox). Data was exported to Prism 6.0 to plot the graphs.

2.9.4 Bivariate correlations

For analyzing bivariate correlations of different nominal parameters, e.g. for the correlation matrix provided in **Table 21**, Spearman's rank correlation coefficient (r_s or ρ) was calculated using SPSS. Statistical significance was determined in a two tailed approach using SPSS's standard test for r_s . For analyzing bivariate correlations of metric parameters, e.g. methylation values determined by HRM vs. methylation values determined by pyrosequencing, were calculated with Pearson's product moment correlation coefficient (R). Statistical significance was determined in a two tailed approach using SPSS's standard test for R.

Material & Methods

2.9.5 Statistical hypothesis testing

Tests for statistical significance of the observed results were performed with appropriate statistical methods using Prism 6.0. The null hypothesis was rejected upon p values below 0.05 (*). Lower p values are indicated with asterisks: 0.01 (**), 0.001 (***), 0.0001 (****). For values above 0.05, the null hypothesis was not rejected and differences are indicated as not significant (ns).

Normal distribution was assumed for the conducted experiments. Comparing the means of two unmatched samples, Student's unpaired t test was used. To compare three or more unmatched groups One way ANOVA was carried out. Two way/ two factor ANOVA was used to test a response depending on the factors, e.g., cell cycle phase and knockdown. Multiple comparison post hoc testing for One way and Two way ANOVA are indicated in the particular experiment. All p values were calculated in two tailed tests.

2.10 Assays for determining DNA repair

2.10.1 DNA-dependent protein kinase assay

For quantification of the DNA dependent protein kinase (DNA PK) activity SignaTECT DNA PK assay system (Promega) was used. This assay uses radioactively labeled [γ 32 P] ATP (PerkinElmer) for transferring 32 P to a p53 derived peptide substrate by DNA PK. Due to the relatively short half life of 32 P, radioactivity had to be ordered separately for each assay performed. The biotinylated substrate is captured on a streptavidin matrix (SAM2[®] Biotin Capture Membrane) and radioactivity is then measured in a liquid scintillation counter (Canberra Packard Central Europe). Two cell pellets were generated for each treatment/ time points. For analysis of the DNA PK activity, nuclear extracts were prepared with lysis buffer 1 (see 2.3.1). The cell pellet was resuspended in lysis buffer 1 with 0.5 % NP 40, containing protease inhibitors. For cell lysis, the suspension was incubated on ice for 5 min and then centrifuged (5 min, 3200 rpm, 4 °C). Supernatant was discarded. To retain functionality of the DNA PK catalytic subunit (CS) nuclei were resuspended in lysis buffer 1 (without NP 40) to get rid of remaining detergent. After centrifugation (5 min, 3200 rpm, 4 °C), nuclei were resuspended in 100 ml extraction buffer (20 mM HEPES, 450 mM NaCl, 0.2 mM EDTA, 25 % glycerol). Protease inhib

itors were added freshly to the extraction buffer (0.5 mM DTT, 0.5 mM PMSF and 1 x Complete (Roche)). Samples were then subjected to 5 repeated freeze thaw cycles between liquid N₂ and 37 °C. After centrifugation (5 min, 18407 g, 4 °C), the cleared supernatant was then analyzed for total protein amount by Bradford protein assay. No DNA PK activator (calf thymus DNA) was used for this experiment (refer to the manufacturer's protocol), since the removal step of endogenous DNA by treatment with DEAE sepharose was omitted. Thus, endogenous DNA was used as intrinsic activator of the DNA PK enzyme, instead of an artificial activator of DNA PK.

All subsequent working steps were performed under adequate radiation protection measures for the work with beta emitters in a laboratory designated for radioactive working. An assay reaction mix was prepared as follows:

Reaction mix	Volume
DNA PK control buffer	2.5 µl
5X Reaction buffer	5.0 µl
DNA PK Biotinylated peptide substrate	2.5 µl
BSA (10 mg/ ml)	0.2 µl
[γ ³² P] ATP mix*	5.0 µl

*containing 4.5 µl 0.1 mM ATP + 0.5 µl [γ ³²P] ATP

The reaction mix was pre incubated at 30 °C for 5 min. According to the enzyme sample with the lowest total protein concentration, remaining samples were adjusted to the same amount of protein in 9.75 µl maximum volume. Enzyme dilution buffer was prepared, using 1X Reaction buffer with a final BSA concentration of 0.1 mg/ ml. 9.75 µl enzyme sample were incubated with 15.2 µl of Reaction mix for 5 min at 30 °C. Upon termination with 12.5 µl termination buffer, samples were kept on ice before being spotted onto a prenumbered streptavidin membrane square (provided). Several washing steps of the membrane were performed to rinse off excess free [γ ³²P] ATP and non biotinylated proteins under repeated shaking:

- 1 x 30 s with 100 ml 2 M NaCl
- 3 x 2 min with 100 ml 2 M NaCl
- 4 x 2 min with 100 ml 2 M NaCl + 1 % H₃PO₄
- 2 x 30 s with 100 ml deionized water

Material & Methods

Radioactive waste was collected according to general regulations. After washing, the membrane was allowed to dry at RT for 30 – 60 min. Membrane squares were separated and transferred into vials for liquid scintillation, filled with 2 ml scintillation cocktail (Rotiszint, Carl Roth). Radiation in each sample was detected as counts per minute (CPM) on a liquid scintillation analyzer with 3 min counting time.

2.10.2 Homologous Recombination assay

A non radioactive, real time PCR based approach was chosen for quantification of the HR activity in different cell clones and under Survivin knockdown, respectively. Homologous recombination assay kit (Norgen Biotek Corporation) was used for measuring the efficiency of HR. Upon co transfection of two plasmids, intermolecular recombination may generate a characteristic recombined plasmid due to inherent homologies of the plasmids. After DNA isolation, the abundance of this recombination product can be quantified with by real time PCR.

Cells were seeded in different densities to avoid confluency at later time points. 12 h before the end of the incubation period (e.g. the treatment with TMZ or Survivin knockdown), cells were transfected with the HR assay plasmids using Effectene transfection reagent (Qiagen) according to the manufacturer's protocol (24 well). For positive control 0.5 µg positive plasmid was used for transfection. Samples were transfected with 0.5 µg DL 1 and 0.5 µg DL 2 plasmid to test HR efficiency. Negative controls were transfected with 0.5 µg of either plasmid. After 12 h of incubation, the (plasmid) DNA was isolated from the transfected cells by PCI extraction (see 2.6.1). In brief, cells were lysed in the 24 well plate, using 300 µl TE9 buffer, with freshly added SDS (1 %) and 182.5 µg proteinase K, for 3 h at 48 °C under constant shaking (500 rpm). The additional incubation with proteinase K was omitted. The cell lysate was then transferred to a 1.5 ml reaction tube and subsequent steps were performed as described already, starting by adding the PCI solution. The isolated DNA was resuspended in 25 µl DNase free H₂O and DNA concentration and purity was determined by UV spectrophotometry.

For detection of the relative plasmid quantity qPCR was carried out with 2 µl primers³, 10 µl GoTaq qPCR Master Mix 2x (Promega) and 50 ng DNA diluted in 8 µl. Following qPCR protocol was used for amplification:

Step	°C	min	cycle
1	95	3:00	
2	95	0:15	
3	61	0:30	40x
4	72	1:00	
detection of fluorescence			
detection of melting curves			

The abundance of the backbone plasmids was determined using the “universal primers” and served as normalization. “Assay primers” allowed the detection of the recombined plasmid only. C_T values were not detectable for the NTC, while the positive control showed the highest abundance of the recombined plasmid. C_T values were exported to Excel (Microsoft) and the HR efficiency was calculated as normalized fold expression according to the $\Delta\Delta C_T$ method [197]. The C_T of the untreated control served as calibrator to calculate ΔC_T . ΔC_T of the recombined plasmid samples (assay primers) were then normalized to the ΔC_T of the backbone plasmids (universal primers):

$$\Delta\Delta C_t = \frac{2^{C_{t(\text{Con AssayPrimer})} - C_{t(\text{Sample AssayPrimer})}}}{2^{C_{t(\text{Con UnivPrimer})} - C_{t(\text{Sample UnivPrimer})}}}$$

³ concentration not specified by the kit's manufacturer

3 Results

To initiate this project, transgenic cell lines with overexpression of Survivin were generated based on the glioblastoma cell line LN229 (see 3.1). This model allowed the analysis of the influence of Survivin's expression and localization on different cellular endpoints upon treatment with cytostatic drugs involved in the treatment of gliomas. Furthermore, the clinical relevance of Survivin localization in glioma patients was analyzed. Results regarding the analyses of survival, cell death, senescence, DNA damage, DNA repair are summarized in chapters 3.3 and 3.4. Data describing the clinical implications of the epigenetic regulation of Survivin and the tumor suppressor XAF1 are presented in chapters 3.5 and 3.6, respectively. Here, the epigenetic silencing of both factors was analyzed in glioma cell lines and HGG patient samples.

3.1 Cell model

A glioblastoma cell model was established to investigate the influence of the IAP member Survivin on cellular processes like apoptosis, necrosis, senescence, and DNA repair. LN229 cells were either stably transfected with a plasmid carrying the CDS of *BIRC5* as wild type (wt) copy or as mutated Survivin variant (Survivin NESmut) with two inactivating mutations in the NES. To track cellular changes of the distribution of Survivin, both variants were fused to an eGFP tag (further named GFP). Utilizing this glioblastoma cell model, the influences of Survivin overexpression and especially its subcellular localization on the response to an anticancer therapy was investigated.

3.1.1 Stable expression of a Survivin-GFP fusion protein in glioblastoma cells

Different clones positive for both selection markers (neomycin resistance and puromycin resistance) were analyzed for expression of the Surv GFP fusion protein. Western blot revealed several stable cell clones with overexpression of Surv GFP. Cell clones "D6", "9b", and "5a" showed the strongest expression, while Surv GFP was found moderately expressed in "C1" and "A2", while being expressed at low level in "C4" and "C2" clones (**Figure 17**, upper panel). "D6" was selected for further analysis and is labeled "LN229 Surv GFP" if not stated otherwise. For reasons of clarity, parental cell line LN229 is plotted as control in the presented experiments. A comparison between LN229 cells and transfection control (LN229 con) transfected with empty pSV2_neo + empty pSuper plasmids is provided in the supplemental material

(Suppl. Figure 2 – 3). No differences in cellular survival, the induction of apoptosis, or DNA damage (except for 72 h, where DNA damage was higher in LN229 con, see Suppl. Figure 2) was observed between parental cells and cells transfected with the empty plasmids.

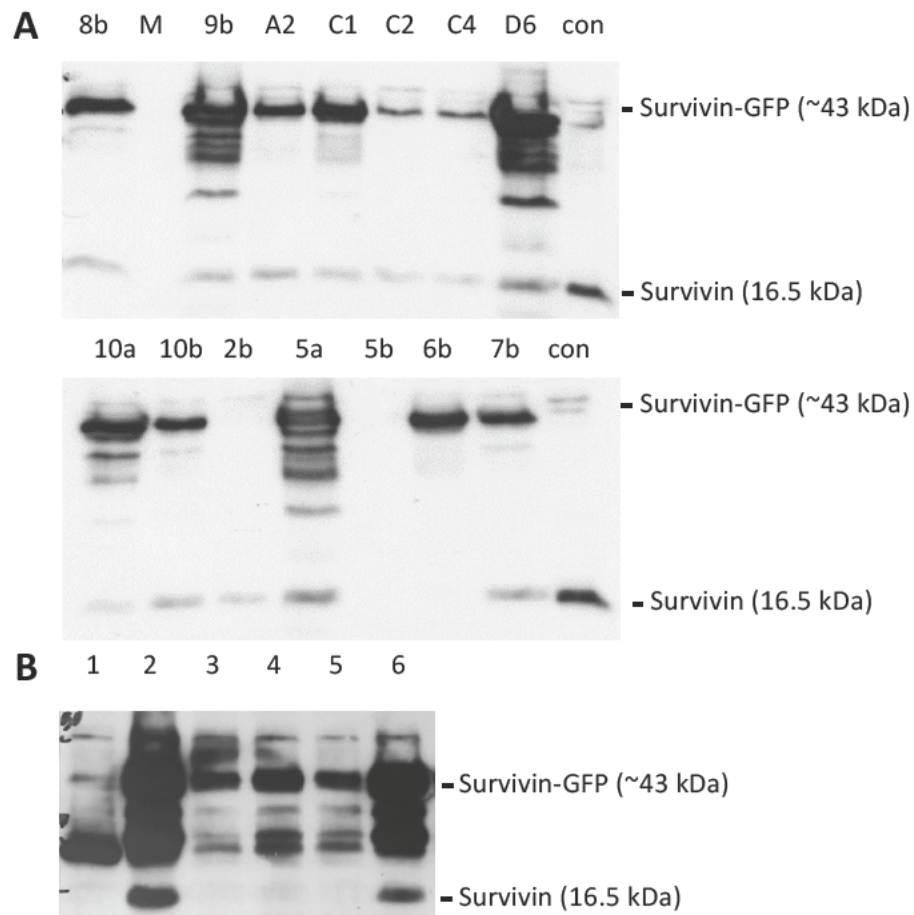


Figure 17: Western blot detection of endogenous Survivin (16.5 kDa) and Survivin-GFP (~43 kDa) in cell extracts from different Surv-GFP cell clones and untransfected LN229 cells (con). Survivin protein levels were analyzed in (A) Surv-GFP transfected and (B) SurvNESmut-GFP transfected cells. 20 μ g total protein were loaded for each sample. Signals were detected using ECL.

Analogously to Surv GFP expressing clones, cell clones with expression of NES deficient Survivin were selected among different positive clones (Figure 17, lower panel). LN229 SurvNESmut GFP (clone “2”) was chosen for further experiments, as this cell clone showed a strong, stable overexpression of the protein. A comparison of all three selected clones with parental LN229 cells is shown in Figure 18. While LN229 cells do not show a signal at the molecular weight of the Survivin GFP fusion protein (43 kDa), a strong protein expression is seen in LN229 Surv GFP and LN229 SurvNESmut GFP. The Surv GFP cell clone “C4” showed a moderate protein level. Endogenous Survivin is detected at 16.5 kDa in each cell line.

Results

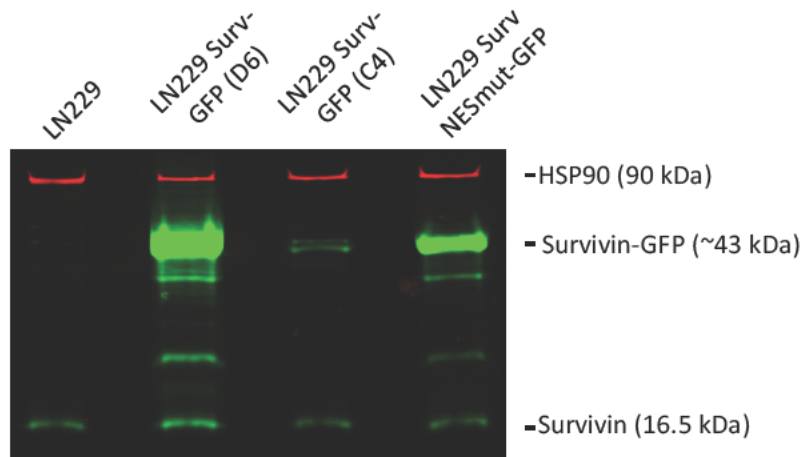


Figure 18: Western blot for the selected Surv-GFP cell clones and LN229 SurvNESmut-GFP cell clone used for further experiments. Signals were detected on the Odyssey infrared imaging system (LI-COR), using anti-mouse Ab for detection of HSP90 (red) and anti-rabbit Ab for detection of Survivin (green).

To confirm the impact of the NES mutations L96A and L98A on the subcellular distribution of the Survivin GFP fusion protein, the localization of both, the wt and mutated Survivin was analyzed by IF. Wild type Survivin was predominantly localized in the cytoplasm, showing a weak GFP signal in the nuclear compartment (**Figure 19**, upper panel). Strikingly, a nuclear trapping could be observed for cell clones expressing the NES deficient Surv GFP variant (lower panel). Here, more Survivin GFP was localized in the nucleus.

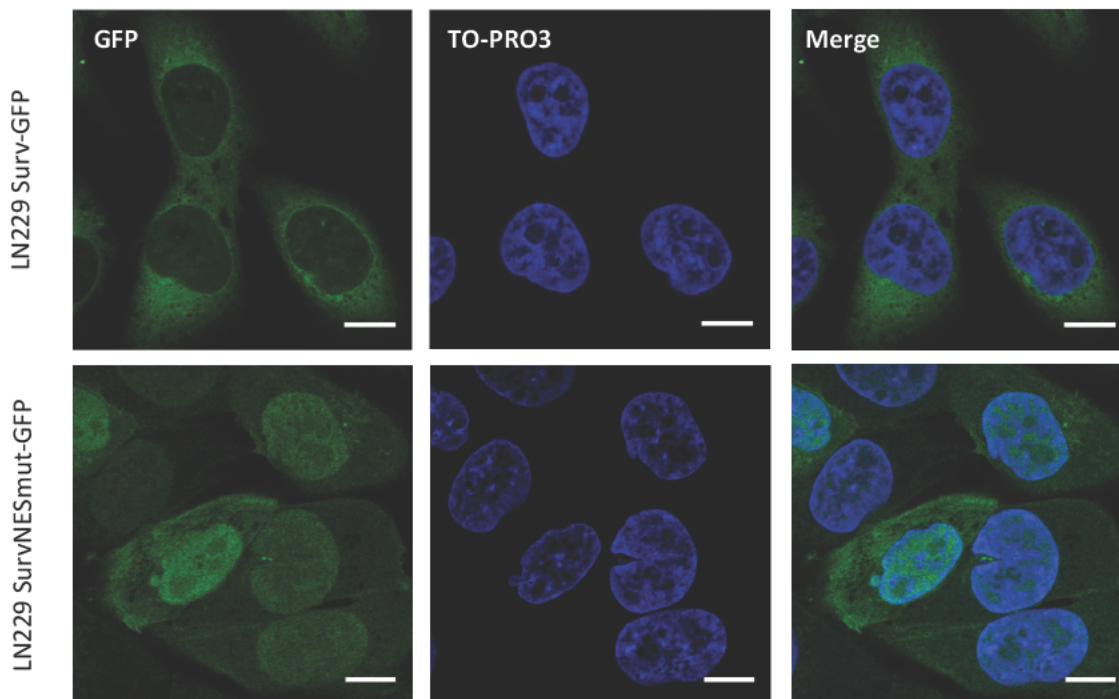


Figure 19: Immunofluorescence images of the selected FA-fixed cell clones with stable expression of SurvivinGFP-wt (upper panel) or SurvivinGFP-NESmut (lower panel). Nuclear staining was performed with TO-PRO3 (blue), and GFP fluorescence is shown in green. Scale bars equate 10 μ m.

3.1.2 NES-inactivating mutation in SurvNESmut-GFP clones

The identity of the mutational NES inactivation was further validated by sequencing of the SurvNESmut plasmid used for transfection. The alignment with *BIRC5* wt sequence (NM_001168.2) revealed both mutations at the anticipated site within the NES (**Figure 20**). One transversion and one transition in each codon caused the substitution of the unpolar amino acid leucine with the isofunctional alanine at positions 96 (L96A) and 98 (L98A), respectively.



Figure 20: Alignment of *BIRC5* CDS (NM_001168.2) and sequencing data obtained from sequencing of the pcDNA 3.1 SurvNESmut-GFP plasmid. Sequences were aligned with SnapGene (Trial Version).

3.1.3 Doubling time of Surv-GFP cell clones

Growth curves for the different cell clones were determined to check whether doubling time was altered due to the transfection of the Survivin plasmids. As the response to TMZ is strongly dependent on the rate of growth, this experiment was crucial to exclude a growth dependent effect. **Figure 21** shows the exponential growth curves for the parental cell line LN229, LN229 Surv GFP, and LN229 SurvNESmut GFP determined by flow cytometry. Derived growth equations were used to calculate doubling times given in **Table 13**.

Results

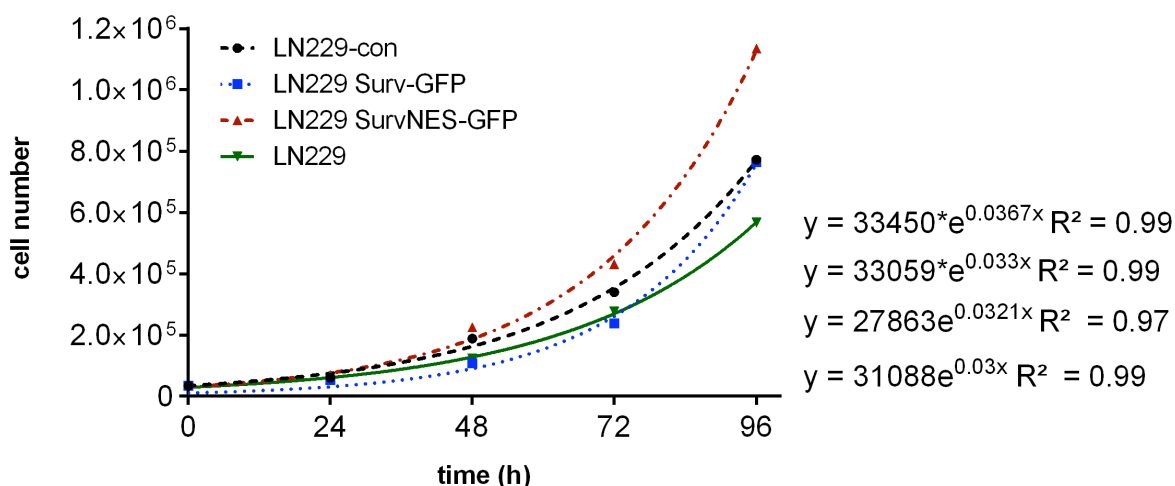


Figure 21: Growth curves for different LN229 cell clones determined by flow cytometry. The cell number determined every 24 h was used to calculate an exponential growth equation. Growth equations are provided from top to bottom, starting with the fastest growth.

The doubling time of the clones investigated was found to be within the same range. The overexpression of Survivin, especially of SurvNESmut, shortened the doubling time. This suggests a faster progression through the cell cycle, which would imply a slight growth advantage in these cells. The doubling time of SurvNESmut GFP cells was shortened by 4.2 h in comparison to LN229 cells.

Table 13: Doubling times (T2-T1) deduced from interpolated time-points for reaching cell numbers of 200000 (T1), 400000 (T2).

	T1 (h)	T2 (h)	T2-T1 (h)
LN229-con	54.5	75.5	21.0
LN229 Surv-GFP	61.4	82.9	21.6
LN229 SurvNESmut-GFP	48.7	67.6	18.9
LN229	62.0	85.1	23.1

3.2 Localization of Survivin in the response to anticancer drugs

To clarify whether Survivin changes its subcellular localization upon DNA damage, the localization changes were monitored via live cell imaging in LN229 Surv GFP cells. Additionally, localization of endogenous Survivin was determined in untreated glioblastoma cells. As discussed above, IR was reported to cause a nuclear accumulation of Survivin. Therefore, IR was used as positive control in the following experiments. To avoid long incubation periods for live cell imaging, the topoisomerase I inhibitor topotecan (TPT), used as second line therapeutic

drug, was used to follow changes upon chemotherapy. Both types of DNA damage were tested for their influence on Survivin's cellular distribution, while nuclear export inhibitor LMB served as second positive control to demonstrate a nuclear trapping of Survivin GFP.

3.2.1 Localization of Survivin-GFP upon CRM1-inhibition, TPT, and IR

LMB concentrations ranging from 0.5 to 20 nM were administered, and localization of Surv GFP was observed after 60 min upon treatment with the CRM1 inhibitor. At the highest concentration of 20 nM LMB, Surv GFP was equally distributed between the cytoplasmic and nuclear compartment (**Figure 22**). Concentrations of 5 nM and 1 nM led to an increased accumulation of the fusion protein in the nucleus. This demonstrates that the Surv GFP fusion protein is targeted correctly by CRM1 which shuttles the protein out of the nucleus. Upon specific inhibition of this exporter by LMB, a nuclear accumulation could be observed. In the following, the influence of TPT and IR on the localization of Survivin GFP was analyzed.

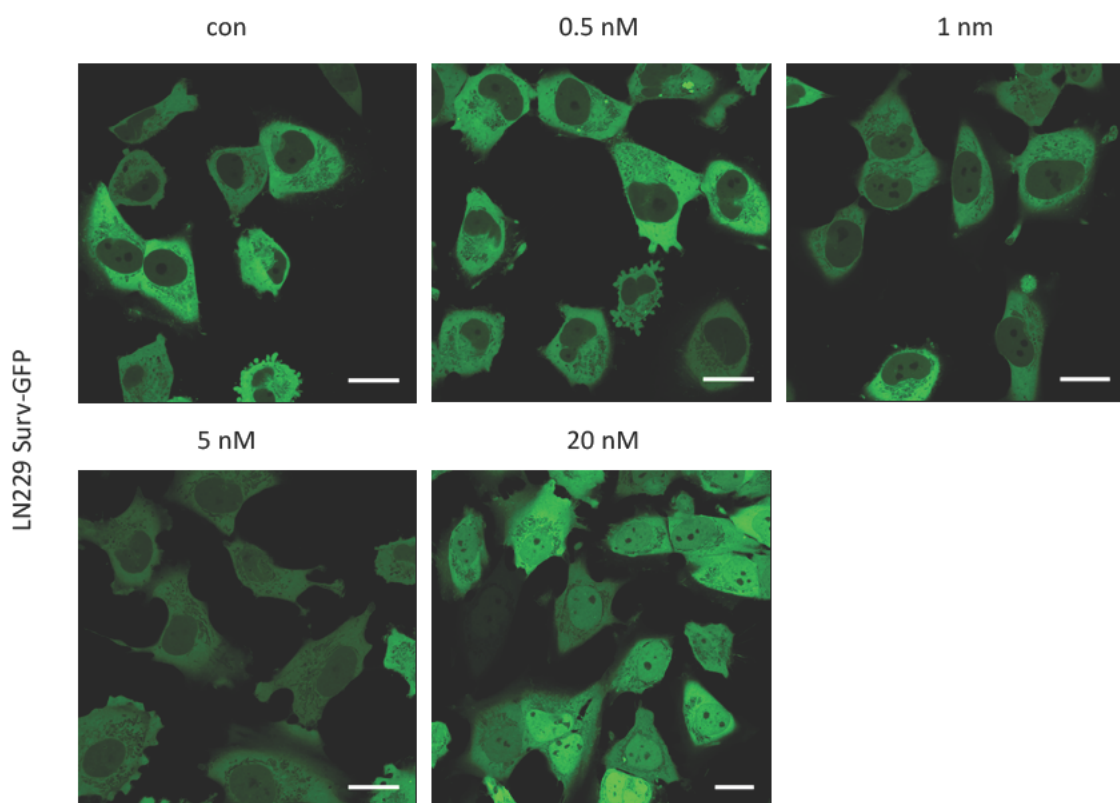


Figure 22: Live cell imaging of LN229 Surv-GFP cells 60 min after treatment with the CRM1 inhibitor LMB. GFP fluorescence is shown in green. Scale bars equate 20 μ m.

Results

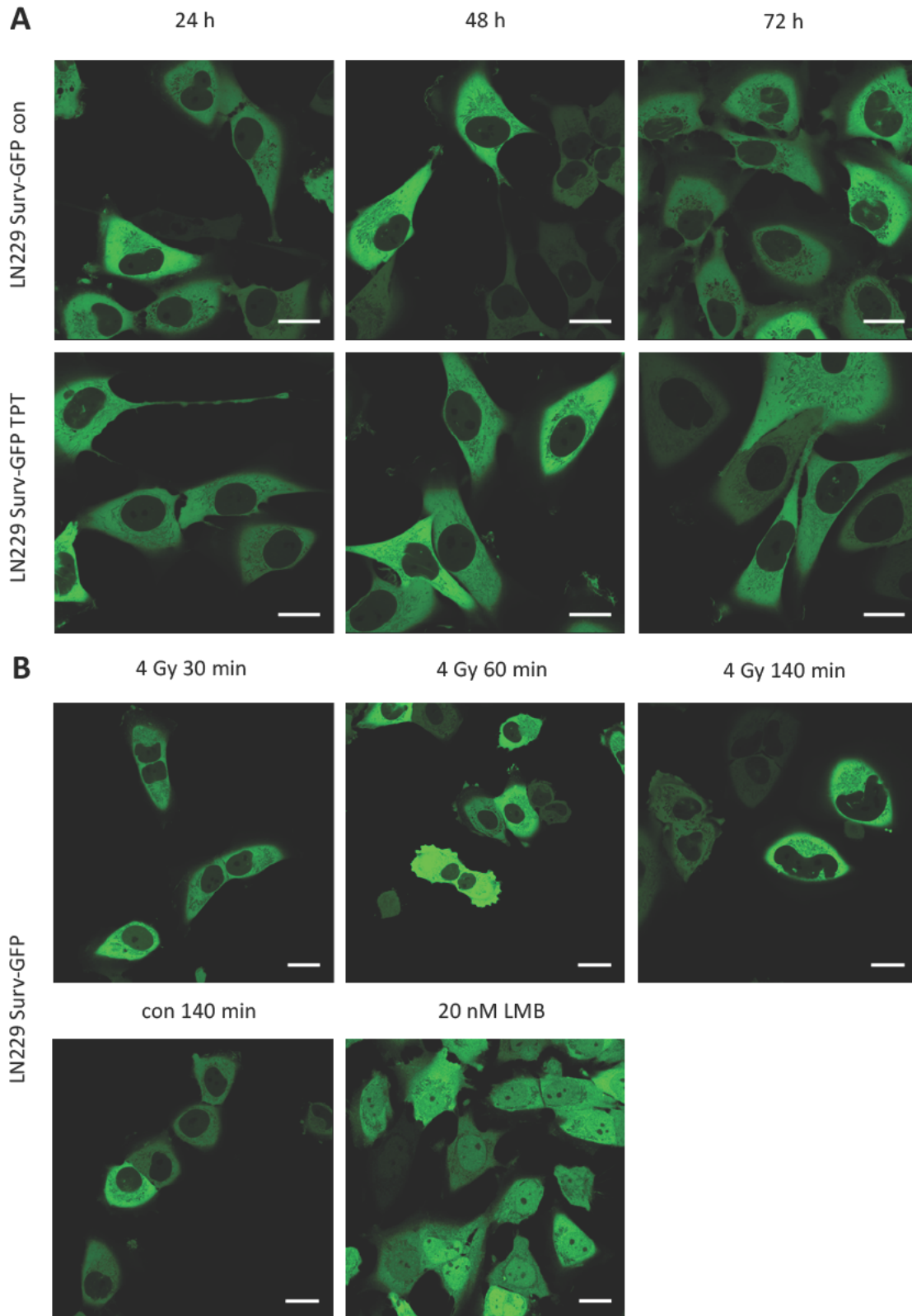


Figure 23: Live cell imaging of LN229 Surv-GFP cells at different time points after treatment with topotecan (A, TPT) or after irradiation (B). Treatment with 20 nM LMB was used as positive control. GFP fluorescence is shown in green. Scale bars equate 20 μ m.

To test whether therapy relevant DNA damaging stimuli can trigger redistribution of Survivin from the cytoplasm to the nucleus, LN229 Surv GFP cells were treated with TPT and IR in **Figure 23 A and B**, respectively. Neither for TPT nor for IR a change in the localization pattern of Surv GFP could be observed over the indicated time period, as determined by live cell imaging. The predominantly cytoplasmic subcellular distribution of Survivin did not change upon treatment. Thus, a nuclear accumulation could not be observed.

3.2.2 Localization of endogenous Survivin in glioma cell lines

In addition to the localization of the recombinant Surv GFP fusion protein, the localization of endogenous Survivin was investigated in GB cell lines (LN229, A172, and U87). Upon fixation, localization of Survivin was determined in untreated cells (**Figure 24**).

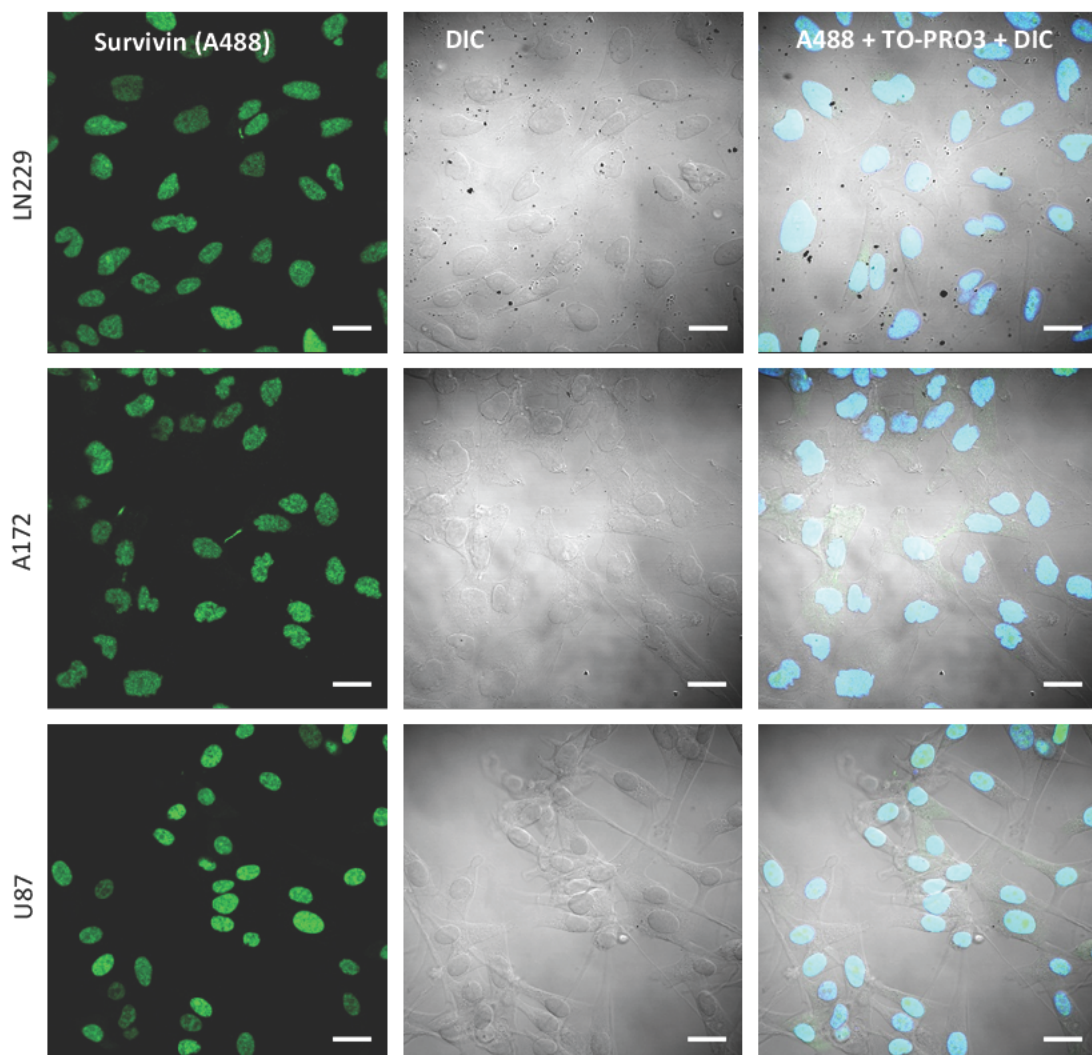


Figure 24: Immunofluorescence images of FA-fixed GB cells lines stained for Survivin (green). Nuclear staining was performed with TO-PRO3 (blue), and differential interference contrast (DIC) images were overlaid (grayscale) to visualize cell structures. Scale bars equate 20 μm .

Results

All cell lines showed a strong nuclear expression of Survivin. Differential interference contrast (DIC) images were acquired for a better visibility of the cytoplasmic dilatations. Interestingly, Survivin specific localization to the midbody could be observed in post mitotic cells (see center image of A172 and **Figure 25**). These structures reflect remnants of the mitotic apparatus. Amongst others, Survivin is localized to centromeres in prophase, kinetochores of the metaphase and anaphase spindle [205]. Thus, specificity of the antibody was specific for Survivin, which was additionally confirmed by single staining with the secondary Ab or Survivin Ab alone (data not shown).

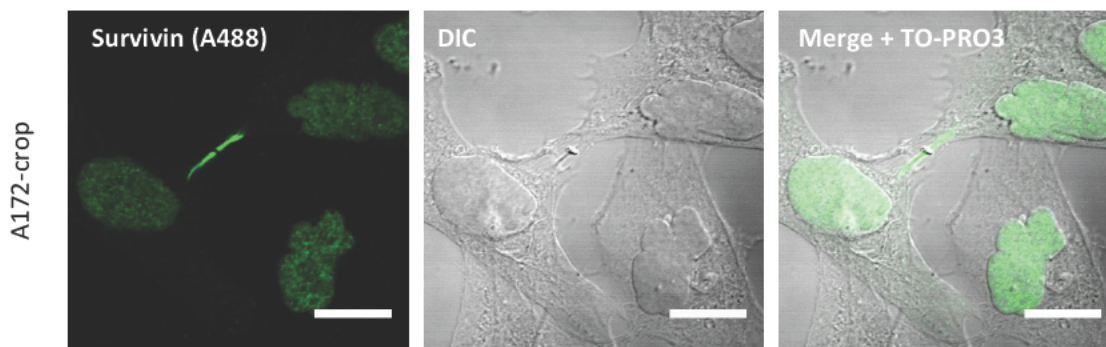


Figure 25: Immunofluorescence images of FA-fixed A172 cells (crop) stained for Survivin (green). Differential interference contrast (DIC) images were overlaid to visualize cell structures (grayscale). Scale bars equate 15 μ m.

3.2.3 Localization of endogenous Survivin after IR

To further consolidate the data regarding the localization of Survivin after genotoxic stress, endogenous Survivin was analyzed in LN229 cells exposed to IR (**Figure 26**).

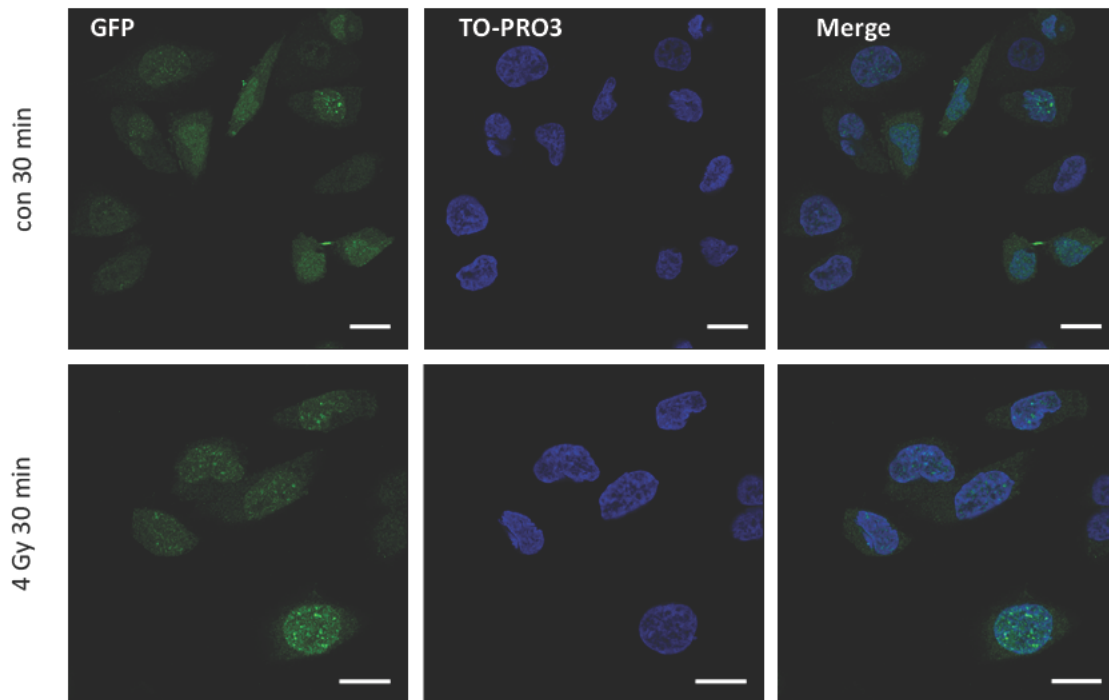


Figure 26: Immunofluorescence images of FA fixed LN229 cells stained for Survivin (green). Nuclear staining was performed with TO-PRO3 (blue). Cells were untreated (upper panel) or irradiated with 4 Gy. Fixation was performed after 30 min. Scale bars equate 20 μm .

In untreated LN229, Survivin was predominantly found in the nucleus as demonstrated already (**Figure 24**). Irradiation with 4 Gy did not cause any changes in the localization pattern of Survivin.

For validation of these findings, fractionated cell extracts were obtained from irradiated cells (4 Gy) and control cells after different time points. Western blot analysis of nuclear and cytoplasmic proteins is shown in **Figure 27**. The cell fractions were found to be highly pure, as minimal contaminations with the cytoplasmic protein HSP90 were detected in nuclear extracts, whereas nucleus specific Poly(ADP ribose) polymerase 1 (PARP 1) was detectable in the nuclear fraction only. The signal below the PARP1 detection band arises from the strong binding of the HSP90 Ab. However, at 113 kDa (black arrow) no PARP 1 signal could be detected in the cytoplasmic fraction. In these fractionated cell extracts no nuclear accumulation of Survivin was observed upon irradiation. Furthermore, endogenous Survivin seems to be

Results

predominately found in the nucleus, as the detected expression is stronger in all nuclear extracts, which reflects the localization determined by IF in untreated GB cells (**Figure 24**) and irradiated LN229 (**Figure 26**).

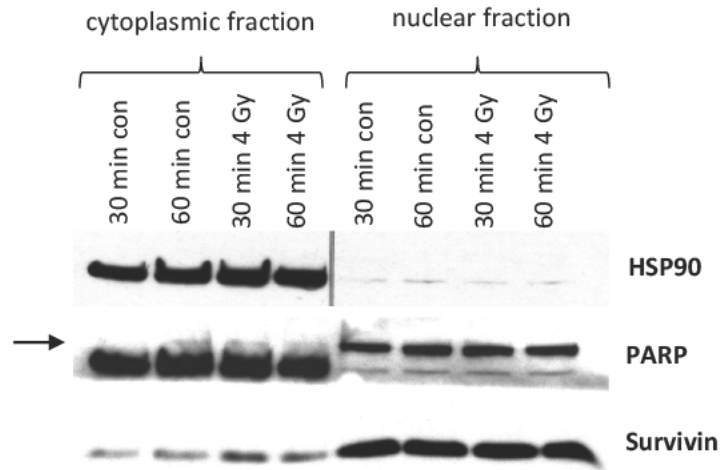


Figure 27: Western blot of fractionated cell extracts of LN229 cells. Cells were irradiated with 4 Gy and harvested after the time points indicated. HSP90 was used as cytoplasmic loading control, whereas nuclear loading control was PARP-1. Cytoplasmic cell fraction and nuclear fraction were analyzed separately. Signals were detected using ECL.

3.2.4 Localization of Survivin in high-grade glioma tumor sections

The clinical implications of the intracellular Survivin localization on the prognosis are discussed controversially. Some studies find an improved prognosis for tumors with predominant nuclear accumulation of the protein in tumor cells. As discussed earlier, other reports show the opposite. To test whether a differential localization of Survivin can be found in high grade gliomas, and whether this might correlate with survival, tumor sections were stained for Survivin by IHC. A representative staining of a 10 μm FFPE section is shown in **Figure 28**. Beside weakly stained cytoplasmic areas, a strong co localization of Survivin and nuclear TO PRO3 was observed. In concordance with the cell culture data, Survivin was mainly localized in the nucleus in all sections analyzed (N = 3). Overall, the localization pattern was homogenous in different areas of the tumor sections.

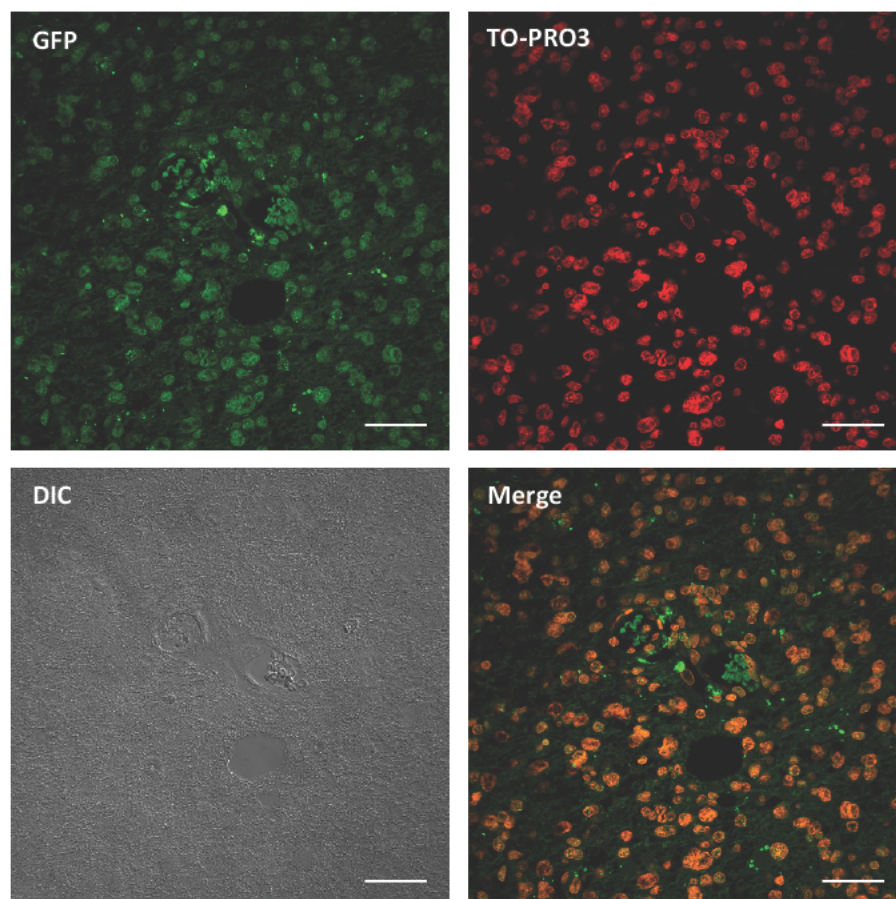


Figure 28: IHC of a FFPE tumor section of an anaplastic oligodendroglioma (grade III) stained for Survivin (green). Nuclear staining was performed with TO-PRO3 (red). Differential interference contrast (DIC) images were overlaid to visualize cell structures (grayscale). Scale bars equate 50 μm .

Results

3.2.5 Screening for NES inactivating somatic mutations in HGG tumor samples

In order to allow larger screening for differential Survivin localization in brain tumors, pyrosequencing for known mutations in the NES was performed. This should clarify whether NES mutations occur in HGG, and whether a link with patient's survival can be deduced. DNA isolated from high grade glioma samples was thus sequenced for specific mutations in the nuclear export sequence of *BIRC5*. Mutations annotated in **Figure 29** have been described to cause a nuclear accumulation in HNSCC. Pyrosequencing primers were set up to identify two NES inactivating transitions in genomic DNA at bp 278 T>C and bp 292 C>T as well as one silent transition in between (A288G).



Figure 29: Setup of PCR and pyrosequencing primers, covering inactivating mutations in the NES of *BIRC5*. Two transition mutations at position 278 and 292 and one silent mutation at position 288 were analyzed in HGG samples.

Primer specificity was verified by PCR with genomic DNA isolated from LN229 cells. At a T_M of 56.1 °C, a specific amplification of the 153 bp product was found (**Figure 30**). To ensure assay specificity, a PCR for a combination of rev primer and sequencing primer (SeqP) was run additionally, yielding the predicted 93 bp fragment.

After establishing the PCR conditions, pyrosequencing of 91 HGG DNA samples returned a reliable signal in 86 cases. Five samples were excluded from further analysis due to low sequencing quality. In total, all tumors showed wild type sequence of *BIRC5* (**Figure 31, A**). In some patients, a low percentage (< 13 %) of C to T transitions at position 292 and silent transitions at position 288 (A to G) was detected (**Figure 31, B**). However, transitions from T to C (position 278) could not be detected.

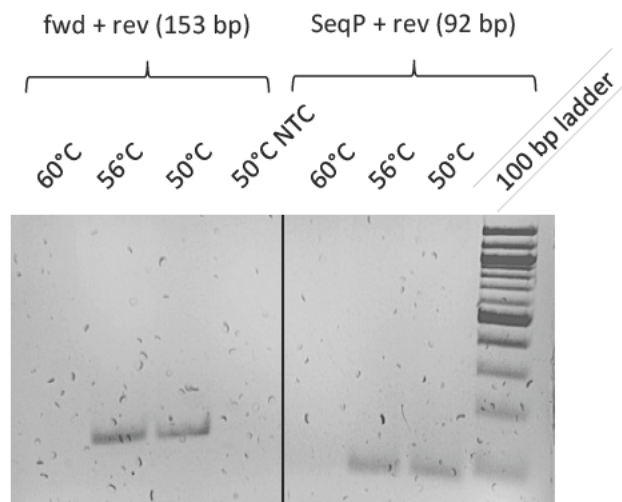


Figure 30: Agarose gel separation of PCR products of different combinations of SurvNESmut pyrosequencing primers. SurvNESmut fwd and rev primer were used for amplification (left side), and a combination of SurvNESmut sequencing primer (SeqP) and SurvNESmut rev primer was used additionally. Amplification products were separated on a 2 % agarose gel, stained with EtBR, and visualized on a UV transilluminator.

The SNPs found in some samples indicated a low frequency of the particular mutations. Assuming that only some tumor cells within the tumor might bear a *BIRC5* NES mutation, these patients were analyzed for peculiarities in the survival. Patients with a detected mutation frequency above 5 % were designated as “noticeable”, and Kaplan Meier survival curves were calculated (data not shown). No significant association between putative *BIRC5* NES mutations and survival, progression free survival, age, or tumor grade could be observed. Thus, the sequencing data support the in vitro experiments and IHC staining, showing that Survivin is mainly localized in the nucleus of glioma cells.

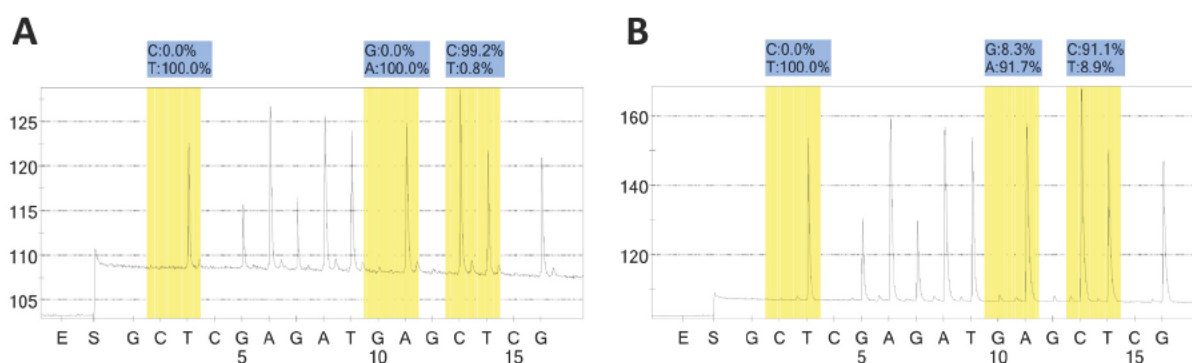


Figure 31: Pyrosequencing results for detection of NES mutations in HGG patient samples. (A) One patient sample (1221/12) showing wild type Survivin sequence is compared to (B) one patient sample (1739/11) showing deviations from wild type Survivin sequence.

3.3 Impact of Survivin expression and localization on the response to TMZ

To characterize the impact of Survivin expression and especially the influence of its localization on the response to TMZ induced genotoxic stress, different cellular endpoints were analyzed in Survivin expressing cell clones (see 3.1). In the background of Survivin (wt) and NES deficient Survivin expression, cellular survival, cell death, senescence, DNA damage, and DNA repair was analyzed.

3.3.1 Survivin protects glioblastoma cells from TMZ-induced cell death

The sensitivity of LN229 Surv GFP and SurvNESmut GFP cells towards anti cancer drugs, used in the therapy of glioma, was investigated by colony formation assay (CFA). All tested cell lines show a dose dependent reduction in the survival upon TMZ (**Figure 32 A**) and TPT (**B**). The LN229 Surv GFP clone was strongly protected against the treatment with both anti cancer drugs, when compared to LN229 SurvNESmut GFP and parental LN229 cells. At a higher concentration of 10 μ M TMZ, still 42.6 % of the LN229 Surv GFP cells survived. In contrast, only 13.8 % of the LN229 cells were able to form colonies. Most strikingly, the expression of SurvNESmut GFP even sensitized the cells (4.3 % survival). This effect was visible through the whole concentration range. Similar results were obtained for the treatment with TPT. Expression of Surv GFP strongly protected the cells, which was most evident at the highest concentration of 15 nM TPT. While being highly toxic for LN229 (4.8 %) and SurvNESmut GFP (0.8 %), still 46.0 % of LN229 Surv GFP cells survived the high dose (15 nM).

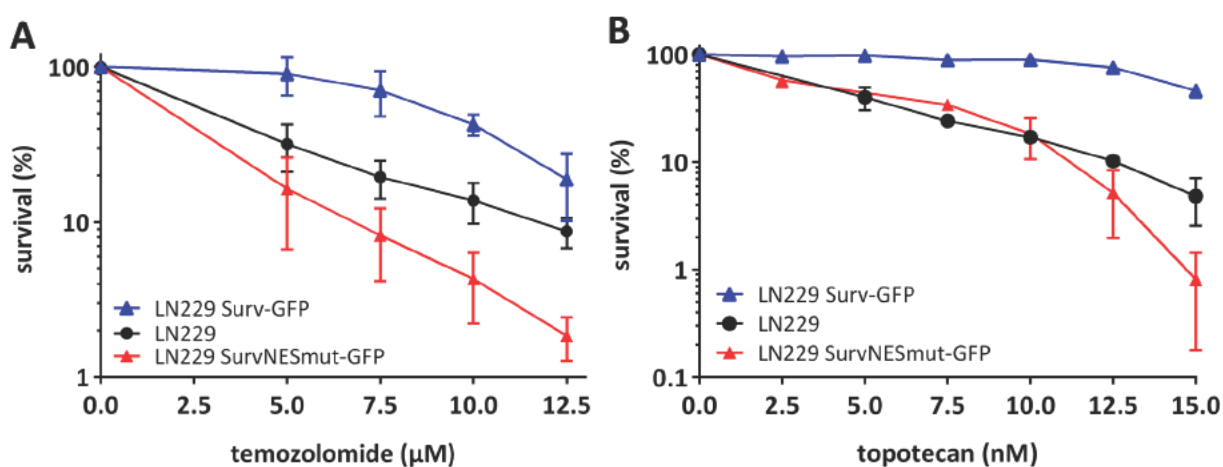


Figure 32: Colony formation assay (CFA) of Survivin cell clones for different concentrations of TMZ (A) and TPT (B). Surviving cells were normalized to control (%) and plotted in a semi-logarithmic graph. Data of at least two independent experiments in technical triplicates is shown ($N = 2$) with error bars indicating SD.

Besides, no striking differences could be observed for the survival curves of parental LN229 cells and SurvNESmut cells. At 15 nM, the survival of LN229 SurvNESmut GFP was worse in comparison to parental cells.

Additionally, survival was validated for selected TMZ concentrations (**Figure 33**). Due to a lesser cell number seeded for this colony assay (500 cells instead of 1000 cells), a lower overall survival percentage was achieved. Nevertheless, the survival data are in line with the data presented above. While the LN229 Surv GFP clone was protected from TMZ treatment at 2.5 and 7.5 μ M, LN229 SurvNESmut GFP cells showed the lowest survival, with parental survival percentages of LN229 cells lying in between.

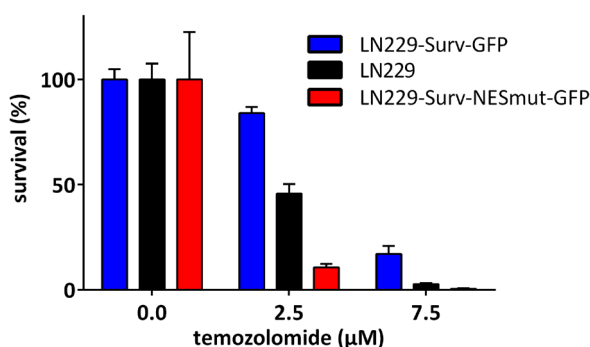


Figure 33: Colony formation assay of Survivin cell clones for selected concentrations of TMZ. Surviving cells were normalized to control (%) and plotted in a semi-logarithmic graph. Data of one experiment are shown ($N = 1$) with error bars indicating SD among triplicates.

3.3.2 Induction of apoptosis and necrosis in LN229 cell clones

As the Survivin's anti apoptotic properties are well described in the literature, apoptosis inhibition is one possible mechanism that might explain the strong survival differences in LN229 cell clones. To test whether this accounts for an increased survival of LN229 Surv GFP cells, levels of apoptosis and necrosis were measured by AnnexinV/ PI staining. The amount of apoptotic/ necrotic cells of the whole cell population was calculated as cell death above control (induced cell death). At 120 h, no significant differences could be determined (**Figure 34**). The apoptotic cell fraction was equal in case of LN229 and LN229 Surv GFP cells. Apoptosis in LN229 SurvNESmut GFP was slightly reduced, albeit the differences were not significant. Necrotic cell death was detectable in $\sim 8\%$ for all cell lines. At the later time point (144 h), parental as well as SurvNESmut expressing cells showed a slight induction of necrotic cell death, again not reaching statistical significance.

Results

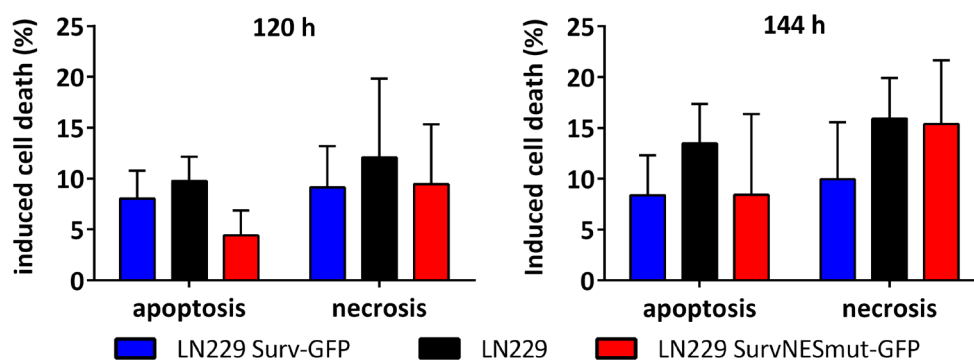


Figure 34: Induced apoptosis and necrosis in LN229 cell clones 120h and 144h after treatment with 100 μ M TMZ. Different cell populations were gated for AnnexinV-APC/ PI positivity.

3.3.3 Activation of Caspase 3/ 7 in LN229 cell clones

Furthermore, activation of effector caspases 3 and 7 was determined via luminescent Caspase Glo 3/ 7 assay. To clarify whether a differential caspase activation is measurable at early and late time points after TMZ treatment, caspase 3/ 7 activity was determined after 72 and 144 h (**Figure 35**). At 72 h, LN229 cells showed the highest activity levels (3 fold above untreated control). At this time point, LN229 Surv GFP and LN229 SurvNESmut GFP cells showed only a slight increase in caspase activity of 1.7 fold and 1.3 fold, respectively. This indicates that both Survivin variants were capable of mediating a caspase inhibition. After 144 h, caspase activity in both Survivin clones was augmented. A 3.7 fold increase was determined in LN229 Surv GFP cells and a 2.5 fold increase in LN229 SurvNESmut GFP, whereas caspase activity decreased in LN229 to 2.1 fold. Thus, the cell clone with expression of Surv GFP showed the highest activity of the caspases 3 and 7.

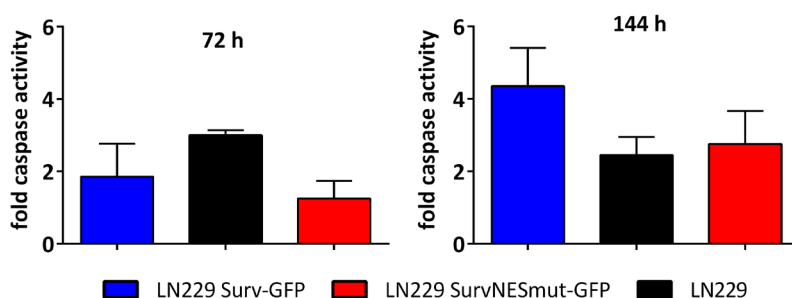


Figure 35: Activation of Caspase 3 and 7 in response to 100 μ M TMZ treatment as fold luminescence relative to control. Mean values of duplicates from independent experiments are plotted for 72 h and 144 h (N = 2).

3.3.4 Induction of senescence

Cellular senescence can be caused by various types of genotoxic treatments including TMZ. To examine whether Survivin or SurvNESmut can prevent or promote cellular senescence, β Galactosidase (β Gal) staining for senescence associated β Gal activity was conducted. β Gal becomes active during the cellular senescence program, which is utilized to cleave an artificial β Gal substrate (X Gal). The cleavage products may dimerize and are oxidized to a blue indigo dye by which senescent cells can be identified.

Interestingly, the percentage of senescent cells was significantly reduced in LN229 Surv GFP cells following TMZ treatment (**Figure 36**). At 120 h, also LN229 SurvNESmut cells showed a significantly lower number of senescent cells when compared to parental LN229 cells. However, this effect was not persisting at 144 h. Here, again Surv GFP expressing cells showed the lowest induction of cellular senescence. This indicates that wt Survivin but not NES mutated Survivin was consistently able to prevent TMZ induced senescence. Representative images for every time point investigated are provided in **Figure 37**.

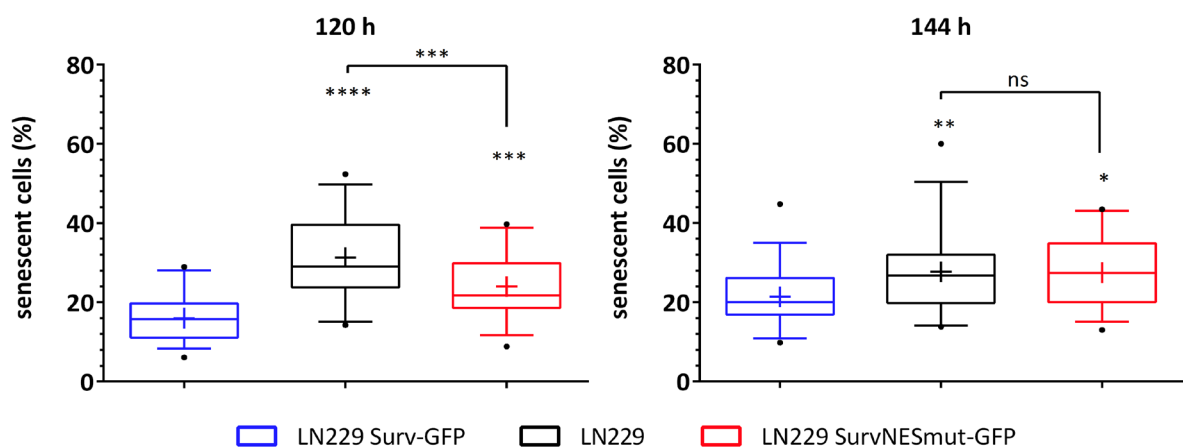


Figure 36: Box-plots for senescence induction as fraction of positive cells in Survivin cell clones 120 and 144 h after treatment with 100 μ M TMZ. Single cells were counted and characterized for positive X-Gal staining. Both time-points represent three independent experiments. Between 255–568 cells were counted for each group in each independent experiment ($N = 3$). Whiskers indicate 5th and 95th percentile, with boxes representing first, second (median), and third quartile (from top to bottom). Geometric means are marked with “+”. Outliers (values out of 5–95 percentile range) are marked as “•”. Test for statistical significance was performed by One-Way ANOVA with Bonferroni post hoc analysis. Significant differences are indicated with *.

Results

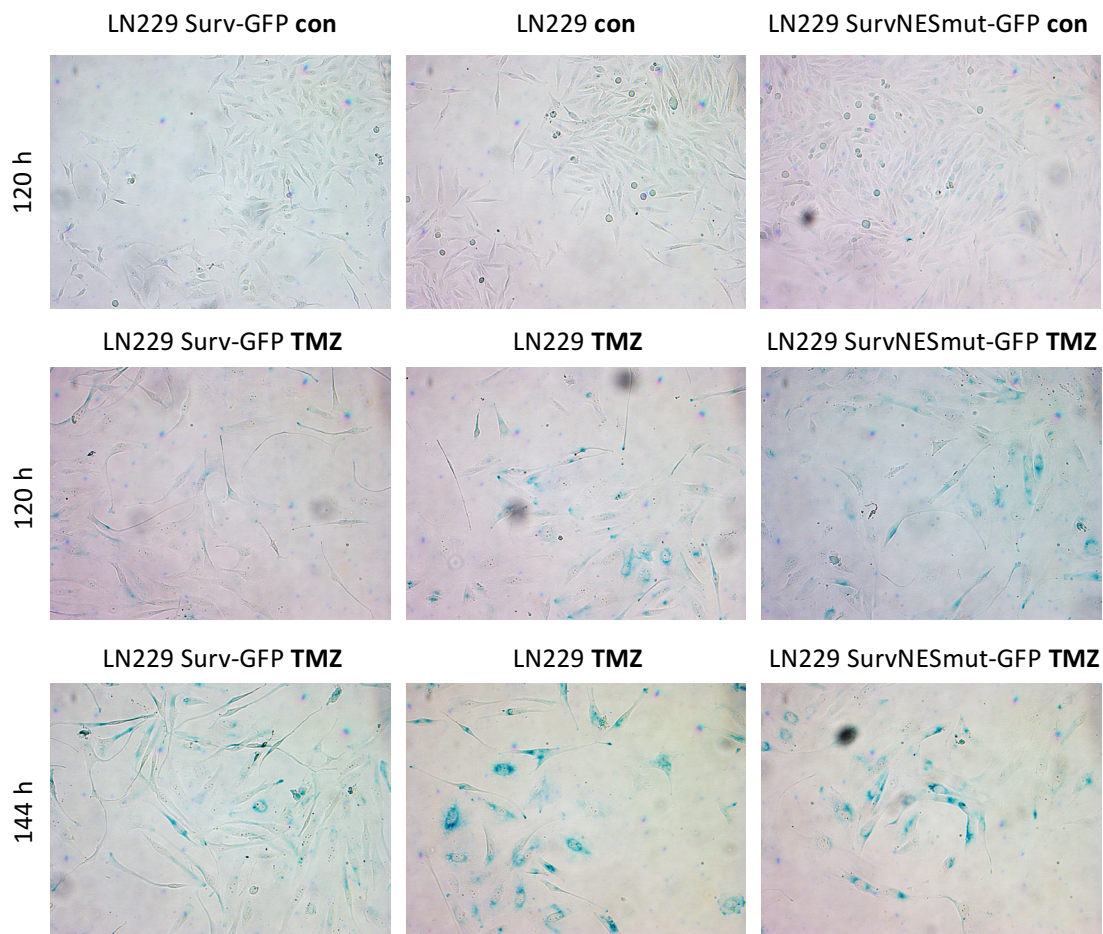


Figure 37: Representative bright field images of different LN229 cell clones stained for SA- β -Gal activity. Positive cells (strong blue) and total cells were counted on each image.

3.3.5 Cellular response to TMZ-induced DNA damage

To address the question whether the DDR to TMZ is different in LN229 Surv GFP compared to LN229 SurvNESmut GFP cells, the phosphorylation (activation) of different DDR key proteins was analyzed in both cell clones (**Figure 38**). The phosphorylation of CHK1 (Ser345) was increased in response to TMZ in a time frame of 48 – 96 h when compared to untreated cells. Both cell clones showed a strong activation of CHK1 (pChk1), indicating the presence of stalled replication forks and SSBs. In line with this, the downstream target of CHK1 p53 was strongly phosphorylated at serine 15 and serine 46. 96 h after treatment, the phosphorylation of both p53 residues already declines in LN229 Surv GFP, whereas the phosphorylation is slightly more prominent in LN229 SurvNESmut GFP. Most strikingly, phosphorylation of the DNA DSB marker H2AX was strongly pronounced in LN229 SurvNESmut GFP after 96 h, whereas it was

almost lost in LN229 Surv GFP. This finding hints at the involvement of the DNA DSB repair in the enhanced survival of LN229 Surv GFP cells. Thus, the phosphorylation of H2AX was analyzed in more detail.

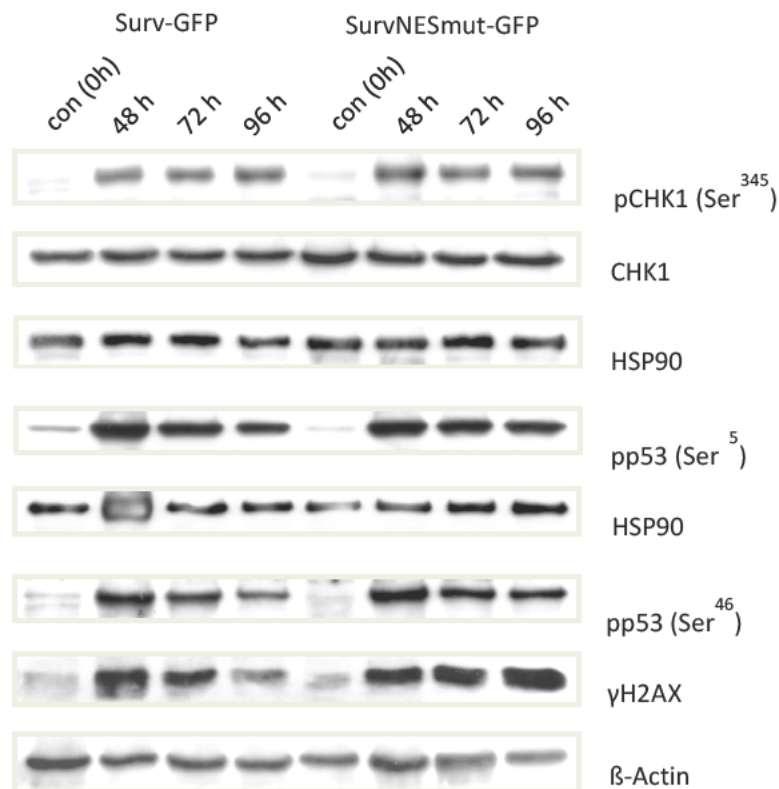


Figure 38: Western blot for different phosphorylation forms of DDR proteins. HSP90 was used as loading control for the detection of CHK1/ pCHK1 (top), and detection of pp53 (Ser¹⁵; middle). β-Actin served as loading control for the detection of γH2AX and pp53 (Ser⁴⁶; bottom). Signals were detected using ECL.

3.4 Induction of DNA double-strand breaks in Survivin cell clones

The role of Survivin in the repair of DSB remains largely obscure. For radiation, a facilitation of the main repair pathway (NHEJ) of this lesion was reported (see 1.5.3). Whether Survivin plays a role in other DNA repair pathways is not known. A major part of this work was to investigate the contribution of Survivin to the repair of TMZ induced DSBs. TMZ causes highly cytotoxic DSBs (see 1.4.1). As this type of DNA damage leads to cell cycle arrest in the G2 phase, the main pathway for the repair is HRR. To elucidate the impact of Survivin and SurvNESmut on this pathway, DNA damage induction and DNA repair efficiency was analyzed in the corresponding cell clones.

Results

3.4.1 γ H2AX and co-localization with 53BP1

DSB lesions induce DNA damage sensing, signaling, and repair pathways, which involve diverse repair factors. An early event during the DSB recognition is the phosphorylation of the histone variant H2AX. The active sites of DNA repair can be visualized by IF imaging as distinct foci by staining of proteins accumulating at sites of DNA repair, especially γ H2AX. These foci are formed in proximity to the DNA DSB and allow a quantification of the amount of double strand breaks within a cell. An additional factor involved in DSB repair is 53BP1 that was checked for its colocalization with γ H2AX in the following experiment for further validation of the detection of DSBs and not of other lesions also involving the phosphorylation of H2AX (see 1.4.3.1). **Figure 39** shows three representative series of an IF co staining of γ H2AX and 53BP1 in LN229 cells treated with 50 μ M TMZ (96 h).

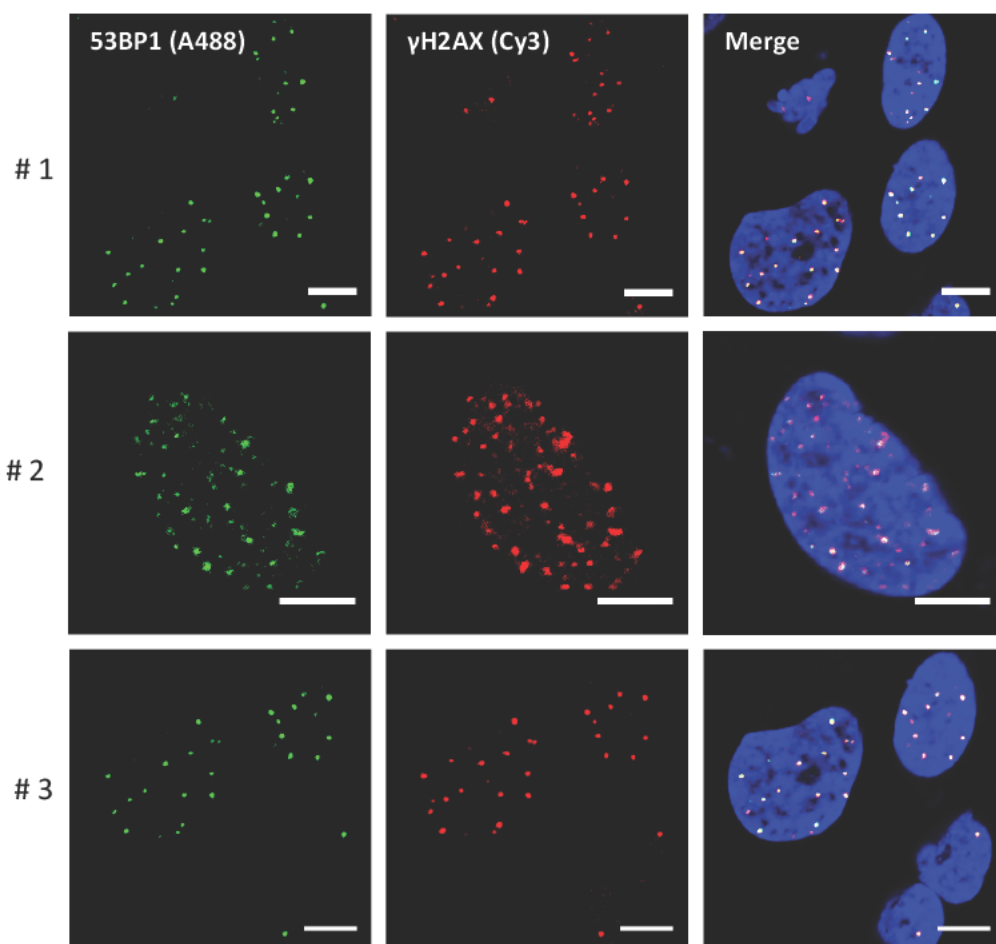


Figure 39: Immunofluorescence images showing the co-localization of 53BP1 and γ H2AX 96 h after TMZ treatment (50 μ M). 53BP1 was stained with A488-conjugated (green) and γ H2AX with Cy3-conjugated (red) secondary Ab. TO-PRO3 was used for nuclear staining (blue). Scale bars equate 10 μ m.

Both factors show distinct nuclear foci pattern and besides, γ H2AX and 53BP1 foci are perfectly co localized, as the comparison of the single channels and the merge image reveals. The experimental settings tested here were used for further experiments to determine the quantity of DNA DSBs upon TMZ treatment.

3.4.2 γ H2AX induction after TMZ treatment in Survivin clones

To determine the induction of DSBs caused by TMZ, phosphorylation of H2AX was analyzed. Distinctly visible γ H2AX foci within cell nuclei were counted manually on immunofluorescent images. Detailed, representative pictures for the different cell clones and time points are presented in **Figure 40**. The number of γ H2AX foci was strikingly different among the cell clones. LN229 Surv GFP cells exhibited the lowest induction of γ H2AX foci at all time points, while foci numbers were increased in LN229 and LN229 SurvNESmut GFP cells.

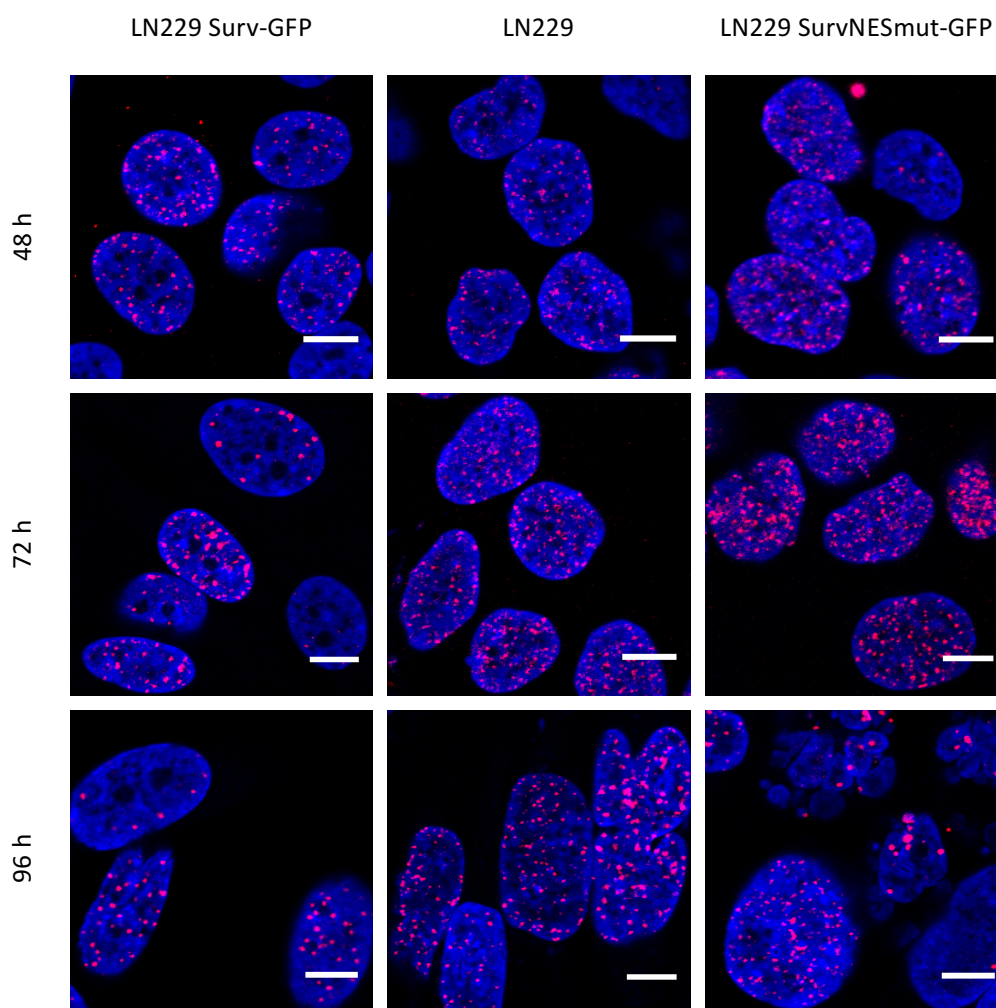


Figure 40: Immunofluorescence images of γ H2AX foci (red) in LN229 cell clones upon treatment with 50 μ M TMZ for different time points. Representative cells were cropped from larger images. TOPRO-3 (blue) was used for nuclear staining. Scale bars equate 10 μ m.

Results

Thus, quantitative analysis of the foci numbers per nucleus was performed 48, 72, and 96 h upon TMZ treatment (50 μ M). The mean foci numbers per nucleus were significantly decreased in LN229 Surv GFP cells at 48, 72, and 96 h after treatment when compared to LN229 cells and cells expressing NES mutated Survivin (**Figure 41**).

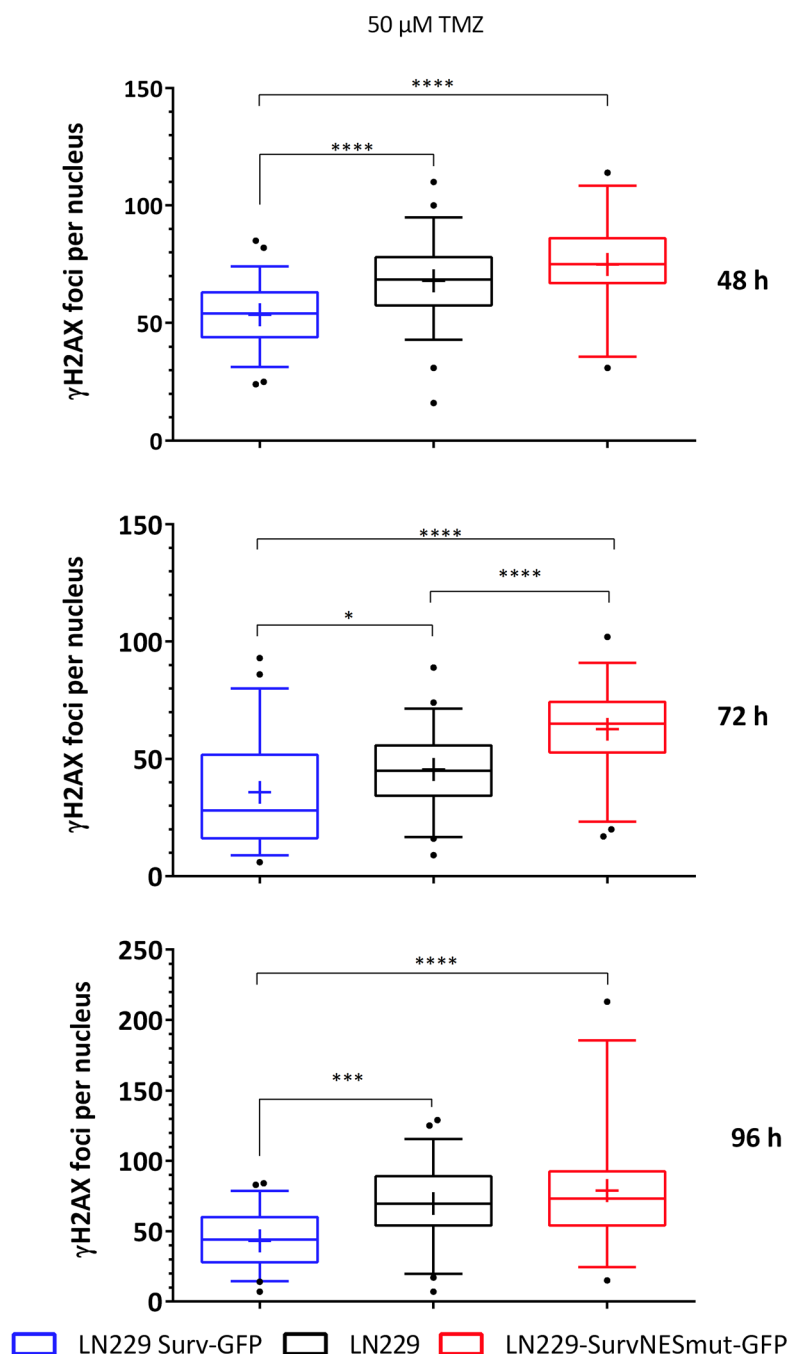


Figure 41: Box-Blots of γ H2AX foci numbers per nucleus in Surv-GFP cell clones after treatment with 50 μ M TMZ. Whiskers indicate 5th and 95th percentile, with boxes representing first, second (median), and third quartile (from top to bottom). Geometric means are marked with "+". Outliers (values out of 5 – 95 percentile range) are marked as "•". Test for statistical significance was performed by One-Way ANOVA with Tukey's post hoc analysis. Significant differences are indicated with *. 35 to 56 nuclei were evaluated for each cell line and time point in this analysis.

This effect was most prominent 72 h after treatment. In average, Surv GFP cells showed 36 foci per nucleus, while the induced foci number was significantly higher in LN229 cells (46). Expression of NES deficient Survivin variant (SurvNESmut GFP) led to an even increased foci number (63). Comparison between parental cell line LN229 and SurvNESmut GFP clone revealed significantly increased number of γ H2AX foci ($p < 0.0001$) in the clone expressing the NES deficient Survivin after 72 h. Also, 48 h and 96 h after the treatment, the NES deficient clone tended to show more γ H2AX foci than parental cells, although not reaching statistical significance. LN229 SurvNESmut GFP showed the highest variance at 48 h and 96 h. Here, the foci numbers observed varied greatly from 213 to 41.

In direct comparison (**Figure 42**), the time course of γ H2AX foci formation revealed an initial high number of foci 48 h after treatment, which was reduced at 72 h in all cell lines. Interestingly, after 96 h foci numbers increased again. This observation might reflect a complex balance of ongoing DNA repair and the formation of new DSB upon O^6 MeG lesions over time. However, in LN229 Surv GFP cells, foci numbers stayed below 44 foci per nucleus after 96 h, while in LN229 and SurvNES mut cells, the foci counts were even higher than the initial values after 48 h.

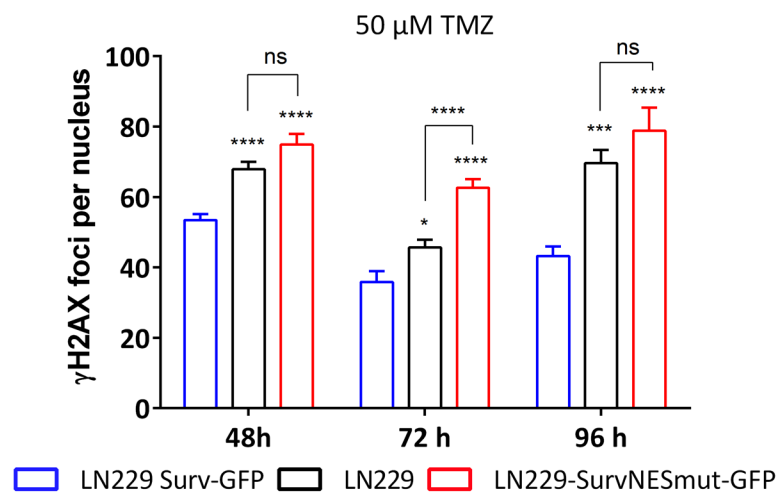


Figure 42: Summary of γ H2AX foci formation per nucleus in Surv-GFP cell clones after treatment with 50 μ M TMZ. Error bars indicate SEM. Test for statistical significance was performed by One-Way ANOVA with Tukey's post hoc analysis. p -values (*) indicated above each column were calculated between LN229 Surv-GFP (blue) and the corresponding column. Other comparisons are indicated above the bars.

Results

Differences in the number of the remaining DSBs might reflect variances in the efficiency of DNA repair in clones. Further experiments were conducted to measure repair rate and sensitivity of the cells upon inhibition of either DSB repair pathway.

3.4.3 Influence of NHEJ on TMZ-induced DNA damage in Survivin clones

One possible pathway for the repair of DSB is NHEJ. As mentioned earlier, Survivin facilitates NHEJ upon IR. Although TMZ induced DNA lesions are mainly repaired by HR, a putative involvement of Survivin in NHEJ was investigated.

3.4.3.1 DNA PK activity assay

The rate limiting enzyme of NHEJ is DNA PK, which activates downstream kinases by phosphorylation. DNA PK activity was determined in cellular protein extracts of LN229, LN229 Surv GFP, and SurvNESmut GFP cell clones. An enhanced activity of DNA PK was measured for LN229 Surv GFP and slightly in LN229 SurvNESmut GFP cells irradiated with 4 Gy (**Figure 43, A**). Without irradiation, the enzyme's activity was comparable to that of parental LN229 cells. To check whether a similar influence can be observed after TMZ induced DNA damage, DNA PK activity was determined 72 h after treatment with the alkylating agent. Interestingly, a reduction of the DNA PK activity was observed in LN229 Surv GFP as well as in LN229 SurvNESmut GFP cells (**Figure 43, B**). Due to inherent fluctuations of the radioactivity of the γ ³²P ATP used, a direct comparison of both experiments is not possible. Therefore, the fold activity of control (**Figure 43, C**) was calculated to compare the effect of IR and TMZ on DNA PK activity in both Survivin cell clones. A 1.4 fold increase was observed in LN229 Surv GFP upon IR, while LN229 SurvNESmut GFP cells showed only a marginal difference to control (1.1 fold). In contrast, 72 h after the treatment with TMZ both clones showed a reduced DNA PK activity of 0.5 fold and 0.8 fold, respectively.

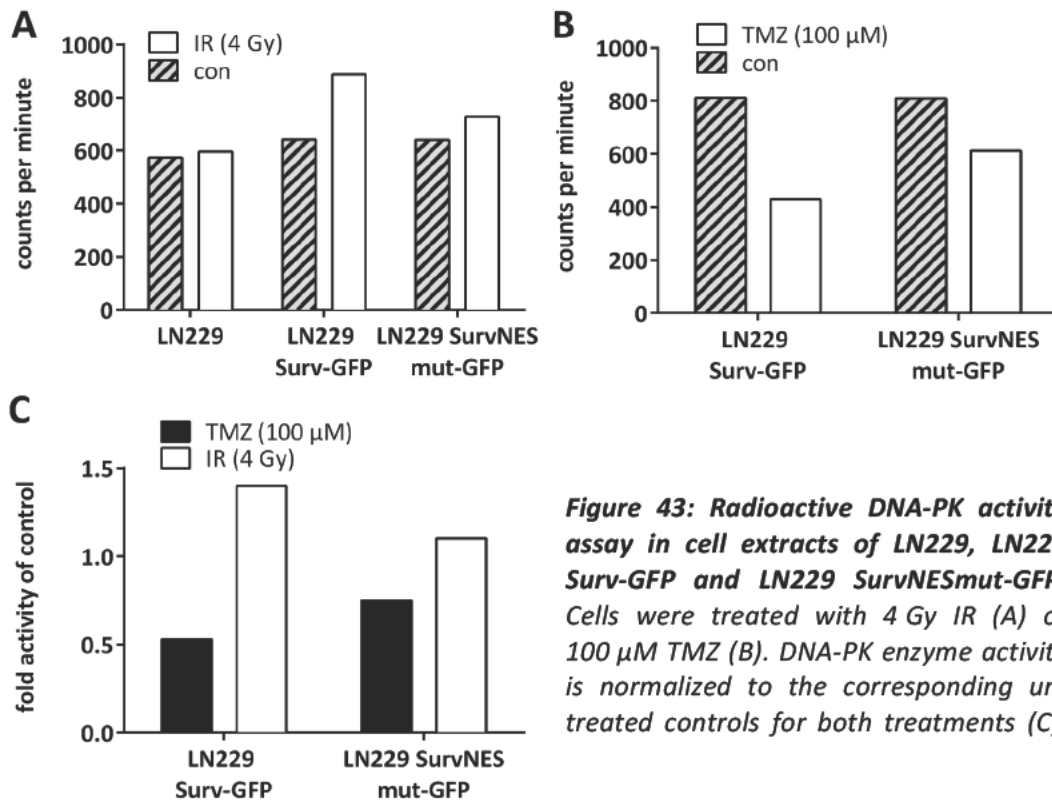


Figure 43: Radioactive DNA-PK activity assay in cell extracts of LN229, LN229 Surv-GFP and LN229 SurvNESmut-GFP. Cells were treated with 4 Gy IR (A) or 100 μM TMZ (B). DNA-PK enzyme activity is normalized to the corresponding untreated controls for both treatments (C).

3.4.3.2 Inhibition of NHEJ

To further investigate the putative interplay of Survivin and components of the NHEJ, the cellular viability of LN229 Surv GFP was compared to LN229 SurvNESmut GFP in the background of DNA PK inhibition. Metabolic competence, i.e. cell viability, was impaired upon TMZ treatment in all cell lines in a concentration dependent manner as determined by MTT assay (**Figure 44**). 72 h after the treatment with 25 μM TMZ, LN229 Surv GFP cells showed a viability of 51 % comparable to LN229 SurvNESmut GFP cells (47 %) and LN229 cells (48 %). At the higher TMZ concentration, viability was equally reduced in all cells (43 – 44 %). Inhibition of the NHEJ pathway alone did not show toxic effects. At both time points, the cells showed a slightly increased viability upon the treatment with the DNA PK inhibitor Nu7026. Also, the combination treatment with TMZ did not cause additional toxicity.

Results

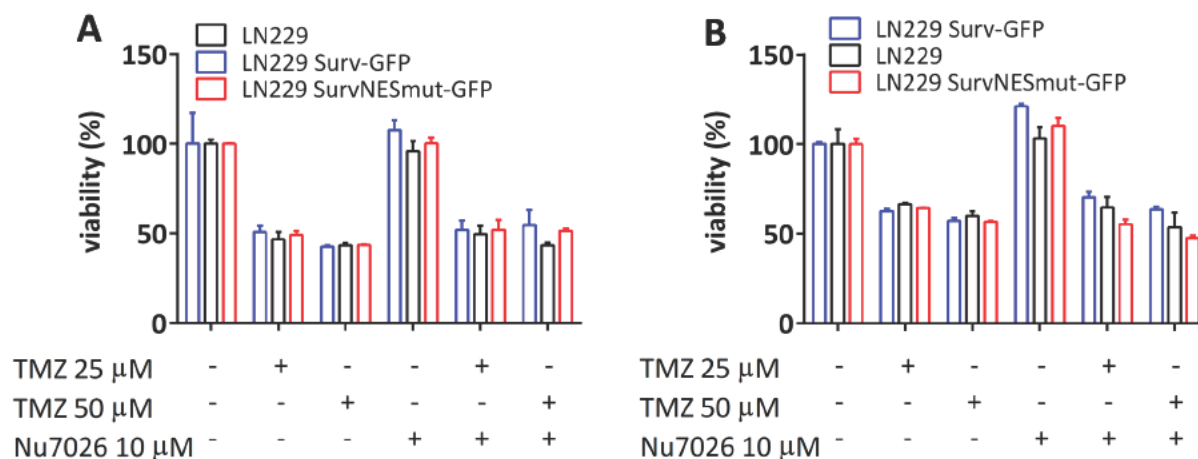


Figure 44: MTT cell viability assay of Survivin expressing cell clones 72 h (A) and 96 h (B) after single- and combination treatment with TMZ and the DNA-PK inhibitor Nu7026. Cellular viability was normalized to control treated cells (DMSO). Experiment was performed in technical triplicates for each time point. Error bars indicate the SD.

Furthermore, clonogenic survival was analyzed after the inhibition of NHEJ and the treatment with TMZ (**Figure 45**). LN229 Surv GFP retained their survival advantage, upon combination treatment with TMZ (100 μ M) and NU7026 (10 μ M). Irrespective of NHEJ inhibition, Surv GFP expressing cells still survived better than SurvNESmut GFP expressing cells. However, survival percentages were dramatically lower than in the treatment with TMZ alone (see 3.3.1), which might be caused by the treatment with high concentrations of the solvent DMSO. At a concentration of 2.5 μ M TMZ, the survival of LN229 Surv GFP was 45.3 %, while only 3.7 % of Surv NESmut expressing cells survived.

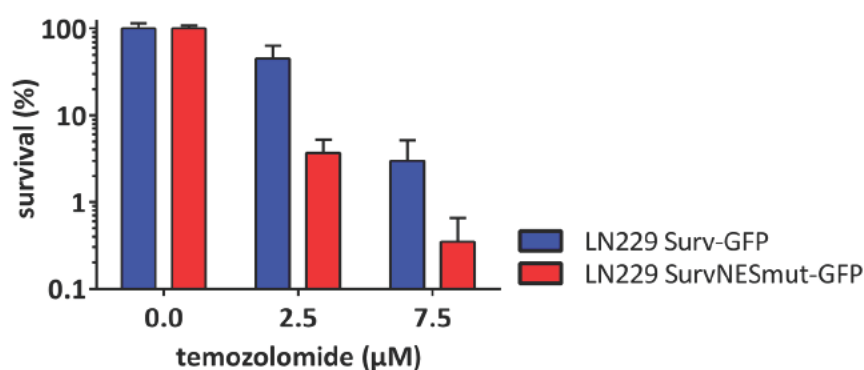


Figure 45: Colony formation assay of Survivin cell clones for different concentrations of TMZ upon co-treatment with 10 μ M Nu7026. Surviving cells were normalized to control (%) and plotted in a semi-logarithmic graph. Data of three independent experiments are shown ($N = 3$) with error bars indicating SD.

3.4.4 Survivin in the homologous recombination repair of TMZ-induced DSB

To clarify whether Survivin has an influence on HR, Surv GFP was overexpressed in the background of an additional knockdown of RAD51, a key player of the HR. Clonogenic survival and the induction of γ H2AX foci was analyzed in this cell model. Furthermore, the HR activity was measured in different LN229 clones (with normal expression of Rad51).

3.4.4.1 Survivin expression rescues survival of Rad51 knockdown clones

LN229 cells, stably transfected with Rad51_shRNA, are drastically sensitive towards treatment with TMZ, as this is the main pathway of repair for TMZ induced DSB [185]. Cells with a stable Rad51 knockdown (LN229 RAD51_sh) were additionally transfected with Surv GFP expression plasmid. **Figure 46** shows the clonogenic survival of LN229 RAD51_sh + Surv GFP and LN229 Rad51_sh alone upon different concentrations of TMZ. LN229 cells with RAD51 knockdown were hypersensitive towards TMZ treatment. At the lowest concentration of 2.5 μ M, a survival of 10 % was observed. Interestingly, this sensitive phenotype can be almost completely rescued by the expression of Surv GFP (94 %). In comparison to LN229 Surv GFP cells, survival was slightly reduced at 5 μ M TMZ in the RAD51 deficient “Survivin” cells (83 % vs. 90 %). An observation that can also be confirmed at 7.5 μ M (55 % vs. 71 %). However, when compared to LN229 RAD51_sh, Survivin expression led to a strong survival advantage at all concentrations observed. Upon 5 μ M or 7.5 μ M TMZ, the survival of LN229 RAD51_sh cells dropped to 1 % or below. In contrast, LN229 RAD51_sh + Surv GFP cells showed a high survival at these concentrations. At higher concentrations, no colonies were observed for LN229 RAD51_sh.

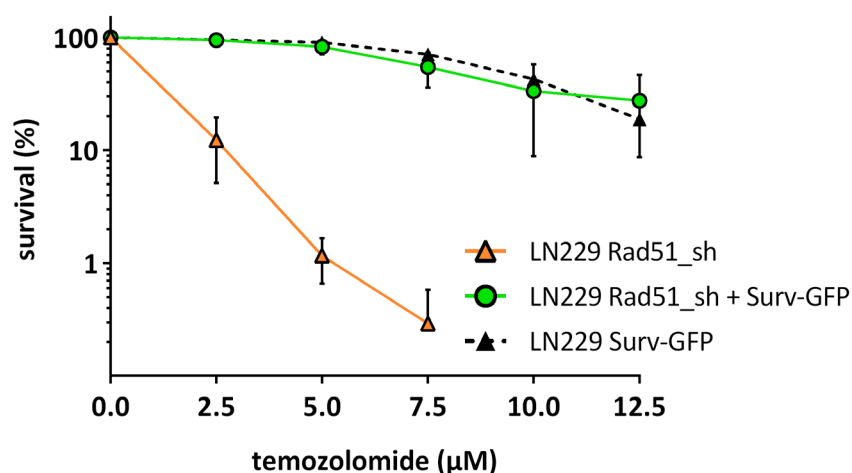


Figure 46: Colony formation assay of LN229 Rad51_sh and LN229 Rad51_sh + Surv-GFP for different concentrations of TMZ. Surviving cells were normalized to control (%) and plotted in a semi-logarithmic graph. Data of three independent experiments is shown ($N = 3$) with error bars indicating SD.

Results

3.4.4.2 Survivin expression reduces DNA DSB in RAD51 knockdown clones

Similar to LN229 Surv GFP cells, the observed protective effect of Survivin in LN229 RAD51 knockdown cells, might also be attributed to a lower amount of DNA DSB. Therefore, the formation of γ H2AX was analyzed. In line with the survival data, LN229 RAD51_sh + Surv GFP cells were significantly protected from TMZ induced DSB at 48 h (**Figure 47**). No significant difference was detected for LN229 Rad51_sh + Surv GFP cells when compared to LN229 cells. In contrast, after 72 h foci numbers were significantly lower in LN229 cells than in both RAD51 knockdown clones. However, γ H2AX foci number was significantly reduced at this time point when compared to cells with RAD51 knockdown alone. In comparison to the foci numbers determined in LN229 cell clones (see 3.4.2), the number of detected DSBs was overall higher in both Rad51 deficient cells. Thus, the effect of a Rad51 knockdown could not be completely reversed by Survivin expression.

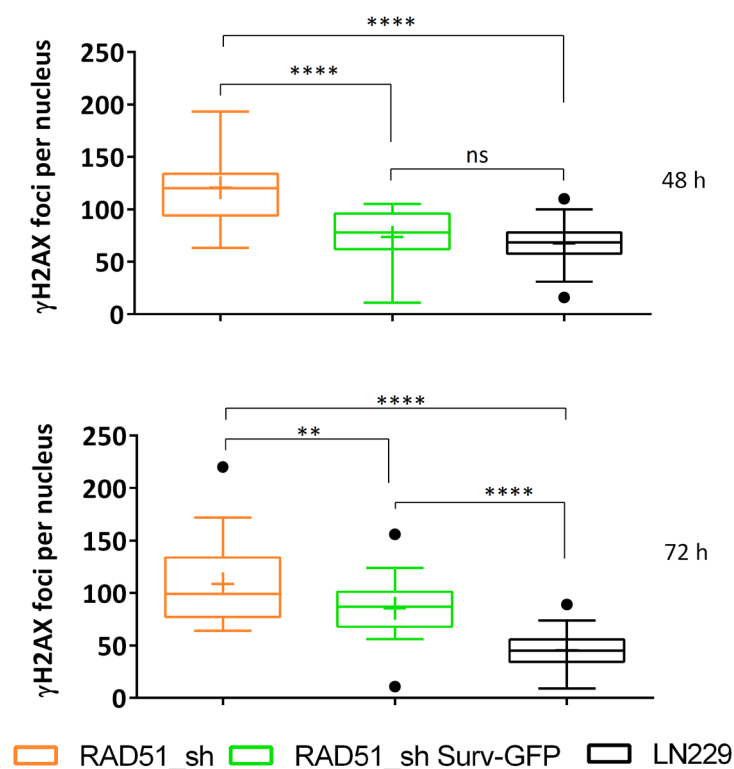


Figure 47: Box-Blots of γ H2AX foci numbers per nucleus in RAD51 knockdown cells with and without overexpression of Surv-GFP upon treatment with 50 μ M TMZ. Whiskers indicate 5-95 percentiles, with boxes representing 75th, 50th (median), and 25th quartiles (from top to bottom). Geometric means are marked with "+". Outliers are marked as "•". 26 to 56 nuclei were evaluated for each cell line and time point in this analysis.

However, the data provided clearly shows that an overexpression of Survivin dampens the effect of a RAD51 shRNA mediated HR deficiency. Survivin might thus facilitate the repair of DSBs by enhancing HR.

3.4.5 Survivin increases capacity of HR DSB repair

The data presented above show that Survivin expression increases the resistance of LN229 glioblastoma cells to TMZ and rescues the hypersensitive RAD51 knockdown phenotype. The amount of measurable DNA damage was significantly reduced upon overexpression of Survivin. To determine the repair rate in the HRR, activity was determined in dependency of Surv GFP and SurvNESmut GFP expression (**Figure 48, A**) and knockdown of Survivin (**Figure 48, B**). The abundance of a recombined (repaired) HR plasmid was quantified by relative qPCR as measure of the recombination activity. In line with the lower number of γ H2AX foci in LN229 Surv GFP cells (see 3.4.2), HR activity in this clone was 1.5 fold higher when compared to LN229 cells. Vice versa, the knockdown of Survivin caused a 0.6 fold reduction of the HRR activity (**Figure 48, B**). Interestingly, also LN229 SurvNESmut GFP showed an impaired HRR, which might reflect the higher amount of γ H2AX foci and the increase in the sensitivity to TMZ.

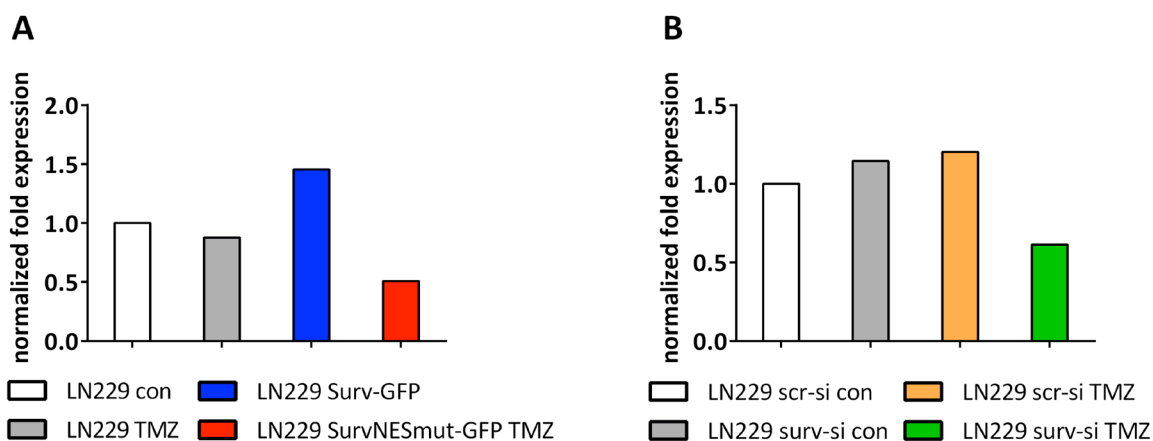


Figure 48: qPCR results of the HR activity assay (A) in different LN229 cell clones and (B) upon Survivin knockdown with and without treatment with TMZ. The normalized fold expression is shown, using untreated LN229 cells/ untreated scr-siRNA-transfected cells as calibrator control and the internal reference plasmid sequence for normalization ($\Delta\Delta C_T$). Experiment was performed in technical duplicates.

Results

The HR activity data show that wt Survivin but not NES mutated Survivin is capable of enhancing the repair of TMZ induced DSBs via HR. Thus, overexpression of Survivin protects cells from DNA damage and thereby from cell death.

3.5 Evaluation of Survivin as biomarker in high grade gliomas

Survivin is one of the most frequently up regulated genes in tumors. Evidence provided here shows that cellular survival is increased by its influence on cell death pathways and DNA repair mechanisms in vitro. Thus, the level of Survivin expression in gliomas might correlate with increased malignancy and therapy resistance. An accurate method for predicting Survivin expression in tumor cells would provide valuable information that could clarify the role of Survivin for the prognosis. Besides, transcriptional regulation mechanisms, also gene silencing by DNA methylation, plays a role in the regulation of *BIRC5* (see introduction). To elucidate whether epigenetic silencing of *BIRC5* occurs in glioma cell lines and high grade glioma samples, the methylation of a regulatory gene region was analyzed.

As there are contradicting reports regarding the impact of *BIRC5* methylation, on e.g. the therapy response and tumor malignancy, a putative prognostic value of *BIRC5* methylation was analyzed. Therefore, the DNA methylation in the exon 1 of *BIRC5* was determined in bisulfite treated DNA of different glioblastoma and astrocytoma cell lines. Methylation specific PCR (MSP) showed that all cell lines investigated bore no CpG methylation. **Figure 49** shows representative MSP results for LN308 glioblastoma cells. No amplification product was detected for the primer pair being specific for an unmethylated template. Additionally, a methylation standard with a methylation value of 75 % was analyzed. Here, PCR products for the unmethylated (UM) and the methylated (M) primer pair could be detected, indicating the presence of both templates. Since the percentage of the methylated template was higher (75 %), a stronger amplification was observed for the M primer pair. Thus, reliability of both primer pairs at the specific annealing temperatures could be demonstrated.

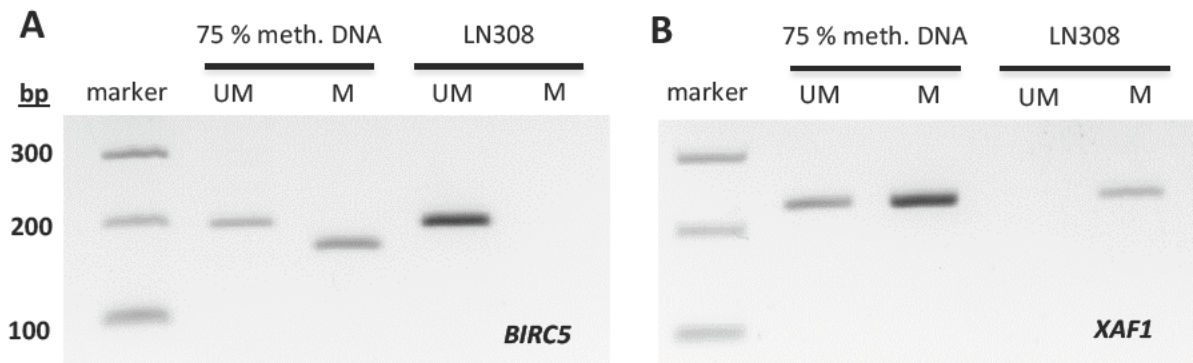


Figure 49: Agarose gel separation of MSP amplicons for UM- and M-pairs targeting (A) *BIRC5* and (B) *XAF1* in methylation standard (75 %) and glioblastoma cell line LN308. Amplification products were separated on a 1.5 % agarose gel, stained with EtBR, and visualized on a UV transilluminator.

Since MSP is limited to a small number of CpGs contained within the primer binding site, and the quantification of the results is difficult, a high throughput approach was chosen for a broader study of *BIRC5* as epigenetic marker. Methylation sensitive high resolution melt analysis (MS HRM) was established for the methylation analysis of a promoter region reaching into the exon 1 of *BIRC5*, containing 36 CpGs. Some of these CpGs were also targeted in the conventional MSP analysis reported above. In GB cell lines, no methylation of the investigated region of *BIRC5* was found. The melting curves were congruent with the unmethylated DNA standard (Figure 50 upper panel), and thus no signs of methylation were detectable.

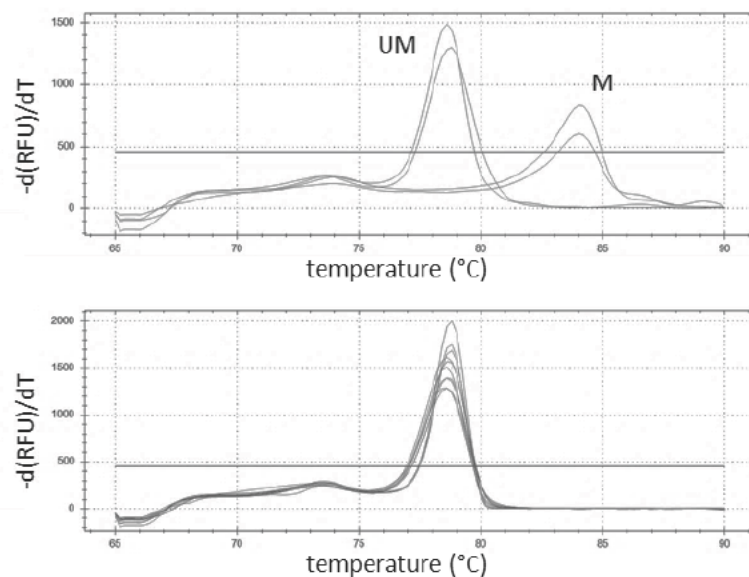


Figure 50: Representative qPCR melting curves of *BIRC*-targeted MS-HRM amplification of unmethylated (UM) and methylated (M) bisulfite-converted DNA standards (upper panel) and bisulfite-converted DNA from GB cell lines (lower panel). Values are shown in technical duplicates.

Results

Representative melting curves for five glioma cell lines (U87, GBP61, U118, D247, U343) are provided in **Figure 50** (lower panel). In confirmation of the MSP results, these data indicate that *BIRC5* might not be epigenetically silenced in gliomas.

A summary of methylation values of 13 GB cell lines is provided in **Table 14**. All cell lines included in this analysis had no detectable level of methylation in the region analyzed. Negative methylation values arise from the theoretical methylation value of the fully methylated standard, which was set to 100 % for interpolation. All melt curves were identical to those of the UM standard, therefore a correction for the empirical methylation value of the UM and M standard was omitted for *BIRC5*. This correction step was performed for *XAF1* as described (see 3.6.1). The arising differences between theoretical and true methylation values, e.g. negative methylation percentages, are most likely caused by an incomplete in vitro methylation of the standard DNA, prior to bisulfite conversion.

Table 14: Methylation values of the *BIRC5* promoter region determined by MS-HRM in GB cell lines. Percentage of methylation was interpolated from the area under the curve (AUC) of normalized melt curves of methylation standards with 0, 25, 50, 75, and 100 % methylation.

sample	interpolated methylation (%)	AUC
LN18	16.3	1.4
U87	18.4	1.4
GBP61	20.6	1.3
LN229	19.9	1.3
U118	17.5	1.4
D247	16.1	1.5
U343	17.2	1.4
U138	16.4	1.4
LN308	16.1	1.5
U251	16.4	1.4
LN373	14.8	1.5
A172	21.0	1.3
LN319	17.0	1.4

To exclude that a demethylation in *BIRC5* is a result of in vitro culturing of tumor cells, methylation levels were also determined in 40 randomly chosen high grade glioma tumor samples. In line with the data obtained in GB cell lines, none of these samples showed signs of *BIRC5*

promoter methylation (**Suppl. Table 4**). Since no evidence for an epigenetic regulation of *BIRC5* could be found, epigenetic silencing of *BIRC5* probably does not occur in gliomas.

3.6 IAP-antagonist XAF1 is epigenetically silenced in glioblastoma cell lines

The evidence provided here suggests that epigenetic silencing of *BIRC5* does not occur in glioma cell lines and high grade gliomas. Thus, the use of *BIRC5* as prognostic or predictive marker seems implausible for gliomas. As there is an urgent need of new markers and/ or putative therapeutic targets, we further focused on other promising factors in the context of IAPs. XAF1 is closely linked to posttranslational regulation of Survivin and XIAP. Its pro apoptotic, tumor suppressing properties make this protein an interesting factor that might play an important role during glioma development and treatment. Since XAF1 was reported to be epigenetically silenced, in different tumor entities, the motivation for this analysis was to establish a method for a fast and accurate determination of the XAF1 expression in tumor specimens. Analogously to *BIRC5* methylation analysis, MS HRM was utilized for this purpose. Other than for *BIRC5*, a heterogenous methylation pattern could be detected for *XAF1* in first experiments with established MSP primers [199]. For example, the cell line LN308 exhibited a methylated promoter in MSP analysis, while no UM band was detectable (**Figure 49, B**).

3.6.1 Establishing MS-HRM promoter methylation analysis for XAF1 in GB cell lines

Byun *et al.* previously linked CpG methylation in the promoter region ranging from -234 bp (upstream) to +7 bp (downstream) to a reduced XAF1 expression in human gastric adenocarcinomas [179]. In this study, the methylation of 3 CpGs in this region of -236 bp to -196 bp was analyzed for its impact on XAF1 regulation (**Figure 51**). For verification, a second region lying proximal to the transcription start site was additionally analyzed using primer pair "HRM2". The methylation values were determined in randomly selected matched HGG samples (N = 39). Both regions were found to be coincidentally methylated, thus a strong positive correlation between both methylation percentages could be observed ($R = 0.730$; $p \leq 0.0001$).

Results

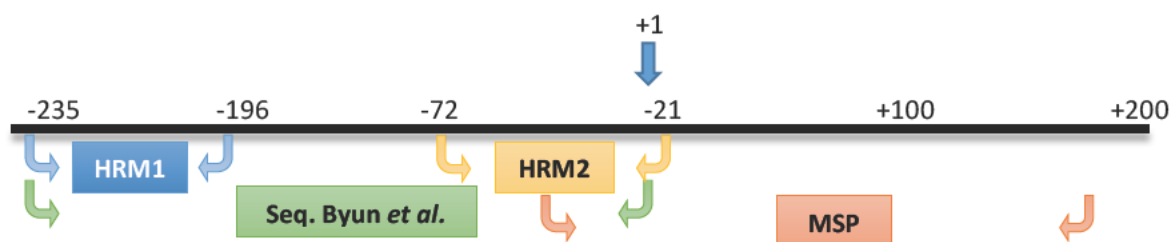


Figure 51: Schematic XAF1 promoter with different primer binding sites for the analysis of the XAF1 promoter methylation by sequencing (Byun et al.), MSP, and MS-HRM used for the conducted analysis. Bp in the diagram indicate the location relative to the transcription start site.

The sequence of the amplified HRM1 region was verified by pyrosequencing to ensure the specificity of this assay. Using the HRM1 fwd primer and HRM1 biotinylated rev primer with an appropriate sequencing primer, the predicted amplicon sequence (TGYGGTTGTGATAGTAGTAAAGAATGAYGGTTAAGGGYGATA) could be confirmed for unmethylated and fully methylated DNA standards (**Figure 52**) and for selected cell lines (**Table 15**). C to T transitions caused by bisulfite conversion were detected and quantified. The actual methylation values of both standards were thereby determined and compared to the theoretical level of methylation (0 %; 100 %). In the XAF1 promoter, UM DNA showed an average methylation of 2.6 %, whereas M DNA was methylated to 84.1 % as average of all three CpGs. The position of the CpGs within the amplicon, and the methylation are indicated in **Figure 52**. As an overall methylation below 100 % may be caused by incomplete in vitro methylation, this empirically determined methylation values were used for sample interpolation during MS HRM analysis. Furthermore, the low background methylation of 2.6 % was corrected in the analysis, thereby yielding methylation standards of 23.0 % (75:25), 43.35 % (50:50), and 63.73 % (25:75).

Table 15: Methylation percentage of the XAF1 promoter in GB cell lines, determined by pyrosequencing and MS-HRM.

cell line	Pyrosequencing			MS HRM	
	CpG1	CpG2	CpG3	mean	
LN308	92.7	85.6	87.2	88.5	90.3
LN18	23.9	18.5	13.9	18.8	2.5
T98G	16.4	26.3	16.7	19.8	13.1
M059J	62.5	33.7	40.0	45.4	48.9
LN319	42.5	16.3	12.1	23.7	8.3
GBP44	40.8	38.2	37.3	38.8	48.9

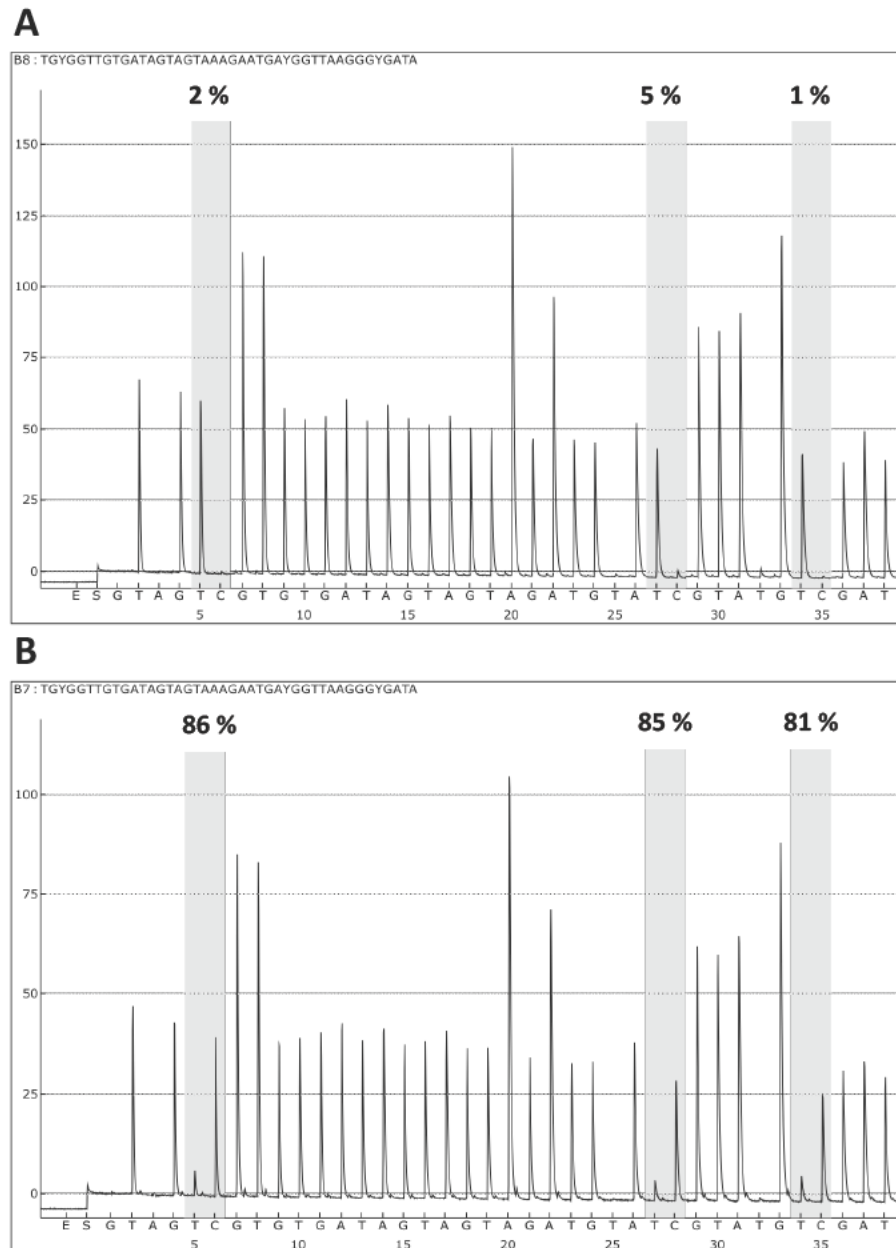


Figure 52: Pyrosequencing results for the XAF1 HRM1 amplicon using (A) unmethylated DNA and (B) methylated DNA standard as template. Gray bars indicate CpG sites with methylation/ SNP percentages. A transition from C to T was introduced at unmethylated Cs by bisulfite-conversion.

XAF1 methylation determined by MS HRM was compared to the results obtained by pyrosequencing in six GB cell lines. Results from both methods (Table 15) showed a very strong correlation ($R = 0.965$; $p = 0.0018$) as determined by Pearson's product moment correlation. Despite an overall high concordance of both methods, a discrepancy between pyrosequencing and MS HRM was observed in cell lines LN18 (15.3 %) and LN319 (15.4 %). However, these deviations did not affect the grouping as UM or M.

Results

3.6.2 *XAF1* methylation predicts *XAF1* mRNA expression in glioma cells

To clarify whether the methylation in the analyzed promoter region is predictive for the expression of *XAF1*, methylation levels were compared to mRNA levels quantified by qPCR. mRNA expression was normalized to the cell line GBP61 with two reference genes (*ENOX2*, *ACTB*). The comparison of 16 GB cell lines showed a heterogeneous *XAF1* methylation pattern. Cell lines with the lowest methylation showed the highest expression of *XAF1* mRNA (**Figure 53**). U118 have a *XAF1* methylation of 17.6 % with the corresponding high relative mRNA levels (1.7 fold). Thus, a detected methylation of 17.6 % seems not to be sufficient for gene silencing. For cell lines with higher methylation values, the relative expression was strikingly reduced (below 0.185 fold). In the cell line panel, LN229 with 33.9 % showed the next higher methylation level adjacent to U118. As the relative expression was markedly reduced for LN229 (0.137 fold), the existence of a methylation threshold between the methylation percentages of U118 (~18 %) and LN229 (~34 %) is to be assumed. At a methylation ≥ 34 %, all cell lines investigated here did not show a convincing mRNA expression, thus a cut off point at this methylation value might be suitable for dichotomizing the samples. Supporting this, a higher promoter methylation was detected in cell lines A172 (0.139) and U251 (0.184), although the relative mRNA expression was slightly higher than in LN229. This indicates that expression levels are already at the detection limit, because of which a relative expression equal to or below 0.184 (U251) was considered as “negative”.

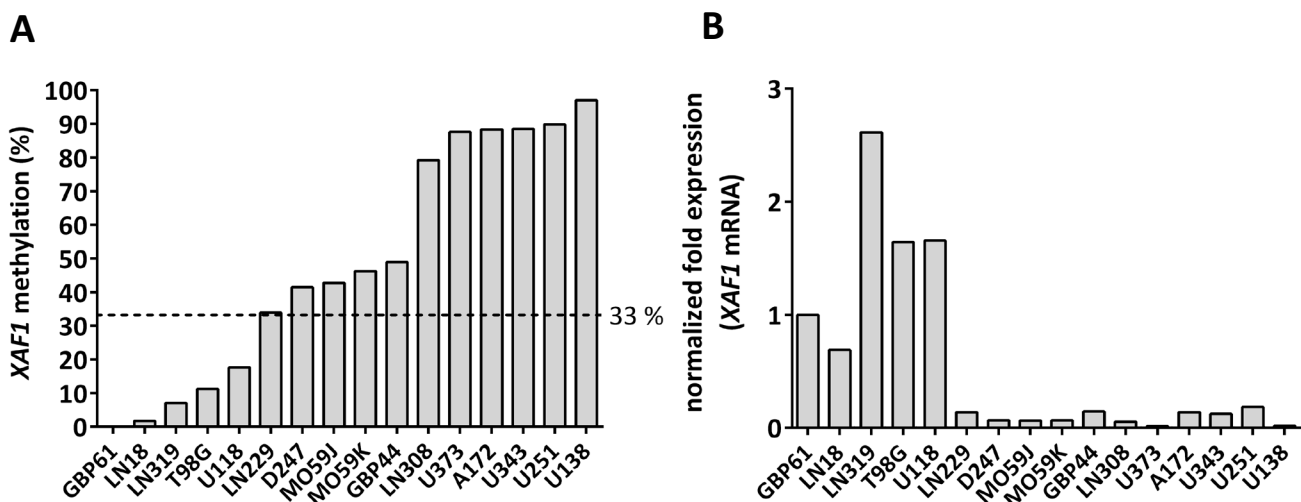


Figure 53: Comparison of *XAF1* promoter methylation (A) with *XAF1* mRNA expression (B) in 16 glioma cell lines. Bars represent mean values of two technical duplicates. mRNA expression was normalized to verified reference genes *ENOX2* and β -Actin and GBP61 as calibrator using the $\Delta\Delta C_T$ -method.

According to these findings, a cut off point of 34 % *XAF1* promoter methylation was applied for classifying the cell lines as either *XAF1* UM (< 34 %) or *XAF1* M (\geq 34 %). To show that *XAF1* methylation in this particular promoter region can predict the expression level of *XAF1*, both cell line groups were compared with regard to their relative expression level. Differences in the expression were found to be highly significant ($p < 0.001$), as depicted in **Figure 54**.

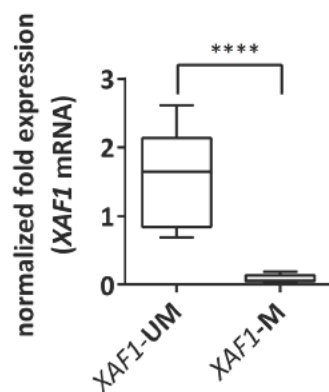


Figure 54: *XAF1* mRNA expression in 16 glioma cell lines, classified either as *XAF1*-UM or *XAF1*-M according to the determined methylation threshold. Test for statistical significance was performed by Student's unpaired t-test (two-tailed). Significant differences are indicated with *.

Using this methylation threshold indicative for *XAF1* mRNA expression, tumor samples could be classified as either *XAF1* M or UM. To elucidate, whether this regulation affects protein expression also, WB experiments were conducted in methylated and unmethylated cell lines. Strongly methylated cell lines showed no detectable protein expression (LN308, U251). However, cell lines exhibiting an intermediate level of methylation still showed low amounts of the *XAF1* protein. Cell lines with unmethylated *XAF1* promoter or a low methylation percentage showed the highest protein level when considering the loading control (HSP90).

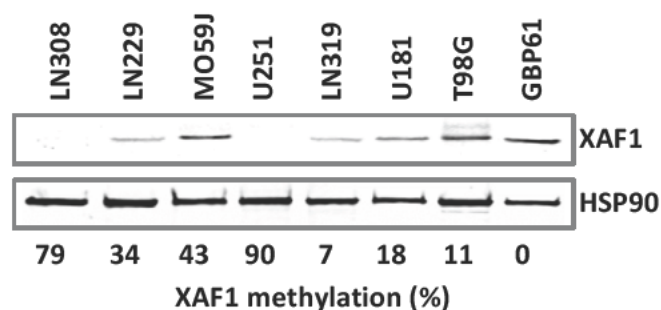


Figure 55: Western Blot analysis of *XAF1* protein levels in selected HGG cell lines. Methylation levels determined by MS-HRM are indicated for each cell line. HSP90 was used as loading control.

Results

3.6.3 Methylation of the XAF1 promoter in high-grade brain tumors

After demonstrating the role of epigenetic silencing of *XAF1* in gliomas and determining a threshold of methylation for sample classification, the role of *XAF1* in malignant gliomas could be analyzed. The *XAF1* promoter methylation levels were determined in bisulfite treated tumor DNA obtained from histologically confirmed tumor areas on FFPE sections of high grade (WHO III and IV) brain tumors. The methylation was determined and the impact on clinical parameters like age, sex, PFS, OS, and *IDH1* status was evaluated in a retrospective study.

3.6.3.1 Patient characteristics

A total of 80 tumor specimens were analyzed during this study (see **Suppl. Table 4** for patient's data). Patients with a newly diagnosed malignant brain tumor were included in the analysis. In accordance with the WHO Guideline for "Classification of Tumours of the Central Nervous System" 2007 [25], the tumors had been classified by a neuropathologist as WHO grade III AA, AO, AOA, or grade IV GB. The composition of the different tumor entities in the dataset is summarized in **Table 16**. Most of the tumors are GB with 67.5 %, while the remaining 32.5 % are made up by grade III astrocytic, oligodendroglial tumors as well as the less well defined AOA.

Table 16: Frequencies of different tumor entities in the HGG cohort analyzed. Tumors were diagnosed on the basis of histopathological features at the Institute of Neuropathology of the University Medical Center Mainz. (abbr.: AA anaplastic astrocytoma; AOA anaplastic oligoastrocytoma; AO anaplastic oligodendroglioma; GB glioblastoma)

WHO grade		N	Percent	N
III	AA	14	17.5	26
	AOA	8	10.0	
	AO	4	5.0	
IV	GB	54	67.5	54
	Total	80	100	80

3.6.3.2 Receiver operating characteristics: Verification of the promoter methylation threshold in HGG patient samples

To test possible methylation thresholds with the best predictive potential for classifying the tumors as either *XAF1* M or *XAF1* UM, a receiver operating characteristics (ROC) curve was calculated. The ROC analysis provides an unbiased method to define a threshold the highest possible true positive rate (sensitivity) and a preferably low false positive rate (1 specificity). ROC curves are used in different clinical setups to test variables with binary outputs for their suitability, e.g. as cancer risk factor, imaging biomarker, high risk predictor, or other applications [206 209]. For this purpose, *XAF1* methylation was set as classifier (test variable), and its value for predicting an OS or PFS > 24 months (state variable) was calculated for all possible discrimination thresholds (**Figure 56, Suppl. Table 2 and 3**). Both parameters were graphed with the sensitivity lying on the ordinate and 1 specificity on the abscissa. A perfect classifier (red dot) is found in the upper left corner of the diagram (**Figure 55**). A point at the diagonal (line of no discrimination) has no discriminating value, as random guess would yield the same results. The AUC of the ROC curve is 1 for a perfect classifier and 0.5 for a curve identical with the line of no discrimination. Thus, the higher the AUC (> 0.5), the better is the diagnostic performance of the analyzed variable [210].

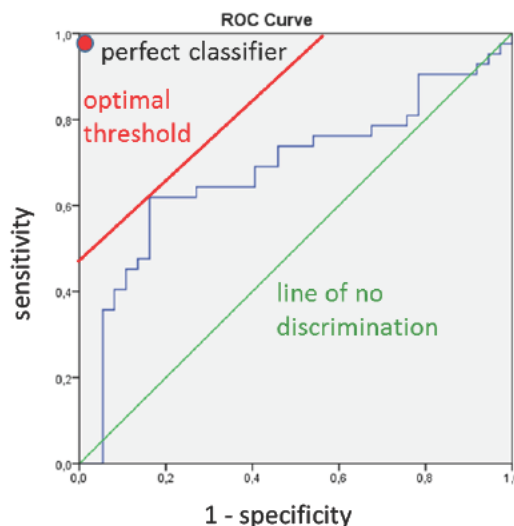


Figure 55: Explanation of a receiver operating characteristics (ROC) curve plotting the sensitivity (ordinate) against 1-specificity (abscissa) for a test variable (blue graph). The optimal threshold for discrimination is indicated (red line) at the best possible compromise for the lowest possible false-positive and highest true-positive rate. The line of no discrimination with an AUC of 0.5 is plotted in green.

Results

The ROC curve calculated from *XAF1* methylation data for predicting the OS and PFS (**Figure 56**, blue graph) shows an AUC of 0.76 and 0.87, respectively. This points to a strong classifier with a good predictive value for the state variable (i.e., survival). According to this ROC curve, an optimal threshold with lowest possible false positive and highest true positive rate for as signing patients to the group of either *XAF1* UM or *XAF1* M can be derived at a sensitivity of 0.697 for the OS or at 0.857 for PFS. This corresponds to a methylation value of 17.4 % and 36 %, respectively, which can be read off the coordinates of the curve (see suppl. tables).

The analysis of the predictor “*XAF1* methylation” by a ROC curve thus yields almost identical results as derived from the observations made in glioma cell lines (see 3.6.2). The very strong value of *XAF1* methylation for predicting the PFS (AUC = 0.857) provides additional evidence that dichotomizing patients according to this factor provides valuable prognostic information. On basis of the ROC data, a threshold at 34 % *XAF1* promoter methylation is justified and was thus used for grouping of the patient samples.

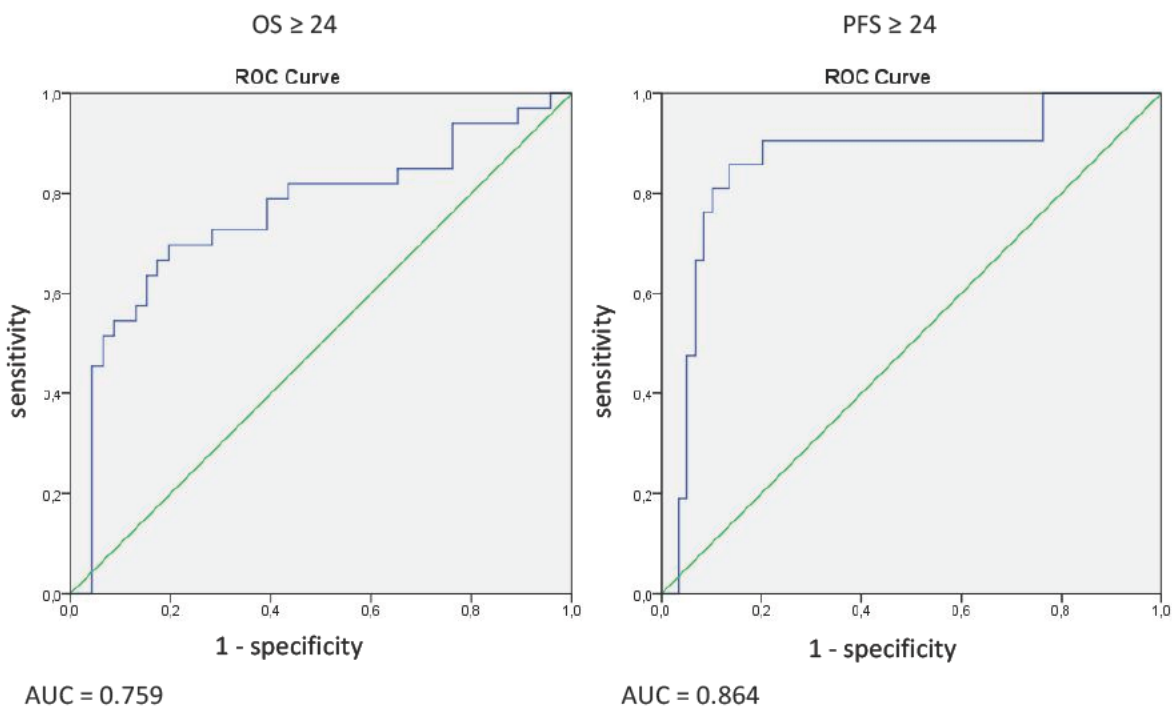


Figure 56: Receiver operating characteristics (ROC) curve for the sensitivity (ordinate) and 1- specificity (abscissa) for *XAF1* methylation (blue graph) with the state variable OS ≥ 24 (left) and PFS ≥ 24 (right). Area under the curve is provided below. For better orientation, the line of no discrimination is plotted in green.

3.6.3.3 XAF1 methylation is associated with an improved survival in malignant gliomas

32.5 % of the patients showed a methylated *XAF1* promoter within their tumor tissue (**Table 17**). No prevalence was found for sex, whereas older patients (> 70 y) tend to exhibit a methylated *XAF1* promoter less frequently than patients of younger age (< 70 y) at diagnosis (41.1 % vs. 12.5 %). Interestingly, a high percentage of patients with WHO grade III tumors (69.2 %) were methylated in the *XAF1* promoter, compared to only 14.8 % of grade IV gliomas.

Table 17: XAF1 promoter methylation in different subgroups of HGG patients.

	N total	XAF1-M	
		%	N
All patients	80	32.5	26
Women	24	29.2	7
Men	56	33.9	19
Age < 70 years	56	41.1	23
Age ≥ 70 years	24	12.5	3
Grade III	26	69.2	18
Grade IV	54	14.8	8

The clinical implications of *XAF1* promoter methylation were analyzed by Kaplan Meier survival estimates. Time to event in months was calculated for the endpoints of experiencing a progress (PFS) or death (OS). Four patients had to be excluded from OS analysis due to a loss of follow up. Dichotomizing the patients for *XAF1* status revealed significant differences in the survival and progression of the disease. Methylation of the *XAF1* promoter was associated with a significantly prolonged PFS (**Figure 57, A**) for and an improved OS (**Figure 57, B**).

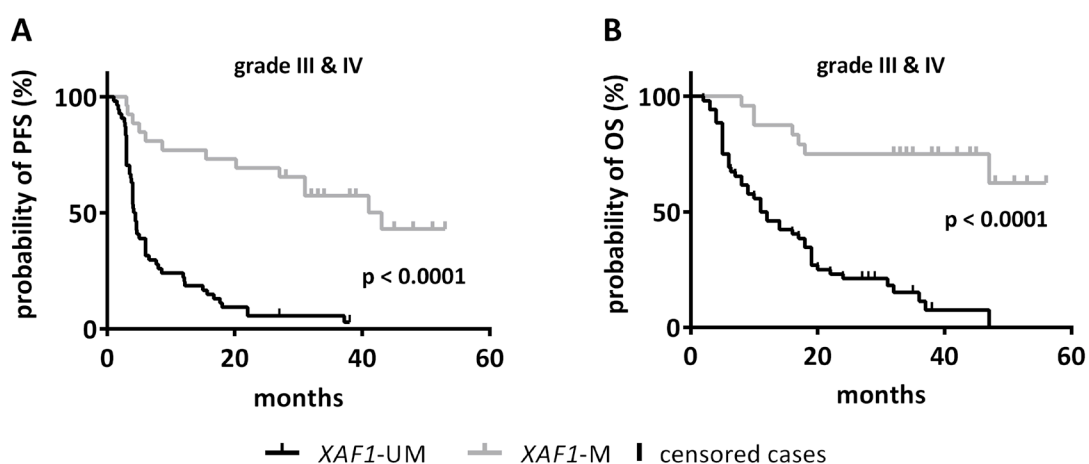


Figure 57: Kaplan-Meier survival analysis for HGG patients (N = 80). Group separation was performed for *XAF1* promoter methylation status as determined by MS-HRM. Progression free survival (PFS; A, C) and overall survival (OS; B, D) was compared between both groups. Survival differences were tested for statistical significance by Log-rank test.

Results

Further subgrouping of the dataset according to the tumor grade (WHO III vs. WHO IV) revealed that *XAF1* methylation is associated with improved clinical outcome in patients with AA, AO, and AOA (grade III). The separate analysis of both tumor groups (**Figure 58**) shows that the effect was even more pronounced in tumors of grade III (C, D). However, there was no significant difference for PFS and OS in WHO grade IV GB (E, F) in Kaplan Meier analysis. The presented data reveals that, depending on the tumor grade, patients with a methylation in the *XAF1* promoter have an overall survival advantage and suffer later from a relapse of the tumor.

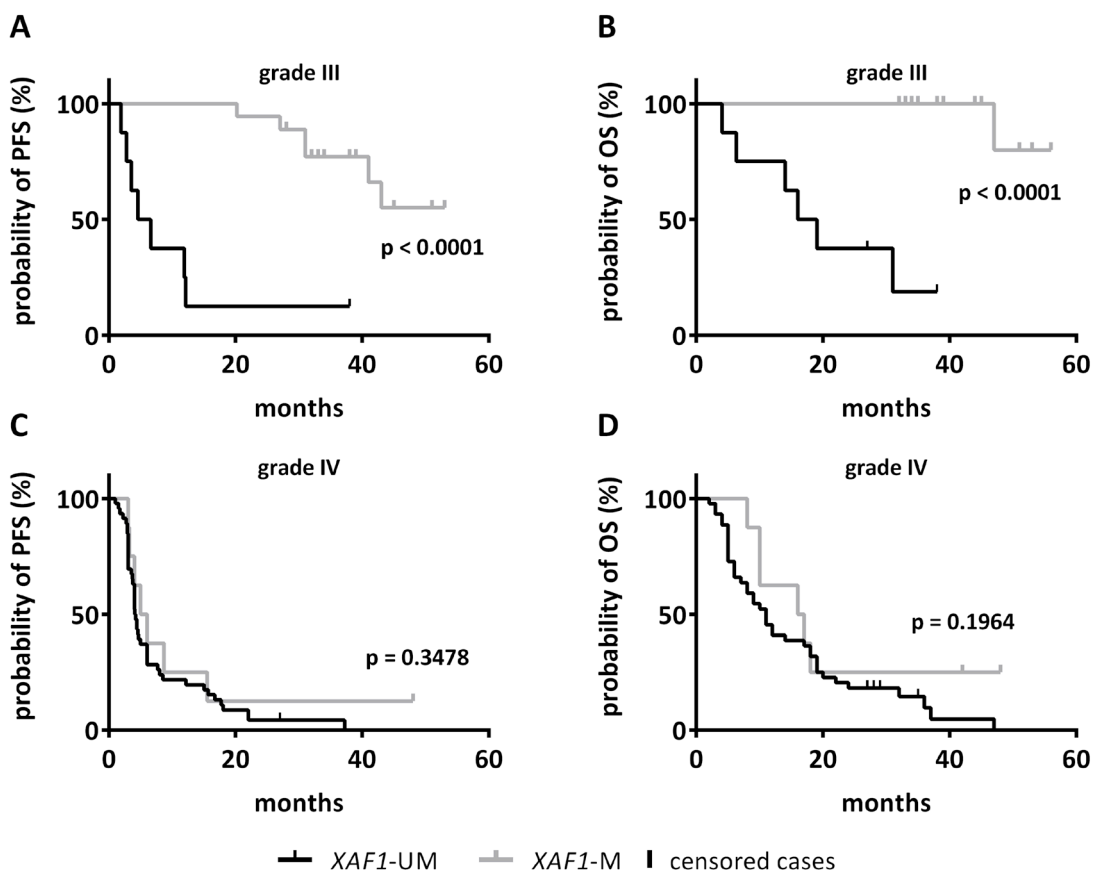


Figure 58: Separate Kaplan-Meier survival analysis for patients with WHO grade III (A; B) and grade IV (C, D) tumors. Group separation was performed for *XAF1* promoter methylation status as determined by MS-HRM. Progression free survival (PFS; A, C) and overall survival (OS; B, D) was compared between both groups. Survival differences were tested for statistical significance by Log-rank test.

For further investigation, the frequencies of *IDH1* mutations and *XAF1* methylation were calculated for different patient subsets. Among 26 grade III gliomas, 18 (69.2 %) showed a mutation in the *IDH1* gene (**Table 18**). Most strikingly, all 18 tumors showed a methylation in the *XAF1* promoter. In line with this, among the eight *IDH1* wt tumors, none was methylated, leading to a 100 % association between both values in this tumor subtype ($r_s^4 = 1$; N = 26).

Table 18: Crosstabulation^a frequencies of the *IDH1* mutation and *XAF1* methylation in grade III gliomas. *XAF1*-UM and *IDH*-wt are indicated with "0", while occurrence of *XAF1*-M and *IDH1*-mut is coded with "1".

		IDH1mut		Total
		0	1	
XAF1_Methylation 0	Count	8	0	8
	% within XAF1_Methylation	100.0%	0.0%	100.0%
	% within IDH1mut	100.0%	0.0%	30.8%
	% of Total	30.8%	0.0%	30.8%
1	Count	0	18	18
	% within XAF1_Methylation	0.0%	100.0%	100.0%
	% within IDH1mut	0.0%	100.0%	69.2%
	% of Total	0.0%	69.2%	69.2%
Total	Count	8	18	26
	% within XAF1_Methylation	30.8%	69.2%	100.0%
	% within IDH1mut	100.0%	100.0%	100.0%
	% of Total	30.8%	69.2%	100.0%

a. Grade III/ AA, AO, AOA

⁴ Spearman's rank correlation coefficient for *IDH1*-mut vs. *XAF1*-M in WHO grade III gliomas; significance level cannot be determined due to an absolute correlation

Results

In contrast, among 54 WHO grade IV tumors (**Table 19**) representing GB merely eight were *XAF1* M (14.8 %). Among these, only two tumors showed an *IDH1* mutation. Since this mutation is exclusive for lower grade gliomas, these tumors most likely represent a small fraction of GB that have evolved from lower grade tumors (secondary glioblastomas). In contrast to the findings in grade III tumors, GB (grade IV) showed a small subgroup of six tumors which exhibited a methylated *XAF1* promoter despite being *IDH1* wt. Beside the discrepancy in these six tumors, a significant positive correlation between *IDH1* mut and *XAF1* M was observed ($r_s = 0.470$; $p \leq 0.0001$; $N = 54$). Most tumors (85.5 %) neither showed an *IDH1* mutation nor exhibited a methylated *XAF1* promoter.

Table 19: Crosstabulation^a frequencies of the *IDH1* mutation and *XAF1* methylation in grade IV gliomas (GB). *XAF1*-UM and *IDH*-wt are indicated with “0”, while occurrence of *XAF1*-M and *IDH1*-mut is coded with “1”.

		IDH1mut		Total
		0	1	
XAF1_Methylation 0	Count	46	0	46
	% within XAF1_Methylation	100.0%	0.0%	100.0%
	% within IDH1mut	88.5%	0.0%	85.2%
	% of Total	85.2%	0.0%	85.2%
1	Count	6	2	8
	% within XAF1_Methylation	75.0%	25.0%	100.0%
	% within IDH1mut	11.5%	100.0%	14.8%
	% of Total	11.1%	3.7%	14.8%
Total	Count	52	2	54
	% within XAF1_Methylation	96.3%	3.7%	100.0%
	% within IDH1mut	100.0%	100.0%	100.0%
	% of Total	96.3%	3.7%	100.0%

a. Grade = Grade IV /GB

Since IHC detection of the *IDH1* status might miss rare mutations not being recognized by the R132H specific Ab, *IDH1* wt status of these patients was additionally confirmed by pyrosequencing (data not shown). Furthermore, the position R172 of the *IDH2* gene was analyzed by pyrosequencing, since mutations at this position also can give rise to the G CIMP (**Figure 59**). *IDH1/2* wild type status could be confirmed in all samples, thus leading to the conclusion that in grade IV gliomas *XAF1* methylation might occur independently of a general G CIMP.

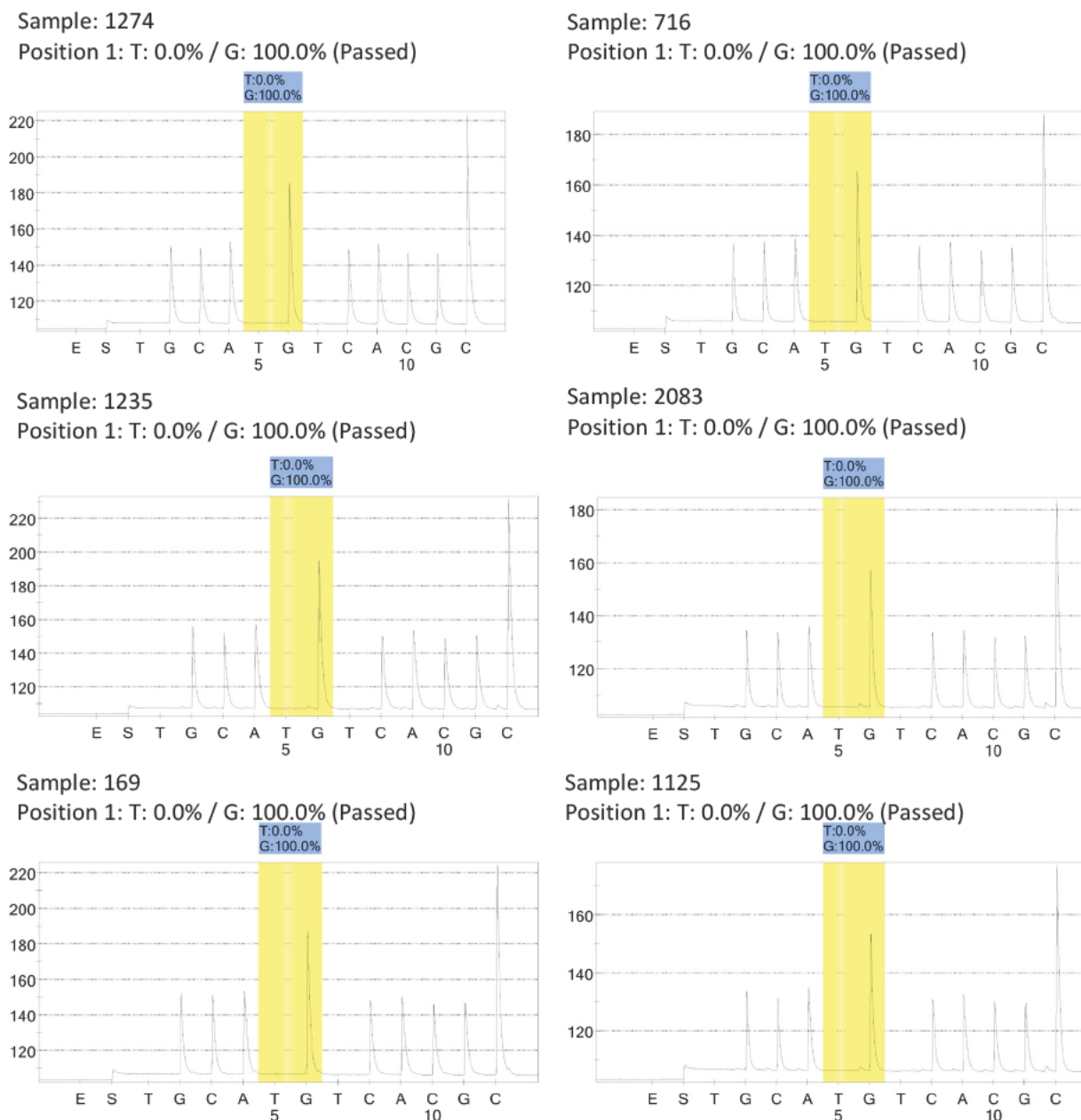


Figure 59: Pyrosequencing results analyzing SNPs at position 172 of the *IDH2* gene. DNA from six GB *XAF1*-M and *IDH1*-wt samples was subjected to PyroMark PCR and analyzed by pyrosequencing. The wt *IDH2* sequence was detected in all six samples.

In summary, the comparison between the cases positive for *IDH1* mutation and *XAF1* methylation are identical in grade III tumors, whereas no absolute association was observed in WHO IV tumors. Here, six tumor samples showed a methylated *XAF1* promoter despite *IDH1* and *IDH2* wt status. Furthermore, patients above an age of 70 did not show a mutation in *IDH1*, which points to an association with younger age (Table 20). Correspondingly, *XAF1* promoter methylation was observed more frequently in the group of patients below 70 years of age, while frequencies in men and women were equal.

Results

Table 20: Summary of XAF1 promoter methylation and IDH1 mutation frequencies in HGG.

	N	XAF1-M (%)	N	IDH1-mut (%)	N
All patients	80	32.5	26	25.0	20
Women	24	29.2	7	25.0	6
Men	56	33.9	19	25.0	14
Age < 70 years	56	41.1	23	35.7	20
Age ≥ 70 years	24	12.5	3	0.0	0
Grade III	26	69.2	18	69.2	18
Grade IV	54	14.8	8	3.7	2

XAF1 methylation was tested for correlation with other clinical parameters in the dataset (**Table 21**). XAF1 M was significantly correlated with OS ($r_s = 0.565$) and PFS ($r_s = 0.503$). No correlation was found with sex and an inverse correlation was observed for age ($r_s = -0.457$), indicating that XAF1 M occurs less frequently in older patients. Most strikingly a strong, significant correlation could be observed between IDH1 mutation and XAF1 methylation (0.832). As described earlier, this mutation occurs frequently in younger patients with low grade (WHO II) and grade III gliomas. Thus, a strong inverse correlation of IDH1 mut with grade ($r_s = -0.709$) and age ($r_s = -0.568$) was observed. The strongest correlation with OS and PFS was observed with IDH1 mutation (0.693; 0.666), underlining the high prognostic value of this tumor marker.

Table 21: Bivariate correlations determined by Spearman's rank-order correlation coefficient (r_s) for different clinical parameters in the HGG cohort. Significance level (two-tailed) is indicated by asterisks.

		XAF1 Meth.	OS	PFS	OS24	PFS24	IDH1 mut	Age	<70 y	Sex	Grade
XAF1 Meth.	r_s	1									
	N	80									
OS	r_s	,565**	1								
	N	79	79								
PFS	r_s	,588**	,763**	1							
	N	80	79	80							
OS24*	r_s	,472**	/	/	1						
	N	79			79						
PFS24*	r_s	,678**	/	/	,710**	1					
	N	80			79	80					
IDH1mut	r_s	,832**	,693**	,666**	,664**	,837**	1				
	N	80	79	80	79	80	80				
Age	r_s	-,457**	-,515**	-,453**	-,515**	-,554**	-,568**	1			
	N	80	79	80	79	80	80	80			
<70 y	r_s	,264*	,359**	,345**	,317**	,379**	,367**	/	1		
	N	80	79	80	79	80	80	80	80		
Sex	r_s	-0,047	0,045	-0,014	0,054	-0,019	0	-0,009	-0,066	1	
	N	80	79	80	79	80	80	80	80	80	
Grade	r_s	-,544**	-,534**	-,545**	-,527**	-,678**	-,709**	,442**	-,264*	-0,012	1
	N	80	79	80	79	80	80	80	80	80	80

* OS24/ PFS24 is a binary classifier, indicating an OS or PFS ≥ 24 months

3.6.3.4 Identification of a false negative *IDH1* wt diagnosis using *XAF1* methylation

One particular case in the subgroup of grade III tumors was outstanding, as the patient sample showed *XAF1* methylation in spite of a *IDH1* wt status. Since all other cases of *XAF1* M (17 out of 18) were also diagnosed with *IDH1* mut, this patient sample was subjected to pyrosequencing for *IDH1*. As the clinical diagnosis of the patient's *IDH1* status was performed by IHC, the possibility arose that false negative result was produced due to a rare *IDH1* mutation, not being recognized by the R132H specific antibody. Indeed, a very rare SNP was detected in this sample. Pyrograms (Figure 60) show the *IDH1* wt sequence compared to the common heterozygous *IDH1* mutation G395A and the patient sample analyzed. A heterozygous SNP was found at position 394 (C ⇌ G) which causes the substitution of an arginine (R) to glycine (G) at position 132, thus the mutation is not being recognized by the R132H specific IHC antibody. The majority of all *IDH1* mutations is of G395A (R132H), which is found in approximately 92.7 % of the tumors [32]. However, in the same study the mutation identified here, has been described for 0.9 % of the cases. Using MS HRM, we could identify a false negative IHC result via analysis of the *XAF1* status. The diagnosis aided by pyrosequencing was adjusted in the patient's data (Table 18), thereby leading to a 100 % correlation of *XAF1* M and *IDH1* mut.

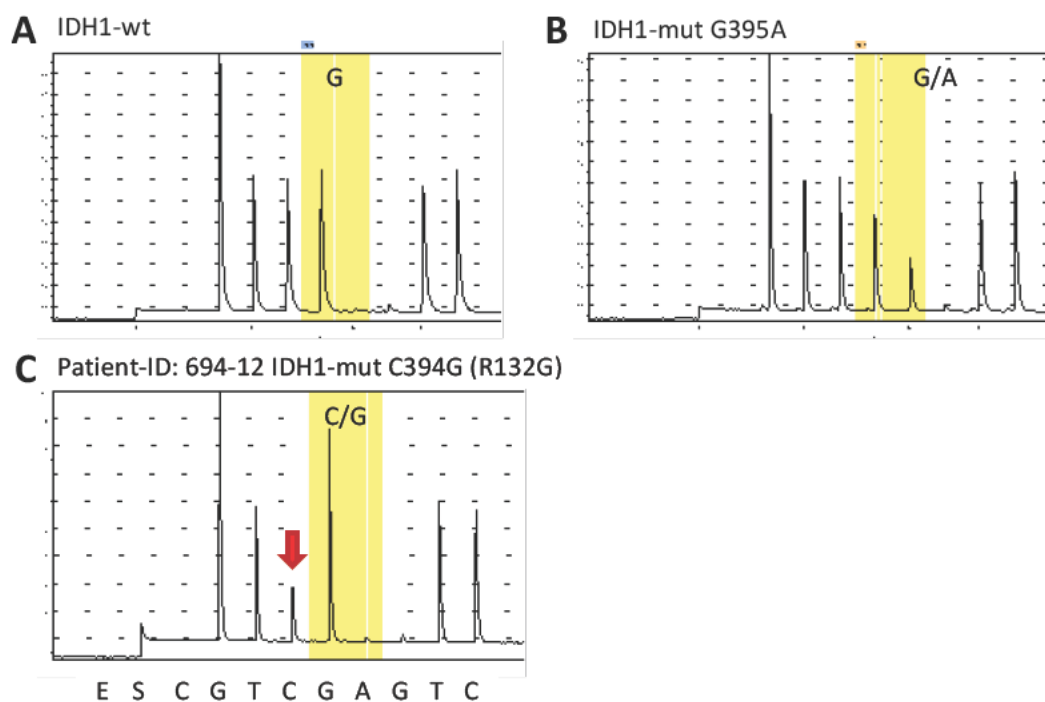


Figure 60: Pyrosequencing results for detecting SNPs in the *IDH1* gene. The yellow bar indicates position 395/132 which is commonly mutated in gliomas. Results are shown for A) an *IDH1*-wt sample, B) a sample showing the heterozygous G395A mutation, and C) one patient sample with a rare heterozygous C394G mutation (red arrow indicates position 394). Pyrosequencing dispensation order is indicated below diagram C.

Results

3.6.4 A lack of XAF1 changes response of glioma cells to TMZ

To investigate the molecular influence of *XAF1* silencing and elucidate its association with survival benefits beyond *IDH1* mutation, knockdown experiments were conducted in LN229 cells. Although the effect of *XAF1* silencing in tumors might be overshadowed by the far reaching impacts of G CIMP, the influence on the response to TMZ was hereby analyzed in an *IDH1* wt background. The presented data provide evidence that a lack of the tumor suppressor XAF1 can alter the response to TMZ. Cellular survival, cell cycle distribution, and proliferation were analyzed after XAF1 knockdown and overexpression of XAF1.

3.6.4.1 XAF1 knockdown abrogates the TMZ induced G2 arrest

In search of possible molecular explanations for the positive prognosis associated with XAF1 methylation, further studies were conducted in GB cell line LN229. Colony formation was analyzed for different TMZ concentrations (**Figure 61**). To mimic XAF1 promoter methylation, cells were transfected with siRNA targeted against XAF1 mRNA. The ability of LN229 cells to form colonies was not impaired after the knockdown of the protein compared to con siRNA transfected cells. Both survival curves were in line with the colony survival presented earlier for LN229 cells (see 3.3.1).

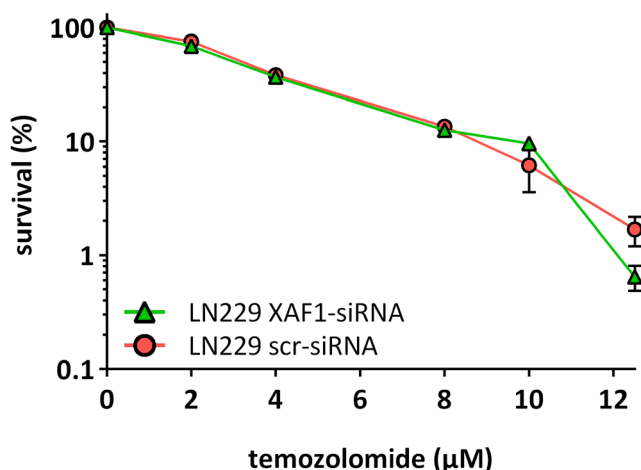


Figure 61: Colony formation assay (CFA) in LN229 cells with (*XAF1*-siRNA) and without (*scr*-siRNA) knockdown of XAF1 upon the treatment with 100 μM TMZ. Surviving cells were normalized to control (%) and plotted in a semi-logarithmic graph. Data of three independent experiments is shown ($N = 3$) with error bars indicating SD.

To address not only long term effects of *XAF1* silencing, a cell viability assay (MTT) was performed 96 and 120 h after the treatment with TMZ (**Figure 62**). Cells were transfected with *XAF1* siRNA and scramble siRNA (scr) 24 h prior to the treatment. Interestingly, at both time points a slightly increased viability could be observed upon *XAF1* knockdown when compared to scr siRNA. A slight protective effect from TMZ treatment can thus be assumed for *XAF1* knockdown at both time points.

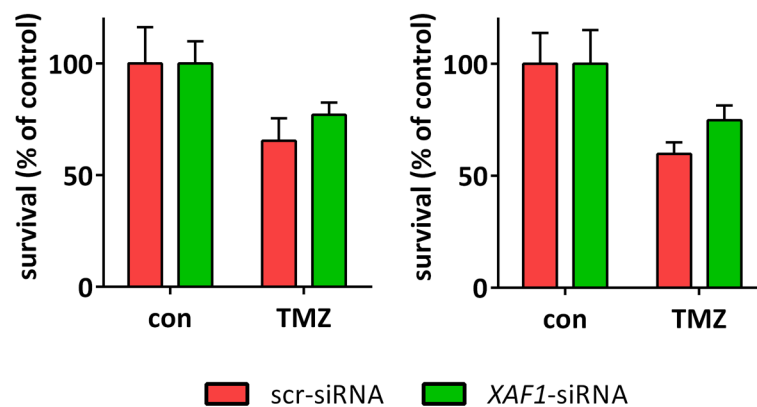


Figure 62: MTT cell viability assay for scramble-siRNA (scr) and *XAF1*-siRNA transfected LN229 cells A) 96 and B) 120 h upon the treatment with 100 μ M TMZ. Viability was normalized to untreated control. Error bars indicate SD of technical triplicates.

3.6.4.2 *XAF1* knockdown abrogates TMZ induced cell cycle arrest in glioma cells

Upon *XAF1* knockdown, a severe impact on the cell cycle distribution could be observed for the treatment with TMZ. **Figure 63** shows representative histograms of the SubG1 analysis in LN229 cells 96 h after treatment. For an unbiased analysis of the cell cycle distribution, cell cycle phases were calculated using ModFit 3.3 analysis software. Untransfected cells (A, D) were compared to cells transfected with scramble siRNA (B, E) and *XAF1* siRNA (C, F). In untreated cells (A, C), no differences were observed in the cell cycle distribution. Upon TMZ treatment, LN229 and scr siRNA transfected cells showed a characteristic cell cycle block in G2 (**Figure 63 D, E**). Here, 75 % of parental LN229 and 61 % of scr siRNA transfected cells were arrested in G2. Most strikingly, this G2 arrest was not evident when *XAF1* expression was attenuated by knockdown (**Figure 63 F**). Despite TMZ treatment, these cells showed only a moderate increase in G2 cells and instead a cell cycle distribution comparable to untreated cells (compare **Figure 63 C, F**).

Results

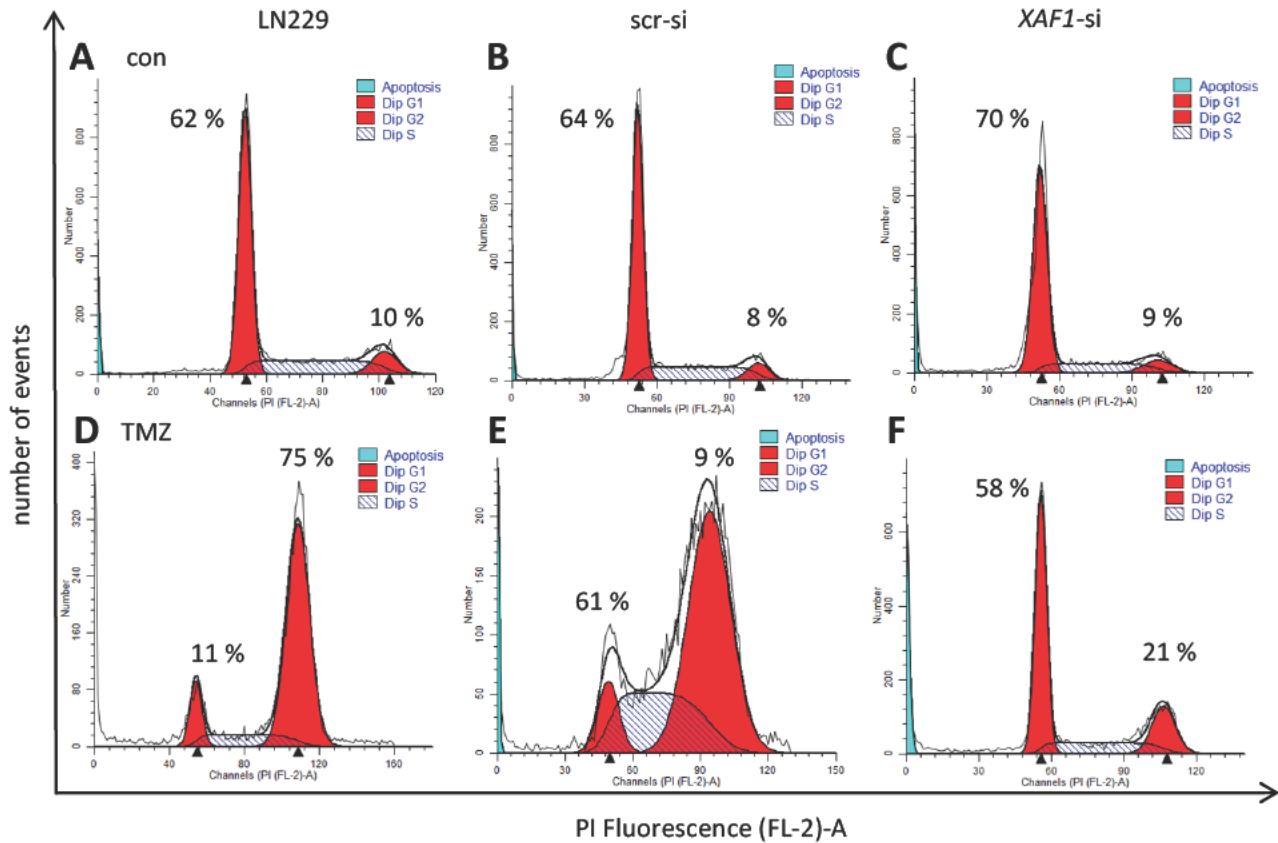


Figure 63: Cell cycle analysis of LN229 cells 96 h upon treatment with 100 μ M TMZ and XAF1 knock-down. Parental LN229 cells (A; D) were compared to LN229 cells transfected with scr-siRNA (B; E) and XAF1-siRNA (C; F). Percentages indicate portion of cells in G1-phase (left peak) and G2-phase (right peak). Data were analyzed and plotted with ModFit 3.3. Histograms of the number of events (ordinate) vs. PI fluorescence measured as FL2-A (abscissa) are shown.

The abrogation of the TMZ induced G2 arrest by XAF1 kd was consistently observed at 96 h as summarized for three independent experiments in **Figure 64**. XAF1 kd almost completely abrogated the TMZ induced G2 block observed in scr siRNA transfected (control) cells (16.9 % vs. 65.7 %). A small but significant increase in the number of G2 cells upon treatment could be observed in XAF1 kd cells though. In contrast scr siRNA transfected cells showed a strongly increased percentage of G2 cells upon TMZ treatment. Strikingly, G2 fractions did not differ significantly between the untreated control and TMZ treated XAF1 kd cells. Furthermore, an accumulation of cells in the G1 phase (63.9 % vs. 11.5 %) was observed for XAF1 kd + TMZ when compared to scr siRNA transfected cells. Interestingly, cells transfected with XAF1 siRNA and treated with TMZ showed the same fraction of G1 cells as untreated control cells since no significant difference was observed. S phase fractions seemed to be slightly reduced upon XAF1 kd, although differences were not significant. In the background of XAF1 kd, strong

differences in the percentage of cells in G1 and G2 were observed upon TMZ treatment. This indicates that the underlying response to TMZ is completely changed in the absence of XAF1.

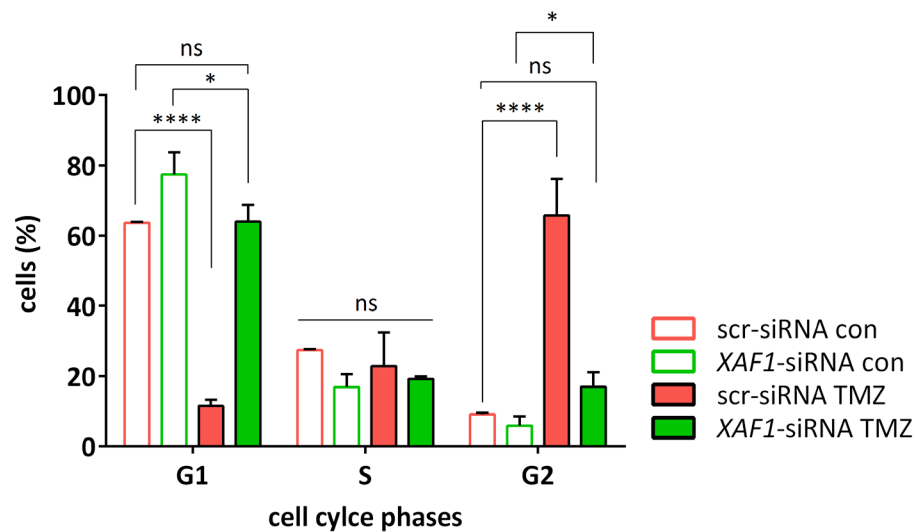


Figure 64: Cell cycle distribution of LN229 cells 96 h upon treatment with 100 μM TMZ. Cells were transfected with scramble siRNA and XAF1 siRNA. Cell cycle phases were analyzed, using Modfit 3.3 in at least three independent experiments ($N \geq 3$) with error bars indicating SD. Test for statistical significance was performed by Two-Way ANOVA with Tukey's post hoc analysis.

3.6.4.3 Implications of XAF1 knockdown for proliferation

To consolidate the data concerning the S phase distribution (**Figure 64**), cell proliferation was measured after XAF1 kd by a BrdU incorporation assay (**Figure 65**). scr siRNA and XAF1 siRNA transfected cells were incubated with BrdU for two hours at different time points after the treatment with TMZ. The total incorporation of BrdU was normalized to the control (untreated cells) at 24 h. While the incorporation rate was slightly increased in both transfections 24 h upon TMZ, BrdU DNA labeling constantly decreased over the rest of the observation period. This indicates the presence of replication blocking lesions without showing striking differences between scr siRNA and XAF1 siRNA transfection. Though, a slight reduction in the BrdU incorporation can be seen for the XAF1 knockdown in a time frame of 48 – 120 h.

Results

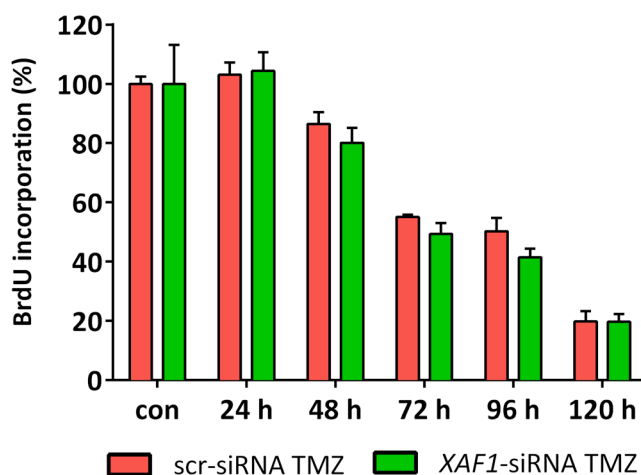


Figure 65: ELISA BrdU incorporation assay for different time points upon treatment with TMZ (100 μ M). LN229 cells were transfected with scr-siRNA or XAF1-siRNA prior to treatment with TMZ. Error bars indicate SD of technical triplicates.

3.6.5 Overexpression of XAF1 TMZ-treated glioma cells

To address the question whether XAF1 overexpression has an impact on the cellular response to TMZ, LN229 cells were transfected with an XAF1 GFP expression plasmid prior to treatment (Figure 66). Automated cell cycle analysis was performed using ModFit 3.3 analysis software. Expression of XAF1 GFP was verified flow cytometrically by the determination of GFP positive cells. Upon overexpression of XAF1 GFP, the percentage of cells in G1 and G2 phase was reduced when compared to mock transfected cells (Figure 66, A B). In contrast, the percentage of S phase cells was increased upon XAF1 GFP expression (31 % vs. 44 %). Upon TMZ treatment, the characteristic G2 block in XAF1 GFP transfected cells was still eminent (Figure 66, D) but strongly decreased from 72 % to 44 % (Figure 66, C). This may indicate a blockage of cells in the S phase for an abundant amount of XAF1 protein. However, upon overexpression of XAF1 GFP, no induction of apoptosis could be observed for the treatment with TMZ (and control).

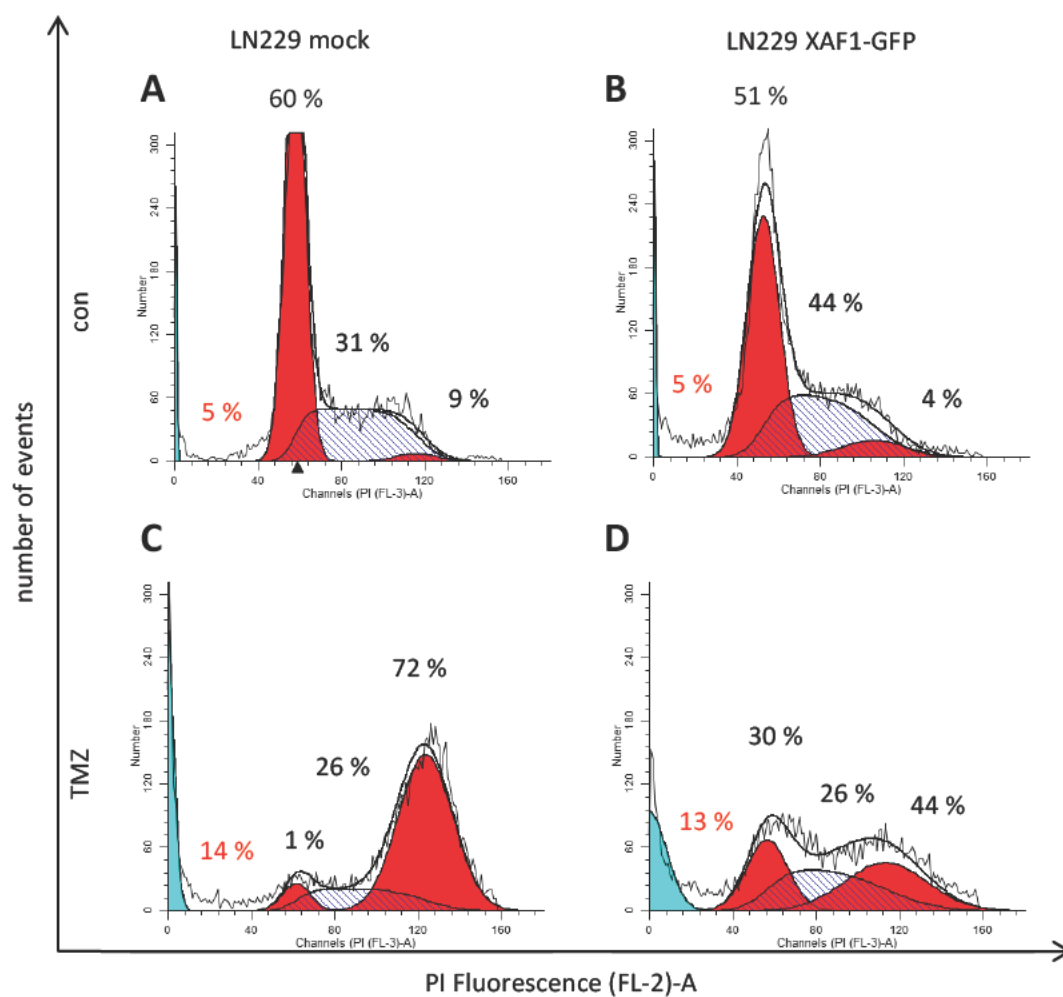


Figure 66: Cell cycle distribution of LN229 cells 72 h upon treatment with 100 μ M TMZ. Mock transfected LN229 cells (A; C) were compared to LN229 cells transiently transfected with an XAF1-GFP expression plasmid (B; D). Cells were treated with 100 μ M TMZ (B; D). Percentages indicate portion of cells in G1-, S-, and G2-phase (from left to right). The proportion of apoptotic cells is indicated. Data were analyzed and plotted with ModFit 3.3. Histograms of the number of events (ordinate) vs. PI fluorescence measured as FL2-A (abscissa) are shown.

4 Discussion

The proteins of the IAP family exhibit multi nodal functions involved in diverse cellular pathways. IAPs and especially Survivin is among the top cancer associated genes [211], being strongly expressed in almost all human malignancies including esophageal, lung, ovarian, central nervous system, breast, colorectal, bladder, gastric, prostate, pancreatic, laryngeal, uterine, hepatocellular, and renal cancers, as well as some hematologic malignancies in a cell cycle independent manner [212]. Survivin overexpression is generally associated with a poor clinical prognosis in terms of shorter relapse free survival and OS in oesophageal cancer [213,214], BC [215,216], hepatocellular carcinoma [217], pancreatic cancer [218], and astrocytomas [219] for example. In another study on 106 BC patients, the authors demonstrate no significant correlation between the mRNA expression of different Survivin splice variants and disease outcome [220]. However, the vast majority of reports links an increased Survivin expression to a worse, clinical prognosis. This association is further emphasized by the correlation between an overall higher Survivin level and an advanced tumor stage/ grade in different tumor entities. This was observed in malignant astrocytomas [219], meningiomas [221], and HCC [222,223] for example. Furthermore, Survivin expression did strongly correlate with the TNM stage (Tumor, Node, Metastasis) in CRC patients [224]. Interestingly, the impact of the localization of the protein, i.e. either occurring predominantly cytoplasmic or within the nucleus, is discussed controversially. It has become evident that especially the intracellular localization of Survivin is a good prognostic and sometimes predictive⁵ marker. Though, whether nuclear Survivin is associated with survival benefits seems to stay a matter of debate. Survivin, with a high cytoplasmic to nuclear ratio was found to be an independent predictor of an improved OS in BC [225]. In gastric cancer, a positive nuclear IHC staining for Survivin was associated with a favorable prognosis, while a cytoplasmic staining had no prognostic implications as well [226]. On the contrary, nuclear Survivin was significantly correlated with a shorter OS [227,228] and a worse five year survival in NSCLC [229]. Also for oral squamous cell carcinoma (OSCC), patients with a high expression of nuclear Survivin in their tumors showed a poorer prognosis [230]. Furthermore, similar observations have been made in CRC, where nuclear

⁵ Predictive markers have a value for predicting the response to a certain therapy, while prognostic markers are associated with survival, irrespective of an applied therapy.

Survivin and a combined nuclear and cytoplasmic localization was linked to prognostic parameters indicating a poorer prognosis [231].

For gliomas, there are only few reports analyzing the impact of Survivin's expression on the clinical outcome. While some investigators see no prognostic impact of Survivin expression in glioblastomas [232], others suggest the use of Survivin expression as biomarker for this disease, as a decreased 3 year OS rate was observed [233]. A meta analysis by Lv *et al.* analyzed 91 studies investigating the prognostic value of Survivin in gliomas and selected 15 articles to carefully chosen criteria [234]. Pooled hazard ratios were calculated, based on data of eight eligible studies and revealed a worse 2 year survival of patients with positive Survivin scores (hazard ratio: 0.17; 95 % CI: 0.11 – 0.26). However, the influence of the localization of Survivin was not considered.

In summary, these and other reports demonstrate the discordant situation for evaluating the prognostic value of Survivin expression and especially its localization in gliomas. In search of possible molecular explanations, we analyzed the influence of Survivin expression and localization on TMZ induced DNA damage in a glioblastoma cell model.

4.1 Survivin in the resistance of glioma cells to TMZ-induced cell death

The in vitro data presented here confirms the findings discussed above, showing a worse prognosis for patients with high Survivin levels. Colony formation assays (**Figure 32**, p. 84) showed a strong protective effect of the expression of Survivin GFP (further referred to as Survivin expression). This protection was seen for the treatment with the first line alkylating anti cancer drug TMZ as well as for TPT used for the treatment of pediatric gliomas or in second line therapy. In both cases, the expression of a Survivin variant, deficient for its NES, led to the opposite effect. Cell clones expressing NES deficient Survivin were even sensitized towards the applied treatment. Especially for TMZ, survival fractions were strongly reduced in comparison to control cells. In line with other reports [167,235], the data show the importance of an intact NES for successfully enhancing cellular survival. In contrast to these studies, we observed not only a loss of Survivin's protective effect but even a sensitizing effect upon expression of this Survivin variant.

Discussion

Regarding the induction of apoptosis (**Figure 34**, p. 86), the protective effect of Survivin was rather not reflected by the increased fractions of apoptotic or necrotic/ late apoptotic cells in a time frame of 120 – 144 h after the treatment with TMZ. Neither were the survival disadvantages of LN229 SurvNESmut GFP. Putatively, the expression of the IAP Survivin might reduce the apoptotic signaling upon genotoxic stress, thereby enhancing cellular survival. Due to the mechanism of action of TMZ, several cell cycles and the involvement of DNA repair processes are needed to exert its cytotoxic effects (see 1.4.1). Here, 120 h were sufficient to induce cell death (apoptosis + necrosis). The differences between LN229 Surv GFP and LN229 SurvNESmut GFP cells, however, were not significant at the time points investigated. Also, the activation of caspases 3 and 7 (**Figure 35**, p. 86) was not able to explain the huge survival differences in both cell clones. Although Survivin wt and Survivin NESmut expressing cell clones showed a slightly lower caspase activity 72 h after the treatment, this effect was no longer evident at the later time point of 144 h. Thus, the anti apoptotic properties of Survivin alone seem not to explain the long term survival benefits. However, a detailed analysis of the caspase activation in a time frame of 48 to 144 h could clarify whether a differential caspase activity can be measured at other time points.

In search for other cellular endpoints that can explain the increased survival of LN229 Surv GFP cells, in terms of an increased proliferative potential, induction of cellular senescence was analyzed. TMZ treatment was shown to induce premature cellular senescence (stress induced senescence) in LN229 GB cells (in contrast to replicative senescence) [236]. Here, the protection of Survivin overexpressing cells against the TMZ mediated induction of senescence might be linked to a sustained potential of these cells to proliferate (**Figure 36**, p. 87). Thus, induction of premature senescence was significantly reduced in LN229 Surv GFP cells. Consequently, LN229 Surv GFP cells retain their ability to proliferate and thus to form colonies, while senescence induction was significantly increased in LN229 and SurvNESmut expressing cells. This corresponds to an overall worse reproductive survival of LN229 and LN229 SurvNESmut GFP cells but does not explain the sensitization effect observed in LN229 SurvNESmut GFP cells.

4.1.1 Survivin reduces the number of TMZ-induced double-strand breaks

A first hint pointing to a possible role of Survivin during DNA repair was found when analyzing proteins involved in the DDR (**Figure 38**, p. 89). CHK1 is the distal transducer kinase, primarily

being activated by ATR via phosphorylation in response to stalled replication forks and ssDNA ends/ SSBs [82,237]. These ssDNA ends can also be generated during the processing (end resection) of DSBs [77]. However, an activation of CHK1 via the DSB sensing kinase ATM is also likely, since there is crosstalk between the ATM CHK2 and ATR CHK1 pathways [78]. Therefore, CHK1 (Ser345) phosphorylation was analyzed to address the question, whether initially different amounts of DNA damage could account for the beneficial outcome in LN229 Surv GFP cells. In both clones CHK1 becomes activated 48 h after the treatment with TMZ. The pCHK1 signal is stable for up to 96 h, indicating the presence of severe DNA damage. An equal CHK1 activation indicated an equal amount of DNA damage in both cell clones (LN229 Surv GFP vs. LN229 SurvNESmut GFP).

The affinity of p53 for its target promoters is strongly influenced by post translational protein modification at different residues. Phosphorylation at Ser15 is mediated by ATM and ATR and is considered to be a fundamental event upon DNA damage, allowing subsequent modifications of different p53 residues [238]. p53 mutated for Ser15 fails to mediate transcription or growth arrest [239] and therefore seems to be crucial for the adequate DDR. Following DNA damage, the p53 mediated induction of apoptosis is also dependent on the phosphorylation of this residue [240]. Here, a strong initial activation of p53 at serine 15 was observed in both LN229 clones. This corresponded with the following phosphorylation of Ser46, generally associated with a transactivation activity at the promoter of pro apoptotic genes. A slightly higher induction in LN229 SurvNESmut GFP cells at 96 h when compared to LN229 Surv GFP cells indicates the persistence of DNA damage. LN229 Surv GFP cells are seemingly able to better handle the induced amount of DNA damage. Most strikingly, this was reflected by the induction, i.e. phosphorylation, of the DNA DSB marker γ H2AX. While LN229 Surv GFP cells showed a strong decrease in the phosphorylation of the histone variant between 72 and 96 h, the phosphorylation level stayed high in LN229 SurvNESmut GFP cells. This indicates the presence of unrepaired DSBs in SurvivinNESmut expressing cells and vice versa a facilitated DNA repair in LN229 Surv GFP cells.

To elucidate the role of Survivin in the repair of TMZ induced DSBs, the sites of double strand breaks were visualized as distinct repair foci in LN229 cell clones. An early event during the DSB recognition is the phosphorylation of the histone variant H2AX at the C terminal Ser139 [241] which can occur up to megabases away from the initial break [242]. The resulting γ H2AX

Discussion

foci serve as surrogate marker of DSBs. However, the phosphorylation of H2AX is not limited to DSB sensing kinases ATM, DNA PK_{cs}, and their downstream kinases but can be carried out by ATR as well. Base alkylation, other than O⁶ MeG, arising from TMZ treatment can cause the stalling of replication forks and replication stress which activates ATR [78], ultimately causing H2AX phosphorylation. The detection of DSBs via γ H2AX should thus be validated by the co localization of γ H2AX with other proteins of the DSB repair. One such factor that was shown to co localize with γ H2AX during the processing of DSBs is 53BP1. 53BP1 localizes to nuclear foci in parallel to γ H2AX and thus provides an independent marker for the existence of DSBs at the site of a γ H2AX focus [243]. The exact co localization of γ H2AX and 53BP1 (**Figure 39**, p. 90) points to an activation of the DSB response and the subsequent phosphorylation of H2AX by ATM/ DNA PK_{cs} and their downstream kinases. This confirmation was important to narrow the observed effects to processes of DNA DSB repair.

In line with the initial finding in the western blot analysis, the expression of Survivin led to a decrease of DSBs induced by TMZ. This was most evident in a time frame of 48 – 96 h (**Figure 41**, p. 92) but could also be confirmed at the late time point 144 h (data not show). The observed foci numbers also reflected the sensitization effect towards TMZ in LN229 SurvNESmut GFP cells, as the induction of DSBs was highest in this cell clone. An intact NES was reported to be required to tether the Survivin/ Aurora B complex to the mitotic machinery and thereby being essential for proper cell division [167]. Inactivating mutations in the NES were associated with cell division defects, especially the occurrence of multinuclear cells, and furthermore with a loss of Survivin's cytoprotective function [*ibid.*]. Since endogenous Survivin might compensate for the NESmut mediated inhibition of mitosis, no signs of mitotic defects were observed in untreated LN229 SurvNESmut GFP cells. However, upon TMZ treatment, LN229 SurvNESmut GFP cells showed a strongly increased amount of DNA damage. Therefore, it might be assumed that under additional genotoxic stress NES deficient Survivin might contribute synergistically to genomic instability, thereby leading to mitotic catastrophe and a decreased survival.

Although NHEJ plays a minor role in the repair of TMZ induced DSB (see 1.4.1), a putative influence of Survivin expression was analyzed. Survivin was shown to facilitate the repair of IR induced DSBs via the NHEJ pathway (as discussed above). Indeed, a slight induction in the DNA PK activity was registered in both Survivin expressing cell clones upon irradiation when

compared to parental LN229 cells. This effect was pronounced in Survivin wt expressing cells and was virtually not detectable in the LN229 SurvNESmut GFP cells. In the case of parental LN229, this effect was not evident, indicating a link to an overexpression of Survivin. Interestingly, a decrease in DNA PK activity was observed for the treatment with TMZ. This could indicate a shift from NHEJ to the pathway of choice for the repair of TMZ induced DSB: the HRR. To further exclude that the survival enhancing and DNA damage reducing effects upon Survivin expression are linked to an increased NHEJ activity, a combination treatment with TMZ and a DNA PK inhibitor (Nu7026) was performed. No additional cytotoxic effects were observed in MTT assay and CFA. This underlines the expected minor role of NHEJ in the cellular defense against the alkylating agent TMZ. If an enhanced DNA repair via NHEJ was mediated by Survivin wt but not NES deficient Survivin, the survival differences between LN229 Surv GFP and LN229 SurvNESmut GFP cells should be diminished by NHEJ inhibition. However, CFAs with combination of TMZ and Nu7026 did show survival differences. In conclusion, a shift from the repair pathway of choice (HRR) to the NHEJ seems implausible for TMZ induced DSBs.

4.1.2 Survivin enhances double-strand break repair via HRR

Here, strong evidence for a putative participation of Survivin in the repair of TMZ induced DSBs is provided. In a closer investigation of the homologous recombination repair in this context, the assisting role of Survivin became evident in the background of a RAD51 knockdown. RAD51 is the major recombinase driving the homology search and strand invasion during HRR. Since DSBs are considered to be the main cytotoxic events, arising from TMZ treatment, the inhibition of this pathway was observed to be highly toxic for GB cells [185] which could be confirmed (**Figure 46**, p. 97). Upon Survivin expression, this sensitive phenotype could be rescued and the survival was strongly increased. This effect probably points to a compensation of the lack of RAD51 by Survivin. Whether this is due to a directly increased repair capacity or due to a putative restoration of the RAD51 expression remains elusive. The analysis of the H2AX foci formation suggests that several effects may lead to an enhanced survival of this cell clone (LN229 RAD51_sh + SurvGFP C1). In detail, foci numbers are significantly reduced in the C1 cell clone, when compared to the RAD51 knockdown cells. Compared to the parental cell line LN229, however, there is a still significantly increased number of foci per nucleus in both RAD51 depleted clones. Thus, the protection from DSB observed upon Survivin expression, cannot solely explain the strong survival differences mentioned before. Here, also the anti

Discussion

apoptotic functions of Survivin may play a major role. To further elucidate this finding, additional studies on the induction of apoptosis and caspase activation are strongly required. Gene expression studies on HRR genes in the background of Survivin overexpression might yield additional insights into the participation of Survivin in HRR, thereby leading to the identification of putatively regulated target genes. Furthermore, co immunoprecipitation experiments could reveal molecular interaction partners.

To prove the assumption of a facilitation of the HRR by Survivin, a functional qPCR based assay for the detection of the HRR activity was established. By this, it was clearly demonstrated that HRR activity is increased upon overexpression of Survivin wt and, conversely, was impaired upon knockdown of endogenous Survivin upon TMZ treatment. Furthermore, it was shown that the expression of NES deficient Survivin leads to an even more pronounced impairment of this pathway than the knockdown. Thus, NES deficient Survivin seems to interfere with the HRR. Probably, an intact NES might be required for Survivin's supportive role during HRR. Similar observations were made for Survivin's anti apoptotic functions, as discussed above.

Here, a new role of Survivin was described, showing that Survivin renders tumor cells less vulnerable to TMZ by increasing the cellular DSB repair activity. Most probably this also applies to other DNA lesions, repaired via HRR. Survivin's functions in developing therapy resistances seem to reach further than a mere inhibition of apoptosis. However, the role of Survivin in the processes of the HRR yet has barely been investigated. In confirmation of the data presented here, a recent report by Véquaud *et al.* showed an impaired HR activity after Survivin depletion in breast cancer cells [244]. Furthermore, the RNAi mediated knockdown of Survivin led to a state of "BRCAness" (see [6] and Introduction) in these cells, due to a downregulation of the DNA repair genes *EME1*, *BLM*, *EXO1*, *BRCA1*, *BRCA2*, and *RAD51*. According to the authors, this creates a susceptibility to DNA DSBs via targeting the recombinase *RAD51* and the nucle ase *MUS81/ EME1* both being important for HRR. Véquaud *et al.* further speculate that Survivin might take action in the transcriptional regulation of DNA repair genes [244]. These interesting findings support the data presented here and allow to assume that an upregulation of HRR genes upon overexpression of Survivin might explain the enhancement of HRR and the compensation for the *RAD51* knockdown.

Yet, another publication pointing into this direction analyses the impact of the Survivin inhibitor YM155 on HRR. A prolonged γ H2AX signal and a reduced formation of repair associated

RAD51 foci was detected for combination treatment with IR and YM155 when compared to irradiation alone [245]. The authors conclude that YM155 inhibits HRR by inhibition of the RAD51 foci formation. Indeed, these data indicate a putative role of Survivin in the response to IR. However, the use of YM155 for Survivin inhibition is highly controversial, since YM155 was shown to have many off target effects [reviewed in 246]. Additionally, the protective effects of Survivin upon irradiation are described as being dependent on NHEJ by others [68,157]. This explanation is more plausible, since NHEJ is the main pathway for the repair of IR induced lesions (see 1.4.2).

To our best knowledge, we are the first to establish a link between the expression of Survivin and an increased resistance towards TMZ due to decreased DNA damage. To utilize these findings, in diagnostic approaches, Survivin's expression and especially its localization could serve as biomarker for predicting the therapy response in different tumor types and particularly in gliomas. A method which allows an accurate analysis of both parameters in tumor tissue would thus be of great diagnostic value.

4.1.3 The use of nuclear Survivin as predictive marker for TMZ-based chemotherapy

Here, nuclear Survivin was shown to render tumor cells vulnerable to TMZ. Thus, patients with tumors expressing predominantly nuclear Survivin should benefit from this treatment. Our molecular observations support the association of nuclear Survivin with a better prognosis in HGG, and promote the use of Survivin's localization as predictive marker. One possibility to address the localization accurately is the detection of NES inactivating mutations in the *BIRC5* gene. To clarify, whether these mutations occur in HGG tumors, a panel of 100 HGG tumor and tumor samples and tumor relapses was analyzed for specific point mutations by pyrosequencing (see 3.2.5). The SNPs T278C, A288G (silent), and C292T have been described to occur in HNSCC and to correlate with a nuclear accumulation of Survivin [235]. In xenograft experiments, tumors bearing these mutations responded better to a chemotherapeutic treatment [*ibid.*]. A study regarding the survival of patients bearing these mutations has not been conducted so far. Thus, we aimed at the identification of these mutations in HGG tumors to test for an association with survival. In a high throughput approach, no SNP at position 278 of the *BIRC5* CDS was detected. However, deviations from the wt *BIRC5* sequence at position 292 were detected in low percentages. Unfortunately, no survival differences could be observed

Discussion

upon dichotomizing the patients as “noticeable” or “wt”. Although the sensitizing effect of a nuclear Survivin localization was clearly demonstrated in vitro, an effect associated with survival could not be observed in situ. NES mutated cells might represent a rather small cell population, as only some tumor cells within the tumor may exhibit this mutation [235]. Interestingly, the results of the IF staining show a strong nuclear localization of Survivin (without treatment) in all GB cell lines and HGG tumor sections investigated (**Figure 24**, p. 77 and **Figure 28**, p. 81). This indicates a predominantly nuclear localization of Survivin in HGG. A deregulation of processes of the nuclear cytoplasmic shuttling might explain this specific localization pattern, since NES inactivating mutations could be excluded.

Since a nuclear accumulation has been reported for the response to IR in GB cells [68] and a colorectal cancer cell line [157], localization changes upon genotoxic stress were analyzed to see whether this correlates with an increased DNA repair. Though, no nuclear accumulation of Survivin could be observed upon different types of DNA damage, neither for endogenous Survivin (**Figure 26**, p. 79) nor Survivin GFP (**Figure 23**, p. 76). At least for endogenous Survivin, this might be attributed the already nuclear localization pattern in these cells. The localization of Surv GFP, however, was predominantly cytoplasmic. Live cell imaging at different time points after treatment/ irradiation revealed that the localization was not influenced either. This leads to the conclusion that a nuclear accumulation of Survivin’s is not necessary for an enhanced HRR and that the protein is typically localized within the nucleus in HGG cells and tumors. Importantly, the pharmacological inhibition of the CRM1 mediated transport by LMB convincingly demonstrated the correct targeting of the GFP fusion protein by the CRM1 receptor, since a strong nuclear accumulation was evident upon inhibition.

4.2 Evaluation of *BIRC5* as epigenetic prognostic marker in gliomas

The contradicting reports dealing with the prognostic impact of Survivin expression in gliomas indicate the urgent need for clarification of the importance of Survivin as biomarker in HGG and other cancers. Due to the findings discussed above, the clear determination of Survivin’s localization in gliomas for prognostic purposes seems difficult. On the one hand, the detection of Survivin’s localization via IHC was shown to be sometimes misleading and difficult to interpret [247]. On the other hand, mutations inactivating the NES could not be detected in the dataset analyzed here.

Thus, we sought to establish a fast and accurate method to determine the Survivin status in glioma samples to test, whether the overall Survivin expression might correlate with survival in HGG. The method of choice should have been applicable to fixed tumor material to allow the conduction of retrospective studies as well. A methylation of CpGs in a promoter region reaching into the exon 1 of *BIRC5* was shown to occur more frequently in non cancerous ovaries when compared to ovarian cancer [149]. This could explain the generally high expression in cancer tissues vs. the low expression in normal tissue and might imply a role of Survivin during tumorigenesis. Convincing reports are missing, so this assumption remains highly speculative. Whether a *BIRC5* methylation occurs in gliomas, and even more interesting, whether this methylation has clinical implications, is not known up to now.

In the glioma cell lines analyzed here, no promoter methylation was detectable by MSP and MS HRM. 36 CpGs in the *BIRC5* promoter region were analyzed. This sequence reaches into the exon 1 and includes the p53 binding site [154] and also the MSP primers used by Wagner *et al.* [150]. To exclude that a demethylation in *BIRC5* is a result of in vitro culturing of tumor cells, methylation levels were also determined in 40 high grade glioma tumor samples. In accordance to the data in the cell lines, no signs of methylation could be detected either. The accuracy of this assay was verified by analyzing different methylation standards with defined methylation value (**Figure 50**, p. 101). In conclusion, no signs of methylation in the *BIRC5* promoter region were observed in gliomas. In line with the findings made in astrocytomas by Yu *et al.*, the *BIRC5* promotor appears to be unmethylated in all cases investigated here [153]. This leads to the conclusion that epigenetic silencing of *survivin/ BIRC5* does not occur in HGG and can therefore not be used as prognostic marker. Since glioma cells are rapidly dividing, a long term silencing of the *BIRC5* promoter might be avoided in order to allow proper cell division. Thus, expression of *BIRC5* most likely is essential for tumor to progress.

In search for other suitable biomarkers in gliomas, an important protein involved in IAP regulation was analyzed. XAF1 negatively regulates Survivin expression via post translational means and inhibits XIAP. Both factors have been proven clearly to account for the resistance to chemotherapeutic drugs in gliomas (see introduction and Tomicic *et al.* [248]). Although being considered as tumor suppressor, no genomic mutations involved in XAF1 inactivation and thus cancer formation have been identified so far [249]. This suggests other mechanisms by which cancer cells might get rid of XAF1.

4.3 *XAF1* promoter methylation is a promising biomarker in high-grade gliomas

Promoter hypermethylation associated with *XAF1* silencing was observed in gastric adenocarcinomas [179], urogenital malignancies [181], colon [180], esophageal [199], and ovarian cancer [250] and cancer cell lines [251]. Together these studies propose that the promoter region between -234 to +164 bp is most tightly associated with *XAF1* gene silencing. In this study, the methylation of three CpG sites in the region -236 to -196 bp upstream of the transcription start site (**Figure 51**, p. 104) was proven to be indicative of a loss of *XAF1* expression in a panel of 16 HGG cell lines. The majority (11) of these tumor cell lines showed a strong methylation of the *XAF1* promoter (**Figure 53**, p. 106). Correspondingly, methylation was inversely correlated with the *XAF1* mRNA expression, which is in accordance to reports by others, indicating a preferential low expression of the tumor suppressor *XAF1* in tumor cells [176,177,252].

4.3.1 *XAF1* promoter methylation accounts for gene silencing in high-grade gliomas

Here, the method of MS HRM was successfully established for the accurate detection of the *XAF1* promoter methylation, in a larger retrospective clinical study in HGG patients. The accuracy of this assay was validated by pyrosequencing of the HRM amplicon (**Table 14**, p. 102). Crucial for the application of this technique in the analysis of clinical samples was the definition of a valid threshold, allowing the dichotomization of patients for an unmethylated (*XAF1* UM) or methylated (*XAF1* M) promoter. Based on the observations made in HGG cell lines, a cut off value between 18 % in U118, where mRNA expression still was detectable, and 34 % in LN229, where *XAF1* expression was lost, seemed reasonable. A methylation threshold of ≥ 34 % was assumed, which allowed the classification of the cell lines as either *XAF1* M or *XAF1* UM. The resulting groups showed a significantly different mRNA expression for *XAF1* (**Figure 54**, p. 107). Most importantly, this threshold was validated in the analyzed patient collective (N = 80). Utilizing ROC analysis, an unbiased threshold could be deduced from all possible *XAF1* cut off levels determined in patient samples. Here, the value of *XAF1* methylation for predicting the 24 months OS or PFS was calculated, allowing the determination of a threshold of 17.4 % or 36 %, respectively (see 3.6.3.2). Both results exactly reflected the assumption of a threshold between ~ 18 % and ~ 34 % discussed above. Aided by the ROC results, the threshold deduced from HGG cells at a methylation of ≥ 34 % was chosen for dichotomiz

ing samples according to the *XAF1* methylation. Here, the highest true positive rate was associated with the lowest false positive rate (**Suppl. Table 2 and 3**). On the basis of this threshold, an association of *XAF1* methylation and different clinical parameters could be analyzed.

4.3.2 *XAF1* promoter methylation is strictly linked to 2-HG-producing *IDH1* mutations and prolonged survival in grade III gliomas

The role of *XAF1* as tumor suppressor which is involved in different pro apoptotic processes is well established. Accordingly, an epigenetic silencing [179,184] or more general a loss of *XAF1* expression [253] was associated with a poorer disease outcome in different types of cancer. However, the use of *XAF1*, especially of its methylation status as a biomarker, has not found its way into clinical diagnosis, yet. Particularly in malignant gliomas, new biomarkers could help to guide therapy or at least offer the possibility of a more accurate diagnosis.

Analyzing *XAF1* methylation in tumor samples from 80 HGG patients, a beneficial impact of the methylation on the survival was anticipated due to the tumor suppressing nature of *XAF1*. Unexpectedly, a methylation of the *XAF1* promoter was found to predict an improved OS and PFS in HGG patients. The survival differences were highly significant as determined by Kaplan Meier survival analysis (log rank test). In search of possible explanations for this interesting association, the dataset was analyzed in more depth. Stratifying according to the histological tumor grade revealed that *XAF1* methylation was mostly associated with WHO grade III tumors (AA, AO, AOA). In line with this, a significantly different mean PFS (13.3 vs. 42.0 months) and mean⁶ OS (21.9 vs. 49.8 months) was observed in *XAF1* UM vs. *XAF1* M tumors, respectively. In contrast, a beneficial impact of *XAF1* methylation was not evident in GBs of grade IV stratified for *XAF1* UM vs. *XAF1* M (7.8 vs. 11.0 months PFS; 15.3 vs. 20.6 months OS). A slightly improved PFS and OS upon *XAF1* methylation might be hypothesized on the basis of this data, however, not reaching statistical significance ($p = 0.348$).

Strikingly, *XAF1* M was found to be absolutely linked to the occurrence of the *IDH1* mutations R132H and R132G. 18 out of 18 WHOIII/ *IDH1* mut tumors showed a methylated *XAF1* pro

⁶ The median OS for grade III tumors could not be calculated by Kaplan-Meier survival analysis as the survival in this group did not drop below 50 %. Therefore, the mean survival is discussed here.

Discussion

moter also (**Table 18**, p. 113). Among the eight GBs positive for *XAF1* methylation, two exhibited an *IDH1* mutation. These two tumors most likely represent secondary GB, having progressed from a lower grade lesion, since *IDH1* mutations are not found in primary GBs. The low frequency of *IDH1* mut GBs in the dataset is in accordance with the frequencies (< 5 %) reported in the literature [45]. Regarding the strict association of *XAF1* M and *IDH1* mut observed in grade III tumors and secondary GB, the subgroup of six *IDH1* wt/*XAF1* M GBs is of special interest. Importantly, the occurrence of 2 HG producing *IDH1* R132 and *IDH2* R172 mutations has been excluded by pyrosequencing in these samples. This implies that *XAF1* methylation can occur independently of *IDH* mutations in these tumors and thus might represent an independent prognostic factor. Since the sample size of this subgroup was quite small (N = 6; **Table 19**, p. 114), a larger cohort is needed to clarify whether GB (*IDH1* wt) patients also benefit from *XAF1* M or whether *XAF1* M predicts a worse prognosis here.

4.3.3 *XAF1* methylation as surrogate marker for IDH mutations

The *IDH* mut associated production of the oncometabolite 2 HG is mechanistically involved in the development of the so called CpG island methylator phenotype (CIMP). As discussed earlier, this phenotype is associated with an extensive, coordinated hypermethylation at specific gene loci [41,42]. Due to the absolute correlation observed between *IDH1* mut and *XAF1* M in grade III gliomas and secondary GB, the 2 HG producing *IDH1* mutation might potentially be responsible for *XAF1* methylation at early stages of gliomagenesis. This would link the CIMP, generally being associated with malignant progression, with the coordinated silencing of the tumor suppressor gene *XAF1*. This hypothesis is supported by a large study on the genome wide methylation in CIMP positive vs. CIMP negative cells and tumors by Turcan *et. al* [41]. Upon screening the supplemental Illumina Infinium HumanMethylation450 bead array data provided by the authors (supplemental material), *XAF1* was found among the hypermethylated genes. In human astrocytes, expressing mutant *IDH1* (R132H), a 7.35 fold increased methylation in CpGs, belonging to the *XAF1* 5' UTR is reported. Furthermore, methylation data of a cohort of low grade glioma (LGG) samples were provided. Again, *XAF1* was found among the hypermethylated genes, showing a 3.23 fold increased methylation in CIMP positive vs. CIMP negative LGG.

Despite not being an independent prognostic marker in grade III gliomas, *XAF1* methylation might provide a suitable surrogate marker for *IDH* mutations due to its strict association with *IDH1* mut observed here. This includes the 2 HG producing mutations R132H and R132G identified in the presented cohort and probably similar *IDH2* mutations. Unfortunately, no *IDH2* mutations could be detected in the dataset.

Interestingly, a case of a false negative IHC guided *IDH1* diagnosis became evident among the grade III gliomas when *IDH1* status and *XAF1* M were compared. One tumor was seemingly *IDH1* wt but showed a methylated *XAF1* promoter. Due to the otherwise strict coincidence of both markers, this particular tumor was subjected to *IDH1* targeted pyrosequencing. Indeed, the *XAF1* methylation helped to identify a rare 2 HG producing SNP in the *IDH1* gene. Upon sequencing, a transversion at position 394 (C > G) was revealed, causing the substitution R132G. A frequency 0.9 % was reported for this rare SNP in another study [32]. The MS HRM based detection of the *XAF1* promoter methylation status in combination with the identified threshold, thus could provide a fast and cheap diagnostic tool for assessing the *IDH* status in tumor samples or complementing IHC based diagnosis.

A link to *IDH2* mutations also, would strengthen the hypothesis of a causative influence of the G CIMP on *XAF1* methylation. On the one hand, this would clearly indicate the potency of *XAF1* methylation as surrogate marker for various 2 HG producing *IDH* mutations or to represent G CIMP in general. Hereby, the quality of the diagnosis could be enhanced, as MS HRM provides superiority over conventional IHC in terms of being an observer independent, thus unbiased, and quantitative technique. Furthermore, as putative downstream target of *IDH1* mutations, the use of *XAF1* methylation as surrogate marker would allow the detection of rare mutations, not being recognized by the widely used IHC mAb [254]. Although pyrosequencing is the gold standard for SNP detection, recent studies indicate that pyrosequencing based detection of *IDH1* SNPs shows some discrepancies to corresponding IHC stainings [255,256]. The methods of DNA sequencing are described as “labor intensive, requiring trained personal and sophisticated equipment (which is) not available in every center” [255]. Therefore, the method of *XAF1* targeted MS HRM could aid the diagnosis of the *IDH* status in gliomas, as it provides great reproducibility, high sensitivity, and accuracy. On the other hand, a causal connection between CIMP and *XAF1* M also might suggest the silencing of *XAF1* as a critical event

Discussion

during gliomagenesis, since the loss of *XAF1* expression was linked to malignant transformation and tumor progression in other tumor entities as well. However, to elucidate *XAF1* methylation in G CIMP, further experiments are needed. Mechanistic investigations of the long term influence of 2 HG treatment on *XAF1* UM cells could clarify if *XAF1* methylation is selectively introduced by elevated levels of 2 HG.

The unexpected finding of a beneficial impact of *XAF1* silencing might be attributed to the overall better prognosis for patients with CIMP positive tumors [257]. In this case, the tumor suppressing functions of *XAF1* may be overshadowed by the general G CIMP. However, since the key changes in this phenotype are still not well characterized, the loss of *XAF1* might also contribute to the clinical features of this phenotype. The following chapter gives an overview of the different functions of *XAF1* in cell cycle regulation, regulation of p53 and apoptosis and also suggests a model, linking *XAF1* methylation to an improved response to TMZ based therapy.

4.3.4 The contradictory role of *XAF1* silencing in the response of glioma cells to TMZ

XAF1 was shown to enhance the pro apoptotic p53 signaling, which allows apoptosis induction independent of XIAP inhibition [258]. Complex functions of *XAF1* have been described, involving the increase in p53 expression by antagonizing the targeting of p53 by MDM2 [*ibid.*]. Additionally, HIPK2 phosphorylation of apoptosis associated p53 S46 was increased by *XAF1* and attenuated when *XAF1* induction was blocked [258]. The phosphorylation of p53 at S46 leads to the transcription of pro apoptotic genes including PUMA, NOXA, BAX and the execution of apoptosis [259]. In contrast, S15 phosphorylation drives the expression of the cell cycle regulator p21 [239], which mediates the p53 induced growth suppression [260,261]. Lee *et al.* convincingly demonstrated a *XAF1* induced downregulation of p21 by stabilizing the p21 targeting E3 ubiquitin ligase ZNF313 [258]. Since p21 is mediating G1/ G₀ cell cycle arrest [262], the ubiquitination of p21 regulates the switch from cell cycle arrest/ senescence to apoptosis. In the background of *XAF1* silencing, however, p21 expression might be upregulated in response to DNA damage via the downregulation of ZNF313. Here, a new association between 2 HG producing *IDH1* mutations and methylation of the tumor suppressor gene *XAF1* is described. Combining observations of others with the data presented here, it can be speculated that the unexpected beneficial impact of *XAF1* silencing for glioma patients might be linked to

an increased G1 arrest response via upregulation of p21. In a hypothesized model (**Figure 67**, p. 140) XAF1 is involved in the decision between apoptosis and cell cycle arrest/ senescence upon TMZ treatment by a p21 driven induction of cellular senescence. This would reduce the tumor's proliferative activity and enhance the patients' long term survival. The increased amount of G1 cells observed upon XAF1 knockdown and the treatment with TMZ (**Figure 64**, p. 121) strongly supports this hypothesis. Here, an abrogation of the characteristic G2 arrest was found, while S phase fraction was largely unchanged. Cells accumulated in G1 which indicates an arrest of the tumor cells in this cell cycle phase, probably linked to premature cellular senescence due to decreased amounts of ZNF313 and thus elevated levels of p21.

A recent report by Han *et al.* strongly supports this model, since the authors could show an enhanced G1 arrest response towards DNA damaging agents upon the reduction of ZNF313 activity [263]. Consistently, high levels of ZNF313 were linked to an attenuated G1 arrest followed by apoptosis induction. In agreement with Lee *et al.* [258], the interaction between XAF1 and ZNF313 was shown to contribute to protein stability [263]. The authors also provide evidence that ZNF313 is a negative regulator of cellular senescence, and vice versa that reduction of ZNF313 promotes senescence in a XAF1 dependent and importantly a p53 independent manner [263]. Here, changes in the fraction of apoptotic cells/ cell viability upon XAF1 knock down could not be observed for TMZ. However, the detailed analysis of apoptosis/ cell viability especially at later time points should be conducted.

Transferring these findings to the situation in *XAF1* M gliomas, it is most plausible to deduce that an enhanced level of p21 probably leads to enhanced premature senescence upon irradiation and TMZ treatment. As discussed above, this occurs independently of the tumor's p53 status. The cell cycle analysis (**Figure 64**, p. 121) and BrdU incorporation (**Figure 65**, p. 122) revealed that cell proliferation is not markedly inhibited in XAF1 depleted cells upon TMZ treatment, though, the induction of senescence would demand a reduced proliferation rate.

Further experiments are needed to demonstrate clearly whether XAF1 knockdown induces expression of p21 and most importantly whether this can enhance premature cellular senescence. This should be conducted in in vitro experiments first, and could then be extended to the analysis of p21 expression *XAF1* M and *XAF1* UM tumor sections by IHC.

Discussion

The findings of this work indicate a complex role of *XAF1* methylation in the response of gliomas to CT and RT. The proposed model represents a putative explanation for the prognostic benefits of CIMP positive tumors. The use of *XAF1* methylation in the diagnosis of gliomas is suggested to give valuable information about the *IDH* status, the prognosis, and possibly the response to TMZ.

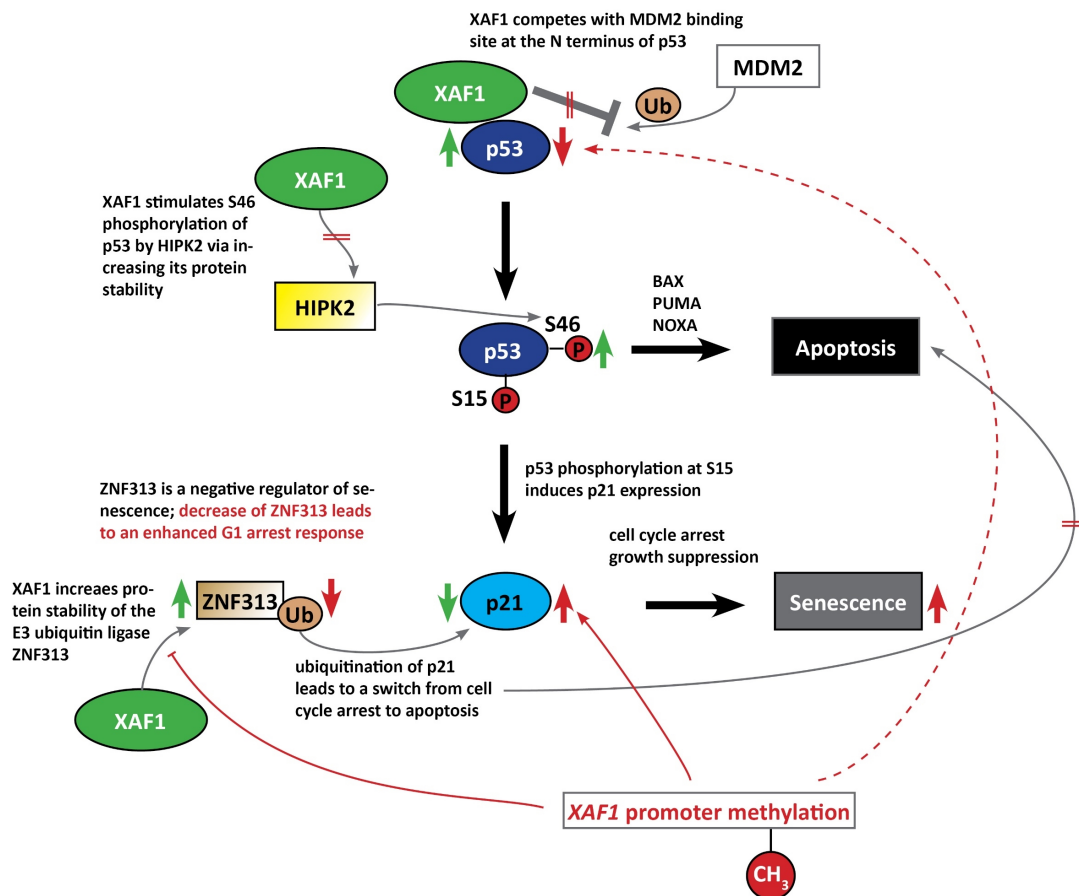


Figure 67: Proposed model for the *XAF1* signaling network in response to TMZ. *XAF1* was shown to be involved in the *p53*-mediated DDR. *p53* levels are elevated via an inhibition of the binding of the E3 ubiquitin ligase MDM2 to the *p53* by *XAF1*. Apoptosis-associated phosphorylation at serine 46 at *p53* protein is induced via stabilization of the protein kinase HIPK2 by *XAF1*. This is associated with the transcription of apoptosis-related genes (*BAX*, *PUMA*, *NOXA*). Phosphorylation at serine 15 mediates the activation of the cell cycle regulator *p21* generally leading to cell cycle arrest and premature senescence. Here, *XAF1* promotes apoptosis via the degradation of *p21* by the *p21*-targeting E3 ubiquitin ligase *ZNF313* in a *p53*-independent manner. This drives cells from DNA damage-induced cell cycle arrest towards apoptosis. Consequently, a loss of *XAF1* (e.g. by methylation) leads an increased G1 arrest response via the upregulation of *p21*, since *ZNF313* stability is reduced. Most importantly, this can occur independently of *p53*. Additionally, pro-apoptotic signaling is reduced, since overall *p53* levels (loss of MDM2 inhibition) and the phosphorylation of *p53* at S46 is attenuated.

5 Literature

1. Wooster, R., Bignell, G., Lancaster, J., Swift, S., Seal, S., Mangion, J., Collins, N., Gregory, S., Gumbs, C., and Micklem, G., *Identification of the breast cancer susceptibility gene BRCA2*. *Nature*, **1995**. 378(6559): p. 789-92.
2. Miki, Y., Swensen, J., Shattuck-Eidens, D., Futreal, P.A., Harshman, K., Tavtigian, S., Liu, Q., Cochran, C., Bennett, L.M., Ding, W., and et al., *A strong candidate for the breast and ovarian cancer susceptibility gene BRCA1*. *Science*, **1994**. 266(5182): p. 66-71.
3. Moynahan, M.E., Pierce, A.J., and Jasin, M., *BRCA2 is required for homology-directed repair of chromosomal breaks*. *Mol Cell*, **2001**. 7(2): p. 263-72.
4. Moynahan, M.E., Chiu, J.W., Koller, B.H., and Jasin, M., *Brca1 controls homology-directed DNA repair*. *Mol Cell*, **1999**. 4(4): p. 511-8.
5. Bouwman, P. and Jonkers, J., *The effects of deregulated DNA damage signalling on cancer chemotherapy response and resistance*. *Nat Rev Cancer*, **2012**. 12(9): p. 587-98.
6. Turner, N., Tutt, A., and Ashworth, A., *Hallmarks of 'BRCAness' in sporadic cancers*. *Nat Rev Cancer*, **2004**. 4(10): p. 814-9.
7. Wolff, A.C., Hammond, M.E., Hicks, D.G., Dowsett, M., McShane, L.M., Allison, K.H., Allred, D.C., Bartlett, J.M., Bilous, M., Fitzgibbons, P., Hanna, W., Jenkins, R.B., Mangu, P.B., Paik, S., Perez, E.A., Press, M.F., Spears, P.A., Vance, G.H., Viale, G., and Hayes, D.F., *Recommendations for human epidermal growth factor receptor 2 testing in breast cancer: American Society of Clinical Oncology/College of American Pathologists clinical practice guideline update*. *J Clin Oncol*, **2013**. 31(31): p. 3997-4013.
8. Hammond, M.E., Hayes, D.F., Dowsett, M., Allred, D.C., Hagerty, K.L., Badve, S., Fitzgibbons, P.L., Francis, G., Goldstein, N.S., Hayes, M., Hicks, D.G., Lester, S., Love, R., Mangu, P.B., McShane, L., Miller, K., Osborne, C.K., Paik, S., Perlmutter, J., Rhodes, A., Sasano, H., Schwartz, J.N., Sweep, F.C., Taube, S., Torlakovic, E.E., Valenstein, P., Viale, G., Visscher, D., Wheeler, T., Williams, R.B., Wittliff, J.L., and Wolff, A.C., *American Society of Clinical Oncology/College of American Pathologists guideline recommendations for immunohistochemical testing of estrogen and progesterone receptors in breast cancer*. *Arch Pathol Lab Med*, **2010**. 134(6): p. 907-22.
9. Robert Koch-Institut und die Gesellschaft der epidemiologischen Krebsregister in Deutschland e.V., *Krebs in Deutschland 2011/ 2012*. Berlin, **2015**.
10. Kleihues, P., Burger, P.C., and Scheithauer, B.W., *The New WHO Classification of Brain Tumours*. *Brain Pathology*, **1993**. 3(3): p. 255-268.
11. Louis, D.N., Perry, A., Reifenberger, G., von Deimling, A., Figarella-Branger, D., Cavenee, W.K., Ohgaki, H., Wiestler, O.D., Kleihues, P., and Ellison, D.W., *The 2016 World Health Organization Classification of Tumors of the Central Nervous System: a summary*. *Acta Neuropathol*, **2016**. 131(6): p. 803-20.
12. Schneider, T., Mawrin, C., Scherlach, C., Skalej, M., and Firsching, R., *Gliomas in Adults*. *Dtsch Arztebl Int*, **2010**. 107(45): p. 799-808.
13. American Brain Tumor Association. *Brain tumor statistics*. [cited 2016 08.21.]; Available from: <http://www.abta.org/about-us/news/brain-tumor-statistics/>.
14. Ostrom, Q.T., Gittleman, H., Fulop, J., Liu, M., Blanda, R., Kromer, C., Wolinsky, Y., Kruchko, C., and Barnholtz-Sloan, J.S., *CBTRUS Statistical Report: Primary Brain and Central Nervous System Tumors Diagnosed in the United States in 2008-2012*. *Neuro Oncol*, **2015**. 17 Suppl 4: p. iv1-iv62.
15. Ostrom, Q.T., Gittleman, H., de Blank, P.M., Finlay, J.L., Gurney, J.G., McKean-Cowdin, R., Stearns, D.S., Wolff, J.E., Liu, M., Wolinsky, Y., Kruchko, C., and Barnholtz-Sloan, J.S., *American Brain Tumor Association Adolescent and Young Adult Primary Brain and Central Nervous System Tumors Diagnosed in the United States in 2008-2012*. *Neuro Oncol*, **2016**. 18 Suppl 1: p. i1-i50.
16. American Cancer Society, *Cancer Facts & Figures 2016*. Atlanta, **2016**.

Literature

17. Preusser, M., de Ribaupierre, S., Wohrer, A., Erridge, S.C., Hegi, M., Weller, M., and Stupp, R., *Current concepts and management of glioblastoma*. *Ann Neurol*, **2011**. 70(1): p. 9-21.
18. Louis, D.N., Pomeroy, S.L., and Cairncross, J.G., *Focus on central nervous system neoplasia*. *Cancer Cell*, **2002**. 1(2): p. 125-8.
19. Stupp, R., Mason, W.P., Bent, M.J., Weller, M., Fisher, B., Taphoorn, M.J., Belanger, K., Brandes, A.A., Marosi, C., and Bogdahn, U., *Radiotherapy plus concomitant and adjuvant temozolomide for glioblastoma*. *N Engl J Med*, **2005**. 352.
20. Louis, D., Ohgaki, H., Wiestler, O., and Cavenee, W., eds. *WHO Classification of Tumours of the Central Nervous System*. 4th Edition Revised ed. WHO/IARC Classification of Tumours. **2016**.
21. Wick, W. and Hau, P., *Personalized therapy for gliomas*. *Nervenarzt*, **2015**. 86(6): p. 692, 694-6, 698-700.
22. Hegi, M.E., Diserens, A.C., Gorlia, T., Hamou, M.F., de Tribolet, N., Weller, M., Kros, J.M., Hainfellner, J.A., Mason, W., Mariani, L., Bromberg, J.E., Hau, P., Mirimanoff, R.O., Cairncross, J.G., Janzer, R.C., and Stupp, R., *MGMT gene silencing and benefit from temozolomide in glioblastoma*. *N Engl J Med*, **2005**. 352(10): p. 997-1003.
23. Wick, W., Platten, M., Meisner, C., Felsberg, J., Tabatabai, G., Simon, M., Nikkhah, G., Papsdorf, K., Steinbach, J.P., Sabel, M., Combs, S.E., Vesper, J., Braun, C., Meixensberger, J., Ketter, R., Mayer-Steinacker, R., Reifenberger, G., Weller, M., and Society, N.O.A.S.G.o.N.-o.W.G.o.G.C., *Temozolomide chemotherapy alone versus radiotherapy alone for malignant astrocytoma in the elderly: the NOA-08 randomised, phase 3 trial*. *Lancet Oncol*, **2012**. 13(7): p. 707-15.
24. Malmström, A., Grønberg, B.H., Marosi, C., Stupp, R., Frappaz, D., Schultz, H., Abacioglu, U., Tavelin, B., Lhermitte, B., Hegi, M.E., Rosell, J., and Henriksson, R., *Temozolomide versus standard 6-week radiotherapy versus hypofractionated radiotherapy in patients older than 60 years with glioblastoma: the Nordic randomised, phase 3 trial*. *The Lancet Oncology*, **2012**. 13(9): p. 916-926.
25. Louis, D.N., Ohgaki, H., Wiestler, O.D., and Cavenee, W.K., eds. *WHO Classification of tumours of the central nervous system*. **2007**, IARC: Lyon.
26. Parsons, D.W., Jones, S., Zhang, X., Lin, J.C., Leary, R.J., Angenendt, P., Mankoo, P., Carter, H., Siu, I.M., Gallia, G.L., Olivi, A., McLendon, R., Rasheed, B.A., Keir, S., Nikolskaya, T., Nikolsky, Y., Busam, D.A., Tekleab, H., Diaz, L.A., Jr., Hartigan, J., Smith, D.R., Strausberg, R.L., Marie, S.K., Shinjo, S.M., Yan, H., Riggins, G.J., Bigner, D.D., Karchin, R., Papadopoulos, N., Parmigiani, G., Vogelstein, B., Velculescu, V.E., and Kinzler, K.W., *An integrated genomic analysis of human glioblastoma multiforme*. *Science*, **2008**. 321(5897): p. 1807-12.
27. Geisbrecht, B.V. and Gould, S.J., *The human PICD gene encodes a cytoplasmic and peroxisomal NADP(+)-dependent isocitrate dehydrogenase*. *J Biol Chem*, **1999**. 274(43): p. 30527-33.
28. Corpas, F.J., Barroso, J.B., Sandalio, L.M., Palma, J.M., Lupianez, J.A., and del Rio, L.A., *Peroxisomal NADP-Dependent Isocitrate Dehydrogenase. Characterization and Activity Regulation during Natural Senescence*. *Plant Physiol*, **1999**. 121(3): p. 921-928.
29. Nekrutenko, A., Hillis, D.M., Patton, J.C., Bradley, R.D., and Baker, R.J., *Cytosolic isocitrate dehydrogenase in humans, mice, and voles and phylogenetic analysis of the enzyme family*. *Mol Biol Evol*, **1998**. 15(12): p. 1674-84.
30. Xu, X., Zhao, J., Xu, Z., Peng, B., Huang, Q., Arnold, E., and Ding, J., *Structures of human cytosolic NADP-dependent isocitrate dehydrogenase reveal a novel self-regulatory mechanism of activity*. *J Biol Chem*, **2004**. 279(32): p. 33946-57.
31. Prensner, J.R. and Chinnaiyan, A.M., *Metabolism unhinged: IDH mutations in cancer*. *Nat Med*, **2011**. 17(3): p. 291-3.
32. Balss, J., Meyer, J., Mueller, W., Korshunov, A., Hartmann, C., and von Deimling, A., *Analysis of the IDH1 codon 132 mutation in brain tumors*. *Acta Neuropathol*, **2008**. 116(6): p. 597-602.
33. Zhao, S., Lin, Y., Xu, W., Jiang, W., Zha, Z., Wang, P., Yu, W., Li, Z., Gong, L., Peng, Y., Ding, J., Lei, Q., Guan, K.L., and Xiong, Y., *Glioma-derived mutations in IDH1 dominantly inhibit IDH1 catalytic activity and induce HIF-1alpha*. *Science*, **2009**. 324(5924): p. 261-5.
34. Dang, L., White, D.W., Gross, S., Bennett, B.D., Bittinger, M.A., Driggers, E.M., Fantin, V.R., Jang, H.G., Jin, S., Keenan, M.C., Marks, K.M., Prins, R.M., Ward, P.S., Yen, K.E., Liu, L.M.,

- Rabinowitz, J.D., Cantley, L.C., Thompson, C.B., Vander Heiden, M.G., and Su, S.M., *Cancer-associated IDH1 mutations produce 2-hydroxyglutarate*. *Nature*, **2009**. 462(7274): p. 739-44.
35. Ward, P.S., Patel, J., Wise, D.R., Abdel-Wahab, O., Bennett, B.D., Collier, H.A., Cross, J.R., Fantin, V.R., Hedvat, C.V., Perl, A.E., Rabinowitz, J.D., Carroll, M., Su, S.M., Sharp, K.A., Levine, R.L., and Thompson, C.B., *The common feature of leukemia-associated IDH1 and IDH2 mutations is a neomorphic enzyme activity converting alpha-ketoglutarate to 2-hydroxyglutarate*. *Cancer Cell*, **2010**. 17(3): p. 225-34.
36. Rendina, A.R., Pietrak, B., Smallwood, A., Zhao, H., Qi, H., Quinn, C., Adams, N.D., Concha, N., Duraiswami, C., Thrall, S.H., Sweitzer, S., and Schwartz, B., *Mutant IDH1 enhances the production of 2-hydroxyglutarate due to its kinetic mechanism*. *Biochemistry*, **2013**. 52(26): p. 4563-77.
37. Tsukada, Y., Fang, J., Erdjument-Bromage, H., Warren, M.E., Borchers, C.H., Tempst, P., and Zhang, Y., *Histone demethylation by a family of JmjC domain-containing proteins*. *Nature*, **2006**. 439(7078): p. 811-6.
38. Kohli, R.M. and Zhang, Y., *TET enzymes, TDG and the dynamics of DNA demethylation*. *Nature*, **2013**. 502(7472): p. 472-9.
39. Noushmehr, H., Weisenberger, D.J., Diefes, K., Phillips, H.S., Pujara, K., Berman, B.P., Pan, F., Pelloski, C.E., Sulman, E.P., Bhat, K.P., Verhaak, R.G., Hoadley, K.A., Hayes, D.N., Perou, C.M., Schmidt, H.K., Ding, L., Wilson, R.K., Van Den Berg, D., Shen, H., Bengtsson, H., Neuvial, P., Cope, L.M., Buckley, J., Herman, J.G., Baylin, S.B., Laird, P.W., Aldape, K., and Cancer Genome Atlas Research, N., *Identification of a CpG island methylator phenotype that defines a distinct subgroup of glioma*. *Cancer Cell*, **2010**. 17(5): p. 510-22.
40. Losman, J.A. and Kaelin, W.G., Jr., *What a difference a hydroxyl makes: mutant IDH, (R)-2-hydroxyglutarate, and cancer*. *Genes Dev*, **2013**. 27(8): p. 836-52.
41. Turcan, S., Rohle, D., Goenka, A., Walsh, L.A., Fang, F., Yilmaz, E., Campos, C., Fabius, A.W., Lu, C., Ward, P.S., Thompson, C.B., Kaufman, A., Guryanova, O., Levine, R., Heguy, A., Viale, A., Morris, L.G., Huse, J.T., Mellinghoff, I.K., and Chan, T.A., *IDH1 mutation is sufficient to establish the glioma hypermethylator phenotype*. *Nature*, **2012**. 483(7390): p. 479-83.
42. Malzkorn, B., Wolter, M., Riemenschneider, M.J., and Reifenberger, G., *Unraveling the glioma epigenome: from molecular mechanisms to novel biomarkers and therapeutic targets*. *Brain Pathol*, **2011**. 21(6): p. 619-32.
43. Xu, D. and Zhang, Y., *Generating triangulated macromolecular surfaces by Euclidean Distance Transform*. *PLoS One*, **2009**. 4(12): p. e8140.
44. Moreland, J.L., Gramada, A., Buzko, O.V., Zhang, Q., and Bourne, P.E., *The Molecular Biology Toolkit (MBT): a modular platform for developing molecular visualization applications*. *BMC Bioinformatics*, **2005**. 6(1): p. 1-7.
45. Yan, H., Parsons, D.W., Jin, G., McLendon, R., Rasheed, B.A., Yuan, W., Kos, I., Batinic-Haberle, I., Jones, S., Riggins, G.J., Friedman, H., Friedman, A., Reardon, D., Herndon, J., Kinzler, K.W., Velculescu, V.E., Vogelstein, B., and Bigner, D.D., *IDH1 and IDH2 mutations in gliomas*. *N Engl J Med*, **2009**. 360(8): p. 765-73.
46. Ichimura, K., Pearson, D.M., Kocalkowski, S., Backlund, L.M., Chan, R., Jones, D.T., and Collins, V.P., *IDH1 mutations are present in the majority of common adult gliomas but rare in primary glioblastomas*. *Neuro Oncol*, **2009**. 11(4): p. 341-7.
47. Nobusawa, S., Watanabe, T., Kleihues, P., and Ohgaki, H., *IDH1 mutations as molecular signature and predictive factor of secondary glioblastomas*. *Clin Cancer Res*, **2009**. 15(19): p. 6002-7.
48. Watanabe, T., Nobusawa, S., Kleihues, P., and Ohgaki, H., *IDH1 mutations are early events in the development of astrocytomas and oligodendrogliomas*. *Am J Pathol*, **2009**. 174(4): p. 1149-53.
49. Brandner, S. and von Deimling, A., *Diagnostic, prognostic and predictive relevance of molecular markers in gliomas*. *Neuropathol Appl Neurobiol*, **2015**. 41(6): p. 694-720.

Literature

50. Dimitrov, L., Hong, C.S., Yang, C., Zhuang, Z., and Heiss, J.D., *New developments in the pathogenesis and therapeutic targeting of the IDH1 mutation in glioma*. *Int J Med Sci*, **2015**. 12(3): p. 201-13.
51. Friedman, H.S., Kerby, T., and Calvert, H., *Temozolomide and Treatment of Malignant Glioma*. *Clinical Cancer Research*, **2000**. 6(7): p. 2585-2597.
52. Fu, D., Calvo, J.A., and Samson, L.D., *Balancing repair and tolerance of DNA damage caused by alkylating agents*. *Nat Rev Cancer*, **2012**. 12(2): p. 104-20.
53. Foster, P.L. and Davis, E.F., *Loss of an apurinic/aprimidinic site endonuclease increases the mutagenicity of N-methyl-N'-nitro-N-nitrosoguanidine to Escherichia coli*. *Proc Natl Acad Sci U S A*, **1987**. 84(9): p. 2891-5.
54. Loeb, L.A., *Apurinic sites as mutagenic intermediates*. *Cell*. 40(3): p. 483-484.
55. Drablos, F., Feyzi, E., Aas, P.A., Vaagbo, C.B., Kavli, B., Bratlie, M.S., Pena-Diaz, J., Otterlei, M., Slupphaug, G., and Krokan, H.E., *Alkylation damage in DNA and RNA--repair mechanisms and medical significance*. *DNA Repair (Amst)*, **2004**. 3(11): p. 1389-407.
56. Engelward, B.P., Allan, J.M., Dreslin, A.J., Kelly, J.D., Wu, M.M., Gold, B., and Samson, L.D., *A chemical and genetic approach together define the biological consequences of 3-methyladenine lesions in the mammalian genome*. *J Biol Chem*, **1998**. 273(9): p. 5412-8.
57. Shrivastav, N., Li, D., and Essigmann, J.M., *Chemical biology of mutagenesis and DNA repair: cellular responses to DNA alkylation*. *Carcinogenesis*, **2010**. 31(1): p. 59-70.
58. Kaina, B., Christmann, M., Naumann, S., and Roos, W.P., *MGMT: key node in the battle against genotoxicity, carcinogenicity and apoptosis induced by alkylating agents*. *DNA Repair (Amst)*, **2007**. 6.
59. Toorchen, D. and Topal, M.D., *Mechanisms of chemical mutagenesis and carcinogenesis: effects on DNA replication of methylation at the O6-guanine position of dGTP*. *Carcinogenesis*, **1983**. 4(12): p. 1591-7.
60. Karran, P. and Bignami, M., *DNA damage tolerance, mismatch repair and genome instability*. *Bioessays*, **1994**. 16(11): p. 833-9.
61. Ochs, K. and Kaina, B., *Apoptosis induced by DNA damage O6-methylguanine is Bcl-2 and caspase-9/3 regulated and Fas/caspase-8 independent*. *Cancer Res*, **2000**. 60(20): p. 5815-24.
62. Tubbs, J.L., Pegg, A.E., and Tainer, J.A., *DNA binding, nucleotide flipping, and the helix-turn-helix motif in base repair by O6-alkylguanine-DNA alkyltransferase and its implications for cancer chemotherapy*. *DNA Repair (Amst)*, **2007**. 6(8): p. 1100-15.
63. Xu-Welliver, M. and Pegg, A.E., *Degradation of the alkylated form of the DNA repair protein, O(6)-alkylguanine-DNA alkyltransferase*. *Carcinogenesis*, **2002**. 23(5): p. 823-30.
64. Kaina, B., Fritz, G., and Coquerelle, T., *Contribution of O6-alkylguanine and N-alkylpurines to the formation of sister chromatid exchanges, chromosomal aberrations, and gene mutations: new insights gained from studies of genetically engineered mammalian cell lines*. *Environ Mol Mutagen*, **1993**. 22(4): p. 283-92.
65. Roos, W.P., Nikolova, T., Quiros, S., Naumann, S.C., Kiedron, O., Zdzienicka, M.Z., and Kaina, B., *Brca2/Xrcc2 dependent HR, but not NHEJ, is required for protection against O(6)-methylguanine triggered apoptosis, DSBs and chromosomal aberrations by a process leading to SCEs*. *DNA Repair (Amst)*, **2009**. 8(1): p. 72-86.
66. Kaina, B., Christmann, M., Naumann, S., and Roos, W.P., *MGMT: key node in the battle against genotoxicity, carcinogenicity and apoptosis induced by alkylating agents*. *DNA Repair (Amst)*, **2007**. 6(8): p. 1079-99.
67. Rajesh, P., Rajesh, C., Wyatt, M.D., and Pittman, D.L., *RAD51D protects against MLH1-dependent cytotoxic responses to O(6)-methylguanine*. *DNA Repair (Amst)*, **2010**. 9(4): p. 458-67.
68. Reichert, S., Rodel, C., Mirsch, J., Harter, P.N., Tomicic, M.T., Mittelbronn, M., Kaina, B., and Rödel, F., *Survivin inhibition and DNA double-strand break repair: a molecular mechanism to overcome radioresistance in glioblastoma*. *Radiother Oncol*, **2011**. 101(1): p. 51-8.
69. Maier, P., Hartmann, L., Wenz, F., and Herskind, C., *Cellular Pathways in Response to Ionizing Radiation and Their Targetability for Tumor Radiosensitization*. *Int J Mol Sci*, **2016**. 17(1).

70. Herskind, C. and Thacker, J., *Inactivation of DNA-mediated transformation of hamster cells by gamma-rays and deoxyribonuclease I*. *Mutat Res*, **1988**. 198(1): p. 169-78.
71. Herskind, C. and Westergaard, O., *Variable protection by OH scavengers against radiation-induced inactivation of isolated transcriptionally active chromatin: the influence of secondary radicals*. *Radiat Res*, **1988**. 114(1): p. 28-41.
72. Hall, E.J. and Giaccia, A.J., *Radiobiology for the radiologist*. 6th ed. **2006**, Philadelphia: Lippincott Williams & Wilkins. ix, 546 p.
73. Chapman, J.R., Taylor, M.R., and Boulton, S.J., *Playing the end game: DNA double-strand break repair pathway choice*. *Mol Cell*, **2012**. 47(4): p. 497-510.
74. Lieber, M.R., *The mechanism of double-strand DNA break repair by the nonhomologous DNA end-joining pathway*. *Annu Rev Biochem*, **2010**. 79: p. 181-211.
75. Lazzaro, F., Giannattasio, M., Puddu, F., Granata, M., Pellicoli, A., Plevani, P., and Muzi-Falconi, M., *Checkpoint mechanisms at the intersection between DNA damage and repair*. *DNA Repair (Amst)*, **2009**. 8(9): p. 1055-67.
76. Zannini, L., Delia, D., and Buscemi, G., *CHK2 kinase in the DNA damage response and beyond*. *J Mol Cell Biol*, **2014**. 6(6): p. 442-57.
77. Kelley, M.R. and Fishel, M.L., *Chapter 1 - Overview of DNA repair pathways, current targets, and clinical trials bench to clinic*, in *DNA Repair in Cancer Therapy (Second Edition)*. **2016**, Academic Press: Boston. p. 1-54.
78. Murfun, I. and Rass, U., *Chapter 8 - Targeting homologous recombination repair in cancer A2 - Kelley, Mark R*, in *DNA Repair in Cancer Therapy (Second Edition)*, Melissa L. Fishel, Editor. **2016**, Academic Press: Boston. p. 225-275.
79. Lee, J.H. and Paull, T.T., *Activation and regulation of ATM kinase activity in response to DNA double-strand breaks*. *Oncogene*, **2007**. 26(56): p. 7741-8.
80. Ciccio, A. and Elledge, S.J., *The DNA damage response: making it safe to play with knives*. *Mol Cell*, **2010**. 40(2): p. 179-204.
81. Shiloh, Y., *Ataxia-telangiectasia and the Nijmegen breakage syndrome: related disorders but genes apart*. *Annu Rev Genet*, **1997**. 31: p. 635-62.
82. Cimprich, K.A. and Cortez, D., *ATR: an essential regulator of genome integrity*. *Nat Rev Mol Cell Biol*, **2008**. 9(8): p. 616-27.
83. Rein, K. and Stracker, T.H., *The MRE11 complex: an important source of stress relief*. *Exp Cell Res*, **2014**. 329(1): p. 162-9.
84. Lukas, J., Lukas, C., and Bartek, J., *More than just a focus: The chromatin response to DNA damage and its role in genome integrity maintenance*. *Nat Cell Biol*, **2011**. 13(10): p. 1161-9.
85. Thorslund, T., Ripplinger, A., Hoffmann, S., Wild, T., Uckelmann, M., Villumsen, B., Narita, T., Sixma, T.K., Choudhary, C., Bekker-Jensen, S., and Mailand, N., *Histone H1 couples initiation and amplification of ubiquitin signalling after DNA damage*. *Nature*, **2015**. 527(7578): p. 389-93.
86. Shanbhag, N.M., Rafalska-Metcalf, I.U., Balane-Bolivar, C., Janicki, S.M., and Greenberg, R.A., *ATM-dependent chromatin changes silence transcription in cis to DNA double-strand breaks*. *Cell*, **2010**. 141(6): p. 970-81.
87. Symington, L.S., *End resection at double-strand breaks: mechanism and regulation*. *Cold Spring Harb Perspect Biol*, **2014**. 6(8).
88. Zimmermann, M. and de Lange, T., *53BP1: pro choice in DNA repair*. *Trends Cell Biol*, **2014**. 24(2): p. 108-17.
89. Panier, S. and Boulton, S.J., *Double-strand break repair: 53BP1 comes into focus*. *Nat Rev Mol Cell Biol*, **2014**. 15(1): p. 7-18.
90. Cannavo, E. and Cejka, P., *Sae2 promotes dsDNA endonuclease activity within Mre11-Rad50-Xrs2 to resect DNA breaks*. *Nature*, **2014**. 514(7520): p. 122-5.
91. Shibata, A., Moiani, D., Arvai, A.S., Perry, J., Harding, S.M., Genois, M.M., Maity, R., van Rossum-Fikkert, S., Kertokallio, A., Romoli, F., Ismail, A., Ismalaj, E., Petricci, E., Neale, M.J., Bristow, R.G., Masson, J.Y., Wyman, C., Jeggo, P.A., and Tainer, J.A., *DNA double-strand break*

Literature

- repair pathway choice is directed by distinct MRE11 nuclease activities.* Mol Cell, **2014**. 53(1): p. 7-18.
92. Zhang, F., Fan, Q., Ren, K., and Andreassen, P.R., *PALB2 functionally connects the breast cancer susceptibility proteins BRCA1 and BRCA2.* Mol Cancer Res, **2009**. 7(7): p. 1110-8.
93. Taylor, Martin R.G., Špírek, M., Chaurasiya, Kathy R., Ward, Jordan D., Carzaniga, R., Yu, X., Egelman, Edward H., Collinson, Lucy M., Rueda, D., Krejci, L., and Boulton, Simon J., *Rad51 Paralogs Remodel Pre-synaptic Rad51 Filaments to Stimulate Homologous Recombination.* Cell. 162(2): p. 271-286.
94. Moldovan, G.L., Madhavan, M.V., Mirchandani, K.D., McCaffrey, R.M., Vinciguerra, P., and D'Andrea, A.D., *DNA polymerase POLN participates in cross-link repair and homologous recombination.* Mol Cell Biol, **2010**. 30(4): p. 1088-96.
95. Rattray, A.J. and Strathern, J.N., *Homologous recombination is promoted by translesion polymerase poleta.* Mol Cell, **2005**. 20(5): p. 658-9.
96. West, S.C., *Molecular views of recombination proteins and their control.* Nat Rev Mol Cell Biol, **2003**. 4(6): p. 435-45.
97. Ciccica, A., McDonald, N., and West, S.C., *Structural and functional relationships of the XPF/MUS81 family of proteins.* Annu Rev Biochem, **2008**. 77: p. 259-87.
98. Fekairi, S., Scaglione, S., Chahwan, C., Taylor, E.R., Tissier, A., Coulon, S., Dong, M.Q., Ruse, C., Yates, J.R., 3rd, Russell, P., Fuchs, R.P., McGowan, C.H., and Gaillard, P.H., *Human SLX4 is a Holliday junction resolvase subunit that binds multiple DNA repair/recombination endonucleases.* Cell, **2009**. 138(1): p. 78-89.
99. Ip, S.C., Rass, U., Blanco, M.G., Flynn, H.R., Skehel, J.M., and West, S.C., *Identification of Holliday junction resolvases from humans and yeast.* Nature, **2008**. 456(7220): p. 357-61.
100. Svendsen, J.M., Smogorzewska, A., Sowa, M.E., O'Connell, B.C., Gygi, S.P., Elledge, S.J., and Harper, J.W., *Mammalian BTBD12/SLX4 assembles a Holliday junction resolvase and is required for DNA repair.* Cell, **2009**. 138(1): p. 63-77.
101. Caldas, H., Honsey, L.E., and Altura, R.A., *Survivin 2alpha: a novel Survivin splice variant expressed in human malignancies.* Mol Cancer, **2005**. 4(1): p. 11.
102. Mahotka, C., Wenzel, M., Springer, E., Gabbert, H.E., and Gerharz, C.D., *Survivin-deltaEx3 and survivin-2B: two novel splice variants of the apoptosis inhibitor survivin with different antiapoptotic properties.* Cancer Res, **1999**. 59(24): p. 6097-102.
103. Ambrosini, G., Adida, C., and Altieri, D.C., *A novel anti-apoptosis gene, survivin, expressed in cancer and lymphoma.* Nat Med, **1997**. 3(8): p. 917-21.
104. Adida, C., Crotty, P.L., McGrath, J., Berrebi, D., Diebold, J., and Altieri, D.C., *Developmentally regulated expression of the novel cancer anti-apoptosis gene survivin in human and mouse differentiation.* Am J Pathol, **1998**. 152(1): p. 43-9.
105. Altieri, D.C., *Survivin, versatile modulation of cell division and apoptosis in cancer.* Oncogene, **2003**. 22(53): p. 8581-9.
106. Altieri, D.C., *Validating survivin as a cancer therapeutic target.* Nat Rev Cancer, **2003**. 3(1): p. 46-54.
107. Kanwar, J.R., Kamalapuram, S.K., and Kanwar, R.K., *Targeting survivin in cancer: the cell-signalling perspective.* Drug Discov Today, **2011**. 16(11-12): p. 485-94.
108. Altieri, D.C., *Targeting survivin in cancer.* Cancer Lett, **2013**. 332(2): p. 225-8.
109. Altieri, D.C., *Survivin, cancer networks and pathway-directed drug discovery.* Nat Rev Cancer, **2008**. 8(1): p. 61-70.
110. Coumar, M.S., Tsai, F.Y., Kanwar, J.R., Sarvagalla, S., and Cheung, C.H., *Treat cancers by targeting survivin: Just a dream or future reality?* Cancer Treat Rev, **2013**.
111. Kerr Jf Fau - Wyllie, A.H., Wyllie Ah Fau - Currie, A.R., and Currie, A.R., *Apoptosis: a basic biological phenomenon with wide-ranging implications in tissue kinetics.* (0007-0920 (Print)).
112. Chang, H.Y. and Yang, X., *Proteases for Cell Suicide: Functions and Regulation of Caspases.* Microbiology and Molecular Biology Reviews, **2000**. 64(4): p. 821-846.
113. Goyal, L., *Cell death inhibition: keeping caspases in check.* Cell, **2001**. 104(6): p. 805-8.

114. Li, P., Nijhawan, D., Budihardjo, I., Srinivasula, S.M., Ahmad, M., Alnemri, E.S., and Wang, X., *Cytochrome c and dATP-dependent formation of Apaf-1/caspase-9 complex initiates an apoptotic protease cascade*. *Cell*, **1997**. 91(4): p. 479-89.
115. Hill, M.M., Adrain, C., Duriez, P.J., Creagh, E.M., and Martin, S.J., *Analysis of the composition, assembly kinetics and activity of native Apaf-1 apoptosomes*. *EMBO J*, **2004**. 23(10): p. 2134-45.
116. Elmore, S., *Apoptosis: A Review of Programmed Cell Death*. *Toxicologic pathology*, **2007**. 35(4): p. 495-516.
117. Sakahira, H., Enari, M., and Nagata, S., *Cleavage of CAD inhibitor in CAD activation and DNA degradation during apoptosis*. *Nature*, **1998**. 391(6662): p. 96-9.
118. Cory, S. and Adams, J.M., *The Bcl2 family: regulators of the cellular life-or-death switch*. *Nat Rev Cancer*, **2002**. 2(9): p. 647-56.
119. Igney, F.H. and Krammer, P.H., *Death and anti-death: tumour resistance to apoptosis*. *Nat Rev Cancer*, **2002**. 2(4): p. 277-88.
120. Hanahan, D. and Weinberg, R.A., *The hallmarks of cancer*. *Cell*, **2000**. 100(1): p. 57-70.
121. Hanahan, D. and Weinberg, R.A., *Hallmarks of cancer: the next generation*. *Cell*, **2011**. 144(5): p. 646-74.
122. Birnbaum, M.J., Clem, R.J., and Miller, L.K., *An apoptosis-inhibiting gene from a nuclear polyhedrosis virus encoding a polypeptide with Cys/His sequence motifs*. *J Virol*, **1994**. 68(4): p. 2521-8.
123. Crook, N.E., Clem, R.J., and Miller, L.K., *An apoptosis-inhibiting baculovirus gene with a zinc finger-like motif*. *J Virol*, **1993**. 67(4): p. 2168-74.
124. Duckett, C.S., Nava, V.E., Gedrich, R.W., Clem, R.J., Van Dongen, J.L., Gilfillan, M.C., Shiels, H., Hardwick, J.M., and Thompson, C.B., *A conserved family of cellular genes related to the baculovirus iap gene and encoding apoptosis inhibitors*. *EMBO J*, **1996**. 15(11): p. 2685-94.
125. Srinivasula, S.M. and Ashwell, J.D., *IAPs: what's in a name?* *Mol Cell*, **2008**. 30(2): p. 123-35.
126. Owens, T.W., Gilmore, A.P., Streuli, C.H., and Foster, F.M., *Inhibitor of Apoptosis Proteins: Promising Targets for Cancer Therapy*. *J Carcinog Mutagen*, **2013**. Suppl 14.
127. Altieri, D.C., *Survivin - The inconvenient IAP*. *Semin Cell Dev Biol*, **2015**. 39: p. 91-6.
128. Suzuki, Y., Nakabayashi, Y., and Takahashi, R., *Ubiquitin-protein ligase activity of X-linked inhibitor of apoptosis protein promotes proteasomal degradation of caspase-3 and enhances its anti-apoptotic effect in Fas-induced cell death*. *Proc Natl Acad Sci U S A*, **2001**. 98(15): p. 8662-7.
129. Gyrd-Hansen, M., Darding, M., Miasari, M., Santoro, M.M., Zender, L., Xue, W., Tenev, T., da Fonseca, P.C., Zvelebil, M., Bujnicki, J.M., Lowe, S., Silke, J., and Meier, P., *IAPs contain an evolutionarily conserved ubiquitin-binding domain that regulates NF-kappaB as well as cell survival and oncogenesis*. *Nat Cell Biol*, **2008**. 10(11): p. 1309-17.
130. Deveraux, Q.L., Takahashi, R., Salvesen, G.S., and Reed, J.C., *X-linked IAP is a direct inhibitor of cell-death proteases*. *Nature*, **1997**. 388(6639): p. 300-4.
131. Deveraux, Q.L., Roy, N., Stennicke, H.R., Van Arsdale, T., Zhou, Q., Srinivasula, S.M., Alnemri, E.S., Salvesen, G.S., and Reed, J.C., *IAPs block apoptotic events induced by caspase-8 and cytochrome c by direct inhibition of distinct caspases*. *EMBO J*, **1998**. 17(8): p. 2215-23.
132. Sun, C., Cai, M., Meadows, R.P., Xu, N., Gunasekera, A.H., Herrmann, J., Wu, J.C., and Fesik, S.W., *NMR structure and mutagenesis of the third Bir domain of the inhibitor of apoptosis protein XIAP*. *J Biol Chem*, **2000**. 275(43): p. 33777-81.
133. Huang, Y., Park, Y.C., Rich, R.L., Segal, D., Myszka, D.G., and Wu, H., *Structural basis of caspase inhibition by XIAP: differential roles of the linker versus the BIR domain*. *Cell*, **2001**. 104(5): p. 781-90.
134. Srinivasula, S.M., Hegde, R., Saleh, A., Datta, P., Shiozaki, E., Chai, J., Lee, R.A., Robbins, P.D., Fernandes-Alnemri, T., Shi, Y., and Alnemri, E.S., *A conserved XIAP-interaction motif in caspase-9 and Smac/DIABLO regulates caspase activity and apoptosis*. *Nature*, **2001**. 410(6824): p. 112-6.

Literature

135. Srinivasula, S.M., Gupta, S., Datta, P., Zhang, Z., Hegde, R., Cheong, N., Fernandes-Alnemri, T., and Alnemri, E.S., *Inhibitor of apoptosis proteins are substrates for the mitochondrial serine protease Omi/HtrA2*. J Biol Chem, **2003**. 278(34): p. 31469-72.
136. Lewis, J., Burstein, E., Reffey, S.B., Bratton, S.B., Roberts, A.B., and Duckett, C.S., *Uncoupling of the signaling and caspase-inhibitory properties of X-linked inhibitor of apoptosis*. J Biol Chem, **2003**. 279(10): p. 9023-9.
137. Lu, M., Lin, S.C., Huang, Y., Kang, Y.J., Rich, R., Lo, Y.C., Myszka, D., Han, J., and Wu, H., *XIAP induces NF-kappaB activation via the BIR1/TAB1 interaction and BIR1 dimerization*. Mol Cell, **2007**. 26(5): p. 689-702.
138. Tamm, I., Kornblau, S.M., Segall, H., Krajewski, S., Welsh, K., Kitada, S., Scudiero, D.A., Tudor, G., Qui, Y.H., Monks, A., Andreeff, M., and Reed, J.C., *Expression and prognostic significance of IAP-family genes in human cancers and myeloid leukemias*. Clin Cancer Res, **2000**. 6(5): p. 1796-803.
139. Baykara, M., Yaman, M., Buyukberber, S., Tufan, G., Demirci, U., Benekli, M., Coskun, U., Ozet, A., and Umit Bagriacik, E., *Clinical and prognostic importance of XIAP and USP8 in advanced stages of non-small cell lung cancer*. J BUON, **2013**. 18(4): p. 921-7.
140. Seligson, D.B., Hongo, F., Huerta-Yepez, S., Mizutani, Y., Miki, T., Yu, H., Horvath, S., Chia, D., Goodglick, L., and Bonavida, B., *Expression of X-linked inhibitor of apoptosis protein is a strong predictor of human prostate cancer recurrence*. Clin Cancer Res, **2007**. 13(20): p. 6056-63.
141. Zhou, S., Ye, W., Shao, Q., Qi, Y., Zhang, M., and Liang, J., *Prognostic significance of XIAP and NF-kappaB expression in esophageal carcinoma with postoperative radiotherapy*. World J Surg Oncol, **2013**. 11: p. 288.
142. Ramp, U., Krieg, T., Caliskan, E., Mahotka, C., Ebert, T., Willers, R., Gabbert, H.E., and Gerharz, C.D., *XIAP expression is an independent prognostic marker in clear-cell renal carcinomas*. Hum Pathol, **2004**. 35(8): p. 1022-8.
143. Mizutani, Y., Nakanishi, H., Li, Y.N., Matsubara, H., Yamamoto, K., Sato, N., Shiraishi, T., Nakamura, T., Mikami, K., Okihara, K., Takaha, N., Ukimura, O., Kawauchi, A., Nonomura, N., Bonavida, B., and Miki, T., *Overexpression of XIAP expression in renal cell carcinoma predicts a worse prognosis*. Int J Oncol, **2007**. 30(4): p. 919-25.
144. Yang, X.H., Feng, Z.E., Yan, M., Hanada, S., Zuo, H., Yang, C.Z., Han, Z.G., Guo, W., Chen, W.T., and Zhang, P., *XIAP is a predictor of cisplatin-based chemotherapy response and prognosis for patients with advanced head and neck cancer*. PLoS One, **2012**. 7(3): p. e31601.
145. Tamm, I., Richter, S., Scholz, F., Schmelz, K., Oltersdorf, D., Karawajew, L., Schoch, C., Haferlach, T., Ludwig, W.D., and Wuchter, C., *XIAP expression correlates with monocytic differentiation in adult de novo AML: impact on prognosis*. Hematol J, **2004**. 5(6): p. 489-95.
146. Li, F. and Altieri, D.C., *Transcriptional analysis of human survivin gene expression*. Biochem J, **1999**. 344 Pt 2: p. 305-11.
147. Li, F., Ambrosini, G., Chu, E.Y., Plescia, J., Tognin, S., Marchisio, P.C., and Altieri, D.C., *Control of apoptosis and mitotic spindle checkpoint by survivin*. Nature, **1998**. 396(6711): p. 580-4.
148. Altieri, D.C., *Targeted therapy by disabling crossroad signaling networks: the survivin paradigm*. Mol Cancer Ther, **2006**. 5(3): p. 478-82.
149. Hattori, M., Sakamoto, H., Satoh, K., and Yamamoto, T., *DNA demethylase is expressed in ovarian cancers and the expression correlates with demethylation of CpG sites in the promoter region of c-erbB-2 and survivin genes*. Cancer Letters, **2001**. 169(2): p. 155-164.
150. Wagner, M., Schmelz, K., Dorken, B., and Tamm, I., *Epigenetic and genetic analysis of the survivin promoter in acute myeloid leukemia*. Leuk Res, **2008**. 32(7): p. 1054-60.
151. Tanaka, C., Uzawa, K., Shibahara, T., Yokoe, H., Noma, H., and Tanzawa, H., *Expression of an inhibitor of apoptosis, survivin, in oral carcinogenesis*. J Dent Res, **2003**. 82(8): p. 607-11.
152. Cho, S., Lee, J.H., Cho, S.B., Yoon, K.W., Park, S.Y., Lee, W.S., Park, C.H., Joo, Y.E., Kim, H.S., Choi, S.K., and Rew, J.S., *Epigenetic methylation and expression of caspase 8 and survivin in hepatocellular carcinoma*. Pathol Int, **2010**. 60(3): p. 203-11.

153. Yu, J., Zhang, H., Gu, J., Lin, S., Li, J., Lu, W., Wang, Y., and Zhu, J., *Methylation profiles of thirty four promoter-CpG islands and concordant methylation behaviours of sixteen genes that may contribute to carcinogenesis of astrocytoma*. BMC Cancer, **2004**. 4: p. 65.
154. Nabils, N.H., Broaddus, R.R., and Loose, D.S., *DNA methylation inhibits p53-mediated survivin repression*. Oncogene, **2009**. 28(19): p. 2046-50.
155. Hoffman, W.H., Biade, S., Zilfou, J.T., Chen, J., and Murphy, M., *Transcriptional repression of the anti-apoptotic survivin gene by wild type p53*. J Biol Chem, **2002**. 277(5): p. 3247-57.
156. Kitagawa, M. and Lee, S.H., *The chromosomal passenger complex (CPC) as a key orchestrator of orderly mitotic exit and cytokinesis*. Front Cell Dev Biol, **2015**. 3: p. 14.
157. Capalbo, G., Dittmann, K., Weiss, C., Reichert, S., Hausmann, E., Rodel, C., and Rodel, F., *Radiation-induced survivin nuclear accumulation is linked to DNA damage repair*. Int J Radiat Oncol Biol Phys, **2010**. 77(1): p. 226-34.
158. Tamm, I., Wang, Y., Sausville, E., Scudiero, D.A., Vigna, N., Oltersdorf, T., and Reed, J.C., *IAP-family protein survivin inhibits caspase activity and apoptosis induced by Fas (CD95), Bax, caspases, and anticancer drugs*. Cancer Res, **1998**. 58(23): p. 5315-20.
159. Dohi, T., Okada, K., Xia, F., Wilford, C.E., Samuel, T., Welsh, K., Marusawa, H., Zou, H., Armstrong, R., Matsuzawa, S., Salvesen, G.S., Reed, J.C., and Altieri, D.C., *An IAP-IAP complex inhibits apoptosis*. J Biol Chem, **2004**. 279(33): p. 34087-90.
160. Dohi, T., Xia, F., and Altieri, D.C., *Compartmentalized phosphorylation of IAP by protein kinase A regulates cytoprotection*. Mol Cell, **2007**. 27(1): p. 17-28.
161. Song, Z., Yao, X., and Wu, M., *Direct interaction between survivin and Smac/DIABLO is essential for the anti-apoptotic activity of survivin during taxol-induced apoptosis*. J Biol Chem, **2003**. 278(25): p. 23130-40.
162. Ceballos-Cancino, G., Espinosa, M., Maldonado, V., and Melendez-Zajgla, J., *Regulation of mitochondrial Smac/DIABLO-selective release by survivin*. Oncogene, **2007**. 26(54): p. 7569-75.
163. Fortugno, P., Beltrami, E., Plescia, J., Fontana, J., Pradhan, D., Marchisio, P.C., Sessa, W.C., and Altieri, D.C., *Regulation of survivin function by Hsp90*. Proc Natl Acad Sci U S A, **2003**. 100(24): p. 13791-6.
164. Stauber, R.H., Mann, W., and Knauer, S.K., *Nuclear and cytoplasmic survivin: molecular mechanism, prognostic, and therapeutic potential*. Cancer Res, **2007**. 67(13): p. 5999-6002.
165. Engels, K., Knauer, S.K., Metzler, D., Simf, C., Struschka, O., Bier, C., Mann, W., Kovacs, A.F., and Stauber, R.H., *Dynamic intracellular survivin in oral squamous cell carcinoma: underlying molecular mechanism and potential as an early prognostic marker*. J Pathol, **2007**. 211(5): p. 532-40.
166. Knauer, S.K., Bier, C., Habtemichael, N., and Stauber, R.H., *The Survivin-Crm1 interaction is essential for chromosomal passenger complex localization and function*. EMBO Rep, **2006**. 7(12): p. 1259-65.
167. Knauer, S.K., Krämer, O.H., Knosel, T., Engels, K., Rodel, F., Kovacs, A.F., Dietmaier, W., Klein-Hitpass, L., Habtemichael, N., Schweitzer, A., Brieger, J., Rodel, C., Mann, W., Petersen, I., Heinzl, T., and Stauber, R.H., *Nuclear export is essential for the tumor-promoting activity of survivin*. FASEB J, **2007**. 21(1): p. 207-16.
168. Turner, J.G., Dawson, J., and Sullivan, D.M., *Nuclear export of proteins and drug resistance in cancer*. Biochem Pharmacol, **2012**. 83(8): p. 1021-32.
169. Cook, A., Bono, F., Jinek, M., and Conti, E., *Structural biology of nucleocytoplasmic transport*. Annu Rev Biochem, **2007**. 76: p. 647-71.
170. Fornerod, M., Ohno, M., Yoshida, M., and Mattaj, I.W., *CRM1 Is an Export Receptor for Leucine-Rich Nuclear Export Signals*. Cell, **1997**. 90(6): p. 1051-1060.
171. Arnaoutov, A., Azuma, Y., Ribbeck, K., Joseph, J., Boyarchuk, Y., Karpova, T., McNally, J., and Dasso, M., *Crm1 is a mitotic effector of Ran-GTP in somatic cells*. Nat Cell Biol, **2005**. 7(6): p. 626-32.
172. Dong, X., Biswas, A., and Chook, Y.M., *Structural basis for assembly and disassembly of the CRM1 nuclear export complex*. Nat Struct Mol Biol, **2009**. 16(5): p. 558-60.

Literature

173. Colnaghi, R., Connell, C.M., Barrett, R.M., and Wheatley, S.P., *Separating the anti-apoptotic and mitotic roles of survivin*. J Biol Chem, **2006**. 281(44): p. 33450-6.
174. Dohi, T., Beltrami, E., Wall, N.R., Plescia, J., and Altieri, D.C., *Mitochondrial survivin inhibits apoptosis and promotes tumorigenesis*. Journal of Clinical Investigation, **2004**. 114(8): p. 1117-1127.
175. Ghosh, J.C., Dohi, T., Raskett, C.M., Kowalik, T.F., and Altieri, D.C., *Activated Checkpoint Kinase 2 Provides a Survival Signal for Tumor Cells*. Cancer Research, **2006**. 66(24): p. 11576.
176. Fong, W.G., Liston, P., Rajcan-Separovic, E., St Jean, M., Craig, C., and Korneluk, R.G., *Expression and genetic analysis of XIAP-associated factor 1 (XAF1) in cancer cell lines*. Genomics, **2000**. 70(1): p. 113-22.
177. Liston, P., Fong, W.G., Kelly, N.L., Toji, S., Miyazaki, T., Conte, D., Tamai, K., Craig, C.G., McBurney, M.W., and Korneluk, R.G., *Identification of XAF1 as an antagonist of XIAP anti-Caspase activity*. Nat Cell Biol, **2001**. 3(2): p. 128-33.
178. Arora, V., Cheung, H.H., Plenchette, S., Micali, O.C., Liston, P., and Korneluk, R.G., *Degradation of survivin by the X-linked inhibitor of apoptosis (XIAP)-XAF1 complex*. J Biol Chem, **2007**. 282(36): p. 26202-9.
179. Byun, D.S., Cho, K., Ryu, B.K., Lee, M.G., Kang, M.J., Kim, H.R., and Chi, S.G., *Hypermethylation of XIAP-associated factor 1, a putative tumor suppressor gene from the 17p13.2 locus, in human gastric adenocarcinomas*. Cancer Res, **2003**. 63(21): p. 7068-75.
180. Zou, B., Chim, C.S., Zeng, H., Leung, S.Y., Yang, Y., Tu, S.P., Lin, M.C., Wang, J., He, H., Jiang, S.H., Sun, Y.W., Yu, L.F., Yuen, S.T., Kung, H.F., and Wong, B.C., *Correlation between the single-site CpG methylation and expression silencing of the XAF1 gene in human gastric and colon cancers*. Gastroenterology, **2006**. 131(6): p. 1835-43.
181. Lee, M.G., Huh, J.S., Chung, S.K., Lee, J.H., Byun, D.S., Ryu, B.K., Kang, M.J., Chae, K.S., Lee, S.J., Lee, C.H., Kim, J.I., Chang, S.G., and Chi, S.G., *Promoter CpG hypermethylation and downregulation of XAF1 expression in human urogenital malignancies: implication for attenuated p53 response to apoptotic stresses*. Oncogene, **2006**. 25(42): p. 5807-22.
182. Victoria-Acosta, G., Vazquez-Santillan, K., Jimenez-Hernandez, L., Munoz-Galindo, L., Maldonado, V., Martinez-Ruiz, G.U., and Melendez-Zajgla, J., *Epigenetic silencing of the XAF1 gene is mediated by the loss of CTCF binding*. Sci Rep, **2015**. 5: p. 14838.
183. Zhu, L.M., Shi, D.M., Dai, Q., Cheng, X.J., Yao, W.Y., Sun, P.H., Ding, Y., Qiao, M.M., Wu, Y.L., Jiang, S.H., and Tu, S.P., *Tumor suppressor XAF1 induces apoptosis, inhibits angiogenesis and inhibits tumor growth in hepatocellular carcinoma*. Oncotarget, **2014**. 5(14): p. 5403-15.
184. Huang, J., Yao, W.Y., Zhu, Q., Tu, S.P., Yuan, F., Wang, H.F., Zhang, Y.P., and Yuan, Y.Z., *XAF1 as a prognostic biomarker and therapeutic target in pancreatic cancer*. Cancer Sci, **2010**. 101(2): p. 559-67.
185. Quiros, S., Roos, W.P., and Kaina, B., *Rad51 and BRCA2--New molecular targets for sensitizing glioma cells to alkylating anticancer drugs*. PLoS One, **2011**. 6(11): p. e27183.
186. Bradford, M.M., *A rapid and sensitive method for the quantitation of microgram quantities of protein utilizing the principle of protein-dye binding*. Anal Biochem, **1976**. 72: p. 248-54.
187. Lowry, O.H., Rosebrough, N.J., Farr, A.L., and Randall, R.J., *Protein measurement with the Folin phenol reagent*. J Biol Chem, **1951**. 193(1): p. 265-75.
188. Mosmann, T., *Rapid colorimetric assay for cellular growth and survival: application to proliferation and cytotoxicity assays*. J Immunol Methods, **1983**. 65(1-2): p. 55-63.
189. Gewirtz, D.A., Holt, S.E., and Grant, S., *Apoptosis, senescence, and cancer*. **2007**, Totowa, N.J.: Humana Press. xvii, 599 p.
190. Debacq-Chainiaux, F., Erusalimsky, J.D., Campisi, J., and Toussaint, O., *Protocols to detect senescence-associated beta-galactosidase (SA-beta-gal) activity, a biomarker of senescent cells in culture and in vivo*. Nat Protoc, **2009**. 4(12): p. 1798-806.
191. Dimri, G.P., Lee, X., Basile, G., Acosta, M., Scott, G., Roskelley, C., Medrano, E.E., Linskens, M., Rubelj, I., Pereira-Smith, O., and et al., *A biomarker that identifies senescent human cells in culture and in aging skin in vivo*. Proc Natl Acad Sci U S A, **1995**. 92(20): p. 9363-7.

192. Kuilman, T., Michaloglou, C., Mooi, W.J., and Peeper, D.S., *The essence of senescence*. *Genes Dev*, **2010**. 24(22): p. 2463-79.
193. Lee, B.Y., Han, J.A., Im, J.S., Morrone, A., Johung, K., Goodwin, E.C., Kleijer, W.J., DiMaio, D., and Hwang, E.S., *Senescence-associated beta-galactosidase is lysosomal beta-galactosidase*. *Aging Cell*, **2006**. 5(2): p. 187-95.
194. Lecoœur, H., *Nuclear apoptosis detection by flow cytometry: influence of endogenous endonucleases*. *Exp Cell Res*, **2002**. 277(1): p. 1-14.
195. Darzynkiewicz, Z., Halicka, H.D., and Zhao, H., *Analysis of cellular DNA content by flow and laser scanning cytometry*. *Adv Exp Med Biol*, **2010**. 676: p. 137-47.
196. Pfaffl, M.W., Tichopad, A., Prgomet, C., and Neuvians, T.P., *Determination of stable housekeeping genes, differentially regulated target genes and sample integrity: BestKeeper--Excel-based tool using pair-wise correlations*. *Biotechnol Lett*, **2004**. 26(6): p. 509-15.
197. Livak, K.J. and Schmittgen, T.D., *Analysis of relative gene expression data using real-time quantitative PCR and the 2(-Delta Delta C(T)) Method*. *Methods*, **2001**. 25(4): p. 402-8.
198. Frommer, M., McDonald, L.E., Millar, D.S., Collis, C.M., Watt, F., Grigg, G.W., Molloy, P.L., and Paul, C.L., *A genomic sequencing protocol that yields a positive display of 5-methylcytosine residues in individual DNA strands*. *Proc Natl Acad Sci U S A*, **1992**. 89(5): p. 1827-31.
199. Chen, X.Y., He, Q.Y., and Guo, M.Z., *XAF1 is frequently methylated in human esophageal cancer*. *World Journal of Gastroenterology*, **2012**. 18(22): p. 2844-2849.
200. Switzeny, O.J., Christmann, M., Renovanz, M., Giese, A., Sommer, C., and Kaina, B., *MGMT promoter methylation determined by HRM in comparison to MSP and pyrosequencing for predicting high-grade glioma response*. *Clinical Epigenetics*, **2016**. 8(1): p. 1-10.
201. Stupp, R., Hegi, M.E., Mason, W.P., van den Bent, M.J., Taphoorn, M.J.B., Janzer, R.C., Ludwin, S.K., Allgeier, A., Fisher, B., Belanger, K., Hau, P., Brandes, A.A., Gijtenbeek, J., Marosi, C., Vecht, C.J., Mokhtari, K., Wesseling, P., Villa, S., Eisenhauer, E., Gorlia, T., Weller, M., Lacombe, D., Cairncross, J.G., and Mirimanoff, R.-O., *Effects of radiotherapy with concomitant and adjuvant temozolomide versus radiotherapy alone on survival in glioblastoma in a randomised phase III study: 5-year analysis of the EORTC-NCIC trial*. *The Lancet Oncology*, **2009**. 10(5): p. 459-466.
202. Wick, W., Roth, P., Hartmann, C., Hau, P., Nakamura, M., Stockhammer, F., Sabel, M.C., Wick, A., Koeppen, S., Ketter, R., Vajkoczy, P., Eyupoglu, I., Kalff, R., Hoppold, C., Galldiks, N., Schmidt-Graf, F., Bamberg, M., Reifenberger, G., Platten, M., von Deimling, A., Meisner, C., Wiestler, B., Weller, M., and Neurooncology Working Group of the German Cancer, S., *Long-term analysis of the NOA-04 randomized phase III trial of sequential radiochemotherapy of anaplastic glioma with PCV or temozolomide*. *Neuro Oncol*, **2016**.
203. Wick, W., Hartmann, C., Engel, C., Stoffels, M., Felsberg, J., Stockhammer, F., Sabel, M.C., Koeppen, S., Ketter, R., and Meyermann, R., *NOA-04 randomized phase III trial of sequential radiochemotherapy of anaplastic glioma with procarbazine, lomustine, and vincristine or temozolomide*. *J Clin Oncol*, **2009**. 27.
204. Kaplan, E.L. and Meier, P., *Nonparametric-Estimation from Incomplete Observations*. *Journal of the American Statistical Association*, **1958**. 53(282): p. 457-481.
205. Caldas, H., Jiang, Y., Holloway, M.P., Fangusaro, J., Mahotka, C., Conway, E.M., and Altura, R.A., *Survivin splice variants regulate the balance between proliferation and cell death*. *Oncogene*, **2005**. 24(12): p. 1994-2007.
206. Hoggart, C., Brennan, P., Tjonneland, A., Vogel, U., Overvad, K., Ostergaard, J.N., Kaaks, R., Canzian, F., Boeing, H., Steffen, A., Trichopoulou, A., Bamia, C., Trichopoulos, D., Johansson, M., Palli, D., Krogh, V., Tumino, R., Sacerdote, C., Panico, S., Boshuizen, H., Bueno-de-Mesquita, H.B., Peeters, P.H., Lund, E., Gram, I.T., Braaten, T., Rodriguez, L., Agudo, A., Sanchez-Cantalejo, E., Arriola, L., Chirlaque, M.D., Barricarte, A., Rasmuson, T., Khaw, K.T., Wareham, N., Allen, N.E., Riboli, E., and Vineis, P., *A risk model for lung cancer incidence*. *Cancer Prev Res (Phila)*, **2012**. 5(6): p. 834-46.
207. Chopra, S., Verma, A., Kundu, S., Engineer, R., Medhi, S., Mahantshetty, U., Gupta, S., and Shrivastava, S.K., *Evaluation of diffusion-weighted imaging as a predictive marker for tumor*

Literature

- response in patients undergoing chemoradiation for postoperative recurrences of cervical cancer. *J Cancer Res Ther*, **2012**. 8(1): p. 68-73.
208. Kim, D.H., Sriharsha, L., Jung, C.W., Kamel-Reid, S., Radich, J.P., and Lipton, J.H., *Comprehensive evaluation of time-to-response parameter as a predictor of treatment failure following imatinib therapy in chronic phase chronic myeloid leukemia: which parameter at which time-point does matter?* *Am J Hematol*, **2010**. 85(11): p. 856-62.
209. Hoggarth, P.A., Innes, C.R., Dalrymple-Alford, J.C., Severinsen, J.E., and Jones, R.D., *Comparison of a linear and a non-linear model for using sensory-motor, cognitive, personality, and demographic data to predict driving ability in healthy older adults*. *Accid Anal Prev*, **2010**. 42(6): p. 1759-68.
210. Carlone, M., Cruje, C., Rangel, A., McCabe, R., Nielsen, M., and Macpherson, M., *ROC analysis in patient specific quality assurance*. *Med Phys*, **2013**. 40(4): p. 042103.
211. Yamamoto, H., Ngan, C.Y., and Monden, M., *Cancer cells survive with survivin*. *Cancer Sci*, **2008**. 99(9): p. 1709-14.
212. Fukuda, S. and Pelus, L.M., *Survivin, a cancer target with an emerging role in normal adult tissues*. *Mol Cancer Ther*, **2006**. 5(5): p. 1087-98.
213. Ikeguchi, M. and Kaibara, N., *Survivin messenger RNA expression is a good prognostic biomarker for oesophageal carcinoma*. *Br J Cancer*, **2002**. 87(8): p. 883-887.
214. Kato, J., Kuwabara, Y., Mitani, M., Shinoda, N., Sato, A., Toyama, T., Mitsui, A., Nishiwaki, T., Moriyama, S., Kudo, J., and Fujii, Y., *Expression of survivin in esophageal cancer: correlation with the prognosis and response to chemotherapy*. *Int J Cancer*, **2001**. 95(2): p. 92-5.
215. Kennedy, S.M., O'Driscoll, L., Purcell, R., Fitz-simons, N., McDermott, E.W., Hill, A.D., O'Higgins, N.J., Parkinson, M., Linehan, R., and Clynes, M., *Prognostic importance of survivin in breast cancer*. *Br J Cancer*, **2003**. 88(7): p. 1077-1083.
216. Span, P.N., Sweep, F.C.G.J., Wiegerinck, E.T.G., Tjan-Heijnen, V.C.G., Manders, P., Beex, L.V.A.M., and de Kok, J.B., *Survivin Is an Independent Prognostic Marker for Risk Stratification of Breast Cancer Patients*. *Clinical Chemistry*, **2004**. 50(11): p. 1986.
217. Ikeguchi, M., Ueda, T., Sakatani, T., Hirooka, Y., and Kaibara, N., *Expression of Survivin Messenger RNA Correlates With Poor Prognosis in Patients With Hepatocellular Carcinoma*. *Diagnostic Molecular Pathology*, **2002**. 11(1).
218. Kami, K., Doi, R., Koizumi, M., Toyoda, E., Mori, T., Ito, D., Fujimoto, K., Wada, M., Miyatake, S.-I., and Imamura, M., *Survivin expression is a prognostic marker in pancreatic cancer patients*. *Surgery*, **2004**. 136(2): p. 443-448.
219. Kajiwara, Y., Yamasaki, F., Hama, S., Yahara, K., Yoshioka, H., Sugiyama, K., Arita, K., and Kurisu, K., *Expression of survivin in astrocytic tumors: correlation with malignant grade and prognosis*. *Cancer*, **2003**. 97(4): p. 1077-83.
220. O'Driscoll, L., Linehan, R., M. Kennedy, S., Cronin, D., Purcell, R., Glynn, S., W. McDermott, E., D. Hill, A., J. O'Higgins, N., Parkinson, M., and Clynes, M., *Lack of prognostic significance of survivin, survivin- Δ Ex3, survivin-2B, galectin-3, bag-1, bax- α and MRP-1 mRNAs in breast cancer*. *Cancer Letters*, **2003**. 201(2): p. 225-236.
221. Kayaselcuk, F., Zorludemir, S., Bal, N., Erdogan, B., Erdogan, S., and Erman, T., *The expression of survivin and Ki-67 in meningiomas: correlation with grade and clinical outcome*. *J Neurooncol*, **2004**. 67(1-2): p. 209-14.
222. Morinaga, S., Nakamura, Y., Ishiwa, N., Yoshikawa, T., Noguchi, Y., Yamamoto, Y., Rino, Y., Imada, T., Takanashi, Y., Akaike, M., Sugimasa, Y., and Takemiya, S., *Expression of survivin mRNA associates with apoptosis, proliferation and histologically aggressive features in hepatocellular carcinoma*. *Oncol Rep*, **2004**. 12(6): p. 1189-94.
223. Su, C., *Survivin in survival of hepatocellular carcinoma*. *Cancer Lett*, **2016**. 379(2): p. 184-90.
224. Goossens-Beumer, I.J., Zeestraten, E.C., Benard, A., Christen, T., Reimers, M.S., Keijzer, R., Sier, C.F., Liefers, G.J., Morreau, H., Putter, H., Vahrmeijer, A.L., van de Velde, C.J., and Kuppen, P.J., *Clinical prognostic value of combined analysis of Aldh1, Survivin, and EpCAM expression in colorectal cancer*. *Br J Cancer*, **2014**. 110(12): p. 2935-44.

225. Brennan, D.J., Rexhepaj, E., O'Brien, S.L., McSherry, E., O'Connor, D.P., Fagan, A., Culhane, A.C., Higgins, D.G., Jirstrom, K., Millikan, R.C., Landberg, G., Duffy, M.J., Hewitt, S.M., and Gallagher, W.M., *Altered cytoplasmic-to-nuclear ratio of survivin is a prognostic indicator in breast cancer*. Clin Cancer Res, **2008**. 14(9): p. 2681-9.
226. Okada, E., Murai, Y., Matsui, K., Isizawa, S., Cheng, C., Masuda, M., and Takano, Y., *Survivin expression in tumor cell nuclei is predictive of a favorable prognosis in gastric cancer patients*. Cancer Letters, **2001**. 163(1): p. 109-116.
227. Atikcan, S., Ünsal, E., Demirag, F., Köksal, D., and Yilmaz, A., *Correlation between survivin expression and prognosis in non-small cell lung cancer*. Respiratory Medicine, **2006**. 100(12): p. 2220-2226.
228. Hu, S., Qu, Y., Xu, X., Xu, Q., Geng, J., and Xu, J., *Nuclear survivin and its relationship to DNA damage repair genes in non-small cell lung cancer investigated using tissue array*. PLoS One, **2013**. 8(9): p. e74161.
229. Bria, E., Visca, P., Novelli, F., Casini, B., Diodoro, M.G., Perrone-Donnorso, R., Botti, C., Sperduti, I., Facciolo, F., Milella, M., Cecere, F.L., Cognetti, F., and Mottolese, M., *Nuclear and cytoplasmic cellular distribution of survivin as survival predictor in resected non-small-cell lung cancer*. European Journal of Surgical Oncology (EJSO), **2008**. 34(5): p. 593-598.
230. Santarelli, A., Mascitti, M., Rubini, C., Bambini, F., Giannatempo, G., Lo Russo, L., Sartini, D., Emanuelli, M., Procaccini, M., and Lo Muzio, L., *Nuclear Survivin as a Prognostic Factor in Squamous-Cell Carcinoma of the Oral Cavity*. Appl Immunohistochem Mol Morphol, **2016**.
231. Adamkov, M., Vybohova, D., Tupa, V., Chylikova, J., Horacek, J., and Bencat, M., *Expression and significance of survivin in colorectal high grade and low grade adenomas*. Acta Histochem, **2015**. 117(6): p. 590-4.
232. Preusser, M., Gelpi, E., Matej, R., Marosi, C., Dieckmann, K., Rossler, K., Budka, H., and Hainfellner, J.A., *No prognostic impact of survivin expression in glioblastoma*. Acta Neuropathol, **2005**. 109(5): p. 534-8.
233. Shirai, K., Suzuki, Y., Oka, K., Noda, S.E., Katoh, H., Suzuki, Y., Itoh, J., Itoh, H., Ishiuchi, S., Sakurai, H., Hasegawa, M., and Nakano, T., *Nuclear survivin expression predicts poorer prognosis in glioblastoma*. J Neurooncol, **2009**. 91(3): p. 353-8.
234. Lv, S., Dai, C., Liu, Y., Shi, R., Tang, Z., Han, M., Bian, R., Sun, B., and Wang, R., *The impact of survivin on prognosis and clinicopathology of glioma patients: a systematic meta-analysis*. Mol Neurobiol, **2015**. 51(3): p. 1462-7.
235. Knauer, S.K., Unruhe, B., Karczewski, S., Hecht, R., Fetz, V., Bier, C., Friedl, S., Wollenberg, B., Pries, R., Habtemichael, N., Heinrich, U.R., and Stauber, R.H., *Functional characterization of novel mutations affecting survivin (BIRC5)-mediated therapy resistance in head and neck cancer patients*. Hum Mutat, **2012**. 34(2): p. 395-404.
236. Knizhnik, A.V., Roos, W.P., Nikolova, T., Quiros, S., Tomaszowski, K.H., Christmann, M., and Kaina, B., *Survival and death strategies in glioma cells: autophagy, senescence and apoptosis triggered by a single type of temozolomide-induced DNA damage*. PLoS One, **2013**. 8(1): p. e55665.
237. Smith, J., Tho, L.M., Xu, N., and Gillespie, D.A., *The ATM-Chk2 and ATR-Chk1 pathways in DNA damage signaling and cancer*. Adv Cancer Res, **2010**. 108: p. 73-112.
238. Meek, D.W. and Anderson, C.W., *Posttranslational modification of p53: cooperative integrators of function*. Cold Spring Harb Perspect Biol, **2009**. 1(6): p. a000950.
239. Loughery, J., Cox, M., Smith, L.M., and Meek, D.W., *Critical role for p53-serine 15 phosphorylation in stimulating transactivation at p53-responsive promoters*. Nucleic Acids Research, **2014**.
240. Unger, T., Sionov, R.V., Moallem, E., Yee, C.L., Howley, P.M., Oren, M., and Haupt, Y., *Mutations in serines 15 and 20 of human p53 impair its apoptotic activity*. Oncogene, **1999**. 18(21): p. 3205-12.
241. Rogakou, E.P., Pilch, D.R., Orr, A.H., Ivanova, V.S., and Bonner, W.M., *DNA double-stranded breaks induce histone H2AX phosphorylation on serine 139*. J Biol Chem, **1998**. 273(10): p. 5858-68.

Literature

242. Rogakou, E.P., Boon, C., Redon, C., and Bonner, W.M., *Megabase chromatin domains involved in DNA double-strand breaks in vivo*. J Cell Biol, **1999**. 146(5): p. 905-16.
243. Chronis, F. and Rogakou, E.P., *Interplay Between γ H2AX and 53BP1 Pathways in DNA Double-Strand Break Repair Response*, in *Apoptosis, Senescence, and Cancer*, David A. Gewirtz, Holt, Shawn E., and Grant, Steven, Editors. **2007**, Humana Press: Totowa, NJ. p. 243-263.
244. Vequaud, E., Desplanques, G., Jezequel, P., Juin, P., and Barille-Nion, S., *Survivin contributes to DNA repair by homologous recombination in breast cancer cells*. Breast Cancer Res Treat, **2016**. 155(1): p. 53-63.
245. Qin, Q., Cheng, H., Lu, J., Zhan, L., Zheng, J., Cai, J., Yang, X., Xu, L., Zhu, H., Zhang, C., Liu, J., Ma, J., Zhang, X., Dai, S., and Sun, X., *Small-molecule survivin inhibitor YM155 enhances radiosensitization in esophageal squamous cell carcinoma by the abrogation of G2 checkpoint and suppression of homologous recombination repair*. J Hematol Oncol, **2014**. 7: p. 62.
246. Rauch, A., Hennig, D., Schafer, C., Wirth, M., Marx, C., Heinzl, T., Schneider, G., and Kramer, O.H., *Survivin and YM155: how faithful is the liaison?* Biochim Biophys Acta, **2014**. 1845(2): p. 202-20.
247. Li, F., Yang, J., Ramnath, N., Javle, M.M., and Tan, D., *Nuclear or cytoplasmic expression of survivin: what is the significance?* Int J Cancer, **2005**. 114(4): p. 509-12.
248. Tomicic, M.T., Christmann, M., and Kaina, B., *Topotecan triggers apoptosis in p53-deficient cells by forcing degradation of XIAP and survivin thereby activating caspase-3-mediated Bid cleavage*. J Pharmacol Exp Ther, **2010**. 332(1): p. 316-25.
249. Plenchette, S., Cheung, H.H., Fong, W.G., LaCasse, E.C., and Korneluk, R.G., *The role of XAF1 in cancer*. Curr Opin Investig Drugs, **2007**. 8(6): p. 469-76.
250. Wang, Y., Mao, H., Hao, Q., Wang, Y., Yang, Y., Shen, L., Huang, S., and Liu, P., *Association of expression of XIAP-associated factor 1 (XAF1) with clinicopathologic factors, overall survival, microvessel density and cisplatin-resistance in ovarian cancer*. Regul Pept, **2012**. 178(1-3): p. 36-42.
251. Micali, O.C., Cheung, H.H., Plenchette, S., Hurley, S.L., Liston, P., LaCasse, E.C., and Korneluk, R.G., *Silencing of the XAF1 gene by promoter hypermethylation in cancer cells and reactivation to TRAIL-sensitization by IFN-beta*. BMC Cancer, **2007**. 7: p. 52.
252. Ng, K.C., Campos, E.I., Martinka, M., and Li, G., *XAF1 expression is significantly reduced in human melanoma*. J Invest Dermatol, **2004**. 123(6): p. 1127-34.
253. Kempkensteffen, C., Hinz, S., Schrader, M., Christoph, F., Magheli, A., Krause, H., Schostak, M., Miller, K., and Weikert, S., *Gene expression and promoter methylation of the XIAP-associated Factor 1 in renal cell carcinomas: correlations with pathology and outcome*. Cancer Lett, **2007**. 254(2): p. 227-35.
254. Capper, D., Zentgraf, H., Balss, J., Hartmann, C., and von Deimling, A., *Monoclonal antibody specific for IDH1 R132H mutation*. Acta Neuropathol, **2009**. 118(5): p. 599-601.
255. Agarwal, S., Sharma, M.C., Jha, P., Pathak, P., Suri, V., Sarkar, C., Chosdol, K., Suri, A., Kale, S.S., Mahapatra, A.K., and Jha, P., *Comparative study of IDH1 mutations in gliomas by immunohistochemistry and DNA sequencing*. Neuro Oncol, **2013**. 15(6): p. 718-26.
256. Li, J., Zhang, H., Wang, L., Yang, C., Lai, H., Zhang, W., Chen, X., and Wang, J., *Comparative study of IDH1 mutations in gliomas by high resolution melting analysis, immunohistochemistry and direct DNA sequencing*. Mol Med Rep, **2015**. 12(3): p. 4376-81.
257. Wang, P.F., Liu, N., Song, H.W., Yao, K., Jiang, T., Li, S.W., and Yan, C.X., *IDH-1R132H mutation status in diffuse glioma patients: implications for classification*. Oncotarget, **2016**. 7(21): p. 31393-400.
258. Lee, M.G., Han, J., Jeong, S.I., Her, N.G., Lee, J.H., Ha, T.K., Kang, M.J., Ryu, B.K., and Chi, S.G., *XAF1 directs apoptotic switch of p53 signaling through activation of HIPK2 and ZNF313*. Proceedings of the National Academy of Sciences of the United States of America, **2014**. 111(43): p. 15532-15537.
259. Pietsch, E.C., Sykes, S.M., McMahon, S.B., and Murphy, M.E., *The p53 family and programmed cell death*. Oncogene, **2008**. 27(50): p. 6507-21.

260. Li, Y., Jenkins, C.W., Nichols, M.A., and Xiong, Y., *Cell cycle expression and p53 regulation of the cyclin-dependent kinase inhibitor p21*. *Oncogene*, **1994**. 9(8): p. 2261-8.
261. el-Deiry, W.S., Tokino, T., Velculescu, V.E., Levy, D.B., Parsons, R., Trent, J.M., Lin, D., Mercer, W.E., Kinzler, K.W., and Vogelstein, B., *WAF1, a potential mediator of p53 tumor suppression*. *Cell*, **1993**. 75(4): p. 817-25.
262. Jung, Y.S., Qian, Y., and Chen, X., *Examination of the expanding pathways for the regulation of p21 expression and activity*. *Cell Signal*, **2010**. 22(7): p. 1003-12.
263. Han, J., Kim, Y.L., Lee, K.W., Her, N.G., Ha, T.K., Yoon, S., Jeong, S.I., Lee, J.H., Kang, M.J., Lee, M.G., Ryu, B.K., Baik, J.H., and Chi, S.G., *ZNF313 is a novel cell cycle activator with an E3 ligase activity inhibiting cellular senescence by destabilizing p21(WAF1).* *Cell Death Differ*, **2013**. 20(8): p. 1055-67.

6 Appendix

6.1 Supplementary data

Suppl. Table 1: Detailed SNP analysis for the BIRC5 NES. TAC indicates the detection of the wt BIRC5 sequence. Deviations from the wt sequence are indicated with percentages.

Patient ID	SNP-analysis	Aberrations SNP Position 3
1041/12	TAC	Position 3: C: 89.4% / T: 10.6%	1922/12	TAC	Position 3: C: 88.7% / T: 11.3%
116/13	failed		1933/12	TAC	Position 3: C: 90.8% / T: 9.2%
1274/11	failed		1950/12	TAC	Position 3: C: 87.9% / T: 12.1%
1566/12	failed		1961/11	TAC	
1807/12	failed		1998/11	TAC	Position 3: C: 93.8% / T: 6.2%
1813/11	failed		2083/11	TAC	
1042/13	TAC	Position 3: C: 88.7% / T: 11.3%	242/12	TAC	Position 3: C: 84.8% / T: 15.2%
1046/13	TAC		292/13	TAC	Position 3: C: 89.2% / T: 10.8%
1047/13	TAC		298/13	TAC	Position 3: C: 89.0% / T: 11.0%
1052/13	TAC		299/13	TAC	Position 3: C: 93.7% / T: 6.3%
1094/12	TAC	Position 3: C: 94.5% / T: 5.5%	308/13	TAC	Position 3: C: 93.0% / T: 7.0%
1151/11	TAC		394/12	TAC	Position 3: C: 92.2% / T: 7.8%
1170/12	TAC	Position 3: C: 91.6% / T: 8.4%	415/12	TAC	Position 3: C: 92.4% / T: 7.6%
1185/13	TAC	Position 3: C: 92.8% / T: 7.2%	416/13	TAC	
1221/12	TAC		436/13	TAC	
1228/13	TAC		438/12	TAC	Position 3: C: 93.7% / T: 6.3%
1237/12	TAC		449/13	TAC	
1294/13	TAC		456/13	TAC	Position 3: C: 94.5% / T: 5.5%
1307/12	TAC		464/12	TAC	Position 3: C: 91.4% / T: 8.6%
1320/11	TAC		54/13	TAC	Position 3: C: 86.7% / T: 13.3%
1321/12	TAC		624/12	TAC	
1369/13	TAC		658/12	TAC	Position 3: C: 92.6% / T: 7.4%
137/13	TAC	Position 3: C: 94.5% / T: 5.5%	678/11	TAC	
1394/13	TAC	Position 3: C: 91.5% / T: 8.5%	71/12	TAC	
1405/13	TAC	Position 3: C: 89.1% / T: 10.9%	716/12	TAC	
1410/12	TAC		743/13	TAC	Position 3: C: 90.5% / T: 9.5%
1435/12	TAC	Position 3: C: 92.7% / T: 7.3%	760/12	TAC	
1436/12	TAC		770/12	TAC	
1458/12	TAC	Position 3: C: 87.0% / T: 13.0%	774/12	TAC	
1464/12	TAC	Position 3: C: 87.7% / T: 12.3%	812/13	TAC	
1469/12	TAC	Position 3: C: 92.7% / T: 7.3%	828/12	TAC	Position 3: C: 94.8% / T: 5.2%
149/12	TAC	Position 3: C: 87.1% / T: 12.9%	848/12	TAC	Position 3: C: 92.8% / T: 7.2%
1495/11	TAC	Position 3: C: 88.2% / T: 11.8%	931/11	TAC	Position 3: C: 93.1% / T: 6.9%
1510/12	TAC		95/12	TAC	
1525/12	TAC		953/13	TAC	Position 3: C: 90.4% / T: 9.6%
162/13	TAC	Position 3: C: 87.7% / T: 12.3%	964/13	TAC	Position 3: C: 91.3% / T: 8.7%
163/13	TAC		LN229	TAC	
1637/12	TAC		U87	TAC	
1649/12	TAC		HCT116	TAC	
1653/12	TAC		LN308	TAC	
1677/12	TAC	Position 3: C: 91.7% / T: 8.3%	LN319	TAC	
169/11	TAC	Position 3: C: 94.8% / T: 5.2%	VH10	TAC	
1694/12	TAC		1877/12	TAC	
1700/10	TAC		1904/12	TAC	
1702/11	TAC	Position 3: C: 90.1% / T: 9.9%	1849/11	TAC	
1712/11	TAC				
1715/11	TAC	Position 3: C: 90.6% / T: 9.4%			
1727/11	TAC				

1739/11	TAC	Position 3: C: 91.1% / T: 8.9%
1765/11	TAC	
1773/11	TAC	
1833/12	TAC	

Suppl. Table 2: Possible ROC cut-off values determined for predicting the 24 OS. Sensitivity and 1 specificity are provided for each possible cut-off point.

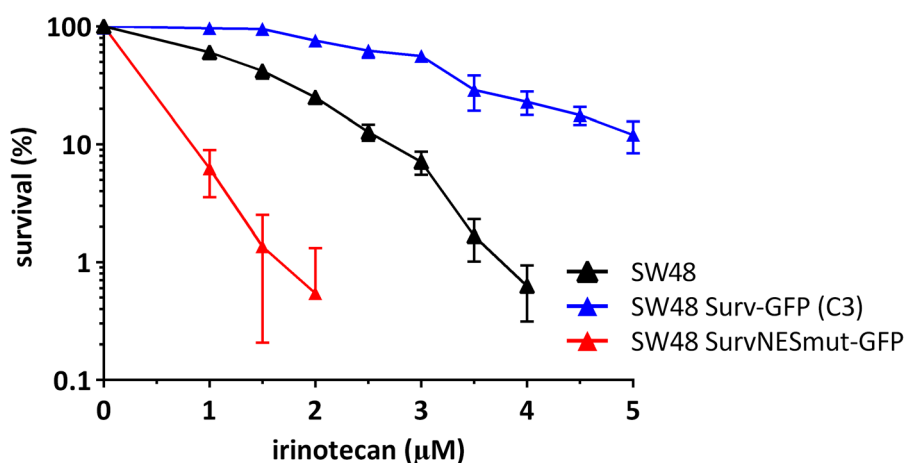
Methylation (%)	Sensitivity	1 - Specificity
-82.785	1.000	1.000	9.689	0.727	0.326
-58.492	1.000	0.978	10.670	0.727	0.304
-32.838	1.000	0.957	12.702	0.727	0.283
-29.768	0.970	0.957	13.946	0.697	0.283
-23.899	0.970	0.935	14.468	0.697	0.261
-17.456	0.970	0.913	14.944	0.697	0.239
-14.754	0.970	0.891	15.643	0.697	0.217
-13.193	0.939	0.891	17.429	0.697	0.196
-12.596	0.939	0.870	20.014	0.667	0.196
-11.863	0.939	0.848	21.970	0.667	0.174
-11.177	0.939	0.826	23.422	0.636	0.174
-10.570	0.939	0.804	25.840	0.636	0.152
-9.951	0.939	0.783	28.284	0.606	0.152
-8.950	0.939	0.761	31.090	0.576	0.152
-7.939	0.909	0.761	35.928	0.576	0.130
-7.335	0.879	0.761	41.850	0.545	0.130
-6.832	0.848	0.761	45.167	0.545	0.109
-6.354	0.848	0.739	52.154	0.545	0.087
-6.162	0.848	0.717	59.735	0.515	0.087
-5.739	0.848	0.696	60.752	0.515	0.065
-5.073	0.848	0.674	64.135	0.485	0.065
-4.527	0.848	0.652	69.422	0.455	0.065
-4.064	0.818	0.652	71.915	0.455	0.043
-3.772	0.818	0.630	73.777	0.424	0.043
-3.174	0.818	0.609	75.133	0.394	0.043
-2.555	0.818	0.587	75.647	0.364	0.043
-2.401	0.818	0.565	77.101	0.333	0.043
-2.362	0.818	0.543	82.143	0.303	0.043
-2.168	0.818	0.522	87.948	0.273	0.043
-1.310	0.818	0.500	91.630	0.242	0.043
0.088	0.818	0.478	93.702	0.212	0.043
1.081	0.818	0.457	94.851	0.182	0.043
1.631	0.818	0.435	97.076	0.152	0.043
1.932	0.788	0.435	99.493	0.121	0.043
2.646	0.788	0.413	101.942	0.091	0.043
3.580	0.788	0.391	104.278	0.061	0.043
5.655	0.758	0.391	105.494	0.030	0.043
7.679	0.727	0.391	107.372	0.000	0.043
8.165	0.727	0.370	131.399	0.000	0.022
9.037	0.727	0.348	154.675	0.000	0.000

Appendix

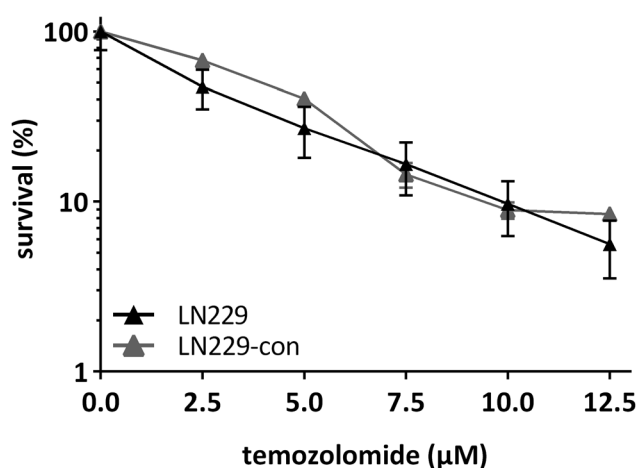
Suppl. Table 3: Possible ROC cut-off values determined for predicting the PFS. Sensitivity and 1 - specificity are provided for each possible cut-off point.

Methylation (%)	Sensitivity	1 - Specificity
-82.785	1	1	9.689	0.905	0.356
-58.492	1	0.983	10.67	0.905	0.339
-32.838	1	0.966	12.702	0.905	0.322
-29.768	1	0.949	13.946	0.905	0.305
-23.899	1	0.932	14.468	0.905	0.288
-17.456	1	0.915	14.944	0.905	0.271
-14.754	1	0.898	15.643	0.905	0.254
-13.193	1	0.881	17.429	0.905	0.237
-12.596	1	0.864	20.014	0.905	0.22
-11.863	1	0.847	21.97	0.905	0.203
-11.177	1	0.831	23.422	0.857	0.203
-10.57	1	0.814	25.84	0.857	0.186
-9.951	1	0.797	28.284	0.857	0.169
-8.95	1	0.78	31.09	0.857	0.153
-7.939	1	0.763	35.928	0.857	0.136
-7.335	0.952	0.763	41.85	0.81	0.136
-6.832	0.905	0.763	45.167	0.81	0.119
-6.354	0.905	0.746	52.154	0.81	0.102
-6.162	0.905	0.729	59.735	0.762	0.102
-5.739	0.905	0.712	60.752	0.762	0.085
-5.073	0.905	0.695	64.135	0.714	0.085
-4.527	0.905	0.678	69.422	0.667	0.085
-4.064	0.905	0.661	71.915	0.667	0.068
-3.772	0.905	0.644	73.777	0.619	0.068
-3.174	0.905	0.627	75.133	0.571	0.068
-2.555	0.905	0.61	75.647	0.524	0.068
-2.401	0.905	0.593	76.737	0.476	0.068
-2.362	0.905	0.576	77.723	0.476	0.051
-2.168	0.905	0.559	82.143	0.429	0.051
-1.31	0.905	0.542	87.948	0.381	0.051
0.088	0.905	0.525	91.63	0.333	0.051
1.081	0.905	0.508	93.702	0.286	0.051
1.631	0.905	0.492	94.851	0.238	0.051
1.932	0.905	0.475	97.076	0.19	0.051
2.646	0.905	0.458	99.493	0.19	0.034
3.58	0.905	0.441	101.942	0.143	0.034
5.655	0.905	0.424	104.278	0.095	0.034
7.679	0.905	0.407	105.494	0.048	0.034
8.165	0.905	0.39	107.372	0	0.034
9.037	0.905	0.373	131.399	0	0.017
			154.675	0	0

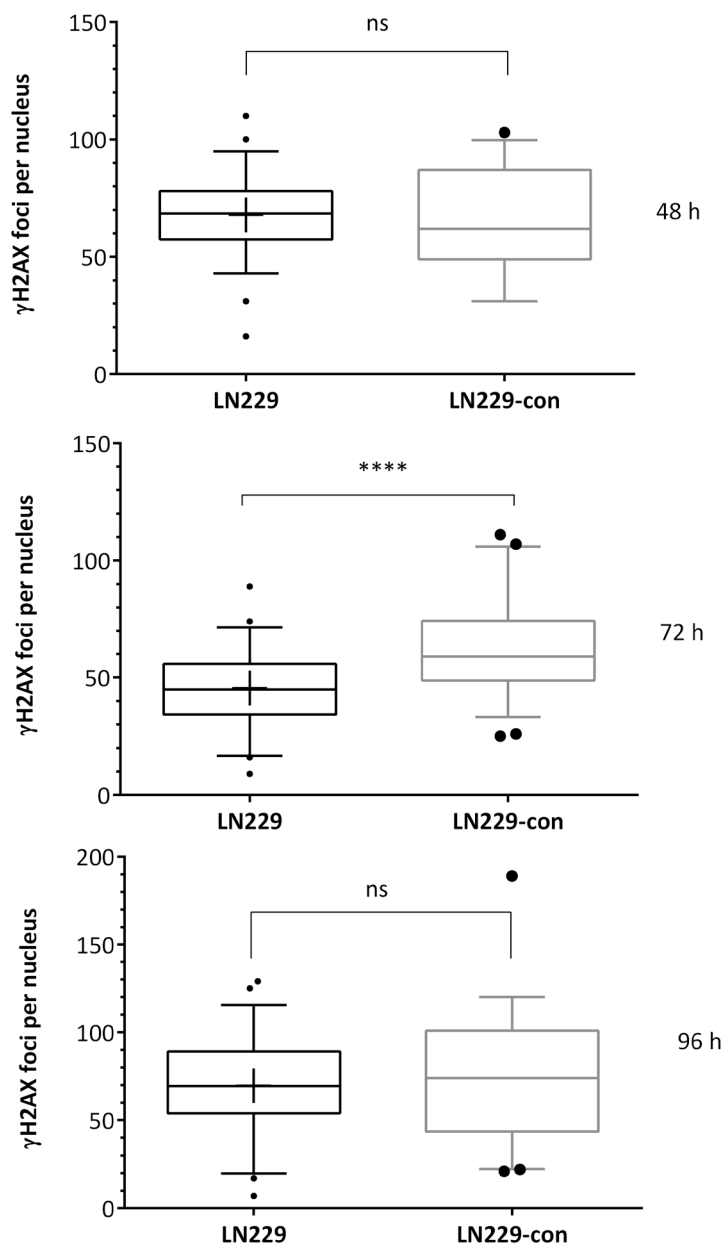
Analogous to the survival studies in GB cells, the impact of Survivin expression was also analyzed in CRC cell line SW48. SW48 cells were transfected with Surv GFP and SurvNESmut GFP, respectively and different cell clones were established. Examples are given in where the response to irinotecan (IT) was analyzed. IT is used in the therapy of CRC. The sensitivity is in line with the observations in glioma cells.



Suppl. Figure 1: Colony formation assay (CFA) of Survivin CRC cell clones for different concentrations of IT. Surviving cells were normalized to control (%) and plotted in a semi-logarithmic graph. Data of three independent experiments in technical triplicates are shown ($N = 3$). Error bars indicate the SD.



Suppl. Figure 2: Colony formation assay (CFA) of parental LN229 cells and transfection control (pSu empty vector) for different concentrations of TMZ. Surviving cells were normalized to control (%) and plotted in a semi-logarithmic graph. Data of three independent experiments in technical triplicates are shown ($N = 3$) with error bars indicating SD.



Suppl. Figure 3: Box-Blots of γ H2AX foci numbers per nucleus of parental LN229 cells and transfection control (pSu empty vector) after treatment with 50 μ M TMZ. Whiskers indicate 5th and 95th percentile, with boxes representing first, second (median) and third quartile (from top to bottom). Geometric means are marked with "+". Outliers (values out of 5–95 percentile range) are marked as "•". Test for statistical significance was performed by One-Way ANOVA with Tukey's post hoc analysis. Significant differences are indicated with *. 35 to 56 nuclei were evaluated for each cell line and time point in this analysis.

Suppl. Table 4: Clinical data of the analyzed cohort of high-grade glioma patients treated at the University Medical Center Mainz between 2011 and 2013. The clinical parameters PFS, OS, Age, Sex, histological tumor grade, and IDH1 status (detected by IHC) were provided by the Department of Neurosurgery of the UM Mainz. IDH1 status was further confirmed by pyrosequencing. Promoter methylation values for XAF1 and BIRC5 were determined as described. According to the "WHO Classification of Tumours of the central nervous system" AA, AO, and AOA resemble WHO grade III gliomas while GB represent WHO grade IV lesions.

ID	PFS months	OS months	Progress months	dead	IDH1 mut	XAF1 Meth. (HRM1)	Age	Sex	XAF1		Grade	>70	OS 24	PFS 24	BIRC5 HRM
									HRM1 (%)	HRM2 (%)					
1041/12	2	2	1	1	0	0	72	1	-11.6	-	GB	1	0	0	-0.7
1042/13	28	33	0	0	1	1	28	1	95.9	-	AA	0	1	1	-29.7
1046/13	34	34	0	0	1	1	29	1	76.1	83.3	AA	0	1	1	-
1047/13	33	33	0	0	1	1	45	1	75.2	-	AA	0	1	1	-51.2
1052/13	32	32	0	0	1	1	44	2	38.9	-	AA	0	1	1	-28.2
1094/12	2	4	1	1	0	0	78	2	0.8	-	AA	1	0	0	-53.5
1151/11	6	14	1	1	0	0	67	1	3.3	-	GB	0	1	0	-7.7
116/13	4	5	1	1	0	0	57	1	-3.7	11.2	GB	0	1	0	-
1170/12	41	47	1	0	1	1	42	1	105.6	-	AO	0	1	1	-
1185/13	6	17	1	1	0	0	56	1	1.9	-	GB	0	1	0	-
1221/12	45	45	0	0	1	1	60	1	93.6	109.8	AO	0	1	1	-33.3
1228/13	3	11	1	1	0	0	67	1	8.5	-	GB	0	1	0	-
1235/11	5	8	1	1	0	1	61	1	71.4	73.5	GB	0	1	0	-12.2
1237/12	3	4	1	1	0	0	67	1	-3.9	12.6	GB	0	1	0	0.6
1274/11	3	16	1	1	0	1	74	1	153.7	59.6	GB	1	0	0	-
1294/13	3	5	1	1	0	0	74	1	-35.2	-	GB	1	0	0	-20.2
1307/12	5	22	1	1	0	0	74	1	1.3	17.5	GB	1	0	0	-
1321/12	45	45	0	0	1	1	51	1	58.8	80.5	AO	0	1	1	-
1349/12	27	35	1	0	1	1	26	1	93.8	-	AA	0	1	1	-
1353/13	15	29	1	0	0	0	71	2	-4.3	-	GB	1	0	1	-
1356/11	3	4	1	1	0	0	63	1	15.0	-	GB	0	1	0	-36.6
1365/12	45	45	0	0	1	1	51	1	67.5	75.6	AOA	0	1	1	-23.6

Appendix

1369/13	27	27	0	0	0	0	0	49	1	-7.5	14.0	GB	0	1	1	1	-10.1
1394/13	22	28	1	0	0	0	0	73	2	1.9	-	GB	1	0	1	0	-
1405/13	3	9	1	1	0	0	0	60	1	14.1	27.9	GB	0	1	0	0	-34.6
1435/12	6	18	1	1	0	0	0	73	1	24.4	-	GB	1	0	0	0	-
1436/12	4	19	1	1	0	0	0	78	2	21.4	-	GB	1	0	0	0	-12.2
1458/12	18	37	1	1	0	0	0	64	1	-13.3	-4.5	GB	0	1	1	0	-28.3
1464/12	7	16	1	1	0	0	0	70	1	-5.4	12.3	AA	1	1	0	0	-6.8
1469/12	31	44	1	0	1	1	1	40	1	89.7	68.5	AOA	0	1	1	1	-
1525/12	4	17	1	1	0	1	1	43	1	109.1	-	GB	0	1	0	0	-
1562/11	53	53	0	0	1	1	1	40	1	105.4	-	AOA	0	1	1	1	-
1566/12	2	18	1	1	0	0	0	68	1	-81.8	-	GB	0	1	0	0	-
162/13	6	7	1	1	0	0	0	69	1	16.3	32.6	GB	0	1	0	0	-13.8
163/13	3	3	1	1	0	0	0	72	1	-6.5	38.6	GB	1	0	0	0	0.0
1637/12	8	10	1	1	0	0	0	73	2	-13.0	0.0	GB	1	0	0	0	-
1653/12	4	9	1	1	0	0	0	57	1	-6.1	36.3	GB	0	1	0	0	-6.0
1677/12	3	11	1	1	0	0	0	81	1	32.9	15.2	GB	1	0	0	0	-30.6
169/11	9	10	1	1	0	1	1	84	1	60.7	77.6	GB	1	0	0	0	-18.7
1712/11	4	5	1	1	0	0	0	77	1	14.9	40.3	GB	1	0	0	0	-13.5
1715/11	2	5	1	1	0	0	0	81	1	-4.8	-1.0	GB	1	0	0	0	2.0
1727/11	4	5	1	1	0	0	0	77	1	-10.8	-	GB	1	0	0	0	0.5
1739/11	4	6	1	1	0	0	0	68	2	-10.4	-	AA	0	1	0	0	4.9
1765/11	43	56	1	0	1	1	1	46	1	75.1	60.6	AA	0	1	1	1	-
1773/11	8	8	1	1	0	0	0	69	1	-0.6	7.5	GB	0	1	0	0	-
1807/12	3	42	1	0	1	1	1	47	2	98.3	-	GB	0	1	1	0	-
1813/11	3	20	1	1	0	0	0	56	1	-6.2	-	GB	0	1	0	0	4.6
1833/12	38	38	0	0	0	0	0	51	2	22.5	-	AA	0	1	1	1	-14.5
1839/11	1	33	1	lost	0	0	0	43	2	29.2	-	GB	0	1	1	0	2.1
1849/11	51	51	0	0	1	1	1	66	1	100.7	35.1	AOA	0	1	1	1	-16.1
1877/12	3	19	1	1	0	0	0	55	1	-2.4	-	AA	0	1	0	0	-
1892/11	12	31	1	1	0	0	0	48	1	27.3	-	AA	0	1	1	0	-

1933/12	3	3	1	1	0	0	76	1	9.8	-	GB	1	0	0	0	-
1940/11	18	24	1	1	0	0	62	1	13.8	-	GB	0	1	1	0	-19.1
1950/12	39	39	0	0	1	1	59	2	86.2	-3.1	AOA	0	1	1	1	-
1961/11	12	14	1	1	0	0	73	2	-16.2	7.5	AA	1	0	0	0	-12.9
1998/11	4	5	1	1	0	0	53	2	11.6	-	GB	0	1	0	0	-
2083/11	6	10	1	1	0	1	54	2	44.8	-	GB	0	1	0	0	-15.5
292/13	3	6	1	1	0	0	69	2	9.6	9.4	GB	0	1	0	0	-
298/13	16	32	1	1	0	0	58	1	7.5	-	GB	0	1	1	0	-
299/13	12	35	1	0	0	0	69	1	3.8	12.5	GB	0	1	1	0	-
308/13	4	6	1	1	0	0	58	2	-2.4	8.2	GB	0	1	0	0	-16.5
394/12	22	36	1	1	0	0	50	1	-8.4	-4.7	GB	0	1	1	0	-
415/12	17	19	1	1	0	0	62	2	-18.7	2.6	GB	0	1	0	0	-53.1
416/13	9	12	1	1	0	0	50	1	-2.7	-	GB	0	1	0	0	9.2
436/13	38	38	0	0	1	1	59	1	78.1	-	AOA	0	1	1	1	-25.8
438/12	4	29	1	lost	0	0	74	2	-30.5	-	GB	1	0	1	0	-43.6
464/12	31	47	1	1	1	1	37	2	72.5	-	AOA	0	1	1	1	-
54/13	5	19	1	1	0	0	74	2	-9.5	-0.1	GB	1	0	0	0	-
694/12	20		1	lost	1	1	33	1	77.4	-	AA	0	1	0	0	-
711/12	38	38	0	lost	1	1	43	2	60.8	48.8	AO	0	1	1	1	-0.7
716/12	16	18	1	1	0	1	78	1	45.6	-	GB	1	0	0	0	-
770/12	4	6	1	1	0	0	23	2	7.9	-0.1	GB	0	1	0	0	-57.3
774/12	48	48	0	0	1	1	62	2	103.2	-	GB	0	1	1	1	-
828/12	4	8	1	1	0	0	71	1	-29.1	-7.8	GB	1	0	0	0	-
848/12	5	27	1	0	0	0	71	1	18.6	-	AOA	1	0	1	0	-
931/11	37	47	1	1	0	0	54	1	-7.2	5.2	GB	0	1	1	1	-
95/12	4	11	1	1	0	0	60	1	-2.4	-	GB	0	1	0	0	-
953/13	5	12	1	1	0	0	57	2	-2.0	-	GB	0	1	0	0	-
964/13	4	5	1	1	0	0	61	1	-12.1	-	GB	0	1	0	0	-

Reprint permission Table 02

International Agency for Research on Cancer



**World Health
Organization**

150 cours Albert Thomas
69372 Lyon cedex 08, France
IARC Communications Group
Tel.: +33 4 72 73 84 78
Fax: +33 4 72 73 83 11
E-mail: com@iarc.fr
<http://www.iarc.fr>

Mr Thomas Reich
University Medical Center Mainz
Obere Zahlbacher Strasse 67
Building 905
Institute of Toxicology
Germany

reich@uni-mainz.de

Ref.: CN/75/1

23 August 2016

Dear Mr Reich,

Following your request, I have pleasure in granting you this non-exclusive permission for print and electronic rights to use:

- the *WHO grading of tumours of the central nervous system*, p. 10–11

from Louis, DN, Ohgaki, H, Wiestler, OD, Cavenee, WK, Ellison, DW, Figarella-Branger, D, Perry, A, Reifenberger, G, Von Deimling, A. [World Health Organization Classification of Tumours of the Central Nervous System, Fourth Edition revised](#). IARC, Lyon, 2016.

for inclusion in a paper tentatively entitled *Role of Inhibitor of apoptosis proteins and XAF1 in resistance development against anti-cancer treatment in brain tumor cells and high-grade glioma patients* to be published in October 2016.

IARC does not require any payment, and the only credit we require is for you to appropriately cite the sources as follows:

- Reproduced with permission from Louis, DN, Ohgaki, H, Wiestler, OD, Cavenee, WK, Ellison, DW, Figarella-Branger, D, Perry, A, Reifenberger, G, Von Deimling, A. [World Health Organization Classification of Tumours of the Central Nervous System, Fourth Edition revised](#). IARC, Lyon, 2016.

I must impress upon you that any real or perceived association between this or other IARC material and a commercial sponsor would entail nullification of this permission, and IARC would reserve the right to legal action.

We also must point out that the material should be reproduced as originally printed, along with proper credit and identification. Permission must be obtained for each and any subsequent edition, translation or whatever use of said material you may wish to plan. Please note that use of the official WHO or IARC logo is prohibited.

We would appreciate it, if you could send us a copy of your publication, or access right to the information concerned. Thank you for your interest in our publications.

Yours sincerely,

A handwritten signature in blue ink, appearing to read 'Nicolas Gaudin'.

Dr Nicolas Gaudin
Head, Communications Group

6.2 Acknowledgments

Zuerst möchte ich mich bei Frau PD Dr. [REDACTED] für das entgegengebrachte Vertrauen bedanken, mir die Bearbeitung des hier dargelegten Projektes zu überlassen. Hier bei schätze ich die größtmögliche Freiheit bei der Planung und Durchführung der Arbeiten, aber auch die stete Ansprechbarkeit und Diskussionsbereitschaft.

Mein besonderer Dank gilt der Stipendienstiftung Rheinland Pfalz, die mir mit der Gewährung eines Promotionsstipendiums über zweimal zwölf Monate ermöglichte, die Dissertation nach intensiven Vorarbeiten erfolgreich und unabhängig fertigzustellen.

Prof. Dr. [REDACTED] danke ich recht herzlich für die Bereitschaft, als weiterer Gutachter zu fungieren, und Frau Prof. Dr. [REDACTED] für die Bereitstellung der Survivin GFP/XAF1 GFP Konstrukte!

Ich möchte mich herzlich bei allen Mitarbeitern des Institutes für Toxikologie, die ich während meiner Zeit als Doktorand kennen lernen durfte, für die kollegiale, freundliche und hilfsbereite Atmosphäre bedanken. Hierbei gilt mein ausdrücklicher Dank meinen ständigen Begleitern und treuen Mitdoktoranden aus dem „Rattenloch 400“ – in alphabetischer Reihenfolge: [REDACTED] für die stets gute Laune und Aufrichtigkeit; [REDACTED] [REDACTED] für emotionalen Support und zahlreiche Späße; [REDACTED] [REDACTED] für die vernünftige Stimme im Schreibraum und viele geführte Wanderungen im Hunsrück; [REDACTED] [REDACTED] [REDACTED] für unzählige wichtige und un wichtige Diskussionen sowie die weit über unsere Themen hinausreichenden Experimente, und die Einführung in die Geheimnisse der HRM.

Weiterhin danke ich [REDACTED] [REDACTED] und [REDACTED] [REDACTED] sehr für die Durchsicht der Arbeit und die Unterstützung.

6.3 Curriculum Vitae

CONTACT INFORMATION

Thomas Reich



reich@uni-mainz.de

born on July 5, 1987 in Ludwigshafen am Rhein

PHD STUDIES & EDUCATION

01/2013	12/2016	Doctoral research study at the University Medical Center Mainz (Institute of Toxicology); Thesis title: "The role of inhibitor of apoptosis proteins and XAF1 in the resistance to anti-cancer treatment in brain tumor cells and high-grade gliomas"
03/2012	01/2013	Diploma thesis at the University Medical Center Mainz (Institute of Toxicology); Thesis title: "Regulation des DNA-Reparaturproteins O6-Methylguanin-DNA Methyltransferase (MGMT) über Promotoraktivierung und miRNA" (1,0) <ul style="list-style-type: none"> • Cell culture studies of DNA repair gene regulation via post-transcriptional means by PCR, qPCR, Western-Blot • Analysis of miRNA expression and promoter activity studies
10/2007	01/2013	Studies of Biology at Johannes Gutenberg-University Mainz; final degree: Diploma with distinction (1,0); graduated in: <ul style="list-style-type: none"> • Molecular genetics • Botany • Toxicology & pharmacology • Additional subjects: microbiology, physiological chemistry
04/2006	12/2006	Military service ABC-Abwehrbataillon 750, Bruchsal
08/1997	03/2006	Heinrich-Böll-Gymnasium (college preparatory school) Ludwigshafen; degree: university-entrance diploma/ Abitur

OTHER

04/2014	04/2015	Scholarship/ PhD grant of the “Stipendienstiftung Rheinland-Pfalz”
04/2015	04/2016	Second year approval of the PhD grant
02/2016		Selected Talk at the 32 ^d German Cancer Congress in Berlin: “Best of (Freier Beitrag): XAF1 is a novel epigenetic marker to predict survival of high-grade brain tumor patients”
06/2015		Travel grant of the German Society for Research on DNA Repair (DGDR) to visit the 1 ^s Tomas Lindahl Conference on DNA Repair in Oslo

CONFERENCES & WORKSHOPS

07/2016		Leica “Light microscopy workshop“ on bright field, fluorescence and confocal laser scanning microscopy, Forschungszentrum für Immuntherapie, Mainz
06/2016		Poster presentation: 18 “Jahrestagung der Neuroonkologischen Arbeitsgemeinschaft (NOA)”, Regensburg
02/2016		Selected talk: 32 ^d German Cancer Congress, Berlin
06/2015		Poster presentation: 1 ^s Tomas Lindahl Conference on DNA Repair, Oslo
03/2015		Poster presentation: 18 International AEK Cancer Congress, Heidelberg
09/2014		Poster presentation: Biennial conference of the DGDR (German Society for Research on DNA Repair), Mainz
05/2014		Oral presentation: GUM-workshop (German Society for Environmental Mutation Research), Düsseldorf
04/2014		Poster presentation: Annual conference of the DGPT (“Deutsche Gesellschaft für experimentelle und klinische Pharmakologie und Toxikologie e.V.”), Hannover

PUBLICATIONS

Reich, T.R., Switzeny, O.J., Renovanz, M., Sommer, C., Kaina, B., Christmann, M., and Tomicic, M.T. - Epigenetic silencing of XAF1 in high-grade gliomas is associated with IDH1 status and improved clinical outcome. Oncotarget, 2017. in press

Reich, T.R., Christmann, M., and Tomicic, M.T. Influence of survivin localization on cell death, senescence, and DNA repair in temozolomide-exposed glioblastoma cells. in preparation

Schafer, C., Goder, A., Beyer, M., Kiweler, N., Mahendrarajah, N., Rauch, A., Nikolova, T., Stojanovic, N., Wiczorek, M., **Reich, T.R.**, Tomicic, M.T., Linnebacher, M., Sonnemann, J., Dietrich, S., Sellmer, A., Mahboobi, S., Heinzl, T., Schneider, G., and Kramer, O.H. - Class I histone deacetylases regulate p53/NF-kappaB crosstalk in cancer cells. Cell Signal, 2016. 29: p. 218-225.

